A heat pipe and porous ceramic based sub wet-bulb temperature evaporative cooler: A theoretical and experimental study

By

Omar Emhemed Amer

BSc (Eng), MSc

Thesis Submitted to the University of Nottingham

for the Degree of Doctor of Philosophy

March 2017

Abstract

Worldwide energy demand in buildings represents about 40-50% of the total energy consumption. In hot climates, such as Middle East and North Africa (MENA) countries, about 30% of the national power demand is used for HVAC applications in buildings. This has led to escalation in power demand in buildings for indoor air-cooling and high energy bills. This is exacerbated further by the widespread adoption of energy intensive and commercially dominant vapour compression air conditioning systems as the technology of choice.

This research aims to address the potential of novel designs of evaporative cooling systems for space cooling and thermal comfort in buildings with reduced water and energy consumption, and low environmental impact as an alternative to vapour compression where climatically is suitable. High water consumption rates and low cooling effectiveness are some of the issues affecting the performance of existing Indirect Evaporative Coolers (IEC). A new configuration of IEC combining heat pipe heat exchanger and porous ceramic tubes is investigated in this work.

The proposed cooler configuration is based on the concept of regenerative IEC system, this system incorporates heat pipes as passive heat transfer elements and porous ceramic tubes as wet medium mounted on the condenser side of the exchanger. The design of the cooler was carried out with consideration for size of the airflows channels, heat pipes for heat transfer, and porous ceramic tubes properties for water evaporation. A mathematical formulation of heat and mass transfer equations was used to develop a computer model to design and optimise the cooling system. Furthermore, a test rig was built to test a laboratory scale cooling unit, evaluate the performance and validate the simulation.

The simulation results reveal that the Wet-bulb (WB) effectiveness of the cooler ranged from 0.524 to 1.053, the COP ranged from 6.33 to 17.01, and water consumption rates of the cooler were around 0.875-1.55 (l/kWh) of cooling capacity. Whereas, the experimental performance

parameters of the cooler show the WB effectiveness was in the range of 0.422-0.908 for all test conditions, the COP was 4.62-13.16, and water consumption rates varied 0.841-2.82 (l/kWh) of cooling capacity. A good agreement was obtained between the experiments data and numerical results, the maximum errors between measured and computed results was around 3.94% and 4.51% of supply air temperature and humidity, respectively, while the discrepancy was in the range of 8.67-12.90% of the WB effectiveness.

The impact of operational and design parameters on the cooler performance was evaluated in a parametric study using the developed numerical model. It was found that increasing the inlet air temperature, decreasing the inlet air flow rate, and/or increasing the working-to-inlet air flow ratio, results in improving the effectiveness and supply air temperature. Whereas, increasing the inlet air wet-bulb temperature depression, increasing the inlet air flow rate, and/or minimising the working-to-inlet air flow ratio leads to enhancing the cooling output and COP of the cooler. Additionally, increasing the thickness and/or the radius of ceramic tube causes a decline of cooler thermal performance. Therefore, it is recommended to operate the cooler at inlet air velocity of 2-2.5 m/s, 50% flow ratio of working-to-inlet air, and inlet air relative humidity below 35% for best results of supply air temperature, WB effectiveness, and COP. Whereas, for desert climate conditions, it is recommended to increase the number of heat pipe rows to 20 to insure sufficient cooling effectivity and performance that meet comfort levels.

Finally, a brief economic assessment of the cooler annual operational performance for a case study was carried out, this IEC system provide sufficient cooling effectiveness to the conditioned space with significantly low power consumption compared to traditional air conditioner with annual saving of 77.60% of operational costs, and also substantially contribute to minimise CO_2 emissions by saving about 86% of electricity consumption.

Publications

- O. Amer, R. Boukhanouf, H. G. Ibrahim, *A review of Evaporative cooling Technologies*, in International Journal of Environmental Science and Development 2015. p. 111.

- R. Boukhanouf, A. Alharbi, O. Amer, H. G. Ibrahim, *Experimental and Numerical Study of a Heat Pipe based Indirect Porous Ceramic Evaporative Cooler*, in International Journal of Environmental Science and Development 2015. p. 104.

- O. Amer, R. Boukhanouf, *Experimental investigation of a novel heat pipe and porous ceramic based indirect evaporative cooler*, in International Heat Transfer Symposium 2016, Nottingham. ISBN: 978-0-9563329-3-6

- R. Boukhanouf, A. Alharbi, H. G. Ibrahim, O. Amer, M. Worall, *Computer modelling and experimental investigation of building integrated sub-wet bulb temperature evaporative cooling system*. Applied Thermal Engineering, 2017. 115: p. 201-211.

Acknowledgement

I would sincerely like to thank my supervisor Dr. Rabah Boukhanouf for his unlimited help and valuable guidance during the course of this study, he has spared no effort in encouraging and supporting me throughout this academic journey.

My thanks to all who helped in the output of this research, to all those who were supporting and helping me;
To Faysal Bahri, David Taylor, David Oliver, and all other technicians in the department. I owe you thanks for all your valuable support and assistance in the technical work.

I am also deeply indebted to the Libyan Higher Education Ministry for the financial support, and to my sponsor in the UK, the Libyan Cultural Attaché.

Finally, I would like to express my special appreciation and thanks to my wife for her support and patience during my study. Also, the encouragement and support from my family, friends, and colleagues are highly appreciated.

Table of Contents

Abstract I
Publications III
Acknowledgement IV
Nomenclature IX
List of Figures XIII
List of Tables XVI
Chapter 1: Introduction 1
1.1 Background 1
1.2 Research aims and objectives 5
1.3 Research methodology 6
1.4 Novelty of the research 7
1.5 Thesis Contents 8
Chapter 2: Overview of evaporative cooling technologies 10
2.1 Evaporative cooling cycle (EC) 10
2.1.1. Classification of evaporative cooling systems 10
2.1.2. Applications 11
2.1.3. Advantages and disadvantages 11
2.2 Direct evaporative cooling coolers (DEC) 12
2.2.1. Active direct evaporative coolers (Active DECs) 14
2.2.2. Passive direct evaporative coolers (Passive DECs) 16
2.3 Indirect evaporative coolers (IECs) 20
2.3.1. Wet-bulb temperature IEC systems (WBT-IEC systems) 21
2.3.2. Sub wet-bulb temperature IEC systems (Sub WBT-IEC) 28
2.4 Combined indirect-direct evaporative coolers (IDEC) 29
2.5 Summary 33
Chapter 3: Review of sub wet-bulb temperature indirect evaporative coolers 34
3.1 Sub wet-bulb temperature coolers (sub WBT-IEC systems) 34
3.2 Porous ceramic as wetting media of IEC systems 45
3.3 Analysis of reviewed work of the sub WBT-IEC systems 48
3.4 Parametric performance of the IEC 56

3.5.1 Wet-bulb effectiveness 56
3.5.2 Dew-point effectiveness 56
3.5.3 Cooling capacity 56
3.5.4 Coefficient of performance (COP) 57
3.5.5 Power demand 57
3.5.6 Water consumption rate 57
3.5 Summary 58
Chapter 4: Design and computer modelling 59
4.1 Configuration of the sub WBT evaporative cooler 59
4.2 Design consideration 60
4.2.1 Heat pipe 60
4.2.2 Determination of the required number of heat pipes 62
4.2.3 Selection of porous ceramic tube dimensions 63
4.2.4 Preliminary design configuration 64
4.3 The Mathematical formulation 65
4.3.1 Energy and mass balance 67
4.3.2 Thermal resistances 70
4.3.3 Heat transfer coefficients 76
4.4 Computer model 78
4.5 Computer model results 81
4.5.1 Effect of channels dimensions 81
4.5.2 Effect of ceramic tube inner and outer diameter 82
4.5.3 Effect of thickness of ceramic tube wall 83
4.5.4 Effect of wettability and contact factors 83
4.5.5 Effect of water film and feed-water rates 84
4.5.6 Effect of number of heat pipes 84
4.5.7 Preliminary computer model results of the cooler performance 85
4.6 Summary 87
Chapter 5: Construction and experimental investigations 89
5.1 Prototype construction 89
5.2 Components assembly 91
5.2.1 Outer casing 91
5.2.2 Heat pipes 92
5.2.3 Porous ceramic pipe 93
5.2.4 Air circulating fan and controller 94
5.3 Fully assembled laboratory prototype 94

5.4 Measuring instruments 96
5.2 Experiment set-up 98
5.3 Test conditions 99
5.4 Test procedure 101
5.5 Experiment observations and limitations 102
5.6 Preliminary results of experimental work 104
5.7 Summary 105
Chapter 6: Results analysis and discussion 106
6.1. Air flows temperature variation 106
6.1.1 Constant inlet air temperature and humidity 106
6.1.2 Variable inlet air temperature and humidity 109
6.2. Temperatures distribution in the air channels 110
6.3. Psychrometric chart plotting and comfort zone 111
6.4. Parametric study 112
6.4.1 Effect of inlet air temperature 112
6.4.2 Effect of inlet air relative humidity 114
6.4.3 Effect of inlet air velocity (inlet air flow rate) 116
6.4.4 Effect of the working-to-inlet air flow rate ratio 118
6.5. Water consumption rate of the cooler 119
6.6. The discrepancy between computed and measured results 120
6.7. Effect of increasing numbers of heat pipe and ceramic tube modules 122
Chapter 7: Simplified economic and environmental evaluation 128
7.1 Building cooling loads assessment 128
7.2 The cooler capacity 131
7.3 Economic assessment 132
7.3.1 Annual electrical energy consumption 132
7.3.2 Annual water consumption 132
7.4 Environmental impact 134
7.5 Summary 135
Chapter 8: Conclusion and future work 136
8.1 Conclusion 136
8.2 Further work 140
References 145

Appendices 151
Appendix A 151
Appendix B 156
Appendix C 158
Appendix D 160
Appendix E 163

Nomenclature

Abbreviations

COP	Coefficient of performance
DEC	Direct evaporative cooler
DP	Dew point
DPT	Dew point temperature
HMX	Heat and mass exchanger
HPC	Heat pipe condenser
HPE	Heat pipe evaporator
HPHX	Heat pipe heat exchanger
IEC	Indirect evaporative cooler
IDEC	Combined indirect and direct evaporative cooler
M-IEC	M-cycle based indirect evaporative cooler
R-IEC	Regenerative indirect evaporative cooler
WBT	Wet-bulb temperature
WBT-IEC	Wet-bulb temperature indirect evaporative cooler

Nomenclature

A	Surface area, m^2
A_1	Total area of a finned heat pipe, m^2
A_b	Exposed area of the fined heat pipe evaporator, m^2
$A_{fin,circ}$	Surface area of circular fan of uniform rectangular cross section, m^2
A_v	Area of vapour space of the heat pipe, m^2
A_{wk}	Cross-section area of heat pipe wick m^2
$C = \dot{m}c_p$	Heat capacity rate; $\mathrm{J/s\,K}$
c_P	Specific heat capacity, $\mathrm{J/kg\,K}$
d_3	Outer diameter of heat pipe, m
d_{wk}	Wire diameter of the mesh, inch
D_H	Hydraulic diameter
F_t	Fin thickness, m
F_P	Fin pitch, m
F_l	Fin length, m
g	Gravity acceleration, m/s^2;
h	Convective heat transfer coefficient, $\mathrm{W/m^2\,K}$
h_m	Mass transfer coefficient, $kg/s\,m^2$
i	Specific enthalpy, $\mathrm{J/kg}$
i_{fg}	Latent heat of water evaporation, $\mathrm{J/kg}$
i_{fg}^0	Latent heat of vaporization heat at zero ℃, $\mathrm{J/kg}$
K	Wick permeability, m^2
l_c	Condenser length of heat pipe, m

l_e	Evaporator length of heat pipe, m
l_{eff}	Effective length of heat pipe m,
l_{fin}	Fin length, m
l_t	Total length of the heat pipe m
Le	Lewis number
$\dot{m}$	Mass flow rate, $\mathrm{kg/s}$
n_i	Number of differential elements
N_{fin}	Number of fins
N_{wk}	Number of mesh wires per 1 in of mesh length
Nu	Nusselt number
p	Pressure, Pa
P_{aux}	Auxiliary power consumption, W
P_v	Vapour pressure, Pa
Pr	Prandtl number
Δp_{air}	Air pressure difference at the inlet and exist of the fan, Pa
ΔP_c	Maximum capillary pressure of heat pipe, Pa
Q_e	Heat transport due to entrainment limit of heat pipe, W
Q_c	Maximum heat transport due to capillary limit, W
Q_b	Maximum heat transfer rate due to boiling limitations, W
Q_v	Heat transport due to the viscous limit, W
Q_s	Sonic heat transport limit, W
q	Heat transfer rate, W
Q_1	Maximum heat transferred by the heat pipe, W
R_1	Convective resistance between evaporator surface and air, m^2K/W
R_2	Conductive resistance of heat pipe wall, m^2K/W
R_3	Conductive resistance of the evaporator wick structure, m^2K/W
R_4	Liquid-vapour interface resistance at the evaporator, m^2K/W
R_5	Vapour space resistance, m^2K/W
R_6	Liquid-vapour interface resistance at the condenser, m^2K/W
R_7	Conductive resistance of heat pipe wick structure of the condenser,m^2K/W
R_8	Conductive resistance of heat pipe wall of the condenser, m^2K/W
R_9	Axial conduction resistance of the adiabatic section wall, m^2K/W
R_{10}	Axial resistance of saturated wick at the adiabatic section, m^2K/W
R_{11}	Water conductive resistance, m^2K/W
R_{12}	Ceramic tube conductive resistance, m^2K/W
R_{13}	Convective resistance between ceramic tube and moist air, m^2K/W
r_{equ}	Equivalent radius of the radial fin, m
r_1	Vapour space radius of heat pipe, m
r_2	Inner radius of heat pipe evaporator, m
r_3	Outer radius of heat pipe, m
r_4	Inner radius of the circular fin, m
r_5	Outer Radius of the circular fin, m
r_6	Inner radius of the porous ceramic tube, m
r_7	Outer radius of the porous tube, m
Re	Reynolds number, -
R_v	Gas constant of vapour, $J/kg\ K$

r_n	Nucleation radius, m
r_c	Capillary radius of the wick surface pores of heat pipe, m
T	Temperature, ℃
t	Time, sec
t_{fin}	Fin thickness, m
U	Overall heat transfer coefficient, W/K
V_d	Air velocity in the dry channel side, m/s
V_a	Air velocity in the wet-air channel, m/s
$\dot{V}$	Air volumetric flow rate, m^3/s
$\dot{V}_w$	Water volumetric flow rate, m^3/s
w_{fin}	Fin width, m

Greek symbols:

σ_1	Surface tension of heat pipe working liquid, N/m
ρ	Air density, kg/m^3
ψ	Surface wettability factor
μ	Dynamic viscosity of air, $kg/m\,s$
ν	Kinematic viscosity of air, m^2/s
λ	Thermal conductivity, $W/m\,K$
ω	Vapour content, $\mathrm{kg}_{\mathrm{vapour}}/\mathrm{kg}_{\mathrm{dry\ air}}$
φ	Inclination angle of the heat pipe
θ	Angle of wettability of the liquid on the heat pipe wick
ε	Effectiveness
ϵ	Wick porosity of heat pipe
η_{fan}	Fan efficiency
η_{pump}	Pump efficiency

Subscripts

1	On dry-air side or inlet air
2	Supply air
a	On wet-air side or Moist air (the working air)
c	Cold or condenser
ce	Ceramic
d	Dry air or on dry-air side
e	Evaporator, or evaporator side of the heat pipe
fin	Fin
h	Hot
i	Inlet of the cooler
L	liquid water
o	Outlet of the cooler
s	On the air-water interface or water surface
v	Water vapour

wf	Water film or water
wb	Wet bulb temperature
wk	Wick of heat pipe

Superscripts

’	Saturated condition at water film temperature

List of Figures

Fig 1-1 Total energy consumption for the world, EU, Africa, China and Middle East [2] 2
Fig 1-2 Global CO_2 emissions by fuel type and sector 1971-2014 [5] 3
Fig 2-1 Classification of evaporative cooling systems 10
Fig 2-2 Working principle and psychrometric chart of a direct evaporative cooler [15] 12
Fig 2-3 Basic structure and main components of drip-type DEC unit (Reproduced from [18] and [19]). 14
Fig 2-4 Types of DEC systems [21], [10] 16
Fig 2-5 Main types of passive cooling systems [1], [22] 17
Fig 2-6 Basic structure of wind tower integrated with evaporative systems [1], [25] 18
Fig 2-7 The Mashrabiya [23] 19
Fig 2-8 Roof-pond cooling systems [1] 20
Fig 2-9 Basic IEC system structure [13] 21
Fig 2-10 Working principle and psychrometric chart of wet-bulb IEC [8] 22
Fig 2-11 Schematic of plate-type IEC system [8], [28] 23
Fig 2-12 Tubular heat exchanger based IEC [8] 25
Fig 2-13 Finned ceramic tube indirect evaporative cooler [38]. 25
Fig 2-14 Schematic of two configurations of Heat pipe based IEC system [50], [52] 27
Fig 2-15 Structure and working principle of M-cycle HMX based IEC 28
Fig 2-16 Schematic of Two-stage IDEC system [13] 30
Fig 2-17 Two-stage IDEC system [58] 32
Fig 2-18 Schematics of solid desiccant/evaporative cooling systems [63], [8] 32
Fig 2-19 Multi-stage IDEC: radiative cooling, cooling coil and two-stage IDEC [67] 32
Fig 3-1 Coolerado Cooler™ [57] 35
Fig 3-2 Configuration and working principle of a regenerative ICE [69], [20] 36
Fig 3-3 Flat-plate based dew point indirect evaporative cooling system [26] 38
Fig 3-4 Four exchanger configurations of IEC system studied by Hasan [74] 39
Fig 3-5 Schematic of sub WBT cooler, a) one-unit module, b) working principle [79] 41
Fig 3-6 Shapes of porous ceramic integrated with building walls; (a) porous ceramic panels [94], (b) structure of porous plate [95] 46
Fig 4-1 Configuration of the cooler; the working principle and air flow pattern 59
Fig 4-2 Cross-section view of the thermosiphon and the heat pipe [115] 61
Fig 4-3 Heat pipe heat exchanger effectiveness [10] 63
Fig 4-4 3D drawing of the HPHX and ceramic tube based IEC system 64
Fig 4-5 Physical model of the system 66
Fig 4-6 Schematic of the heat pipe and ceramic tube module 66
Fig 4-7 Heat pipe thermal resistances; (a) original circuit, (b) simplified circuit [118] 71
Fig 4-8 Efficiencies of circular and straight fins [118] 74
Fig 4-9 Computer model flowchart 80
Fig 4-10 Effect of increasing inner radius of ceramic tube on supply temperature and WB effectiveness at inlet conditions of 40 ℃, 35% RH, 2 m/s, and 50% flow rate ratio 82
Fig 4-11 Thermal resistance of ceramic tube versus tube wall thickness 83
Fig 4-12 Effect of number of heat pipes on the effectiveness and temperature at inlet conditions of 40 ℃, 35% RH, 2 ms, 23 ℃ water temperature and 50% flow rate ratio 85

Fig 4-13 Supply air temperature and relative humidity profiles as function of inlet air temperature at inlet conditions of 20-35%RH, 60-125 m^3/h rates, 18 °C water temperature, and 50% flow ratio 87
Fig 5-1 Isometric and perspective views of the HPHX and ceramic tube based R-IEC system .. 89
Fig 5-2 flow scheme inside the cooler, (a) dry and wet channels, (b) wet channel, (c) dry channel 90
Fig 5-3 Front, sides, and plan views of the cooling unit 91
Fig 5-4 The casing of the prototype unit 92
Fig 5-5 Heat pipe element 93
Fig 5-6 Porous ceramic tubes 94
Fig 5-7 Construction and assembly process of the cooling system 95
Fig 5-8 Heat pipe and porous ceramic tube based R-IEC system 96
Fig 5-9 Measurement instruments' locations on the rig 97
Fig 5-10 Photographs of the measurement instruments: (a) Type K thermocouple; (b) hotwire anemometer; (c) RS-232 humidity and temperature meter; (d) RS-1365 thermometer 97
Fig 5-11 Experiment set-up 99
Fig 5-12 Tests plan 100
Fig 5-13 Water droplets formation over ceramic tubes 103
Fig 5-14 Water puddles formation at the base of ceramic tubes 104
Fig 6-1 Inlet air, supply air and working air temperature profiles over time at inlet conditions of 40 ℃, 25% RH, 150, 105 and 75 m^3/h inlet flow rates, and of 20, 50 and 70% flow ratios ... 107
Fig 6-2 Temperature distribution over the time of dynamic testing under conditions of variable inlet air from 30-45-30 ℃ , at fixed inlet flow rate of 105 $\boldsymbol{m3h}$ and flow rate ratio of 50%; (a) at inlet relative humidity varying 25-30%, (b) at inlet relative humidity 50-55%, ... 109
Fig 6-3 comparision between experimental and numerical temperature curves of the inlet supply air and working air, and moisture content of working air along the cooler channels at inlet conditions of 40℃, 35%, 75 m^3/h air flow rate, 50% flowrate ratio 111
Fig 6-4 Mapping inlet and supply air temperatures on psychrometric chart 112
Fig 6-5 WB effectiveness and inlet air temperature drop versus inlet air temperature at operation conditions of 50% flowrate ratio, 75 m^3/h air flow rate, and 35% RH 113
Fig 6-6 Cooling capacity and COP versus inlet air temperature at flow rate ratio of 50%, 75 m^3/h flow rate ratio and 35% inlet relative humidity 114
Fig 6-7 WB effectiveness and temperature reduction profiles versus various inlet air relative humidity under inlet air conditions of 40℃ temperature, 50% flow ratio, and 75 m^3/h inlet air flow rate 115
Fig 6-8 Cooling capacity and coefficient of performance profiles over various inlet air relative humidity values at inlet conditions of 40 and 30℃, 75 m^3/h air flow rate and 50% flow rate ratio 116
Fig 6-9 WB effectiveness and cooling capacity versus inlet air flow rates at inlet conditions of 40℃, 35% RH and 50% flow rate ratio 117
Fig 6-10 WB effectiveness and cooling capacity variation against flow rate ratio of working-to-inlet air at inlet air speed of 3.5m/s, 35% RH and 40, 35, 30℃ inlet air temperatures 118
Fig 6-11 Water evaporation rate at working conditions of 75 m^3/h air flow rate, 35% RH, and 50% flow rate ratio 120
Fig 6-12 Equavalent radial fin 122

Fig 6-13 Psychrometric plotting of two inlet temperatures under inlet air conditions of 40 and 45℃, constant moisture content of 0.0120 $kgwkgdry\ air$, flow rate ratio of 50%, 60 $m3/h$ flow rate, 23 ℃ water temperature and 15 rows of heat pipe 123
Fig 6-14 Psychrometric plotting of two different inlet temperatures under inlet air conditions of a constant moisture content of 0.0120 $kgwkgdry\ air$, flow rate ratio of 50%, 60 $m3/h$ flow rate, 23 ℃ water temperature and 20 rows of heat pipes 125
Fig 6-15 Effect of heat pipe numbers on the effectiveness for verious inlet temperatures and under fixed operation condtios of 75 m^3/h air flow rate, 35% RH, and 50% flow rate ratio... 126
Fig 7-1 House plan view and 3D sketch of the house 128
Fig 7-2 Structure of house components 129
Fig 7-3 Daily sensible cooling load of the house 130
Fig 7-4 Comparison of annual power consumption between the heat pipe-ceramic based IEC and vapour compression A/C. 132
Fig 7-5 Comparison between annual operation cost of vapour compression A/C and the proposed system of 110 m^2 House 133
Fig 8-1Schematics of axial fin and cross section of finned condenser and ceramic tube..... 141
Fig 8-2 Working air temperature and humidity profiles versus inlet air temperature at inlet air conditions 75 m^3/h of flow rate, 35%RH, and 50% flow rate ratio of working-to-inlet air 142
Fig 8-3 First configuration of the combined system 143
Fig 8-4 Second configuration of the combined system 143
Fig 8-5 Combined configuration of HPHX and ceramic based R-IEC and dry air HX 144

List of Tables

Table 1-1 HVAC systems share of total buildings energy consumption [5]..... 3
Table 1-2 comparison between the some air-conditioning systems [8] 4
Table 2-1 Advantages and disadvantages of the evaporative coolers [11], [12], [13], and [14] 11
Table 2-2 Typical types of active direct evaporative coolers [10], [20] 15
Table 3-1 Summary of reviewed work on sub WBT-IEC systems..... 49
Table 3-2 Summery of comparative studies between different types of the sub WBT-IEC systems 50
Table 3-3 Heat dissipation methods employed in HPHX based IEC systems 54
Table 4-1 Pre-set conditions of the computer model..... 81
Table 4-2 Thermal performance parameters of the cooling system..... 86
Table 5-1 Outer casing specification..... 92
Table 5-2 Heat pipe parameters and specifications 93
Table 5-3 Porous ceramic tubes specification [125]..... 94
Table 5-4 Rig instruments and their corresponding measured parameters 98
Table 5-5 Experimental results of the cooler performance at inlet air conditions of 40 ℃, 25% and 45% RH, and 50% working-to-inlet air flow rate ratio 104
Table 6-1 Pre-set operation conditions and cooler specification..... 110
Table 7-1 House specifications 128
Table 7-2 Input data and assumptions of the house rooms 129
Table 7-3 Specifications of walls, roof, floor, doors, and windows 129
Table 7-4 Thermal performance of the cooling system..... 131
Table 7-5 Daily and annual consumption of electricity and water of the IEC system 131

Chapter 1: Introduction

1.1 Background

Improving thermal comfort in buildings has evolved considerably over time, contributing to the wellbeing and enhanced living conditions of occupants. In hot climates, ancient Greeks and Babylonians used wet mats overhanging doors and windows and water filled clay jars on balconies to capture a cool breeze into the living spaces. Similarly, the Arabs and Persians developed building integrated wind catchers and wet towers to channel cool air flows into buildings. Presently, fully controlled and mechanised air conditioning systems are the ultimate standard for thermal comfort in modern buildings, albeit at a huge cost to the environment and occupants' budget [1]. The market of mechanical cooling systems has expanded significantly in the last few decades causing a surge in demand for electrical power in many countries and putting huge pressure on power grids infrastructures. This has contributed to a steady increase of energy consumption worldwide, leading to strains on the depleted energy sources. Fig 1-1 illustrates the total energy consumption trends for the world and its regions. For instance, between 2000 and 2014 the world energy consumption grew by 36.42%, supported by increased demand from fast developing economies such as China, India and Middle East. The slowdown of energy consumption in Europe over the same period was more than offset by a huge increase in China 173.11% and Middle East region 102.29%, representing 20.48% and 6.43% of the total world energy in 2014 respectively [2].

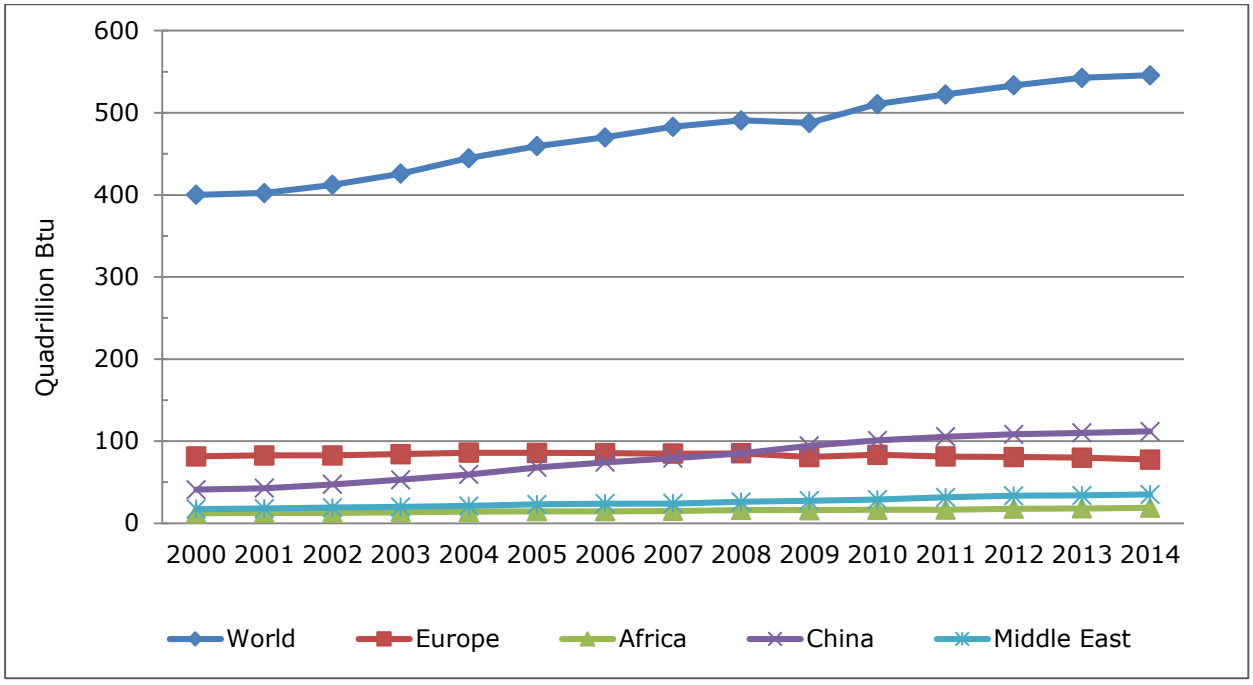


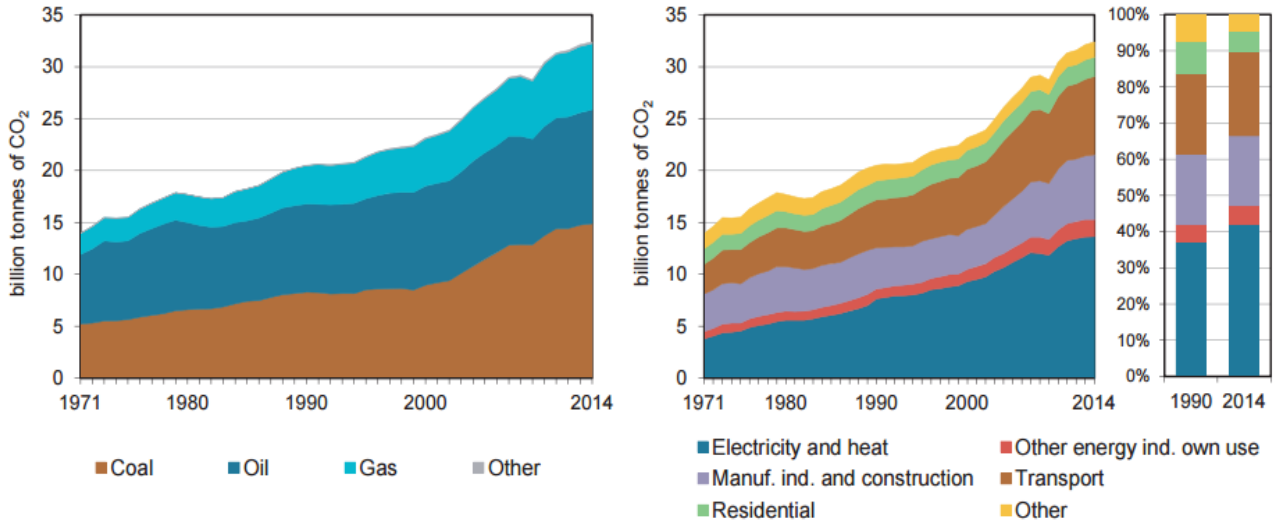
Fig 1-1 Total energy consumption for the world, EU, Africa, China and Middle East [2]

One of the main contributing factors to the surge in demand for power in buildings is increased air-conditioning loads in residential and commercial sectors. This is due to several factors including heat waves and climate change affecting some regions (e.g. southern Europe), improved living standards, growing population where 75% of largest metropolitan cities are in developing countries mostly located in warm climates (e.g., China, India , Australia, and MENA countries), advances in cooling technologies assured high level of comfort and longer time spent indoors [3]. Consequently, the building sector shares 40 to 50% of total primary energy consumption of the world, which is higher than power consumption in other public sectors such as transportation and power generation. The power consumption for heating, ventilation and air-conditioning in buildings accounts almost for as much as 10%-20% of total energy demand [4]. Table 1-1 presents the share of HVAC systems total energy consumption in buildings of selected countries worldwide. It is shown that the energy use for air conditioning can vary from 20% to 70% depending on geographical location, climate conditions, and type of air-conditioning load [4].

Table 1-1 HVAC systems share of total buildings energy consumption [5].

Country	Share of total buildings energy demand
Middle East	70 %
Australia	70 %
US	50 %
India	32 %
China	20.7 %

Environmental concerns associated with global warming and increased public awareness about energy consumption for air conditioning have started to sway the public opinion to seek more energy efficient alternatives to reduce over exploitation of energy resources and the adverse impact on the ecosystems that results from. For example, the total carbon-related emissions increased by about 45.44% for the period from 2000 to 2014 globally, and the main source of these emissions come from conventional energy resources, as shown in Fig 1-2. where 99.5% of world emissions in 2014 were from fossil fuel sources [5]. Furthermore, about 80% of environmental impact of buildings HVAC comes from electricity generation that runs these systems, and the remaining 20% is from the direct effect of refrigerants charges. Refrigerants such as Chlorofluorocarbons (CFCs) and its replacement hydro-chlorofluorocarbons (HCFCs) e.g. R-22 deplete the ozone-layer [5].



(a) Emissions of CO_2 by fuel type

(b) Emissions of CO_2 by sector

Fig 1-2 Global CO_2 emissions by fuel type and sector 1971-2014 [5]

As a result hydro-fluorocarbons which are chlorine-free refrigerant (HFCs), e.g. R-134a, R-410A, were used as replacement alternatives, however still they contribute to global warming [6]. Thus, these factors have led many organisers and researchers to renew their interest in the development of evaporative cooling technology as an environmentally friendly alternative technology for space cooling in buildings where the conditions are favourable [7].

Evaporative coolers offer higher overall energy efficiency than Vapour Mechanical Compression (VMC) and desiccant cooling systems, particularly in hot and dry climates. Table 1-2 shows a comparison between VMC cooling, desiccant cooling and evaporative cooling systems. The VMC systems are well-known for their high cooling effectiveness and stable operation, but their low COP and massive adverse environmental impact are main disadvantages. In contrast, the evaporative cooling systems have low environmental impact and high COP values. Though their performance is strongly dependent on prevailing climatic conditions particularly the temperature difference between the dry-bulb and wet-bulb of the ambient air. For hot and dry climates this temperature difference is large, resulting high cooling effectiveness [7].

Table 1-2 comparison between the some air-conditioning systems [8]

System type	VMC cooling	Desiccant cooling	Evaporative cooling
COP	2 to 3	0.6 to 1.2	5 to 20
Power consumption	High	Medium	Medium
Refrigerants	CFCs, HFCs	Solid/liquid desiccants	Water
Environmental Impact	Extreme	Extreme	Low
Operating range	Any climate	Hot and humid climate	Hot and dry climate

The importance of this research work addresses the energy consumption and comfort dilemma in buildings, as both are strongly interrelated. Air-conditioning cooling energy loads are increasing steadily which impacts on global warming and buildings occupants who are reliant more than ever on air conditioned enclosed spaces, as they spend a large proportion of their time indoors. Therefore, it is important that more efficient and cost-effective cooling means are explored and developed to cope with the increasing demand of air conditioning loads.

1.2 Research aims and objectives

- **Research aims**

The aim of this study is to develop a new configuration of heat pipe based indirect evaporative cooling system. The basic mechanical design is centred on the regenerative configuration of indirect evaporative cooling system which integrates porous ceramic tubes as wetting media material and tubular heat pipes as heat transfer devices. This novel heat pipe and porous ceramic IEC system is intended to overcome some of the disadvantages associated with indirect evaporative coolers; (i.e. large water consumption, and low cooling effectiveness). It is also anticipated that this integrated heat pipe and ceramic IEC would enhance current evaporative cooling technologies i.e. low electricity consumption and low environmental impact.

- **Research objectives**

The main objectives of this thesis are as follows:

- A thorough literature review of evaporative cooling technologies and application in buildings with the focus on sub-wet bulb temperature systems.
- Design and computer modelling of an IEC system to investigate performance parameters.
- Fabrication and testing of a small-scale prototype with integrated heat pipe and ceramic tube under various climate conditions and operating parameters.
- Assessment of the annual economic and the environmental impact of the proposed cooler.

1.3 Research methodology

The research methodology employed to achieve the project objectives is as follows:

- **Literature review**

An overview of the evaporative cooling technologies is provided with particular focus on the indirect evaporative coolers (IEC) for a comprehensive understanding of major evaporative cooling methods employed for building cooling. Additionally, a detailed review of the sub wet-bulb temperature IEC systems is considered for the latest designs and configurations of different types of the IEC systems including the working principle, materials, performance, and efficiency of each system.

This approach would review the literature of the indirect evaporative coolers for building cooling applications, providing a classification of the main of the IEC systems and shedding the light on the latest innovations of the ICE systems and state-of-the-art designs in this domain. Therefore, the research gab and the innovation of this study would be highlighted and distinguished against other similar systems. Consequently, the core idea of the proposed system is defined, and the conceptual design of the cooler is clarified such as system construction, flow scheme, and heat pipes arrangement.

- **Thermal design and computer modelling to investigate performance parameters of the cooler.**

This objective was broken down into two main parts: i) Mathematical formulation of heat and mass transfer conservation laws were applied to model the evaporative cooling system. ii) The performance of the cooling system was then investigated by developing a computer model using MATLAB software.

- **Fabrication and testing of a small-scale unit of the heat pipe and ceramic tube based indirect evaporative cooler under various climate conditions and operating parameters.**

This objective involves construction and assembly of a laboratory-scale cooler and testing under controlled climatic and operational conditions. This allowed:

  - Generate experimental database of the cooler (Cooling capacity, air flow temperature profiles, effectiveness, etc.)
  - Validate the mathematical formulation which underpins the computer model.
  - Improve the accuracy of the computer model.

- **Assessment of the annual economic and the environmental impact of the cooler for an actual case study.**

A simple economic and environmental impact of the proposed evaporative cooler design was analysed to determine its feasibility. This includes determining the operation cost as well as carbon emission savings.

1.4 Novelty of the research

The proposed design of a sub-wet bulb temperature evaporative cooling system include the following;

- Integration of cylindrical ceramic materials, a stable construction material, as wet media for water evaporation with specific structure that allows water evaporation at controlled rate.
- Integrated heat pipe-ceramic tubes design for stand-alone indirect evaporative cooling
- Modular configuration.

This research work encompasses knowledge in materials science, heat and mass transfer as well skills in using laboratory testing instruments, data acquisition and analysis. It is a timely project that will contribute to advancing further development and understanding of efficient evaporative cooling systems and benefiting the wellbeing of building occupants and the environment.

1.5 Thesis Contents

The thesis is structured into 8 chapters:

Chapter 1 covers general background of the global energy consumption with focus on the energy demand of the households, particularly, power consumption of the cooling systems. This chapter also includes the research aims and objectives, the research methodology, and the novelty of the research.

Chapter 2 provides an overview of the most common evaporative cooling methods includes the theory, working principles, and the performance of each cooling system. Furthermore, indirect evaporative cooling system is considered for wider review as being the main domain of interest in this study.

Chapter 3 includes a review of the indirect evaporative coolers with a classification of the IEC systems is provided. Additionally, in-depth review of sub wet-bulb temperature IEC system is conducted, covering theoretical and experimental work conducted, and analysing the performance parameters of current cooling systems in the field.

Chapter 4 is about the numerical modelling process of the proposed design, describes the governing heat and mass transfer equations and heat transfer limitations of the heat pipe. In this chapter, a computer model is developed to simulate the operation and the thermal performance of the proposed cooler.

Chapter 5 concerns the experimental work conducted on a laboratory-scale unit of the proposed cooling system. This chapter describes the cooler's components, fabrication process, experiment set-up, and test procedure that is supported by schematic diagrams or/and photos. Additionally, all the steps of conducting the tests and any special experimental requirements or modifications are presented in this section. Furthermore, preliminary experimental results are highlighted as well.

Chapter 6 analyses and discusses the results of the experiments and the predicted data. This chapter compares the numerical and experimental results and, thus, validation process is considered. Furthermore, a parametric study of the cooler thermal performance is conducted based on the developed computer model for further evaluation and optimisation of the system performance.

Chapter 7 presents a basic economic and environmental analysis of the proposed cooler. The operational costs are covered in the economic assessment, while the environmental evaluation covers the savings of electricity and carbon emissions of this cooler compared with a conventional vapour compression cooler for a real case study of Libyan house.

Chapter 8 concludes the research findings and highlights the main features of this new cooling system. In addition, it will provide recommendations and suggestions for any further work to be conducted. Besides, any limitations of the cooling systems would be stated.

Chapter 2: Overview of evaporative cooling technologies

2.1 Evaporative cooling cycle (EC)

Evaporating cooling (EC) is a process that utilises water evaporation for air cooling, in which heat and mass is exchanged between water and surrounding air. This causes the air temperature to decrease as it transfers sensible heat to water while water vapour is transferred in the opposite direction, increasing the air moisture content [9].

2.1.1. Classification of evaporative cooling systems

Based on the type of heat and mass transfer process between the water and the air, evaporative coolers can be divided into three main types, as shown in Fig 2-1. Accordingly, this overview of evaporative cooler is based on this classification. It includes the theory, working principles, and the effectiveness of each cooling system. After that, chapter three provides a detailed review of the indirect evaporative coolers as being the main area of interest [8].

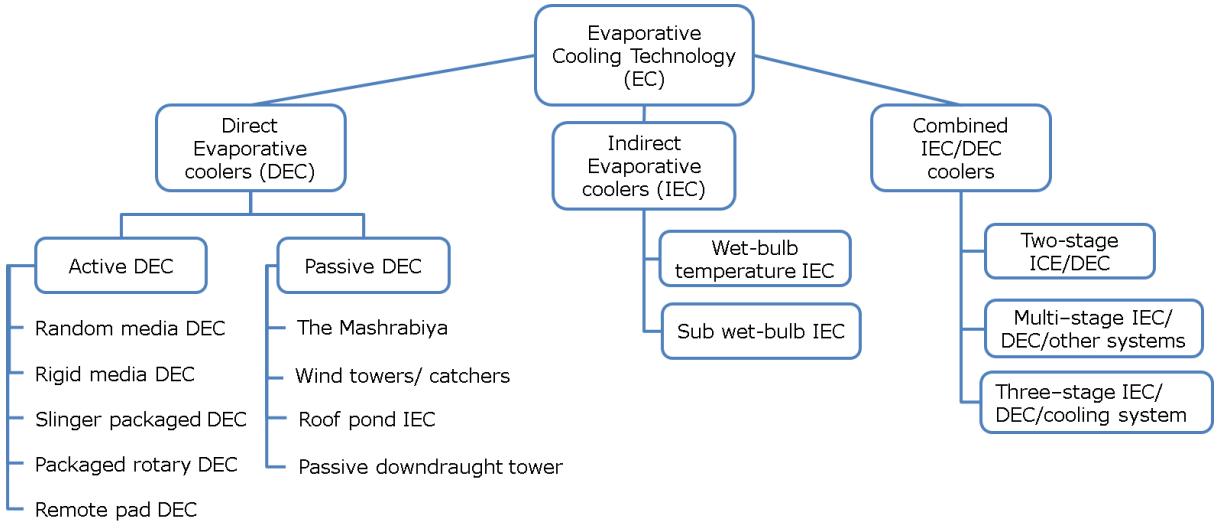


Fig 2-1 Classification of evaporative cooling systems

2.1.2. Applications

Evaporative coolers are existed primarily in several domestic, commercial and industrial cooling applications either as individual coolers or supplementary units of other cooling systems. It is used for air-conditioning for buildings, factories, cold stores, and agricultural greenhouses air-cooling. Furthermore, it is used industrially in cooling towers, evaporative condensers, humidification, and humidity control applications [10].

2.1.3. Advantages and disadvantages

Table 2-1 lists the main features and limitations of the evaporative cooling system, in general, by comparing with mechanical vapour compression cooling systems (MVC).

Table 2-1 Advantages and disadvantages of the evaporative coolers [11], [12], [13], and [14]

Advantages:	Disadvantages
High COP in the range of 5-20. Its COP increases as the ambient temperature rises, which is opposite of MVC cycle.	Accumulated indoor humidity issues (only for DECs) which cause corrosion and condensation risks inside buildings.
Environmentally friendly system uses water as refrigerant.	Discomfort and health issues associated with highly humid environment
Less initial and operation costs.	High humidity decrease the system efficiency.
Much less electricity demand, only for fan and pump. SO, reduce energy usage by around 70%.	Poor water quality could reduce the performance because of related deposits and scales problems (only for DECs).
Easy maintenance and repair comparing to MVC system.	Constant supply of water is needed.
Water consumption is partially offset by the reduction of electricity usage. EC systems consume as much water as conventional electricity-based air conditioners do	Cooling capacity is limited by the ambient wet-bulb temperature.

2.2 Direct evaporative cooling coolers (DEC)

The DEC systems are one of the oldest and simplest configuration used in buildings air-cooling applications. Ingenious techniques were used thousands of years ago by ancient civilisations with variety of configurations and ideas for indoor thermal comfort such as using earthenware porous jar water-contained, wind towers, wetted pads/canvas located in the passages of supply air [1].

In the process of the direct evaporative cooling, as the water comes in contact with the air heat and mass transfer occurs directly between the two working fluids. The water absorbs heat from air and evaporates, and simultaneously water vapour is carried away by the moving air to conditioned space. Consequently, the dry-bulb temperature (DBT) of the supply air decreases while its humidity increases, as shown in Fig 2-2.

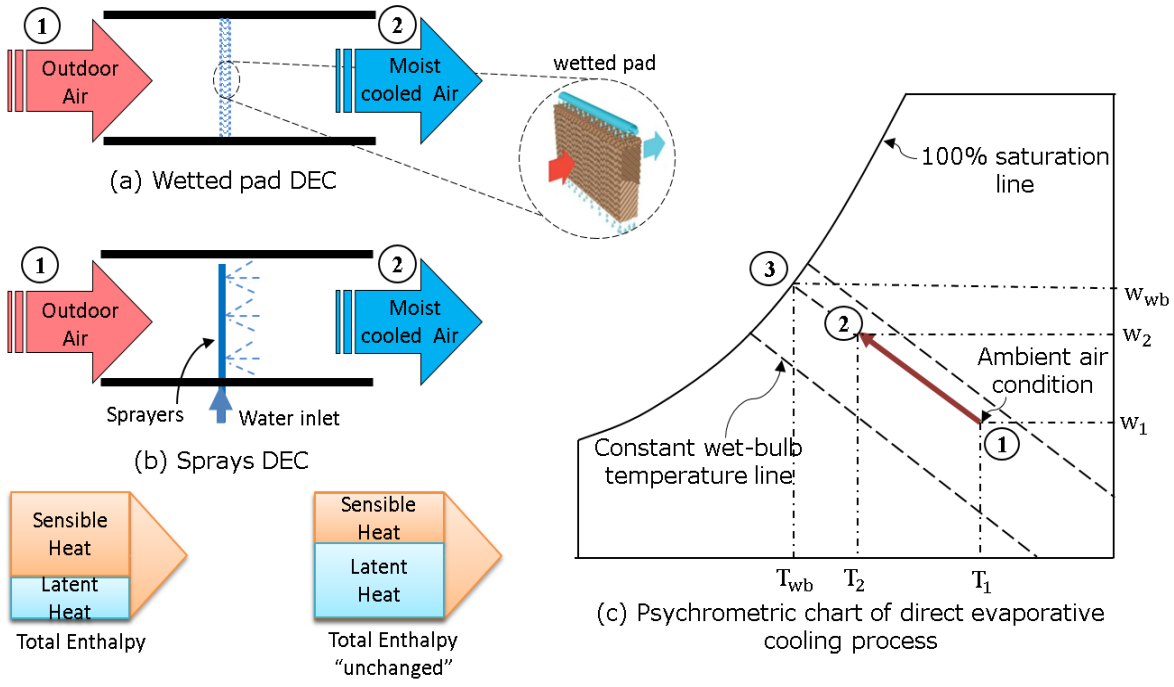


Fig 2-2 Working principle and psychrometric chart of a direct evaporative cooler [15]

During the operation, the hot inlet air (state 1) with high temperature T_1 and moisture content ω_1 is naturally flown or mechanically drawn through wet medium, as seen Fig 2-2 -a and –b. As the air contacts with water, its sensible heat continuously is absorbed by the water and then returned into the air in the form of latent heat of vaporisation. The supply air leaves the system (state 2) with lower temperature T_2 and higher moisture content ω_2 as illustrated on the psychrometric chart in Fig 2-2-c. Thus, the direct evaporative cooling is a constant enthalpy process (isenthalpic process) as shown by a displacement of line 1-2 along the constant wet bulb temperature line on the psychrometric chart.

Theoretically, the process can cool the supply air to 100% saturation i.e. reach (state 3) on the psychrometric chart. But, only 70%-80% of the wet-bulb temperature (WBT) of inlet air is reached due to several limitations. One of which is the WBT of inlet air barrier, that is, the DEC eventually would not be able to cool the inlet air lower than its WBT due to the air and circulated water will reach an equilibrium point equal to the WBT of the inlet air [10]. The other factors are shortness of contact time between the two fluids, and insufficient wettability of the evaporative pad [11]. Nevertheless, the DEC systems are able to provide a reasonable reduction of air dry-bulb temperature, but the high moisture content of the supply air is one of the disadvantages. Furthermore, the microbiological growth and other health hazards are other drawbacks of DEC systems in buildings air-cooling [12] and [16].

Regarding the energy consumption, it is in favour of the DEC system comparing with other conventional cooling cycles. In general, the evaporative coolers require low electricity consumption for operation as they employ fan and water pump only. Also, the direct evaporative coolers vary in terms of operational power consumption from zero power to low power-consuming systems. Accordingly, they can be classified into: Active DECs which are electrically-powered systems, and Passive DECs that are naturally operated systems with almost zero power input [17]. The classification and sub–grouping of the direct evaporative cooling systems is shown in Fig 2-1.

2.2.1. Active direct evaporative coolers (Active DECs)

Active direct evaporative coolers are electricity-driven DEC systems which require power for air and water circulation devices. Nevertheless, these cooling systems are considered to be much less power intensive than other traditional cooling systems such as mechanical vapour compression coolers, with energy saving up to 70% [1].

A typical configuration of an active DEC unit, as shown in Fig 2-3. It comprises of a metal or plastic box enclosure, evaporative media made from wettable materials, blower to circulate ambient air through the evaporative pads to the conditioned space, water tank to collect the falling water, a pump and water distribution system. Alternatively, tiny nozzles can be used, instead of using wetted pads, to create fine sprays of water inside the air streams as presented in Fig 2-2-b [39]. The wet-bulb effectiveness is also called "saturation efficiency" can reach ranges of 0.70-0.95 in the current commercial DEC. It is mainly function of the type and thickness of the evaporative pad, ambient conditions, and inlet air flow rate [11].

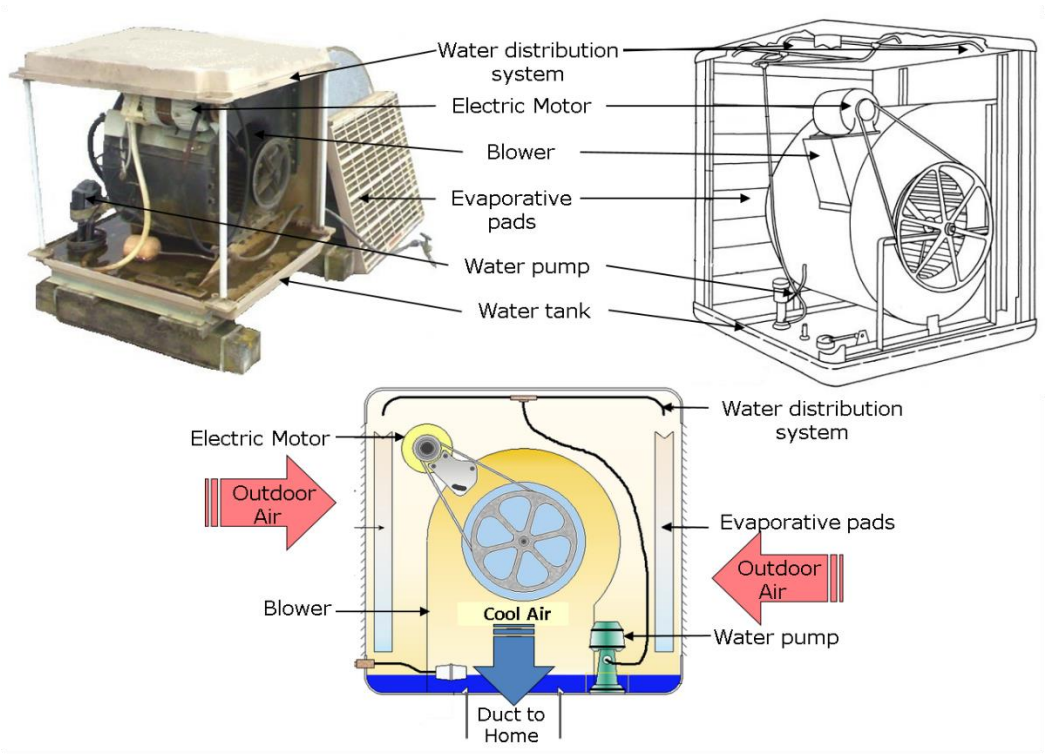


Fig 2-3 Basic structure and main components of drip-type DEC unit (Reproduced from [18] and [19]).

Active direct evaporative coolers are available in variety of configurations for the purpose of increasing the efficiencies and reducing the costs. Based on the type of water distribution system used, the main types of active DEC can be classified into: spray (also called air washer), slinger (a rotating wheel), and drip (Misting) system [15]. Nevertheless, According to ASHRAE Handbook-HVAC Systems and Equipment, active DEC are divided based on the wet medium type into: Random media DEC, Rigid media DEC, and Remote media DEC [10]. Details and characteristics of each type of the DEC systems are beyond the scope of this research. However, Table 2-2 summarises the main features of each type of active DEC systems. Also, Fig 2-4 illustrates schematics of different types of pads and configurations of the DEC systems.

Table 2-2 Typical types of active direct evaporative coolers [10], [20]

system type	Configuration	Medium material	Wet-bulb effectiveness
Random media Fig 2-4-a	Water is pumped from water tank to water distribution system over pads, while fan draws outside air throughout pads into the conditioned space.	Aspen; Plastic fibre; Foam that is fitted and supported by plastic or metallic frame Usually thickness of 50mm	≈0.80
Rigid media Fig 2-4-b	Similar in configuration and operation to Random pad DECs, but it uses stack of cross-corrugated pad which last for longer than Random pads but more expensive.	Sheets of corrugated materials; Cellulose, plastic (Cardboard box/Kraft paper); Fibreglass Pad thickness of 300mm	0.75-0.95
Remote pad Fig 2-4-c	Pads mounted on wall or roof of a building, Water distribution lines sprays water to wet the pads, fan blows the air through the pads to conditioned space. Applied in greenhouses and animals corrals.	Standard random media or Rigid media	0.70-0.95
Slinger packaged Fig 2-4-d	Motor-driven water slinger sprays water on the pads. A fan draws outside air through the wetted pads to conditioned space. Additional power consumption	Latex coated fibre; Fibreglass; Coated nonferrous metal	< 0.80
Rotary packaged Fig 2-4-e	Motor-driven rotary pad through a water trough. A fan draws outside air through the rotary pad to conditioned space. Additional power consumption. No water recirculating system.	Wheel shaped medium made from latex coated fibre; Fibreglass; Rough polyester material; Coated nonferrous metal	0.50
Drip type Fig 2-4-f	Water is pumped from water tank to water distribution lines over the pads, water droplets fall down by gravity effect on the pads, while a blower draws the air throughout the pads to the conditioned space.	Stacks of corrugated materials; Cellulose, plastic; Fibreglass Pad thickness of 300mm	0.70-0.95

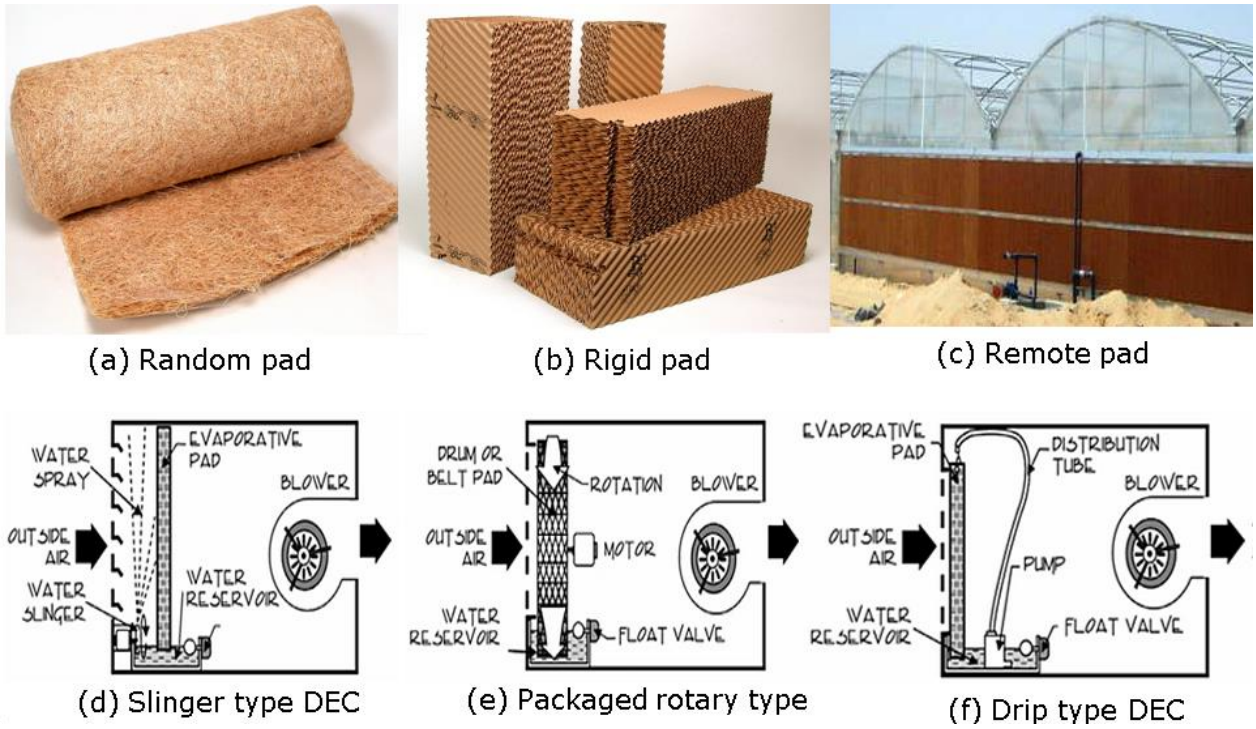


Fig 2-4 Types of DEC systems [21], [10]

2.2.2. Passive direct evaporative coolers (Passive DECs)

Passive DEC systems are one of passive air-cooling techniques which exploit one of natural phenomena, energies, heat sinks, and/or climatic characteristics for air-cooling purposes without the need of electricity to operate the system. Having said that, fan and pump might be used in some designs. Namely, hybrid coolers can be classified under passive cooling systems. Passive architecture cooling systems employ several methods for buildings cooling by solar and heat protection techniques, heat amortization techniques, and heat dissipation techniques. Accordingly, passive cooling systems can be classified in to ventilation cooling, evaporative cooling, radiative cooling, and earth cooling [1], [22]. In this overview, the focus would be on passive evaporative cooling systems rather than other cooling techniques. The passive direct evaporative cooling is divided into direct passive DEC and indirect passive DEC, as shown in Fig 2-5. Main types of building-integrated passive evaporative cooling systems are as follows:

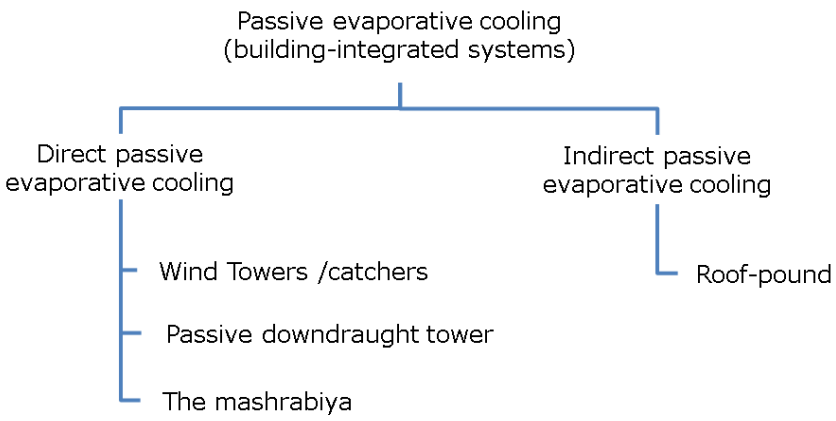


Fig 2-5 Main types of passive cooling systems [1], [22]

(i) Wind Towers

Wind towers, also called wind catchers are a traditional, building-integrated passive air-conditioning system for cooling and ventilation dwellings. This zero power-consuming cooling system built hundreds of years ago in Arabian countries and Iran, some traditional wind tower are still existed till now from the old architectural buildings in MENA region known as 'Burj al Hawaa' i.e. the air tower, as shown in Fig 2-6-a. It exploits the advantage of building geometry, features of local winds, and natural means of water evaporation to provide natural ventilation and/or evaporative cooling of the house. Basic shape of a wind tower and working principles is illustrated Figure Fig 2-6-b, that is, a capped tower with one- or multi-face openings at the top of the tower which is placed on the roof of a dwelling with an average height of 15 m to be away from sand storms and for harvesting greater wind velocities. Wind towers/catchers are divided according to air flow patterns inside the tower into two main types: downward airflow towers and upward airflow towers [1].

(ii) Passive down draught tower (PDEC)

It is also called downward airflow wind catcher which is driven by pressure difference between windward side and leeward sides of the tower. In this configuration, the tower opening faces wind direction, so the ambient air enter at top of the tower and flow down through it into the

building space providing fresh cold air, as shown in Fig 2-6-b. Water distribution system can be integrated into the tower geometry by several means i.e. water pool at bottom of the tower, porous jars filled with water located in the tower airstream (Fig 2-6-c), wetted pads located at the top of the tower (Fig 2-6-b). Thereby, the outside air is cooled and humidified before entering into the indoors.

(iii) Passive upward wind tower

Upward airflow wind tower is driven by temperature difference between building interior and the outside environment. In this system, the tower ports faces away from the wind direction, thus the air is drawn upwards via wind tower. Owing to positive pressure on one sides of the building the hot air is drawn through underground channels, or via courtyard or water fountains before entering into the building as cold air, whereas the hot and stagnant indoor air rises upward via the openings of the wind catcher. Fig 2-6-d illustrates schematically upward wind tower in conjunction with underground cooling passages [23], and [24].

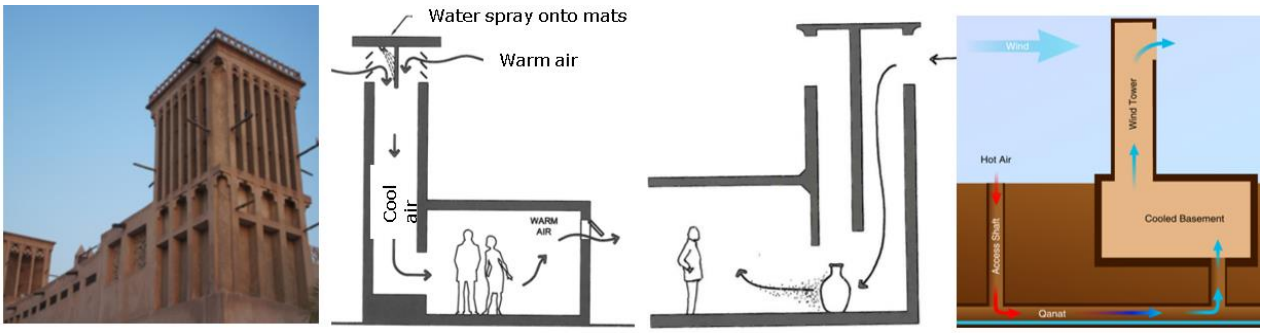
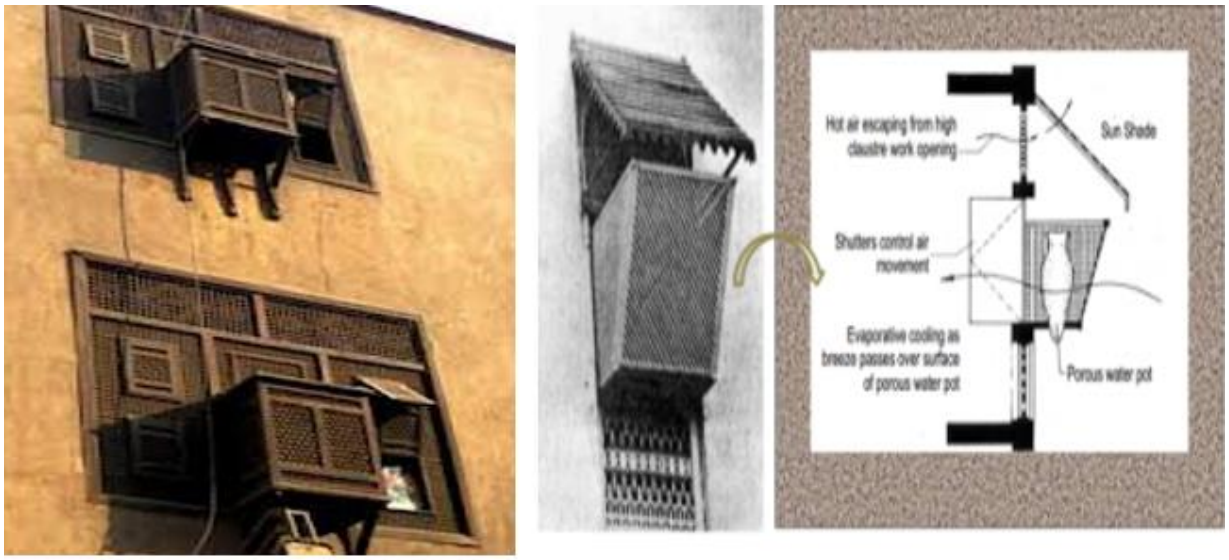


Fig 2-6 Basic structure of wind tower integrated with evaporative systems [1], [25]

(iv) The Mashrabiya

It is considered as one of forms of passive wind-catching techniques. The Mashrabiya is a traditional Islamic architecture element used for natural ventilation and cooling of dwellings without any electricity usage. It is wooden screens/windows provide shad and protection from

the sun, as shown in Fig 2-7-a, which allows breezes to flow through into the house for cooling purpose. Fig 2-7-b shows a Mashrabiya coupled with water-filled porous jars to provide cooling effect of the indoor spaces and cools the drinking water inside the jugs [23].



(a) The mashrabiya of a dwelling (b) Mashrabiya with porous water-jugs for cooling

Fig 2-7 The Mashrabiya [23]

(v) Roof-pond

Roof pond is a building-integrated passive indirect evaporative cooling system i.e. there is no contact between the indoor air and water. This system can highly contribute to mitigate heat by cooling the roof passively. Therefore, the indoor air is cooled without increasing its moisture content, and buildings heat gain is reduced during daytime. Though, circulation fans and pump might be required depending on the design of the system. A typical roof pond consists of water pool in plastic or fibre-glass container stored on top of the roof of the building and water circulation system. A basic configuration of a shaded roof-pond cooling system is shown in Fig 2-8-a. In operation, during summer the ambient air flows over the pond causing the water to evaporate, thus cooling the pond and the roof structure which act as a heat sink of the interior of the building and indoor air. During winter, the pond is emptied and the shad openings are closed. Additionally the pond can be covered by a removable cover, a fixed cover,

or a fixed floating insulation (Fig 2-8-b). Also, roof-pond cooling systems might be incorporated with water spraying system to enhance the evaporative cooling process [1].

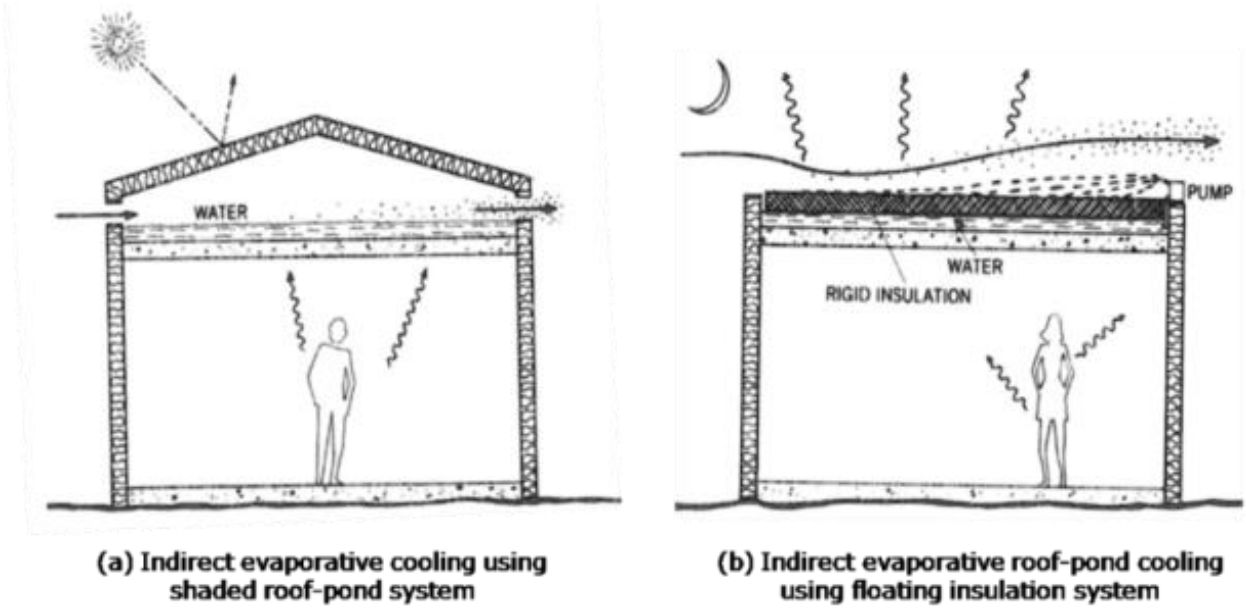


Fig 2-8 Roof-pond cooling systems [1]

2.3 Indirect evaporative coolers (IECs)

This is the second type of the evaporative cooling systems, their primary idea is to decrease air temperature without changing its vapour content by employing heat exchanger. A basic IEC unit comprises of metallic case contains other components, heat exchanger, fan, pump, water tank, and water distribution system, as illustrated schematically in Fig 2-9 [8].

IEC system incorporates heat and mass exchanger (HMX) in which the working fluids are separated by highly conductive plate/wall. Several types and configurations of HMX are used for IECs, such as plate-fin HMX, plate-type HMX, tube-fin HMX, tubular-type HMX, and HPHX. The indirect evaporative coolers can be classified based on their cooling range of the supply air, whether above or below the WBT of the inlet air. Thus, IEC systems are divided into; Wet-bulb temperature IEC systems (WBT-IEC), and Sub wet-bulb temperature ICE systems (Sub WBT-IEC) [13], [26].

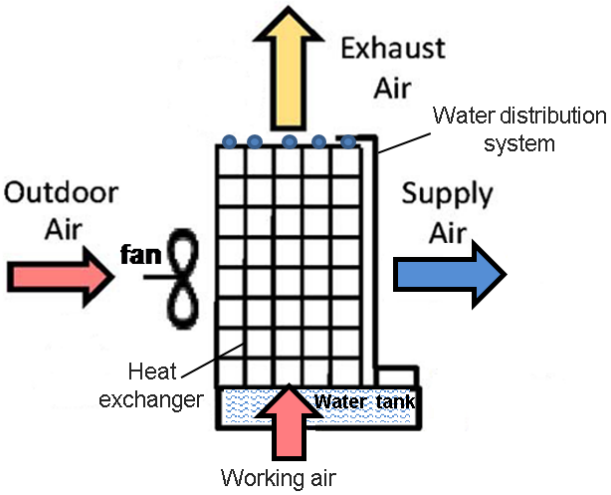


Fig 2-9 Basic IEC system structure [13]

2.3.1. Wet-bulb temperature IEC systems (WBT-IEC systems)

In the WBT indirect evaporative coolers, the main element is a wet surface, air-to-air heat exchanger in which two individual air streams flow throughout two adjacent channels i.e. the wet- and dry-air passages, as shown in Fig 2-10-a. The inlet air, also called the outdoor/ intake air, is cooled via sensible heat transfer to the working air with the aid of water evaporation in the wet-air passages, in where the moisture (latent heat of the vaporised water) is carried away by the working air stream. The cooled air leaves the IEC unit with a temperature close to WBT of the inlet air but not below it [10]. Fig 2-10-b illustrate schematics of the most common HMX employed of a cross-flow flat-plate-stack exchanger based WBT-IEC.

The heat and mass transfer process of wet-bulb IEC is illustrated on the psychrometric chart in Fig 2-10-c. The wet-air channel absorbs heat from the dry-air channel and cools the inlet air by sensible heat transfer in the dry-air passage (process 1-2), while the wet-air stream involves water vaporisation and latent heat transfer between the working air and water film (process 1-3). As a result, the inlet air (state 1) is cooled at constant moisture content toward the WBT of the inlet air (state 2), whereas the working air is gradually saturated and its temperature is decreased (state 2'), and, then, heated again along the 100% saturation line till it is discharged to the atmosphere (state 3) [27].

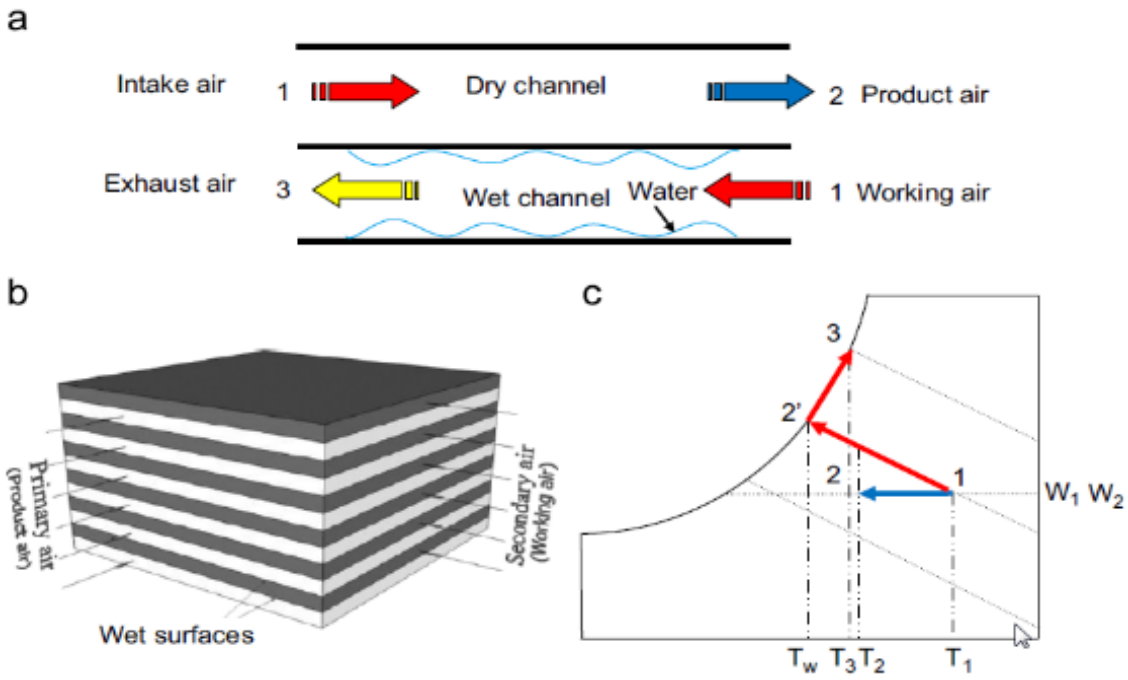


Fig 2-10 Working principle and psychrometric chart of wet-bulb IEC [8]

Despite the fact that the WBT-IEC systems cool the air without any additional moisture to the supply air, the WB effectiveness of the systems is lower than that of the DEC systems, it ranges from 0.40 to 0.80 .The efficiency of these systems is limited by WBT of the inlet air; there has been a considerable amount of research of new designs of WBT indirect exchangers to enhance their efficiency and cool down the supply air temperature below the wet-bulb temperature of the inlet air. Therefore, different types of WBT IEC are developed [8]:

i. Plate-type HMX based wet-bulb IEC (Plate-type WBT-IEC systems).

This is the most used heat exchanger in the WBT-IEC systems i.e. the flat-plate-stack HMX with cross- or counter-flow arrangement. The WB effectiveness is usually in the range of 0.60-0.80. Fig 2-11-a illustrates basic structure of the plate-type wet-bulb temperature IEC system.

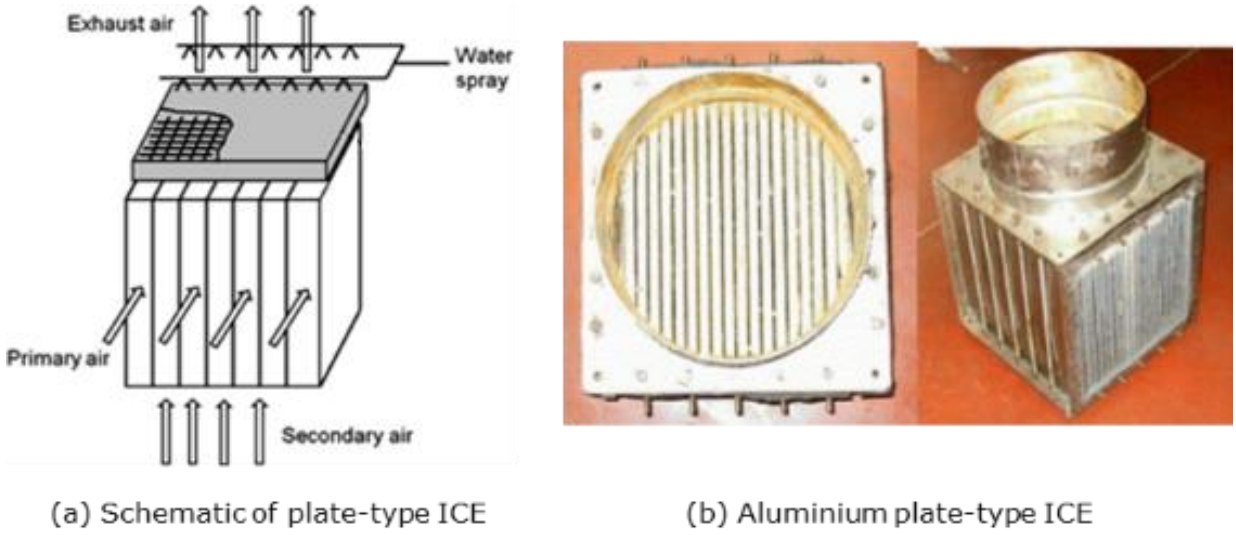


Fig 2-11 Schematic of plate-type IEC system [8], [28]

Several research works conducted on this type of WBT-IEC exchangers. Pescod [29] introduced a simple mathematical design of a plastic, cross-flow, plate-type heat exchanger of wet-bulb IEC for performance evaluation. It was found that the cooler performs effectively in temperate and dry climate and offers good energy savings. However, the cooler's output was not completely satisfactory for hot and humid climate. Martínez et al. [28] fabricated a cross-flow flat-plate-stack HMX of WBT-IEC, as shown in Fig 2-11-b. It consists of 25 aluminium flat sheets, packed and welded together to form pairs of wet and dry adjacent channels. The effectiveness ranged 0.50-0.60. Additionally, a theoretical and experimental investigation of the performance of flat-plate based WBT-IEC unit using a one-dimensional mathematical simulation carried out by [30]. The experimental results were lower than that of the predicted data, possibly, due to poor wettability of the wick material. Equally, Stoitchkov and Dimitrov [31] developed a short-cut and improved method for evaluating the effectiveness based on the numerical model of Maclaine-cross and Banks [30]. Theoretical and experimental findings were found to be satisfactory due to fewer assumptions were made. Also, it found that the effectiveness only was in the range of 0.50–0.60. Furthermore, a simplified heat and mass transfer mathematical model for performance investigation was developed by Alonso et al. [32]. The model can be applied for cross-flow plate-type HMX with different operating

conditions and flow patterns. Further advanced and accurate model was developed by Guo and Zhao [33] for theoretical analysis of the cross-flow plate-type HMX of an indirect evaporative cooler, the investigation covered the effects of channels dimensions, humidity ratio of the inlet working air, inlet and working air velocities, and wettability effect on the thermal performance of the IEC system. It was found that higher effectiveness is at a smaller channel width, lower inlet humidity ratio of the working air, and higher plate wettability. Additionally, Kettleborough and Hsieh [34] conducted similar theoretical analysis but on a counter-flow plate-type HMX.

ii. Tubular-type HMX based wet-bulb IEC (Tubular-type WBT-IEC systems).

This heat exchanger is usually constructed from circular tubes, however, other tubular shapes have been used such as elliptical and rectangular tubes [35]. The common configuration is shell-and-tube heat exchanger which consists of a bundle of round tubes mounted in a cylindrical or rectangular shell. Fig 2-12 illustrates a WBT-IEC system based on tubular HMX in which the inlet air flows inside the tubes and the working air flows across or along the external surface of tubes in the perpendicular direction to the inlet air, while the water is sprayed over the outer surface of the tubes. This configuration of WBT-IEC offers more uniform water film over the tubes and less pressure losses comparing with the plate-type HMX. Additionally, the tubular-type HMX based IEC system can be made from variety of material depending on the required heat transfer rates, thermal conductivity, and costs involved, the tubes are made of either polymer, metal, porous ceramic, PVC, or aluminium [8].

Another common type of tubular HMX is finned-tube HMX [36], [37] in which circular tubes are fitted with external fins to form bundle of tubes hosted in tubular or rectangular metal casing . For example, Velasco Gomez et al. [36] introduced tube-fin HMX based WBT-IEC is shown in Fig 2-13. In this configuration, porous ceramic tubes fitted with metal fins forming two independent air streams separated by ceramic material. The inlet air is cooled as it flows over the external surface of the ceramic tubes which retain sprayed water to aid heat transfer process between the inlet and working air streams that is the return air from the conditioned

space passing inside the porous tubes in the opposite direction of water flow. The experimental results showed that the effectiveness reached 0.60 [38].

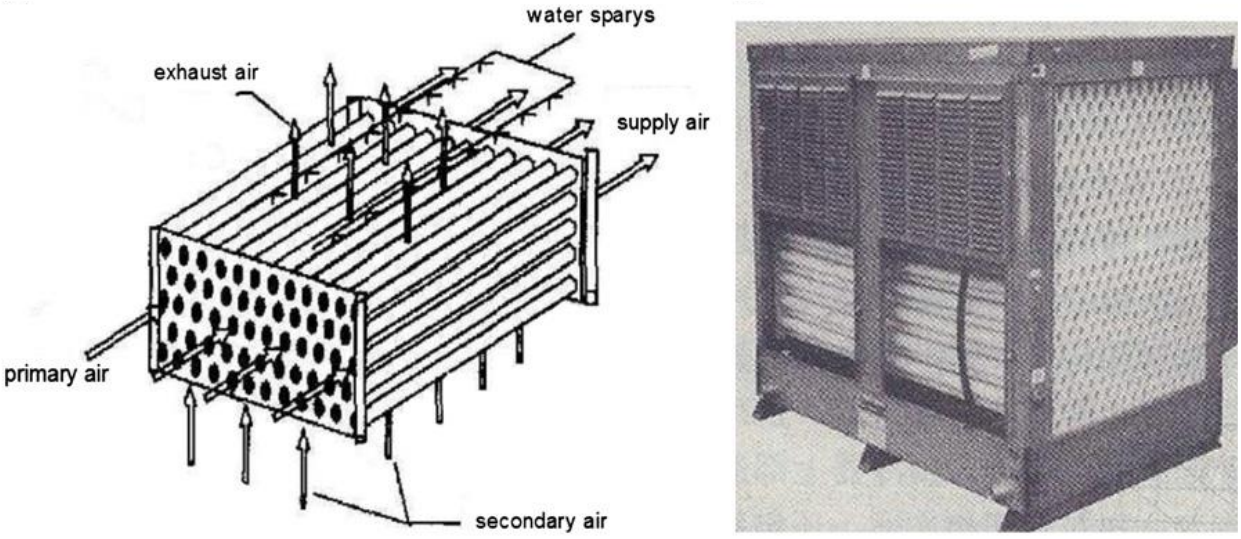


Fig 2-12 Tubular heat exchanger based IEC [8]

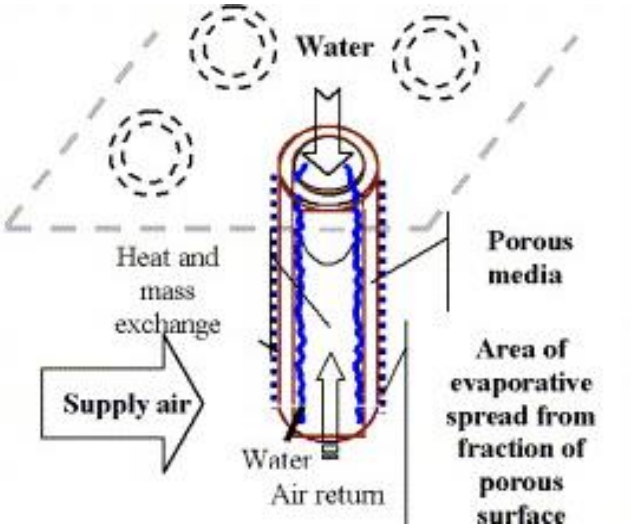


Fig 2-13 Finned ceramic tube indirect evaporative cooler [38].

iii. Heat pipe HMX based WBT-IEC (HPHX WBT-IEC systems)

Heat pipe is a light, simple, reliable, and highly conductive heat transfer element available in different types, configurations, and sizes. Also, they can be applied effectively to transport heat between two passages. In the literature, various researches conducted on heat pipes

applications for building air-conditioning including HVAC systems [39], [40], [41], and [42]; heat recovery systems [43], [44], [45], [46] and [47]; and dehumidification enhancement in air-conditioning systems [48], [49]. But, a few studies have been found on the heat pipe heat exchangers (HPHXs) in the indirect evaporative coolers for buildings air-cooling. for example, Riffat and Zhu [50] developed a mathematical model for building-integrated HPHX based IEC system. The cooling system consists of heat pipes located horizontally cross two individual air streams channels, the evaporator of the heat pipe is placed in the indoor air passage. While, the condenser of the heat pipes are embedded in ceramic containers where the ambient air stream flows over it, the porous water-filled container is to guarantee even water distribution around the condenser. Also, the evaporator is finned to increase convective heat transfer between the heat pipe fins and surrounding indoor air. Fig 2-14-a shows a schematic drawing of one unit of this system. The findings showed that higher cooling capacities can be achieved under dry and windy weather conditions, but for high effectiveness the inlet air velocity must be kept around 0.60 m/s. In another study, Riffat and Zhu [51] experimentally investigated the effects of various parameters of the ceramic container on the performance of a HPHX based IEC such as porosity, wall thickness, and outside diameter. The cooler comprises of a bundle of heat pipes located horizontally across two adjacent air passages, the condensers are embedded in ceramic containers acting as heat sink of the exchanger, while the evaporators are finned in the hot air side. The experimental results revealed that the performance decreases as the container wall thickness increases and when the porosity of the ceramic is reduced. Similarly, Huang et al. [52] and Wang et al. [53] used the same configuration proposed by [50] except of the condenser surface is wrapped with a thin layer of water-absorbent material, and water sprayers are used on the condenser, as shown in Fig 2-14-b. It was found the WB effectiveness was 0.70 [52].

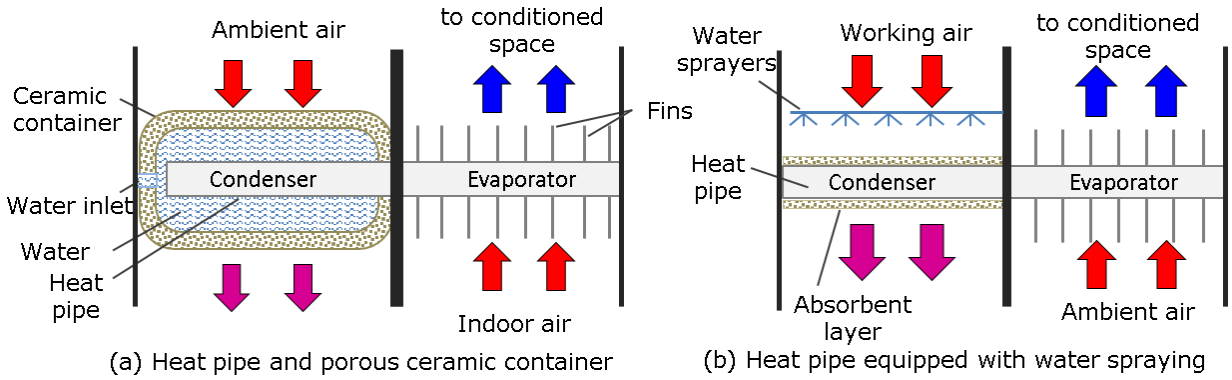


Fig 2-14 Schematic of two configurations of Heat pipe based IEC system [50], [52]

Also, Wang [54] carried out theoretical and experimental investigation of two different heat removal mechanisms from the heat pipe condenser of a HPHX based IEC. One method employs water spraying system directly on the condensers and the ambient air flow through it, while the other technique uses DEC unit before the IEC to pre-cool the ambient air before passing over the condensers. It was found that the cooling efficiency improve by 5% compared with that of conventional heat pipe exchanger. Equally, under the same operational conditions the supply air temperature supplied by the latter method was slightly lower than that of the former.

In another review study [11] reported work by Zheng et al. [55] (available in Chinese only) used four different heat removal techniques for two-stage IDEC system which comprises of HPHX based WBT-IEC as first stage followed by DEC system. The experimentally investigated configurations of the IEC system principally consisted of two air adjacent channels with unmixed air streams, and heat pipes are horizontally positioned across both passages, with four different heat dissipation methods of the condenser side as follows; i) the outdoor air is used for cooling the condenser; ii) an air washer is employed to pre-cool the outdoor air before passing over the condenser; iii) a DEC unit is used to pre-cool the ambient air before entering the HPHX and flowing over the condenser; iv) water spring system is employed to provide fine water droplets over the condenser surface while the outdoor air flows over the condenser;

According to the experimental results, the last heat removal mechanism was the best with higher effectiveness than other configurations of 7-16 %.

2.3.2. Sub wet-bulb temperature IEC systems (Sub WBT-IEC)

This type of IEC systems are known for their ability to cool down the air below the wet-bulb temperature of the inlet air. Valeriy Maisotsenko [56] introduced a new flow configuration of the IEC to overcome some of the disadvantages of DECs and enhance the low effectiveness of the WBT-IEC systems. The Maisotsenko-cycle based IEC, or simply the M-IEC, is a combined design of plate-type heat exchange and evaporative cooling in which the working air is precooled before passing through the wet-air channel, resulting in the supply air temperature to be lower than wet-bulb temperature and approaches dew point temperature of the inlet air. Thus, this type of IEC is also called dew point IEC or sub WBT-IEC [57]. In addition, as the sub wet-bulb indirect evaporative cooling systems are the main area of interest of this research, thereby, it would be broadly reviewed in details in chapter 3. Nonetheless, the following is a brief description of the working principles and concept of this type of IEC system.

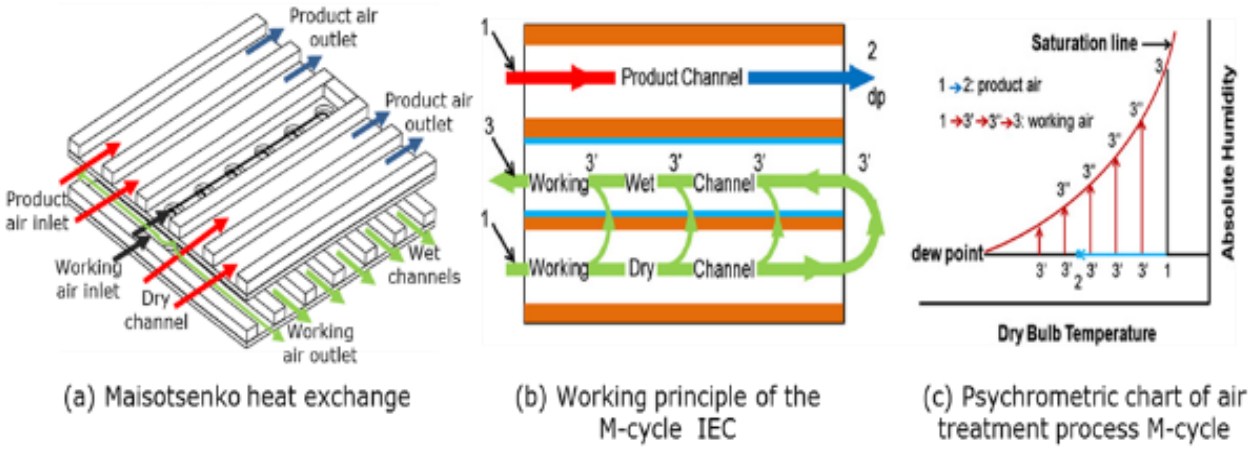


Fig 2-15 Structure and working principle of M-cycle HMX based IEC

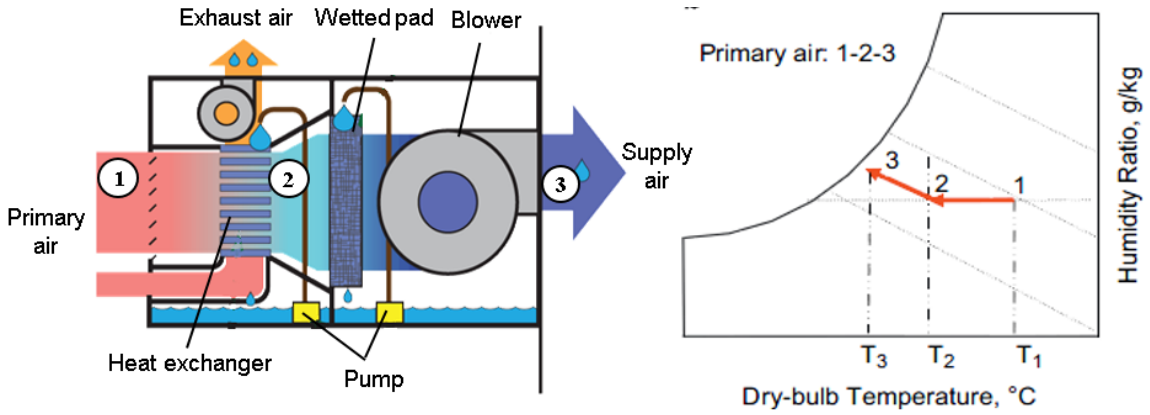
A basic configuration of the M-IEC system, is mainly comprises of a plate-type heat exchanger, as shown in Fig 2-15-a, in which flat-sheets are stacked together and separated by channel guides to form alternating wet- and dry-air channels with cross-flow arrangement. The dry side of the sheets have numerous holes distributed regularly to allow some of the working air to pass through into the wet channel, the dry side of each sheet is sealed to avoid water penetration.

The working principle of this IEC system is presented in Fig 2-15-b. The inlet air is brought into dry channels (state 1) and is cooled down along the dry-air passage due to temperature difference between wet- and dry-air channels. At some point, part of the cooled inlet air is branched into the wet-air passage when passing across the perforated holes (state 3') to become the working air (the secondary air). In the wet channels, the pre-cooled working air flows in perpendicular direction to the inlet air absorbing sensible heat from dry side air and carrying away water vapour from the wet-air channels. As a result, the inlet air is cooled down along its flow paths to a (state 2) below its wet bulb temperature (WBT). Meanwhile, the working air is gradually warming and saturated up (state 3', 3'') on the psychrometric chart in Fig 2-15-c along its flow paths till to be rejected to the surroundings (state 3). It was found the WB effectiveness is in the range of 1.10-1.22 and dew point effectiveness is between 0.55 and 0.85 depending on the inlet air conditions and the system channels dimensions [27].

2.4 Combined indirect-direct evaporative coolers (IDEC)

Since the DEC systems have higher effectiveness but humidity increases indoors, while the IEC systems have lower effectiveness and humidity is almost unchanged, therefore, a combination of both systems together or one of them (IEC or DEC) in conjunction with other cooling cycle might be a favourable choice to achieve the best characteristics from both systems, such as cooling supply air at a constant moisture content, higher system effectiveness. However, the high initial cost and system complexity are obvious drawbacks of the IDEC systems.

The basic structure of the IDEC system is schematically shown in Fig 2-16-a; the main components are heat exchanger of IEC unit, evaporative pads of DEC unit, water recirculation system, water reservoir, and blowers. In operation, as illustrated on psychrometric chart in Fig 2-16-b, the first stage is the IEC unit cools the inlet air without adding moisture (state 1-2), and, then, the DEC stage in which the air flow through the wetted pads for further cooling of the air with moisture being added to the supply air (state 2-3). The effectiveness of these systems is in the range of 1-1.15. Commercially, the IDEC systems are usually coupled with conventional direct-expansion cooling unit to meet variable cooling loads especially in hot and humid climate [58].



(a) Basic structure (b) Psychometric process

Fig 2-16 Schematic of Two-stage IDEC system [13]

The IDEC systems are divided into three main groups as shown in Fig 2-1. The following is a brief explanation of the system configuration, the operational mode, and the main characteristics of each type of the IDEC systems.

Two-stage IDEC: the IDEC comprises of IEC unit followed by DEC system, as illustrated in Fig 2-16-a. The first stage of the IEC (state1) cools the outdoor air, then flows through the DEC (state 2) for further cooling to below the inlet air wet-bulb temperature, but with additional moisture added (state 3). The air cooling process is illustrated on the psychrometric chart Fig 2-16-b. The effectiveness is in the range of 0.90–1.20, the coefficient of performance (COP)

is about 14, and the power saving up to 60% in comparison with MVC systems. But, water consumption increases by 55% [58], [59]. Other configuration of the two-stage IDEC reported by [60], [61] achieved WB effectiveness of 1.09-1.16.

Three-stage IDEC: these systems, generally, consist of the two-stage IDEC integrated with another cooling system. For example, a solid desiccant dehumidification with an IEC and/or DEC unit is common with COP up to 20 [62], [63] and [64]. In operation, as illustrated in Fig 2-18-a, the ambient air is dried and slightly heated up (state 1-2) as it is brought over the desiccant wheel, then flow through heat exchanger transferring heat to the regeneration air (state3), after that the supply air flow through the IEC stage where it is cooled by sensible heat transfer with the working air stream. Depending on required indoor conditions, the inlet air might be further cooled through a DEC unit (Fig 2-18-b) before it is supplied into the conditioned space. Moreover, several configurations have been reported; An IDEC system coupled with cooling coil [65], [66]. For example, the IDEC integrated with a desiccant system for dehumidification, as shown Fig 2-18-b, can offer energy saving of 54%-82% over the conventional cooler [63].

Multi-stage IDEC: hybrid systems of the two-stage IDEC with more than one cooling cycle. For instance, combined system of the two-stage IDEC coupled nocturnal radiative cooler and cooling coil is presented in Fig 2-19. In operation, during the night time in summer, the temperature of water from the panels decrease because of radiative heat transfer between panels and night sky, this water is stored in a storage tank. In the next day, the stored cold water is used as coolant fluid for the coil unit. The hot outdoor air passes through the cooling coil unit to be cooled down and, then, is cooled further through the two stage IDEC unit. This system has higher effectiveness than the two-stage IDEC, and the energy saving is between 75 and 79% compared to MVC systems [67].

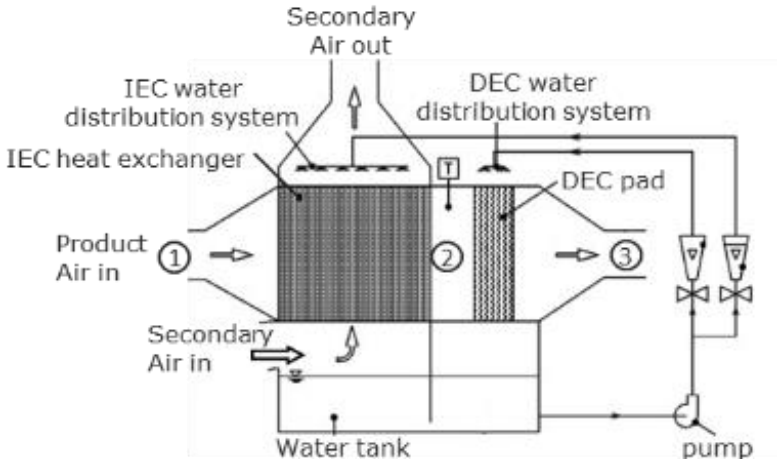


Fig 2-17 Two-stage IDEC system [58]

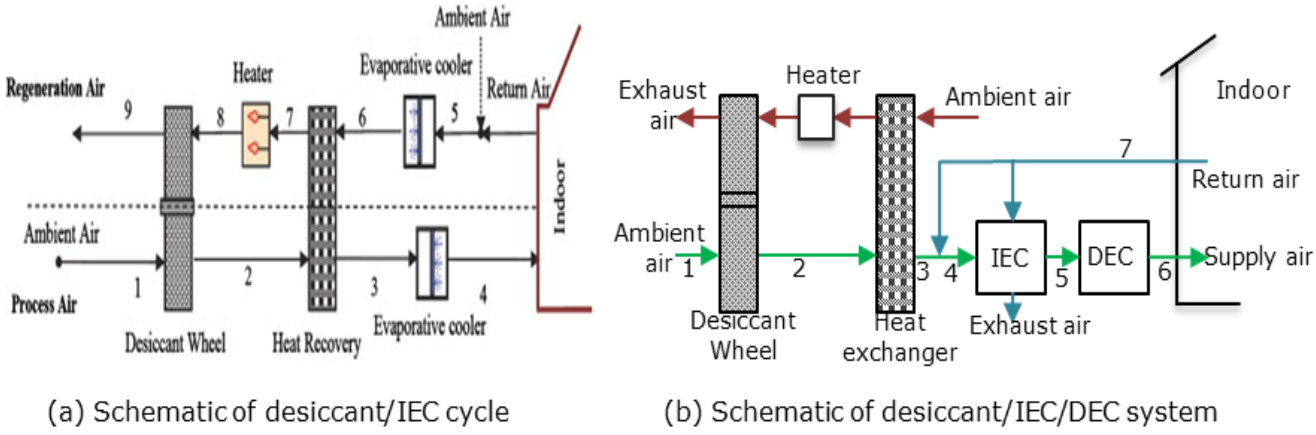


Fig 2-18 Schematics of solid desiccant/evaporative cooling systems [63], [8]

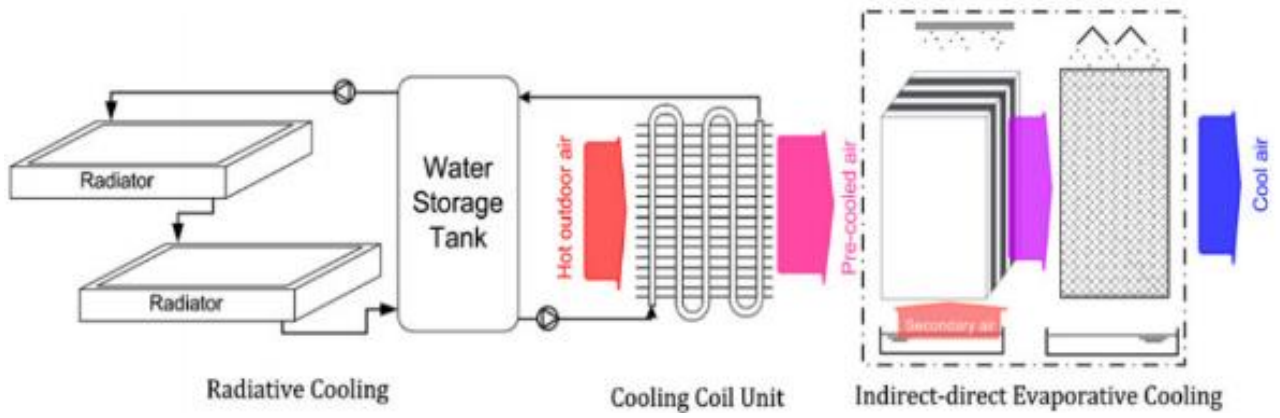


Fig 2-19 Multi-stage IDEC: radiative cooling, cooling coil and two-stage IDEC [67]

2.5 Summary

This chapter provided an overview of evaporative cooling systems, covering the classification, the working principles, and the concept of each system. In addition, a review was carried out of the indirect evaporative coolers (IEC) for buildings air-cooling with particular focus on the WBT-IEC, whereas the sub WBT-IEC would be subject of profound review in the next chapter.

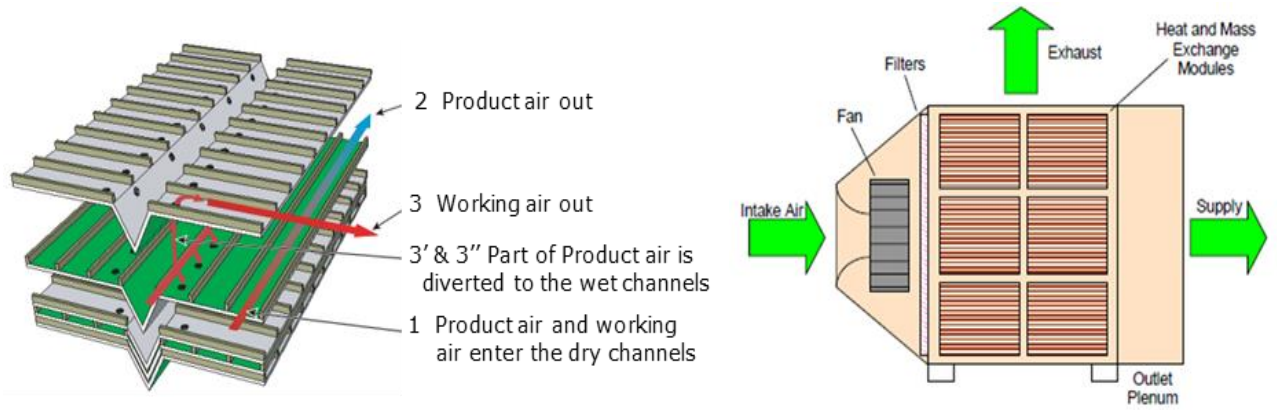
Direct evaporative coolers have high effectiveness, but the uncontrolled indoor humidity levels limit their applications for indoor air-conditioning. In contrast, indirect evaporative coolers showed acceptable and improving values of cooling effectiveness without any additional moisture added to the supply air streams, particularly after the breakthrough brought by the M-cycle configuration of the IEC system. Whereas, the combined IDEC systems have higher values of performance but their system complexity and high initial costs are the major restrictions for wide acceptance.

Indirect evaporative coolers can be divided into WBT-IEC and sub WBT-IEC systems based on their performance i.e. breaking of the WB temperature limit. The WBT coolers are featured with two individual and unmixed airstreams with WB effectiveness ranging from 0.40 to 0.80 i.e. below the unity. These systems are available in different configurations such as plate-type, tubular-type and heat pipe type HMX based IEC systems. Whereas, the sub WBT-IEC systems use part of the cooled inlet air as working air in the wet-air channels, therefore, it possible to cool down the inlet air below its WBT. Yet, several studies carried out to improve the design of the M-IEC system and investigate the possible methods of enhancing the performance and reduce power and water consumption. The following chapter will be dedicated for a detailed review of the sub WBT-IEC systems.

Chapter 3: Review of sub wet-bulb temperature indirect evaporative coolers

3.1 Sub wet-bulb temperature coolers (sub WBT-IEC systems)

To overcome low effectiveness and other disadvantages of wet-bulb temperature IEC systems, a breakthrough in the indirect evaporative cooling technology known as the M-cycle (Maisotsenko cycle) was introduced as early as 1977 by Maisotsenko [68]. Maisotsenko et al. [56] developed the M-cycle based indirect evaporative cooling system. The configuration consists of a cross-flow, multi-perforated flat-plate HMX in which a fraction of supply air, i.e. the cooled inlet air, is used as the working air. Thus, this cooling cycle is able to cool the inlet air below WBT of the inlet air and close to its dew point temperature. Therefore, this configuration would be able to achieve higher effectiveness and COP than WBT-IEC systems. From modelling results, it was reported that the wet-bulb effectiveness for M-cycle systems range from 1.10-1.22, and a dew-point effectiveness of 0.55-0.85. Nevertheless, Elberling (2006) [57] experimentally tested and assessed the performance of Coolerado Cooler which is a cross-flow, M-cycle based IEC, as shown schematically in Fig 3-1, and found that the WB effectiveness ranged 0.81-0.91 during all tests conditions which were less than the theoretically anticipated effectiveness. However, these values of efficiencies were 10%-20% higher than that of the WBT-IEC. The COP of the tested unit was over 8.8 with cooling capacity in the range of 9-12 kW. However, main drawbacks of the cooler were the high initial costs; low air flow rates that is 40-60% less than that of the DEC due to heat exchanger design and pressure losses which probably the main cause of high power consumption of 40-80%.

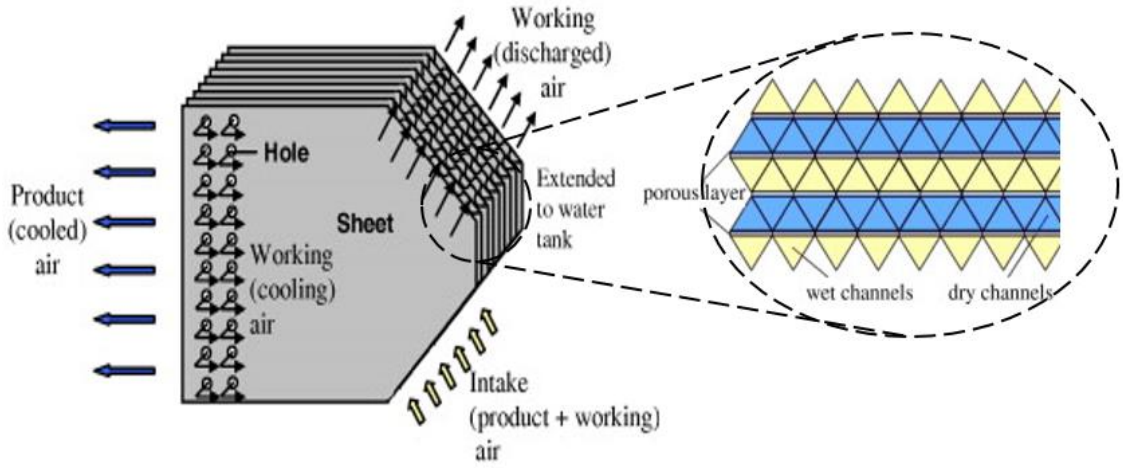


(a) Structure M-cycle heat exchanger (b) Schematic of Coolerado Cooler™ System

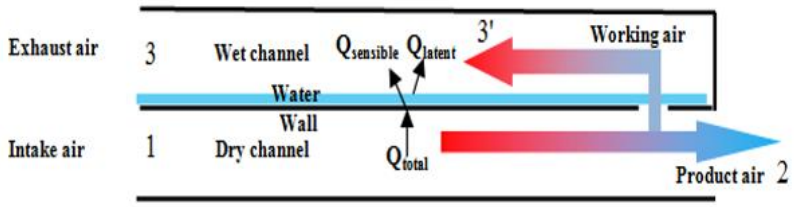
Fig 3-1 Coolerado Cooler™ [57]

Since then, intensive research activities related to sub WBT-IEC carried out aiming to overcome some of the limitations in the M-cycle design such as the unfavourable cross-flow arrangement of heat exchanger, and partly cooled working air due to early diversion from the inlet air flow streams. Zhao et al [69] introduced a novel counter-flow sub WBT-IEC, its concept is based on the M-cycle, but differs in the positions of the perforations and the flow pattern. In some references, this new configuration of the sub WBT-IEC system is also called the regenerative indirect evaporative cooler, or simply the R-IEC [58] and [70]. In this configuration, a polygonal plate-fin HMX was structured from sheets and corrugated triangular cross-section fins stacked together to form the adjacent wet- and dry-air channels, as shown in Fig 3-2. Water-proof material is used to avoid water penetration on the dry side of sheets. Unlike the cross-flow Maisotsenko-cycle HMX, holes are located at end of flow channels. The inlet air flows through and along the dry channels transferring sensible heat to the wet channels, and at the end of dry channels part of the cooled inlet air is delivered to conditioned space, while the remaining is diverted to the wet channel as cold working air flows in counter-flow direction. In another study, Zhao et al. [69] performed numerical investigation of this system by developing computer model to optimise the geometry of the system, and investigate the favourable operating conditions for improved performance. The theoretical results showed that the effectiveness is significantly affected by the dimensions of the air passages, inlet air flow rate,

and working-to-inlet air flow ratio. Also, the supply air temperature was cooled lower that the WBT of the inlet air, and the wet-bulb effectiveness reached 1.30 and dew-point effectiveness of up to 0.90 when the inlet air velocity are below 0.5 m/s, height of air channel is below 6 mm, and the length of the channel is 200 time of the height.



(a) Structure of polygonal plate-fin cross-flow HX



(b) Working principle of counter-flow plate-fin HX based R-IEC

Fig 3-2 Configuration and working principle of a regenerative ICE [69], [20]

Also, Zhan et al [71] carried out a comparative study between cross- and counter-flow M-IEC system. Theoretical and experimental investigation conducted to assess the performance of both systems under the same conditions. It was found that the counter-flow HMX offer distinctive performance over the cross-flow HMX. The counter-flow HMX achieved around 20% higher cooling capacity and 23% higher wet-bulb effectiveness. Contradictory, the cross-flow exchanger has 10% higher COP than that of the counter-flow system due to the increase in power consumption of the counter-flow HMX. The Model results were compared with other studies and showed sufficient agreement with errors ranging 2–10%.

Zhao et al. [72] conducted a feasibility study of a new dew point evaporative cooling system for buildings air-conditioning in China by investigating weather conditions and water availability, as well as evaluating the cooling capacity under various regions of China. They used the IEC system indicated in [69]. The study concluded that the cooling system is suitable for most areas of China apart from hot and humid regions. Tap water can be used for the dew-point IEC and water consumption is in the range 2.6–3 l/kWh cooling output. The cooling output of the unit ranged from 1.1 to 4.3 $W/(1\,m^3/h)$ of the supply air flow rate. Similarly, Zhao et al. [73] carried out another feasibility study for buildings air-conditioning under the UK climate conditions, using the same sub WBT-IEC mentioned in [69] and [72]. It was found that the dew-point IEC system is applicable for most of the UK areas, particularly where the climate is drier in summer. Tap water is suitable as feed water with an adequate temperature for cooling ranging 23-18 ℃, the water consumption rate varied from 2.1 to 2.4 l/kWh cooling output. The system cooling capacity is in the range of 3.1-4.2 $W/(1\,m^3/h)$ supply air flow rate.

Riangvilaikul and Kumar [26] experimentally examined the efficiency of a counter-flow, plate-type sub WBT-IEC based on the regenerative flow scheme under several inlet air conditions of various climatic regions. The R-IEC consists of flat-sheets-stacked structure separated by channel guides located on one side of the sheet to form alternating dry and wet channels as illustrated in Fig 3-3. Polyurethane is used as water-proof material on dry channel side, while the wet channel is coated with a thin-film of cotton sheet as wick material. Feed water is sprayed on the top of the rig. Holes are distributed regularly at the end of dry channels to convert part of cooled inlet air into the wet channel as the working air. The constructed unit involves 4 dry channels and 5 wet channels with wall dimension of 1200mm*80mm and 5 mm of channels height, the working-to-inlet air ratio is 0.44, and water consumption rate of 60 g/h. From the experimental results, it was found that WB effectiveness spanned from 0.92-1.14 and the DP effectiveness ranged between 0.58-0.84 for various inlet air conditions. In another study, they [27] conducted theoretical investigation of the performance of the above cooling

system, a numerical computer model developed to optimise system parameters, and evaluate the effectiveness under various inlet conditions. By comparison, the theoretical results and experimental data showed good agreement with only ±5-10% error. It was found that in order to maintain the WB effectiveness greater than 1 for all inlet air conditions, it is recommended that the inlet air velocity is below 2.5 m/s, channel height is less than 5 mm, channel height is larger than 1 m and the ratio of working-to-intake air is around 35–60%.

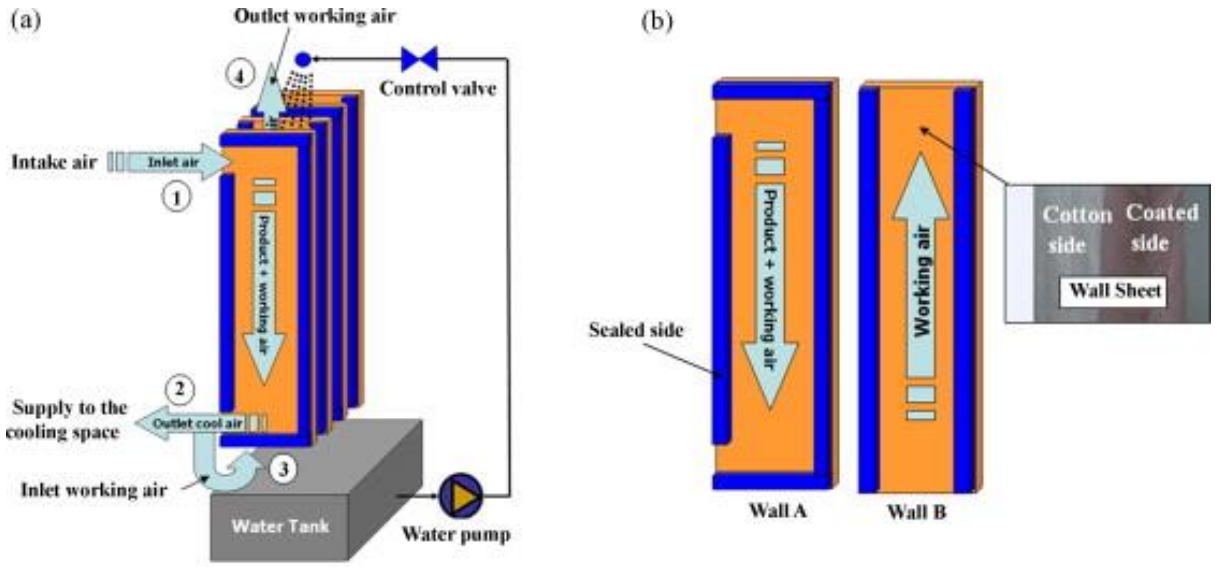


Fig 3-3 Flat-plate based dew point indirect evaporative cooling system [26]

Hasan [74] theoretically conducted a computational model of several configurations and flow arrangements of plate-type HX based indirect evaporative coolers. The thermal performance was investigated of four different flow-configuration of HMX, as illustrated in Fig 3-4, which include: a single-stage counter-flow HMX based R-IEC, and the other three were two-stage cooling system with a parallel flow, a counter flow and a combined parallel-regenerative flow. The results showed that the wet-bulb effectiveness for the systems was 1.16 for the single-stage counter-flow R-IEC, while, 1.26, 1.09 and 1.31 for the two-stage counter-flow, parallel-flow and combined parallel-regenerative cooler, respectively. Although the model results compared with available experimental data from literature, the theoretical findings have not yet been experimentally validated. In another study, Hasan [75] developed mathematical model of

a R-IEC by using a modified effectiveness-NTU method (ε-NTU). The analytical model was used to determine the performance parameters of a counter-flow plate-type HMX of R-IEC system. Despite several assumptions were made, the findings revealed a good matching with results from numerical model using fine-difference-method, and also the validation against experimental data from the literature was satisfactory.

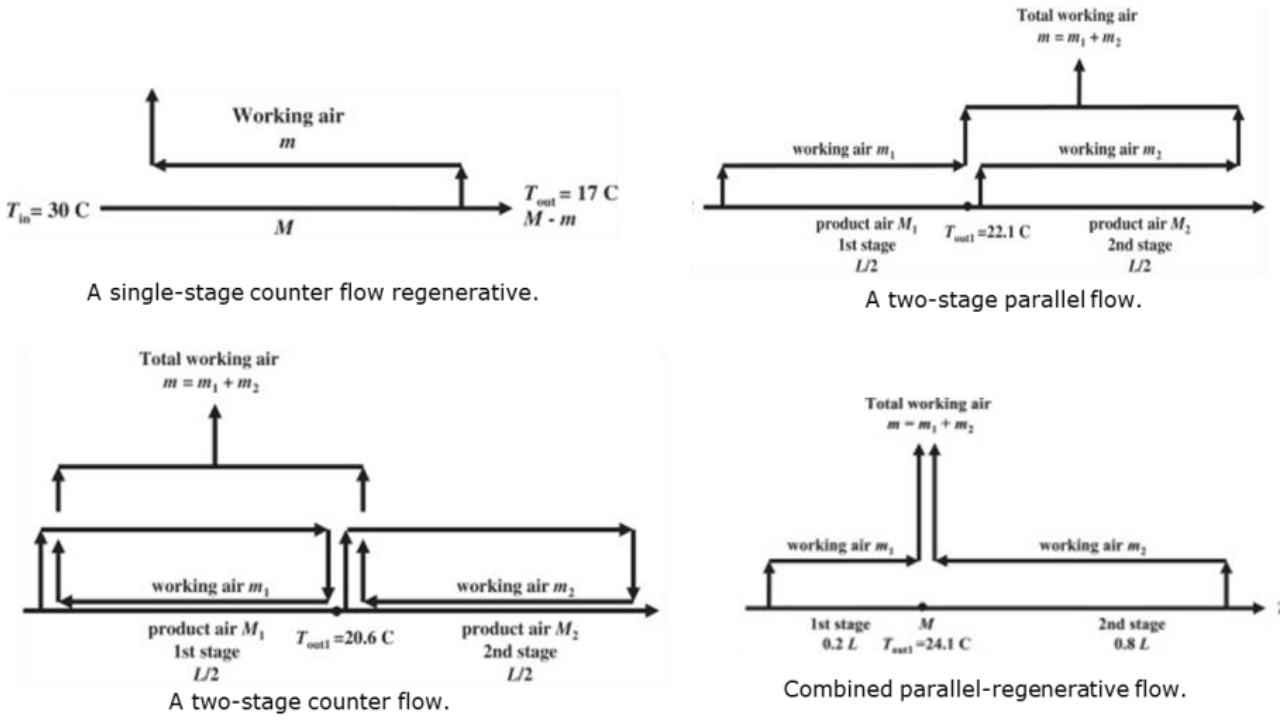


Fig 3-4 Four exchanger configurations of IEC system studied by Hasan [74]

Bruno [76] experimentally investigated the thermal performance a sub wet-bulb evaporative cooler, a module product, for a residential and commercial air-conditioning applications for a wide range of operation conditions. This sub WBT-IEC system equipped with a plate-type HMX based on the R-IEC. The results indicated that for the residential application, an average wet-bulb effectiveness of 1.24 and 0.75 of dew-point effectiveness was achieved. While, for the commercial application the average wet-bulb and dew-point effectiveness was 1.06 and 0.65 respectively. Equally, the cooling capacity ranged from 15-22 kW throughout the day.

Also, Zhan et al. [77] numerically analysed the performance of a cross-flow, flat-plate-stack heat exchanger based R-IEC system. Finite element method and EES software (Engineering Equation Solver) were used to solve the governing equations of heat and mass transfer. From numerical results, higher effectiveness is achieved when the average air velocity in the dry and wet channels are kept below 1.77 m/s and 0.7 m/s respectively, and the working-to-inlet air flow ratio is 50%. The optimum ratio of the channel length to the height must be in the range 100 to 300. The model results showed that this configuration can achieve about 17% higher cooling effectiveness compared with the conventional cross-flow exchanger of WBT-IEC.

Boukhanouf et al. [78] developed a porous ceramic indirect evaporative cooler based on the R-IEC system. The exchanger consists of two adjacent channels with a common porous ceramic wall as wet medium which is water-sealed on one side. The wall is constructed from hollowed rectangular porous panels and filled with water, the porous ceramic panels are sealed by non-permeable layer from dry channel side to prevent water penetration. Experimental and numerical investigation was conducted to evaluate the effectiveness, the cooling capacities and other characteristics of this cooling system. It was found that for hot and dry climate (ambient temperature 30-45 ℃ and humidity <65%) the system is able to cool the supply air below the wet-bulb temperature of inlet air. In additions, the wet-bulb effectiveness reaches 1.17, and cooling capacity of 280 W/m^2 of the wet-ceramic area.

Lee and Lee [70] conducted experimental and theoretical evaluation of the performance of a regenerative indirect evaporative cooler (R-IEC) at various operation conditions. The fabricated core part of the R-IEC is a plate-fin type HMX with counter-flow arrangement, comprises of multiple pairs of Aluminium finned channels brazed with a thin flat plate to form adjacent dry and wet channels. The internal surface of the wet channel is coated with a thin porous layer to increase surface wettability. A guide duct is attached below the wet channel to direct working air to the surroundings. The dimensions of the fin is 100x9.8x0.15 mm (length x height x thickness), and length of the channel is 200 mm with thickness of 0.3 mm. Total of 23 module

pairs are stacked up to form the heat exchanger core of the R-IEC unit. The results showed that the WB effectiveness ranged from 1.18-1.22, and the dew-point effectiveness varied from 0.75 to 0.90.

Cui et al. [79] theoretically evaluated the thermal performance of a counter-flow, closed-loop, flat-plate-stacked HMX of a sub-WBT IEC system under various operating conditions. The study, also, investigated the effect of the channels' surface roughness and effect of using the return air from conditioned space as working air on the overall performance of the system. Fig 3-5 illustrates a schematic of the HMX that comprises of a dry channel and two adjacent wet channels with a closed-loop configuration. The working principle is based on concept of the R-IEC, but the working air is completely separated from the inlet (product) air, i.e. the working air is not fractioned of the product air, as presented in Fig 3-5-b. Therefore, the working air (w_1) passes through the dry channel of the working air then through the wet channel of the working air before it is rejected to the atmosphere (w_3). The product air (P_1) is cooled along the product channel by heat transfer to adjacent wet channels of working air and is finally passed to the conditioned space (P_2).

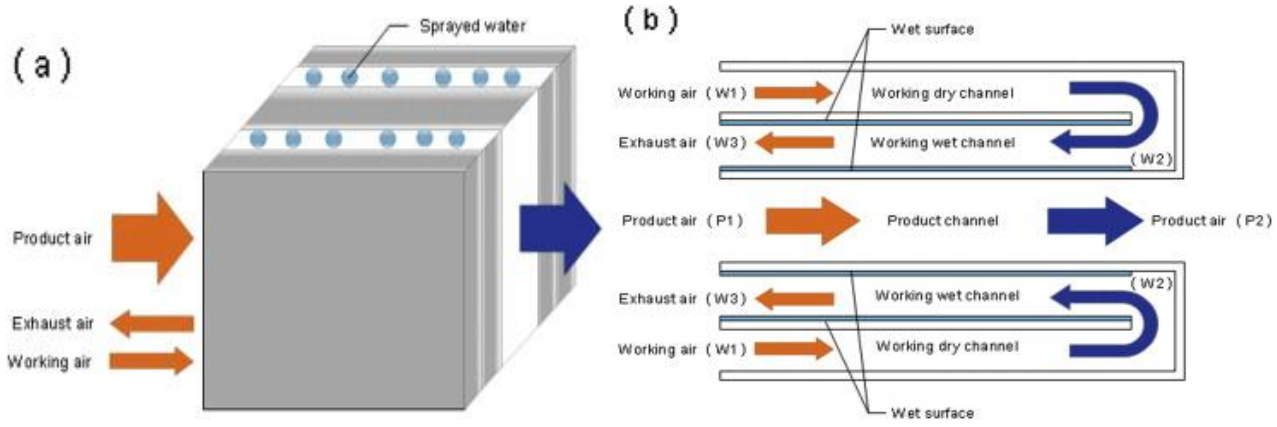


Fig 3-5 Schematic of sub WBT cooler, a) one-unit module, b) working principle [79]

The model was validated by comparing its theoretical results against experimental data from other study of [80]. A sufficient agreement between the model results and experimental data was found within ±7.5-10% discrepancy. The wet bulb effectiveness spanned from 1.22 to 1.32

and dew-point effectiveness ranged from 0.81–0.93. Additionally, it was found that the cooler effectiveness is effectively increased if the room return air was used as working air. Also the roughness of channel surfaces enhances the wet bulb effectiveness by 10–20% when the inlet air velocity was above 1.5 m/s. It is recommended that the length of the channel should be at least 200 times of the height of the working channel. In a similar study, Cui et al. [81] numerically investigated the performance of the previous system using CFD software. The developed computer model was used to examine the effect of ambient conditions and cooler geometry and air flow rates on the thermal performance. Similar results were found, the best performance is associated with low inlet air velocity of 1.5 m/s, 10 mm or less for the dry-air channel height, and the length of the dry-air channel is at least 200 times of the wet-air channel height. By comparison between computed data and experimental results from [69], a good agreement is demonstrated and the discrepancy is within 10%.

Rogdakis et al [82] evaluated theoretically and experimentally a Maisotsenko cycle based indirect evaporative cooler i.e. the M-IEC. An experimental unit was constructed and operated to evaluate the performance of the system under Greek climate conditions. The results showed that the effectiveness was between 0.97 and 1.15, while water consumption ranged from 2.5-3.0 $L\ per\ kW/h$. Moreover, it was found the M-IEC system is applicable for most Greek cities.

Lin et al. [83] introduced mathematical model for a counter-flow plate-type R-IEC. The numerical study concerned the evaluation of the performance parameters under various climatic conditions. Also, the longitudinal heat conduction, water evaporation rate, heat transfer coefficients, and convective heat-mass transfer in the air passages and water film temperature were considered in the simulation. The computer model was validated against experimental data from [80], and against their own experimental work, a discrepancy of 4% was found of the supply air temperature. Furthermore, a parametric study was conducted under various working conditions and for different geometric conditions of the HMX. According to the simulation results, the WB effectiveness ranged 0.42-1.47. Also, it was recommended

that the working-to-supply-air flow ratio is not less than 50%, and the channels height and length are kept at 0.005 m and 1.8 m, respectively to maintain WB effectiveness above 1.

In similar study, the design of plate-type based R-IEC system was optimised. The thermal performance, the cooling capacity, and the effect of design parameters were theoretically and experimentally evaluated [84]. The results revealed that the channel height should be around 0.005 m and the channels length should be between 0.4 and 0.6 m, also, the working-to-inlet air flow rate ratio should be about 40%.

A comparative numerical study carried out by Moshari and Heidarinejad [85] for three different configurations of plate-type IEC systems which involves cross- and counter-flow arrangements. The developed computer model, using MATLAB software, was used to evaluate the performance and investigate of the effect of the longitudinal heat conduction through the coolers walls. The model results compared with experimental data from [86] for verification, and showed a good agreement. Furthermore, it was found that the pre-cooling of the working air led to decrease the inlet air temperature below its WB temperature. Additionally, the counter-flow arrangement of the R-IEC showed higher effectiveness than that of the cross-flow WBT-IEC by 30%.

A numerical investigation carried out by Pandelidis et al. [87] to investigate the performance of three designs of IEC systems employed in a desiccant wheel air-conditioning system. The investigated IEC systems are; (i) cross-flow M-cycle HMX based IEC, (ii) counter-flow R-IEC and (iii) cross-flow WBT-IEC. An analytical simulation model developed based on the modified $\varepsilon - NTU$ method to compare the performance of the different systems under wide range of operational parameters. The numerical results revealed that the desiccant system equipped with the cross-flow M-cycle HMX based IEC provided the lowest supply air temperature, but the HMX configuration is the most complicated and costly among the other two heat exchangers.

Also, counter-flow plate-type HMX was experimentally tested by Duan et al. [88] to evaluate the performance of a regenerative IEC system and, also, to investigate the impact of operating

parameters. From tests results, the WB effectiveness varied from 0.55-1.06, and the COP ranged from 3-15.5. By compared with the WBT-IEC, the WB effectiveness and COP increased by 31% and 40%, respectively. Additionally, it was found that the cooler effectiveness improves by either increasing the inlet air wet-bulb temperature depression, decreasing the inlet air flow rate, or minimising the supply-to-inlet air flow ratio. Whereas, the cooling capacity and COP can be enhanced by either increasing the inlet air wet-bulb temperature depression, or increasing the inlet air flow rate and/or maximising the supply-to-inlet air flow ratio. While, the water temperature has minimal effect on the cooler effectiveness by 5% when the water temperature rises from 19 to 23℃. A good agreement was obtained between the experiments and numerical results.

An experimental and numerical study carried out by Jradi and Riffat [89] on a cross-flow, M-cycle based indirect evaporative cooler. Two-dimensional numerical model was developed to optimise the dimensions of the cooler's channels, evaluate the performance, and investigate the operating parameters impact. The experimental data were compared against simulation results for model validation purposes and showed a good agreement. It was found that the cooler WB effectiveness reached 1.12.

A review study by Porumb et al. [90] of evaporative coolers covering the theory, the working principles, and the type of heat exchanger employed of various systems i.e. DEC, WBT-IEC, M-IEC, and R-IEC systems. It was found that about 80% of the reviewed IEC were constructed from plate-type HMX. In another review study [91], they also presented an up-to–date review of IEC systems concerning the working parameters of both the inlet and working air streams, the geometrical parameters and the thermal performance parameters. Overall, the IEC systems are promising cooling technology with lowest power consumption amongst the other cooling methods. Though high water consumption rates is a key disadvantage.

3.2 Porous ceramic as wetting media of IEC systems

Unlike the DEC system, heat and mass transfer occur indirectly through a common wall for the IEC systems. Therefore, Materials with high thermal conductivity, and wetting material (wick) has uniform water distribution, large contact area and good coating compatibility are always desirable to enable sufficient water evaporation on the wet-side channel which, consequently, enhance the sensible heat transport from the dry-air side channel to the wet-air channel and, also, improve the latent heat transfer in the wet-air passage between the working air and the water film [92].

Several research studies investigated various types of materials and their compatibility as wicking materials of IEC systems. For example, Zhao et al. [92] investigated several types of water wicking materials for IEC system. It was found that aluminium and then cooper were the most suitable material over the others (fibres, ceramics, zeolite and carbon) in terms of their physical and thermal properties and structure for IEC walls. While the sintered, mesh, and grooved wicks type were the best wick structure for IECs. Furthermore, the study found that the shape formation, durability, compatibility with coating material, contamination risk and cost of materials are the most important characteristics in selecting materials. While, material's thermal conductivity and porosity have less impact on selection process [92]. However, these findings are still restricted to a particular configuration of IEC system, and limited to the experiments conditions. In contrast, porous ceramic is considered to be a promising material in heat transport augmentation [93], it was employed hundreds of years ago for several cooling purposes, e.g. for building cooling, drinking water cooling and food preservation [1]. Owing to their durability, accessibility, good thermal conductivity, availability in different porosities, sufficient water-retaining capacity and high contact surface area between solid and fluid phases, porous ceramic materials, recently, have gained intensive attention in the research area for buildings cooling applications. Nevertheless, relatively high prices and possibility of bacteria and mould growth are the main limitations of wider usage of the porous ceramic in

evaporative coolers [92], [36]. However, recently there have been considerable improvements in the conflicting of health issues by developing anti-microbiological growth wick materials, and using chemical treatments, anti-rotting, and filters to eliminate threats of bacteria, mould existence in the wet air channel side [12].

On one hand, ceramic materials have been used in the form of flat plates and panels combined within building walls for solar heat-gain reduction of buildings and indoor air-cooling. Like, Ibrahim et al. [94] performed an experimental investigation of a porous ceramic wall integrated with building external wall. The ceramic wall is made by staking up several hollow, rectangular porous ceramic panels (315 x165 x 35 mm each panel) filled with water, as illustrated in Fig 3-6-a. Performance evaluation carried out under different climate conditions. Three different levels of porosities were tested of 1 m height wall. It was found that the best performance was achieved with high porosity which is associated with highest water consumption. Equally, the supply air temperature dropped by 6-8 ℃, but the indoor air humidity rose by 30%.

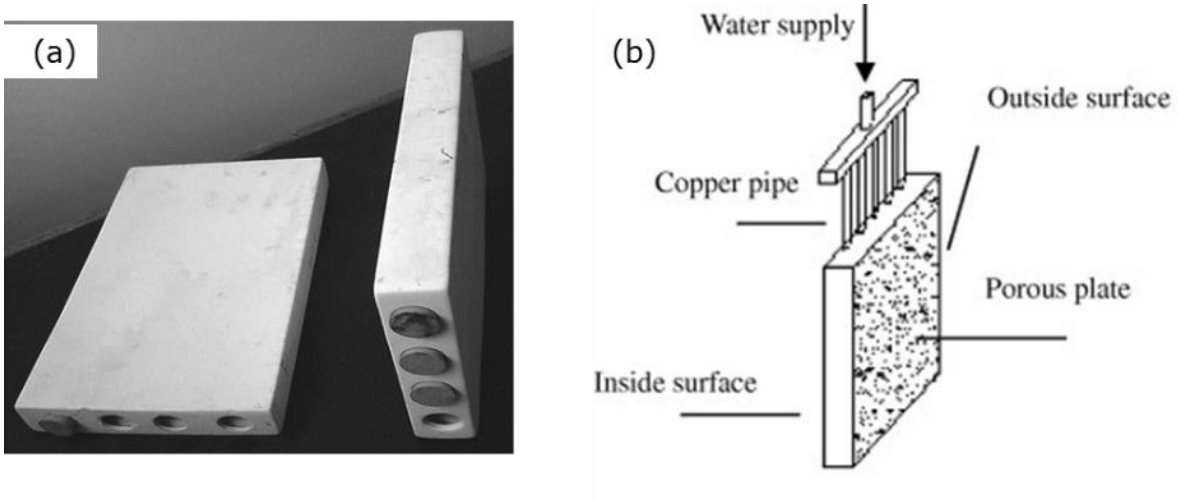


Fig 3-6 Shapes of porous ceramic integrated with building walls; (a) porous ceramic panels [94], (b) structure of porous plate [95]

Similarly, Chen [95] mathematically analysed the performance of a wet porous ceramic plate integrated into building external walls for indoor air-cooling. Additionally, the impacts of

ambient air conditions and the thickness of the porous ceramic plate on the thermal performance were investigated. The wall is constructed from the porous ceramic wall with the outer side of it facing the ambient air, while the inner surface of the wall is coated with thin copper sheets. Water is supplied from the top of the wall via copper pipes that are implanted near the inside surface of the porous plate for water evaporation in the porous wall, as schematically shown in Fig 3-6-b. The results showed that 5-8 ℃ indoor air temperature drop was achieved. In other studies, porous ceramic material with water spraying mechanism was utilised within building facades to minimise building's heat gains through the outer walls [96], [97]. Furthermore, direct evaporative cooling walls comprises of porous ceramic pipes with high capillary force was introduced for thermal comfort of outdoor and semi-outdoor spaces [98].

On the other hand, limited research studies have found on employing porous ceramic material as wetting media for IEC systems, particularly the M-IEC and R-IEC systems. In the literature, Riffat and Zhu [50] used porous ceramic container as wetting medium of heat pipe based indirect evaporative cooler. The ceramic container hosted the heat pipe condenser, filled with water, to work as heat sink of the heat pipe, this system was explained in section 2.3.1. Also, Boukhanouf et al. [78] employed hollow, rectangular porous ceramic panels as a common wall separates between the two adjacent air channels. The model results indicated that the supply air temperature is cooled below the wet-bulb temperature of the intake air and the wet-bulb effectiveness reached 1.17. In another study, Alharbi [99] conducted experimental and numerical investigation using the same porous panels as heat sink of heat pipe exchanger based indirect evaporative cooler. The cooler is constructed of two adjacent channels with a common, impermeable, separating plate. The heat pipe are vertically positioned across both air passages, In the upper air passage, the condensers of the heat pipes are immersed into the water-filled, rectangular porous ceramic panels for heat removal from the condenser. Whereas, the working air flows over the outer surface of the water-soaked panels. While, in the bottom

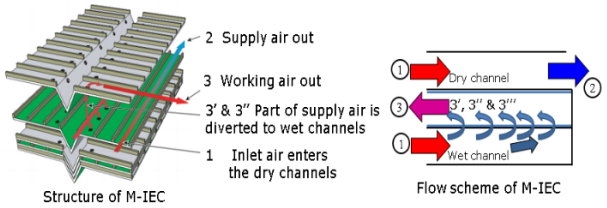
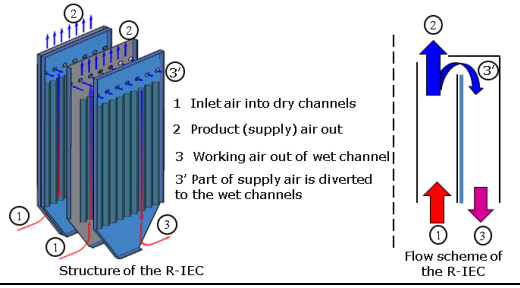
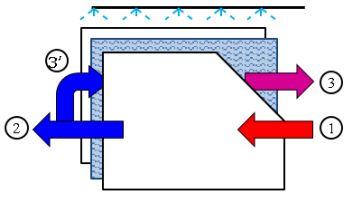
air channel, the inlet air is cooled down as it passes over the finned evaporators of the heat pipes. The experimental results showed that WB effectiveness of 1.10 was achieved. Though higher water demand is required to fill up the ceramic panels, and water evaporation rate ranged 0.22-0.60 l/h.

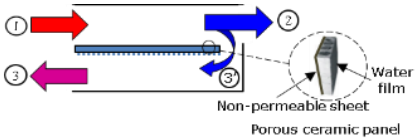
3.3 Analysis of reviewed work of the sub WBT-IEC systems

The sub WBT-IEC systems have been an intensive area of research because of their ability to cool down the supply air below the wet-bulb temperature of inlet air i.e. brake the limit of BWT-IEC, and other distinctive advantages over the DEC systems such as the controlled indoor humidity, less water consumption, and eliminations of odours.

As being the core of any IEC system, the heat-mass exchanger (HMX) principally is the main component of the IEC system to enhance the thermal performance, either by improving the geometry, construction, the flow arrangements, or/and the wicking materials. From the reviewed literature, the most commonly used construction was the plate-type HMX due to fabrication simplicity and availability of several highly conductive material in form of sheets. Two distinctive flow configurations of the plate-type HMX based IEC systems have been found; either the M-cycle or the regenerative flow scheme. Table 3-1 summaries main designs features of most recent sub WBT-IEC systems, it includes the type of HMX employed, flow pattern, research method, performance parameters, and schematics of these configurations. Additionally, Table 3-2 provides a summary of comparative studies conducted to compare the performance parameter between various types the sub WBT-IEC system. It covers theoretical or/and experimental evaluations of different configurations IEC system, but mainly comparing the performance of the M-IEC and the R-IEC systems.

Table 3-1 Summary of reviewed work on sub WBT-IEC systems

Study	Method	HMX type and Flow pattern	Performance parameters	Construction and flow scheme
M-cycle based IEC (The M-IEC system)				
Maisotsenko et al. [56]	Sim.	Horizontal plate-type, Cross flow	ε_{WB}=1.10-1.22	 Structure of M-IEC; Flow scheme of M-IEC
Elberling [57]	Exp.	Horizontal plate-type, Cross flow	ε_{WB}=0.81-0.96, COP=8.8, WC=2.5-3 $l/(kW/h)$, CC=1.33 KW	
Zhan et al. [77]	Sim.	Horizontal plate-type, cross-flow	ε_{WB}=0.50-0.70, CC=200 W	
Ahmed et al [100]	Exp.	Horizontal plate-type, cross-flow	ε_{WB}=0.84-0.96, COP=7-55, WC=16-60 l/h, CC=4-13 KW	
Rogdakis et al. [82]	Sim. and exp.	Horizontal Plate-type HMX, cross-flow	ε_{WB}=0.97-1.15 WC=2.5-3 $l/(kW/h)$	
Jradi and Riffat [89]	Sim. and exp.	Vertical plate-type HMX, cross-flow	ε_{WB}=0.7-1.17, COP=6-14, CC=1.05-1.25 KW	
The regenerative IEC (R-IEC system)				
Zhao et al. [69]	Sim.	Horizontal, Polygonal plate-fin type HMX, Counter-flow	ε_{WB}=0.6-1.3	 Structure of the R-IEC; Flow scheme of the R-IEC
Zhao et al. [72]	Sim.		WC≈3 l/kWh, CC=1.1-4.3 $W/(m^3/h)$ air flow rate	
Zhao et al. [73]	Sim. and Exp.		WC=2.4 $l/kWh_{cooling}$, CC=3-4.2 $W/(m^3/h)$ air flow rate	
Duan et al. [88]	Exp.	Plate-type HMX, counter-flow	ε_{WB}=0.55-1.06, COP=3-16 CC=0.6-1.13 KW	
Riangvilaikul and Kumar [26]	Exp.	Vertical Plate-type HMX, counter-flow	ε_{WB}=0.92-1.14, WC= 60 g/h	 Structure and flow scheme of vertical plate-type HMX
Riangvilaikul and Kumar [27]	Sim.		ε_{WB}=1.06-1.2	
Bruno [76]	Exp.		ε_{WB}=1.06-1.24, COP=5-12, CC=15-22 kW daily	
Bellemo et al. [101]	Sim.		ε_{DP}=0.60-0.76, CC=15-25KW	

Study	Method	HMX type and Flow pattern	Performance parameters	Construction and flow scheme
Hasan [75]	Sim.	Horizontal plate-type HMX, cross-flow	ε_{WB}=0.95-1.16	 Flow scheme of the R-IEC
Lee and Lee [70]	Sim. and exp.	Vertical plate-fin type HMX, counter-flow	ε_{WB}=1.18-1.22, CC=0.9-1.13KW	
Lin et al. [83]	Sim.	Plate-type HMX, counter-flow	ε_{WB}=0.42-1.47, CC=40-200 W/m^2	
Boukhanouf et al. [78], [102]	Sim. and exp.	Vertical plate-type HMX, counter-flow, using porous ceramic material	ε_{WB}=1.17, CC=280 W/m^2	

Sim: simulation, Exp: experiment, ε_{WB}: WB effectiveness, $\varepsilon_{\mathrm{DP}}$: Dew point effectiveness, WC: water consumption rate, CC= Cooling capacity

Table 3-2 Summery of comparative studies between different types of the sub WBT-IEC systems

Study	Method	HMX type and flow pattern	Performance parameters	Research features
Hus et al. [80]	Sim. and exp.	Plate-type HMX of • parallel flow IEC • counter flow IEC • cross flow R-IEC • counter flow R-IEC	ε_{WB}=0.6-0.8 ε_{WB}=0.8-1.0 $\varepsilon_{WB,\mathrm{R-IEC}}$=0.9-1.3 $\varepsilon_{WB,\mathrm{R-IEC}}$=0.9-1.3	the counter- and parallel-flow regenerative configuration (R-IEC) has the highest WB effectiveness
Zhan et al. [71]	Sim.	Cross-flow M-IEC and Counter-flow R-IEC	$\varepsilon_{WB,\mathrm{M-IEC}}$ =1.14 , $\varepsilon_{WB,\mathrm{R-IEC}}$ =1.36	The counter flow R-IEC system has higher performance than the M-IEC system of above 15%.
Hasan [74]	Sim.	Horizontal plate-type HMX of : • counter flow R-IEC • counter flow two-stage R-IEC • parallel flow two-stage R-IEC • Combined parallel- regenerative flow two-stage R-IEC	ε_{WB}=1.16 ε_{WB}=1.26 ε_{WB}=1.09 ε_{WB}=1.31	Numerically analysis heat and mass transfer process for four flow-configurations of IEC systems to evaluate their performances. It was found the combined parallel-regenerative flow two-stage R-IEC system has the best effectiveness. See Fig 3-4 for flow schemes of the IEC systems.

Moshari and Heidarinejad [85]	Sim.	Cross-flow and counter-flow plate-type R-IEC systems and cross-flow plate-type WBT-IEC	N/A	Counter-flow R-IEC has higher effectiveness than that of cross-flow R-IEC by 30%.
Pandelidis et al. [87]	Sim. with exp. Validation	Plate-type HMX of counter-flow R-IEC cross-flow M-IEC cross-flow WBT-IEC	N/A	The cross-flow M-IEC system is the most effective with largest cooling capacities. Whereas, counter-flow R-IEC is more simple and cheaper than the cross-flow M-IEC, but its performance is lower than the M-IEC. While, The Cross-flow WBT-IEC is the simplest and cheapest design, however, its performance is the lowest.
Anisimove and Pandelidis [103]	Sim. with exp. Validation	Plate-type HMX of • parallel-flow WBT-IEC • counter-flow WBT-IEC • cross-flow WBT-IEC • counter-flow R-IEC	N/A	The counter-flow R-IEC is able to achieve the highest effectiveness but with lower cooling capacity
Pandelidis and Anisimove [104]	Sim. with exp. Validation	Horizontal plate-type HMX of an M-IEC system.	N/A	A comparative simulation study of eight flow schemes, i.e. eight different positions of perforations along the plate, of an M-Cycle based IEC. The performance of all selected configurations are investigated and compared in order to improve the construction of the original HMX. It was found that holes' size and positions effect on the cooling capacity. Even distribution of holes and uniform flow rates were recommended.
Bolotin et al. [105]	Sim.	Vertical cross-flow plate-type HMX of WBT-IEC and of R-IEC	$\varepsilon_{WB,\mathrm{WBT-IEC}}$ =0.6-0.99, $\varepsilon_{WB,\mathrm{R-IEC}}$ =0.75-1.45	The R-IEC is characterised with higher effectiveness and COP, while WBT-IEC is favourable when greater cooling capacities are required.

From the aforementioned reviewed studies, the current numerical and experimental research work in the field of the sub WBT-IEC systems concern the following activities:

(i) Investigation studies of the thermal performance characteristics of the proposed IEC system i.e. mostly evaluating the temperature drop of the inlet air, the effectiveness, the COP, the cooling capacity under specific or various climate and operation conditions. Additionally, further performance parameters might be determined that are the water and power consumptions, pressure drop, and heat and mass transfer rates. It can be achieved theoretically by computer simulation of the IEC system, like [69], [75], [77], [79], and [106]; or experimentally via laboratory tests, like [26], [57], [61], [36] and [90], or/and using both approaches for validation purposes. Similarly, on-site evaluations tests of commercial and laboratorial IEC units are considered as well [57], [61] and [76].

(ii) Optimisation studies of the geometric and structural parameters, material type used of IEC system to enhance the performance, like [83], [92], and [107].

(iii) Parametric studies using the computer model to examine the effect of operation parameters on the performance of the cooler [27], [58], [78] and [82] [89].

(iv) Economic assessment studies of the IEC, like [72], [73] and [82], that is usually accompany with investigation of the annual environmental impact, energy saving, and water and power consumption, like [65], [108], [29] and [109].

(v) Comparative studies using computer simulation, such as [74] and [85], or both approaches; the numerical and experimental methods, like [71], between various IEC configurations in order to differentiate between their performance i.e. mainly in terms of the effectiveness, COP, and the cooling output.

From both tables 3-1 and 3-2, all the studies were based on plate-type HMX of either the M-cycle or the regenerative configuration of the IEC systems. For such designs, the research reached saturation in terms of system optimisation and performance investigation. In other words, several studies concluded to similar results. For examples, recent studies by [26], [27], [71], [81], [83], [86], [88], and [89] suggested almost the same specifications of

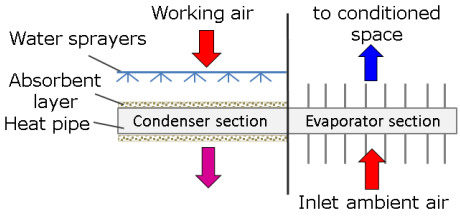
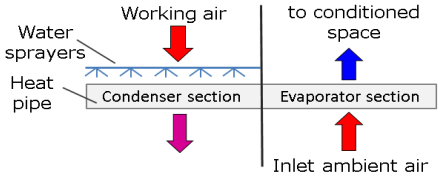
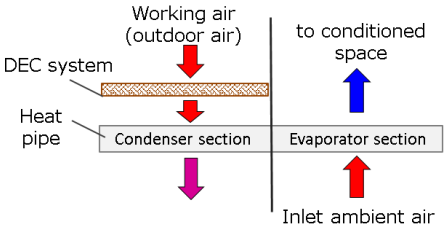
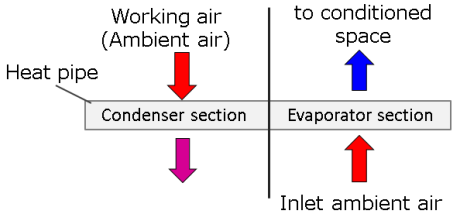
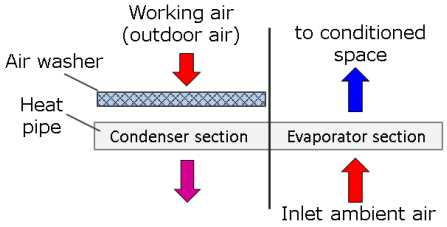
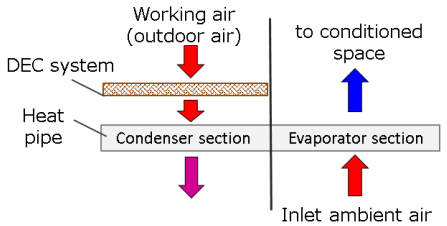
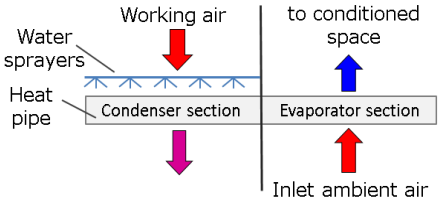
plate-type HMX i.e. the channels dimensions, with relatively close performance. It was recommended that channels height is 5 mm and channel length of around 1m, working-to-inlet-air flow rate ratio between 33%-50%, and air velocity around 1-1.5 m/s. The plate-type HMX based IEC achieved WB effectiveness ranging from 1.0 to 1.4. Yet, the WB effectiveness was below one for most of the experimental work and on-site testing, this might be related to insufficient water distribution. Moreover, the uneven and uncompleted water-saturation of the wick media over the plate require additional water to be pumped and circulated through the system. Thus, an increase of the water and electricity usage is expected. For instance, the best experimental WB effectiveness of the M-IEC was 0.96 [57], [100], though the theoretical studies showed the effectiveness reaches up to 1.22 [56].

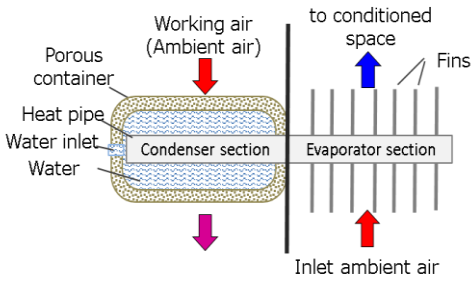
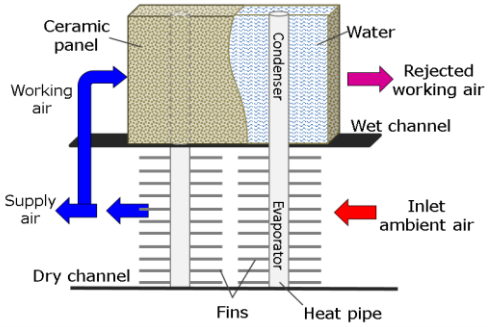
This research introduces a new configuration of heat pipe heat exchanger (HPHX) incorporating ceramic tubes for building air-conditioning, the proposed cooler is anticipated to overcome some of water distribution problem and minimise water consumption by employing heat pipes as heat transfer elements, water-saturated porous ceramic tubes as wet medium, and using the regenerative flow scheme of the R-IEC system. This effort is meant to contribute to the current participations to reduce water and power consumption and improve the performance of the IEC systems for efficient and cost-effective evaporative cooling system.

For heat pipe heat exchanger based IEC system, a proper design of the heat removal mechanism of the heat pipe condenser (HPC) is vital to achieve high heat transfer rates, hence reduce water consumption and cooler size are important as well, which in turn improve the overall performance of the cooler. By analysis the heat removal methods of HPHXs in Table 3-3, some disadvantages and limitations are identified as follows;

- Excessive use of water and the need of continues water supply by employing water spraying system;
- uneven wetting of the HPC surface because of horizontal position of orientation of the heat pipe;

Table 3-3 Heat dissipation methods employed in HPHX based IEC systems

study	Mechanism	Research features	Construction
Huang et al. [52] and Wang et al. [53]	Layer of water-absorbent material stuck on the condenser surface and constantly wetted by water sprayers, while ambient outdoor air flows over it.	0.70 of WB effectiveness [67]	
Wang [54]	(1) Water is sprayed directly on the bare condenser surface using water sprayers, while ambient outdoor air flows over it.	Comparative study of two heat removal systems of a HPHX based IEC. It was found that the supply air temperature by the second method was slightly lower than that of the first system.	
	(2) DEC unit is used to pre-cool ambient air before passing over the HPC, while outdoor air flows over it.		
Zheng et al. [55]	(1) Ambient air is used to cool bare surface of the HPC i.e. no water is introduced	Comparative study of four different heat dissipation methods used for two-stage IDEC system, the HPHX based IEC is the first stage followed by DEC unit. The result showed that the last heat removal mechanism was best with higher efficiency than other configurations of 7-16%.	
	(2) Air washer to pre-cool the ambient air before passing over the HPC		
	(3) DEC unit is employed to pre-cool the outdoor air before flowing over the HPC		
	4) Fine water droplets sprayed over the bra surface of the HPC, while outdoor air passes over the HPC		

Riffat and Zhu [50]	Porous ceramic container filled water hosting the HPC, while the ambient air flow over it	Building integrated indirect evaporative cooling system, 30% more effective that conventional HPHXs	
Alharbi [99]	Hollow, rectangular ceramic panels, filled with water, to host the HPCs, while part of the cooled supply air is diverted to be used as working air	Stand-alone system of regenerative indirect evaporative cooler. 1.05-1.3 of WB effectiveness is achieved	

- The usage of DEC unit upper-stream of the HPHX system requires, also, considerable amount of water for the DEC system, therefore, higher initial and operational cost are anticipated.
- Employing ceramic containers or ceramic panels to host the HPC improved heat removal and attained uniform water film over the HPC surface. Though, water consumption rates were high due to large dimensions and high porosity selected. Also, the thick walls of ceramic might affect the size and performance of the cooler.

In this research, the proposed heat removal method from the condenser is intended to overcome some of the above disadvantages, besides minimising water consumption and enhancing overall heat transfer rates between condenser surface and the working air. Overall, the proposed mechanism for heat removal is based on the design of Riffat and Zhu [50] but differs in terms of using ceramic tubes, instead of porous container, with thinner wall, smaller diameter and less porosity of the ceramic material, and also by employing different flow scheme of the HPHX and heat pipe orientation. Furthermore, this research build on the research work carried out by Boukhanouf et al. [102], [110] and [99] that is principally concerns the applications of ceramic materials and heat pipe for building evaporative cooling.

3.4 Parametric performance of the IEC

The following performance parameters are employed for the evaluation and assessment of the indirect evaporative coolers [76]:

3.5.1 Wet-bulb effectiveness

The wet-bulb effectiveness is defined as the ratio of the actual reduction in DBT of the inlet air though the cooling system to the difference between DBT and WBT of the inlet air. This is expressed as follows,

$$\varepsilon_{\mathrm{wb}} = \frac{\mathrm{T_{db,1}} - \mathrm{T_{db,2}}}{\mathrm{T_{db,1}} - \mathrm{T_{wb,1}}} \qquad (3\text{-}1)$$

where, $\varepsilon_{\mathrm{wb}}$: Wet-bulb effectiveness, $\mathrm{T_{db,1}}$: Inlet supply air dry-bulb temperature, $\mathrm{T_{db,2}}$: outlet supply air dry-bulb temperature, and $\mathrm{T_{wb,1}}$: Inlet supply air wet-bulb temperature.

3.5.2 Dew-point effectiveness

Similarly, dew-point effectiveness is the ratio of the actual temperature drop of the inlet air throughout the cooler to the difference between dry-bulb and wet-bulb temperature of the inlet air, as can be expressed by the following relation,

$$\varepsilon_{\mathrm{dp}} = \frac{\mathrm{T_{db,1}} - \mathrm{T_{db,2}}}{\mathrm{T_{db,1}} - \mathrm{T_{dp,1}}} \qquad (3\text{-}2)$$

where, $\varepsilon_{\mathrm{dp}}$: Dew-point effectiveness, $\mathrm{T_{db,1}}$: Inlet air dry-bulb temperature, $\mathrm{T_{db,2}}$: Supply air dry-bulb temperature, $\mathrm{T_{dp,1}}$: Inlet air dew-point temperature.

3.5.3 Cooling capacity

The cooling capacity is defined as the enthalpy change of the inlet air across the IEC system multiplied by the volumetric flow rate of the supply air. This change of enthalpy can be expressed by temperature difference of the inlet air across the cooler as follow,

$$Q_{cc} = c_p\, \rho_f\, \dot{V}_2 \left(T_{db,1} - T_{db,2}\right) \qquad (3\text{-}3)$$

where, Q_{cc}: Cooling capacity of the system, W; ρ_f: Air density, $\mathrm{kg/m^3}$; $\dot{V}_2$: Supply air volume flow rate, $\mathrm{m^3/s}$; c_f: Specific heat of air, $\mathrm{J/(kg\,K)}$; $\mathrm{T_{db,1}}$: Inlet air dry-bulb temperature, ℃; $\mathrm{T_{db,2}}$: Supply air dry-bulb temperature, ℃.

3.5.4 Coefficient of performance (COP)

Coefficient of performance or Energy efficiency is the ratio between the cooling capacity of a cooler and its power consumption. It can be written as follows [8]:

$$COP = \frac{Q_{cc}}{P_{aux}} \tag{3-4}$$

where, $Q_{cooling}$: Cooling capacity, W; P_{aux}: Power consumption, W.

3.5.5 Power demand

The power demand is mainly related to power required by the air circulating fan and water pump. This is expressed as follows [8],

$$P_{aux} = \frac{\dot{V}_{air}\,\Delta p_{air}}{\eta_{fan}} + \frac{\dot{V}_w\,\rho_w\,g\,h}{\eta_{pump}} \tag{3-5}$$

where, P_{aux}: auxiliary power consumption, $\dot{V}_{air}$: supply air flow rate, Δp_{air}: air pressure difference at the inlet and exist of the fan, η_{fan}: fan efficiency, $\dot{V}_w$: water volumetric flow rate, ρ_w: Water density, g: Gravity acceleration, h: Pumping head, η_{pump}: Pump efficiency.

3.5.6 Water consumption rate

Water consumption of an evaporative cooler depends on several factors including the system effectiveness, the airflow rate, the inlet air conditions, dry bulb temperature depression of the inlet air, the water consumption rate can be calculated by the following equation [8]:.

$$\dot{V}_w = \frac{\dot{V}_{s,out}\,\rho_{s,f}}{\rho_w}\left(w_{a,out} - w_{a,in}\right) \tag{3-6}$$

where, $\dot{V}_w$: Water evaporation rate, m^3/s; $\dot{V}_{s,out}$: Working air flow rate, m^3/s; $\rho_{s,f}$: Working air density, kg/m^3; ρ_w: Water density, kg/m^3; $w_{a,out}$: Moisture content of the outlet working air, $kg_{water}/kg_{\text{dry air}}$; $w_{a,in}$: Moisture content of the inlet working air, $kg_{water}/kg_{\text{dry air}}$.

3.5 Summary

This chapter covered a detailed review of the sub wet-bulb IEC systems including the working principle, design, construction, and thermal performance parameters. The outcomes highlighted the current development area of the indirect evaporative coolers, and provided insights for the research ideas to identify the research gab and highlight the potential of the proposed cooler.

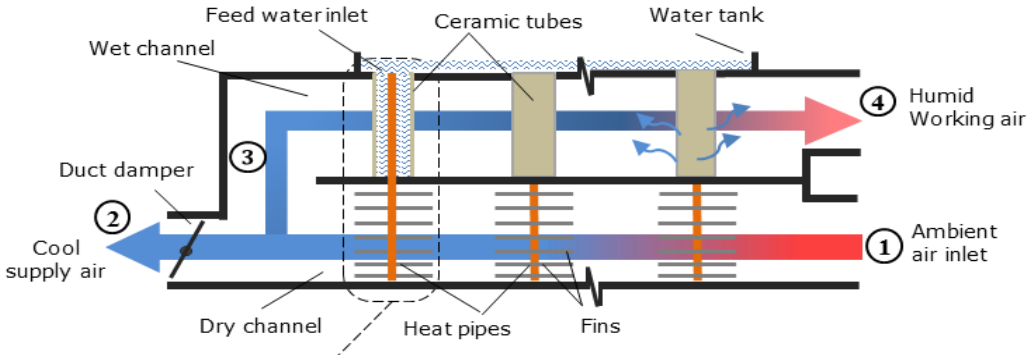
The current sub WBT coolers are typically constructed from the plate-type exchanger with flow scheme are based on either the M-cycle or the regenerative configuration to achieved cooling effect below the WB temperature of the inlet air. Furthermore, it was stressed that most employed heat exchanger of the sub WBT-IEC is the plate-type HMX, while few research work found on other HMX configurations, this motivated the present study.

In this research, a novel configuration of HPHX and porous tubes based R-IEC is considered for building air-conditioning. The new design combines the regenerative flow scheme of the IEC within the heat pipe exchanger configuration, and utilises water-soaked porous ceramic material for heat removal from heat pipe condensers. So, implementing the regenerative flow pattern is expected to improve the heat transport in the working-air passage instead of the traditional flow arrangement. Also, effective and water-saving method is used for heat dissipation from the condensers of the HPHX using water-saturated ceramic tubes. This effort is meant to contribute to the current participations to reduce water and power consumption, and improve the performance of the IEC systems for efficient and cheap evaporative cooling systems of buildings.

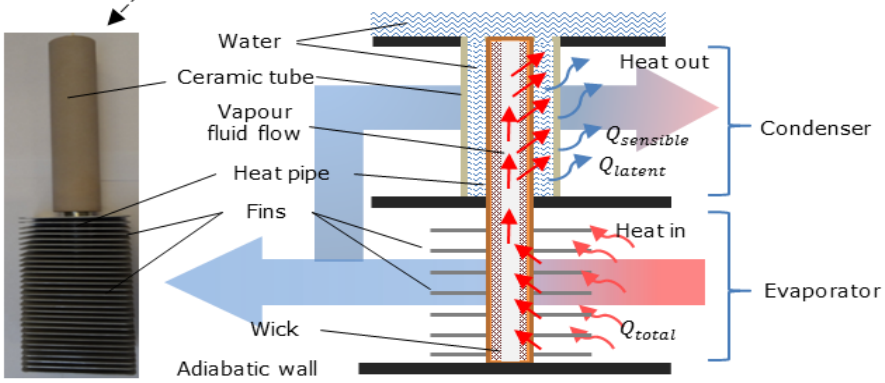
Chapter 4: Design and computer modelling

4.1 Configuration of the sub WBT evaporative cooler

The proposed evaporative cooler design is based on the principle of the regenerative configuration of the IEC, where a portion of the indirectly cooled air is used as working air for water evaporation. The air flow in the cooler is arranged in two separate air channels; dry and wet channels but with one inlet opening for the supply and working air streams. In this work, the heat transfer between the airflows in the dry and wet channels is however accomplished through heat pipe that straddles across the two channels. The evaporator of is finned and located in the dry channel, whereas the condenser is in the wet channel. Additionally, the condenser of the heat pipe is placed in a water saturated porous ceramic tube for heat rejection through water evaporation. The heat pipe-ceramic tube forms a single module that is duplicated along the airflows ducts, as shown in Fig 4-1-a.



(a) Working principle and air flow arrangement of the cooler



(b) Cross-section of heat pipe and ceramic tube module

Fig 4-1 Configuration of the cooler; the working principle and air flow pattern

The working principle is based on the R-IEC system in which the intake ambient air (state 1) is cooled indirectly in the finned heat pipes section (evaporator) at constant moisture content (state 2). A portion of the dry cool air is diverted (state 3) to the wet channel to become the working air and cause evaporate cooling effect with the exposed ceramic tube surface, removing heat from it in the process and becoming saturated air (state 4).

The heat pipe in this arrangement acts as heat transfer enabling device to transport heat between the two air steams. The heat pipe contains a small quantity of a refrigerant that evaporates as it is heated up by the inlet air in the dry channel and rejects heat in the condenser in the wet channels by virtue of refrigerant condensation. The water-soaked porous ceramics allow water to siphon through its structure and form a thin film on its outer surface. A direct evaporation process takes place between the wet air (working air) and the water film causing a drop of the ceramic surface and the bulk water temperatures and increase of the working air temperature and moisture content. This process attains constant removal of heat which would otherwise accumulate in the water and ceramic due to heat transport from the condenser surface to the surrounding water. This heat and mass transfer presses in the wet channel is important as it creates temperature gradient between both channels that is the driving force of the heat pipe.

4.2 Design consideration

The design of the cooler was carried out with consideration of materials and components selection, sizing, and heat and mass transfer processes in the ducts. The design involves sizing the airflows channels, heat pipes for heat transfer and porous ceramic tubes properties for water evaporation.

4.2.1 Heat pipe

The selection and sizing of the heat pipe is important to achieving the correct heat transfer rate between the air streams of the cooler, heat pipe is readily available technology and is

off-the-shelf products from many manufacturers. The main design parameters of the heat pipe in this work are related to operating, heat transfer capacity and size constraints.

Principally, based on the literature [111], [112], suggestions of the manufacture [113], and the cost, a gravity assisted and capillary-driven conventional tubular heat pipe was selected. The type of heat pipe was selected based on availability, cost and material compatibility. Tubular heat pipes are widely available in many standard sizes and are the cheapest as they are manufactured for many applications [114]. In this design, heat is transferred from the dry to the wet channel and the heat pipe is place up right between the two channels with the evaporator below the condenser. This orientation provides additional flexibility to the section of type of heat pipe. The simplest heat pipe configuration is the thermosiphon type where the heat pipe is made of a simple sealed tube containing a fluid and the liquid circulation is mainly accomplished by gravity. For this type of heat pipe to function, the condenser is always above the evaporator, as shown in Fig 4-2-a. In applications, where orientation or high heat transfer densities are required, it is common to select heat pipes with a wick. The wick provides the capillary force required to circulate the working fluid inside the heat pipe more effectively. A wicked heat pipe configuration in shown in Fig 4-2-b.

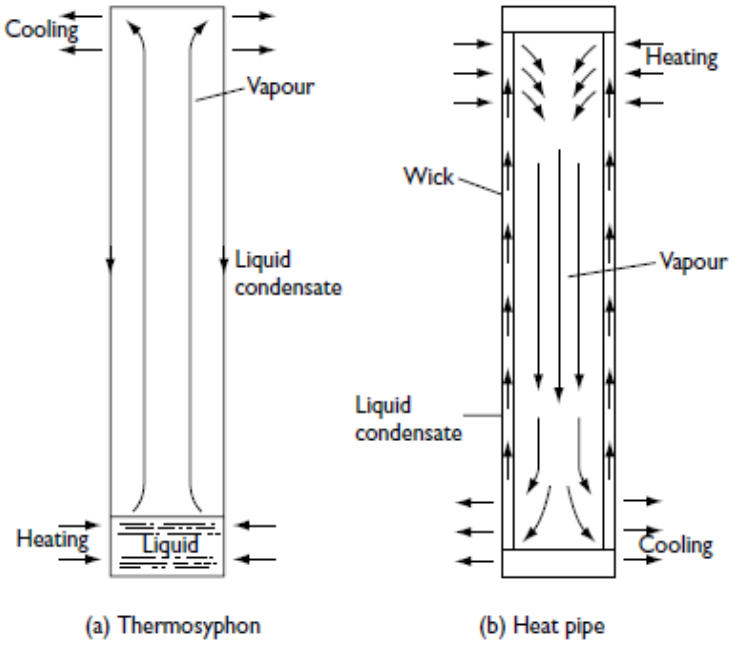


Fig 4-2 Cross-section view of the thermosiphon and the heat pipe [115]

(i) Operation conditions of the heat pipes

The working conditions of the proposed IEC system would be for hot and dry climates, and hot and semi-humid climate in which the maximum and minimum operational temperatures would range from 50-20^{o}C and relative humidity varying from 10 to 50%. The cooling medium of the condenser of the heat pipe is water at average temperature of 23^{o}C at standard ambient pressure.

This allows selecting different charging liquids for the heat pipe. For moderate temperature range of operation Water, methanol and ammonia are the most suitable choices [116]. Water was used in this case as working liquid, as it is a natural fluid, has higher latent heat, and safe if leaked into the air streams.

(ii) Heat pipe tube materials

The heat pipe container is made of various materials including copper, Aluminium, Stainless steel, etc. Copper was the chosen material for the heat pipe container and wick structure because of its compatibility with liquid water, high thermal conductivity, and corrosion resistant [114].

4.2.2 Determination of the required number of heat pipes

Specifying the required number of heat pipe rows for a particular heat pipe heat exchanger (HPHX) is related to heat transfer capacity of heat pipe. Heat pipe heat transfer rate is function of design specifications and orientation of the heat pipe [10]. According to ASHRAE, the effectiveness of the HPHX increases as the number of heat pipe rows increases, as presented in Fig 4-3. Based on average inlet air velocity of IEC system ranging from 1-3 m/s i.e. (200-600 fpm) [8]. Initial number of 14-heat-pipe rows for this cooler is selected to achieve effectiveness ranging from 75-82% (i.e. 0.75-0.82), as it seen from Fig 4-3. However, the exact number of the heat pipes rows would be determined by the mathematical model, since the effectiveness of HPHX, also, related to operation temperatures and velocities of the air streams [10].

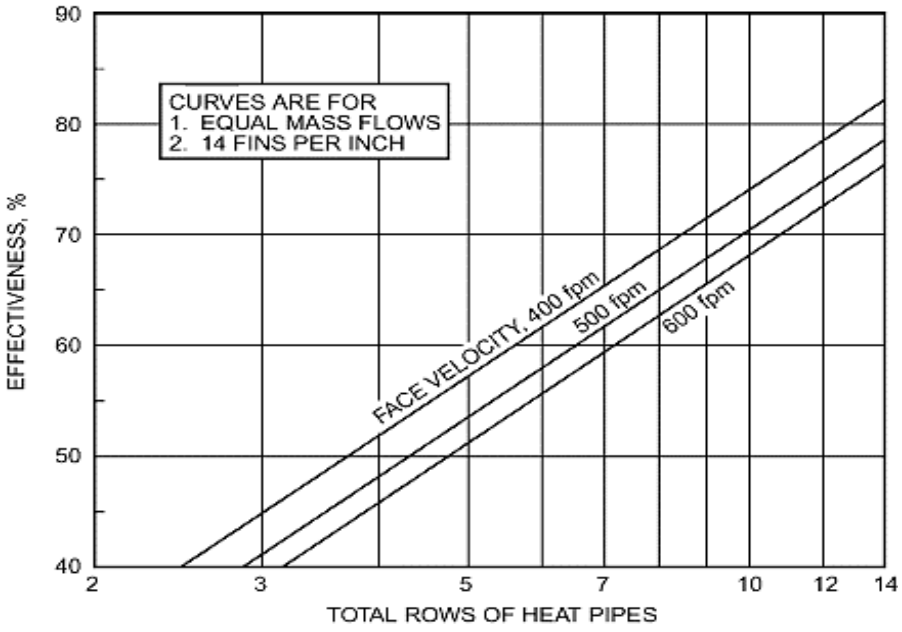


Fig 4-3 Heat pipe heat exchanger effectiveness [10]

4.2.3 Selection of porous ceramic tube dimensions

One of the disadvantages of common evaporative coolers is high water consumption through water being dragged out the wet media material without evaporation and hence a loss in cooling capacity. Hence defining the correct wet media porosity is very important to addressing the problem while minimise surface dry-out spots.

The principle idea of the porous ceramic tube of this cooler is similar to that used in cooling water through evaporation in earthenware water jars. Therefore, the porous ceramic tube is selected to have low porosity to maintain the water inside the tube and allow just enough amount of water syphoning out to form a thin water-film on the ceramic outer surface, and also to have small wall thickness of the tube to reduce the thermal resistance. In a study, Riffat and Zhu experimentally investigated the effect of the dimensions of ceramic container on the performance of HPHX, it showed that the cooling capacity and effectiveness decreases as the ceramic container diameter and wall thickness increases because of the increase of the thermal resistances [51]. Thus, the wall thickness of the porous cylinder is kept small as possible, but within the constraints of ceramic material mechanical requirement from the manufacturer.

4.2.4 Preliminary design configuration

The cooler casing is designed to form two air channels and to accommodate the heat pipes and the ceramic tubes. The casing geometry is sized according to the dimensions of the heat pipe. The heat pipes arrangement inside the casing can be aligned, staggered or in-line. An in-line arrangement is selected for this design and, therefore, the process air would flow over each heat pipe in series that assure sufficient contact time and area between the air and heat pipes with minimum number of heat pipes. Therefore, the cooler ducts dimensions are based on the heat pipe geometry and orientation, this means also the heat sink would be in the upper channel, while the lower channel is the heat source. Additionally, the cooler casing is designed accordingly with particular attention to minimise the gaps between the heat pipe fins and casing wall to reduce the possibility of any air escaping without treatment. Fig 4-4 shows the preliminary configuration arrangement of the cooling system with finned heat pipe evaporator in the dry channel and the ceramic tube fitted heat pipe condenser in the wet channel.

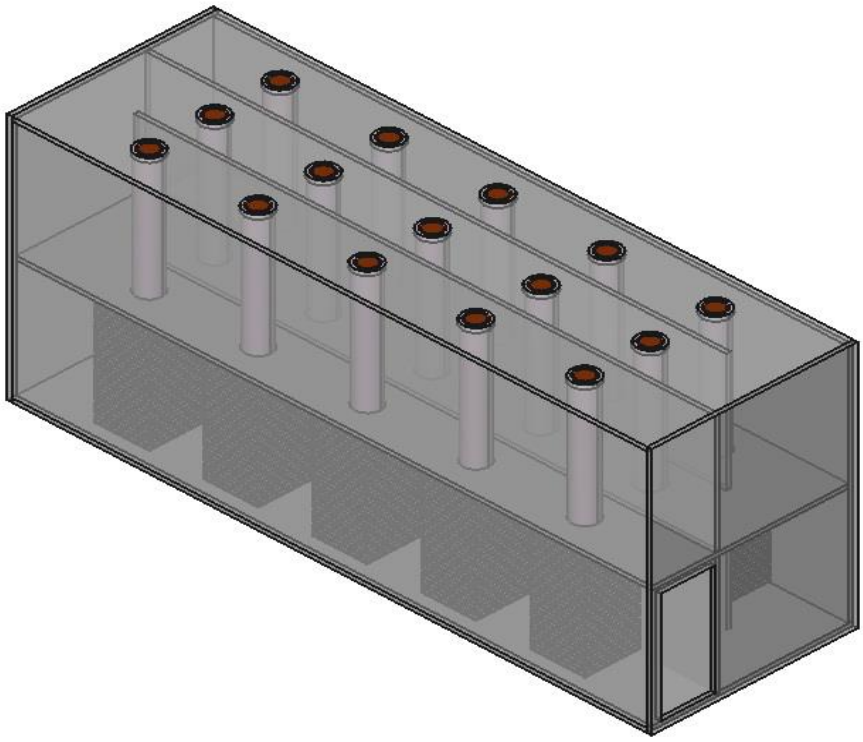


Fig 4-4 3D drawing of the HPHX and ceramic tube based IEC system

4.3 The Mathematical formulation

Theoretical models of IEC rely on the principles of heat and mass transfer processes i.e. energy and mass conservation laws which form a set of ordinary/partial differential equations based on the HMX configuration of a particular IEC system. A mathematical model is developed to simulate the thermal performance and investigate the design parameters of this heat pipe and porous ceramic based R-IEC system.

After understanding the physical of the system, and drawing a schematic sketch of the system, the next step would be making a "list of assumptions" of the physical phenomena under investigation. These assumptions simplify the complex nature of simultaneous heat and mass transfer processes and appropriately alter it to be mathematically modelled to formulate a set governing equations. At this stage, the model development depends on this list as the accuracy of the model and its results may be significantly affected by some of these assumptions. Principally, most simulation models of evaporative coolers share common analysis assumptions which are [117], [74]:

(i) Steady state condition is applied in the process, then $\left(\frac{\partial T}{\partial t} = 0\right)$ in the energy equation, and for the continuity equation $\left(\frac{\partial \rho}{\partial t} = 0\right)$.

(ii) No wall, air and fluid thermal and moisture diffusivity in the flow directions; thus, vapour transport is occurring due to convection only.

(iii) Negligible longitudinal heat transfer in the walls and inside the fluids along flow direction, then $\left(\frac{\partial^2 T}{\partial y^2} + \frac{\partial^2 T}{\partial z^2} = 0\right)$ and $\left(v\frac{\partial T}{\partial y} + w\frac{\partial T}{\partial z} = 0\right)$. Therefore, heat transfer is only in the direction normal to the parallel wall, i.e. one-dimension heat transfer.

(iv) Heat transfer from the device to the surrounding environment is neglected as the system is well insulated i.e. an adiabatic outer surfaces. Additionally, no work or heat source within the control volume of the system, then $(\dot{q} = 0)$.

(v) Constant values of properties, velocities and heat transfer coefficients of the water, air and vapour along the flow direction at each step of the numerical calculation with uniform fluid distribution;

(vi) Water-air interface temperature is equal to the water film temperature;

(vii) Specific heat of moist air $c_{Pa} = c_{Pda} + \omega_a c_{Pv}$;

(viii) Enthalpy of water vapour $i_v = c_{Pv} T_w + i_{fg}$;

(ix) Enthalpy of moist air is expressed as: $i_a = (c_{Pda} + \omega_a c_{Pv}) T_a + \omega_a i_{fg}$

In the model, the domain of interest is divided into "n" elements a cross both the dry- and wet-air channel as shown in Fig 4-5. By considering the "n^{th}" element, as seen in Fig 4-6-a, and applying energy and mass conservation lows, a set of differential governing equations are formulated as explained in the following sections.

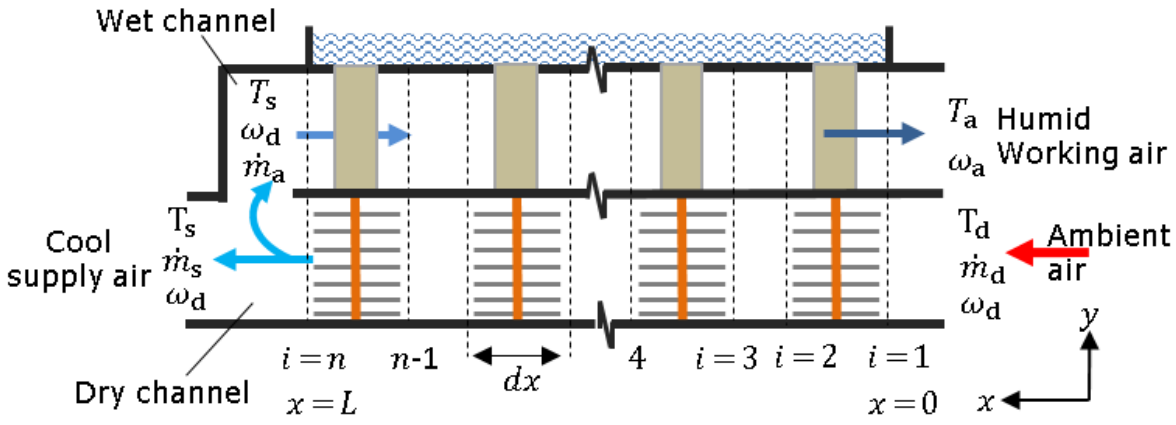


Fig 4-5 Physical model of the system

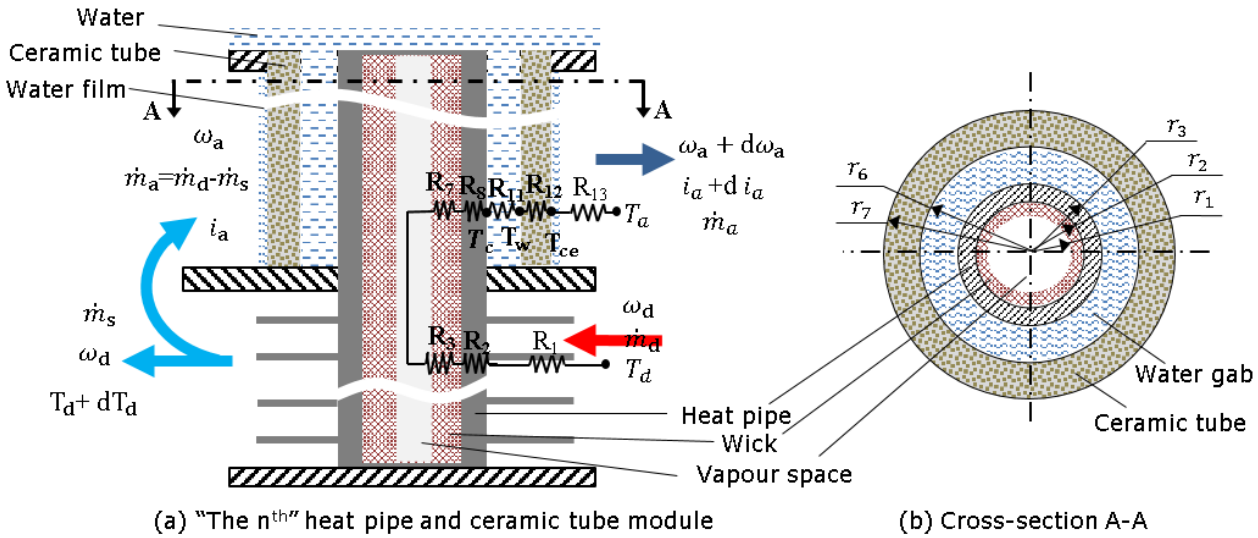


Fig 4-6 Schematic of the heat pipe and ceramic tube module

4.3.1 Energy and mass balance

i. Energy balance of the inlet air in dry channel side

The hot ambient air comes in contact with the finned evaporates of heat pipes as it drawn from outside, the air loses sensible heat to the heat pipes as it flows along the dry-air channel, this can be expressed by the following equation [117].

$$\dot{m}_{\mathrm{d}}\, c_{P,\mathrm{d}}\, dT_{\mathrm{d}} = -\, U_{\mathrm{d}}\, dA\, (\mathrm{T_d} - T_{\mathrm{wf}}) \qquad (4.1)$$

and,

$$\dot{m}_{\mathrm{d}}\, c_{P,\mathrm{d}}\, dT_{\mathrm{d}} = Q_1 \qquad (4.2)$$

where, Q_1 is maximum heat transferred by the heat pipe (W), $\dot{m}_{\mathrm{d}}$ is air flow rate in the dry-air channel (kg/s), $\mathrm{T_d}$ is air temperature in the dry channel (℃), $\mathrm{T_{wf}}$ is water film temperature (℃).

The dry side involved sensible heat transfer between the inlet ambient air and the finned heat pipe, therefore, the heat transfer rate is restricted by limitations of heat transfer of the heat pipe. So, the maximum heat transported by the heat pipe (Q_1) would be the minimum value of heat transfer limitations, it is given as follows [118];

$$Q_1 = min\,(Q_e, Q_c,\, Q_b, Q_s\,, Q_v\,) \qquad (4.3)$$

where,

Entrainment limit: $Q_e = \pi r_1^2 i_v \sqrt{\frac{\rho_v\, \sigma_l}{2\, r_c}}$ (4.5)

Capillary limit: $Q_c = \frac{\rho_l\, i_v\, K\, A_{wk}}{\mu_l\, l_{eff}} \left(\frac{2\sigma_l}{r_c} - \rho_l g l_t \sin\varphi - \rho_l g\, l_t \cos\varphi\right)$ (4.6)

Boiling limit: $Q_b = \frac{4\pi\, l_{eff}\, \lambda_{eff}\, T_v\, \sigma_l}{i_{fg}\, \rho_v\, \ln\frac{r_2}{r_1}} \left(\frac{1}{r_n} - \frac{1}{r_c}\right)$ (4.7)

Sonic limit: $Q_s = A_v\, \rho_v\, i_{fg} \sqrt{\frac{\gamma_v\, R_v\, T_v}{2(1+\gamma_v)}}$ (4.8)

Viscous limit: $Q_v = \frac{A_v\, r_v^2\, \rho_v\, i_{fg}\, P_v}{16\, \mu_v\, l_{eff}}$ (4.9)

where, r_1 is vapour space radius of the heat pipe (m), i_v is latent heat vaporisation of the working liquid (J/kg), σ_l is working liquid surface tension (N/m), r_c is capillary radius of wick surface pores (m), ρ_l is liquid density $(\mathrm{kg/m^3})$, K is wick permeability (m^2), A_{wk} is cross-section area of wick (m^2), g is gravity acceleration (m/s^2), l_t is total length of heat pipe (m), φ is inclination angle of the heat pipe, μ_l is viscosity of the working fluid $(N.s/m^2)$, l_{eff} is effective length of heat pipe (m), ε is wick porosity, λ_{eff} is thermal conductivity of liquid-saturated wick (W/mK), T_v is saturated vapour temperature (K), r_i is the inner radius of heat pipe (m), r_n is nucleation radius (m), A_v is the area of vapour space of the heat pipe, (m^2); R_v is gas constant of vapour $(J/kg\,K)$; P_v is vapour pressure (Pa).

The overall heat transfer coefficient $(\mathrm{U_d})$ between both airstreams equals the inverse of the sum of the total thermal resistances (R_{t1}) between the inlet air and water film on the ceramic surface which include convection thermal resistance in the dry-air channel (R_1), heat pip thermal resistances (R_{HP}), and the thermal resistances of wet-air channel side $(R_{11},\ R_{12})$ as shown in Fig 4-6-a. Section 4.3.2 defines and explains the terms involved in the overall heat transfer coefficient equation which is expressed as;

$$U_{\mathrm{d}} = \frac{1}{\sum R_{t1}} = \frac{1}{R_1 + R_{HP} + R_{11} + R_{12}} \qquad (4.10)$$

ii. Mass balance in the wet-air channel side

Thin water film is formed on the porous tubes surfaces in the wet-air channel, water evaporates as the working air passes over water-saturated porous ceramic tubes. As a result, the working air temperature and moisture content increase along the wet-air channel. The driving force of the vapour mass transfer is expressed by the humidity ratio difference, and the change of vapour mass flow rate is written as follows;

$$\dot{m}_{\mathrm{a}} d\omega_{\mathrm{a}} = h_m\, dA(\omega'_{\mathrm{wf}} - \omega_{\mathrm{a}}) \qquad (4.11)$$

and

$$\dot{m}_{\mathrm{a}} d\omega_{\mathrm{a}} = -d\dot{m}_{\mathrm{wf}} \qquad (4.12)$$

Also, it is assumed the vapour mass flow rate in the wet-air passage is negligible, as its value does have notable effect on the working air flow rate in the wet passage due to very small value of $(\omega'_{\mathrm{wf}} - \omega_{\mathrm{a}})$ in the order 0.01-0.02 [117]; where ω_{a} is moisture content of the moist working air (kg_{wt}/kg_{air}), ω'_{wf} is moisture content of saturated moist air at water film temperature (kg_{wt}/kg_{air}), $\dot{m}_{\mathrm{a}}$ is mass flowrate of moist air (kg/s), h_m is mass transfer coefficient $(kg/m^2\ s)$.

iii. Energy balance in the wet-air channel side

In the wet-air channel, the working air exchanges sensible heat with latent heat of vaporisation from water-soaked ceramic surfaces, this is expressed by the following equation;

$$\dot{m}_{\mathrm{a}} di_{\mathrm{a}} = h_a\ dA(\mathrm{T_{wf}} - T_{\mathrm{a}}) + h_m\ dA(\omega'_{\mathrm{wf}} - \omega_{\mathrm{a}})\ i_{\mathrm{v,wf}} \qquad (4.13)$$

also,

$$h_m = h_a/Le\ c_{pa} \qquad (4.14)$$

and,

$$di_{\mathrm{a}} = c_{\mathrm{Pa}}\ dT_{\mathrm{a}} + \left(c_{P,v}\ T_{\mathrm{a}} + i^0_{\mathrm{fg}}\right) d\omega_{\mathrm{a}} \qquad (4.15)$$

where, $\dot{m}_{\mathrm{a}}$ is moist air mass flow rate in the wet-air channel, i_a is enthalpy of moist air, $\mathrm{h_a}$ is convective heat transfer coefficient in the wet-air channel, $\mathrm{T_{wf}}$ is water film temperature, T_{a} is the moist air temperature, h_m is mass transfer coefficient, ω'_{wf} is saturation air moisture content at water film temperature, ω_{a} is moist air moisture content, $i_{\mathrm{v,ce}}$ is enthalpy of water vapour at temperature of ceramic surface. c_{Pa} is moist air specific heat, $c_{P,v}$ is water vapour specific heat, i^0_{fg} is latent heat of vaporisation of water.

Neglecting the change of the moisture content of the moist working air $(\omega'_{\mathrm{wf}} - \omega_{\mathrm{a}} \approx 0)$ in Eq. (4.13) [117], assuming Lewis Number is equal to unity ($Le \approx 1$ like [75] and [119]) of Eq. (4.14), and, then, substituting Eq. (4.14) and (4.15) into Eq. (4.13). Thus, Eq. (4.13) can be rewritten shortly as

$$\dot{m}_{\mathrm{a}} c_{\mathrm{Pa}} dT_{\mathrm{a}} = h_a\ dA\ (\mathrm{T_{wf}} - T_{\mathrm{a}}) \qquad (4.16)$$

iv. Energy balance of the water film

The energy balance of water film on the ceramic wet surface includes enthalpy change of water film, heat transfer rate from the dry-air passage, energy transported by convection and evaporation from water film. This is expressed as follows,

$$\dot{m}_{\mathrm{wf}}\, di_{\mathrm{wf}} = U_{\mathrm{d}}\, dA(\mathrm{T_d} - T_{\mathrm{w}}) - h_{\mathrm{m}}\, dA(\omega'_{\mathrm{wf}} - \omega_{\mathrm{a}})\left(i_{\mathrm{v,wt}} - i_{\mathrm{l,wt}}\right) - h_a\, dA(\mathrm{T_{wf}} - T_{\mathrm{a}}) \qquad (4.17)$$

$$\dot{m}_{\mathrm{wf}}\, c_{\mathrm{p,wf}}\, dT_{\mathrm{wf}} = U_{\mathrm{d}}\, A(\mathrm{T_d} - T_{\mathrm{w}}) - h_{\mathrm{m}}\, dA(\omega'_{\mathrm{wf}} - \omega_{\mathrm{a}})\, i_{\mathrm{fg,wf}} - h_a A(\mathrm{T_{wf}} - T_{\mathrm{a}}) \qquad (4.18)$$

where, $\dot{\mathrm{m}}_{\mathrm{wf}}$ is feed water mass flow rate, $\mathrm{c_{p,wf}}$ is the specific heat of water film, i_{wf} is enthalpy of water film, $\mathrm{T_{ce}}$ is ceramic surface temperature, $\mathrm{T_w}$ is water temperature.

As the water film over the ceramic surface is a very thin layer, therefore, the temperature difference between the porous ceramic and water film is negligible i.e. $\mathrm{T_{ce}} = T_{\mathrm{wf}}$ [102].

4.3.2 Thermal resistances

To solve energy equation in the dry-air channel, the thermal resistances of the heat pipe should be determined in order to estimate the overall heat transfer coefficient (U_{d}) and analysis heat transfer capacity of the heat pipe. Fig 4-6 illustrates the thermal resistance network of the heat pipe and ceramic tube module. The overall heat transfer coefficient between the inlet air stream in the dry-air passage and the water water-saturated ceramic surface in the wet-air passage is expressed as follows,

$$U_{\mathrm{d}} = \frac{1}{R_1 + R_{HP} + R_{11} + R_{12}} = \frac{1}{R_1 + R_2 + R_3 + R_7 + R_8 + R_{11} + R_{12}} \qquad (4.19)$$

$$U_{\mathrm{d}} = \left(\frac{1}{h_{\mathrm{d}} \eta_o A_1} + \frac{ln(r_3/r_2)}{2\pi l_e \lambda_e} + \frac{ln(r_2/r_1)}{2\pi l_e \lambda_{wk}} + \frac{ln(r_2/r_1)}{2\pi l_c \lambda_{wk}} + \frac{ln(r_3/r_2)}{2\pi l_c \lambda_c} + \frac{ln(r_6/r_3)}{2\pi l_c \lambda_{\mathrm{wt}}} + \frac{ln\left(\frac{r_7}{r_6}\right)}{2\pi\, l_{ce}\, \lambda_{w,ce}} \right)^{-1} \qquad (4.20)$$

where, $h_{\mathrm{d}}$is the convective heat transfer coefficient in the dry-air passage, A_1 is the total area of heat transfer of the finned heat pipe includes the area of exposed surface of the heat pipe plus the area of fins; η_o is the overall surface efficiency of the fin.

It worth explaining that the thermal resistance of the heat pipe adopted in this design is based on simplified resistance network suggested by [118]. The original form of heat pipe thermal resistance ($R_{\mathrm{HP,original}}$) is inferred from Fig 4-7-a, and given by the following equation;

$$R_{\mathrm{HP,original}} = R_2 + R_3 + \frac{1}{\frac{1}{(R_4+R_5+R_6)} + \frac{1}{R_9} + \frac{1}{R_{10}}} + R_7 + R_8 \qquad (4.21)$$

where, R_2 is conductive resistance of the evaporator wall (m^2K/W), R_3 is conductive resistance of the evaporator wick structure (m^2K/W), R_4 is liquid-vapour interface resistance at the evaporator (m^2K/W); R_5 is vapour space resistance (m^2K/W); R_6 is liquid-vapour interface resistance at the condenser (m^2K/W); R_7 is the conductive resistance of the condenser wick (m^2K/W), R_8 is the conductive resistance of condenser wall (m^2K/W); R_9 is axial conduction resistance of the adiabatic section wall (m^2K/W), R_{10} is axial resistance of the saturated wick structure at the adiabatic section(m^2K/W).

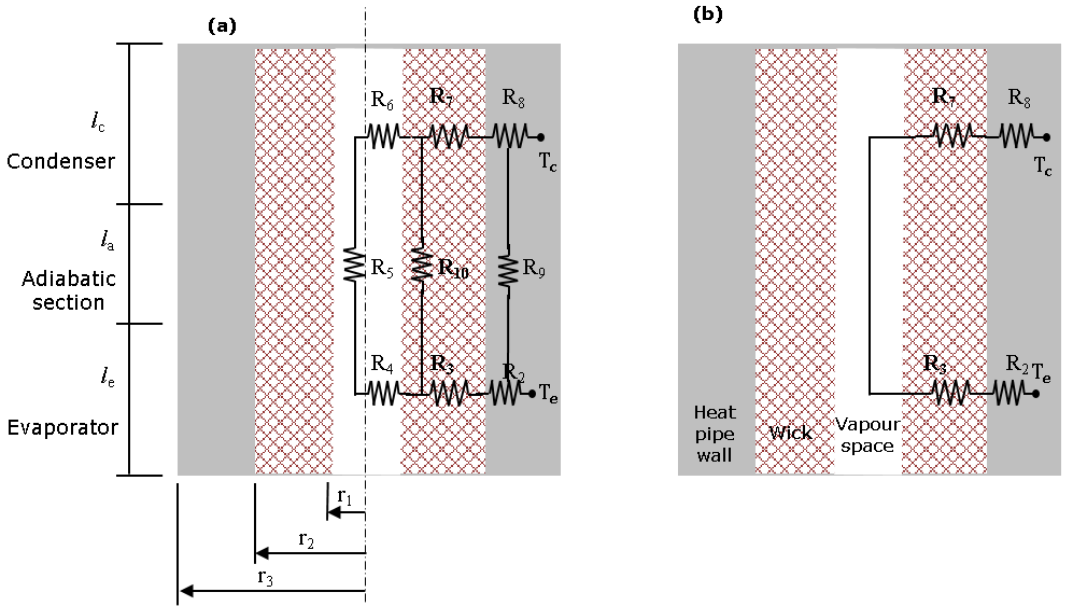


Fig 4-7 Heat pipe thermal resistances; (a) original circuit, (b) simplified circuit [118]

Since some the thermal resistance of heat pipe internal components can be omitted, these resistance are R_9 and R_{10} because of their large values and being connected in parallel in the thermal circuit. Also, the resistances R_4, $R_5$and R_6 have very small values and are in series.

Therefore the value of the term $\left(\frac{1}{\frac{1}{(R_4+R_5+R_6)}+\frac{1}{R_9}+\frac{1}{R_{10}}}\right)$ becomes trivial, in the order of 0.0001 and can be neglected. Accordingly, Eq. (4.21) is reduced to Eq. (4.22),

$$R_{\mathrm{HP}} = R_2 + R_3 + R_7 + R_8 \qquad (4.22)$$

The thermal resistances involved overall heat transfer coefficient, Eq. (4.19), are defined as follows;

- R_1: Convective heat transfer resistance in the dry-air channel of Heat pipe evaporator external surface

$$R_1 = \frac{1}{h_{\mathrm{d}}\eta_o A_1} \qquad (4.23)$$

where, A_1 is the total area of heat transfer of the finned heat pipe includes the area of exposed surface of the evaporative plus the area of fins which can be expressed as follows;

$$A_1 = A_b + N_{fin}\, A_{fin} \qquad (4.24)$$

and,

$$A_b = 2\pi r_3 l_e - N_{fin}\left(t_{fin} * d_3\right) \qquad (4.25)$$

$$A_{fin,rectan} = 2\left(l_{fin}\, \mathrm{w}_{fin} - \pi {r_3}^2\right) + 2\left(l_{fin} + \mathrm{w}_{fin}\right)t_{fin} \qquad (4.26)$$

where, A_b is the base area of heat pipe evaporator, A_{fin} is the surface area of fin, N_{fin} is number of fins on evaporator of heat pipe,

In this study, rectangular fin is used due to the compatibility with the ducts cross section. Yet, finding the fin efficiency of square fins is not straightforward because there is no chart available for such fin geometry. Therefore, an equivalent circular fin with equivalent radius is used to replace the actual square fin, using Eq. (4.27). Then, the calculation can be completed using graphs of the circular fin to determine fin efficiency, as shown in Fig 4-8.

$$r_{eq} = \frac{l_{fin}}{\sqrt{\pi}} \tag{4.27}$$

Nevertheless, this approximation might be one of the sources of discrepancy between calculated and measured results, but, this method of finding the efficiency of a square fin is approved by [118].

Circular fin of uniform rectangular cross section, the surface area is

$$A_{fin,circ} = 2\pi\left({r_{fin}}^2 - {r_3}^2\right) + 2\pi r_3 t_{fin} \tag{4.28}$$

Thus, the total area of a finned heat pipe is;

$$A_1 = A_b + A_{f,circ} = 2\pi r_3 l_e - N_{fin}\left(t_{fin} * d_3\right) + 2N_{fin}\left(2\pi\left({r_{eq}}^2 - {r_3}^2\right) + 2\pi r_3 t_{fin}\right) \tag{4.29}$$

where, r_3 is outer radius of heat pipe (m), l_e is evaporator length of heat pipe (m), N_{fin} is number of fins, t_{fin} is thickness of fin (m), d_3 is outer diameter of heat pipe (m), l_{fin} is length of fin (m), w_{fin} is width of fin (m), η_o is overall surface efficiency which is the ratio of the total heat transfer to the maximum heat transfer by the finned surface. It can be expressed as follows;

$$\eta_o = 1 - N_{\text{fin}}\frac{A_{\text{fin}}}{A_1}(1 - \eta_{\text{fin}}) \tag{4.30}$$

Note that the thermal contact resistance is neglected in the Eq. (4.31), it might present in the thermal resistance network when the fins are mechanically fitted to the heat pipe vessel [35]. And η_{fin} is the fin efficiency which is determined from Fig 4-8, based on the type and geometry of the fin.

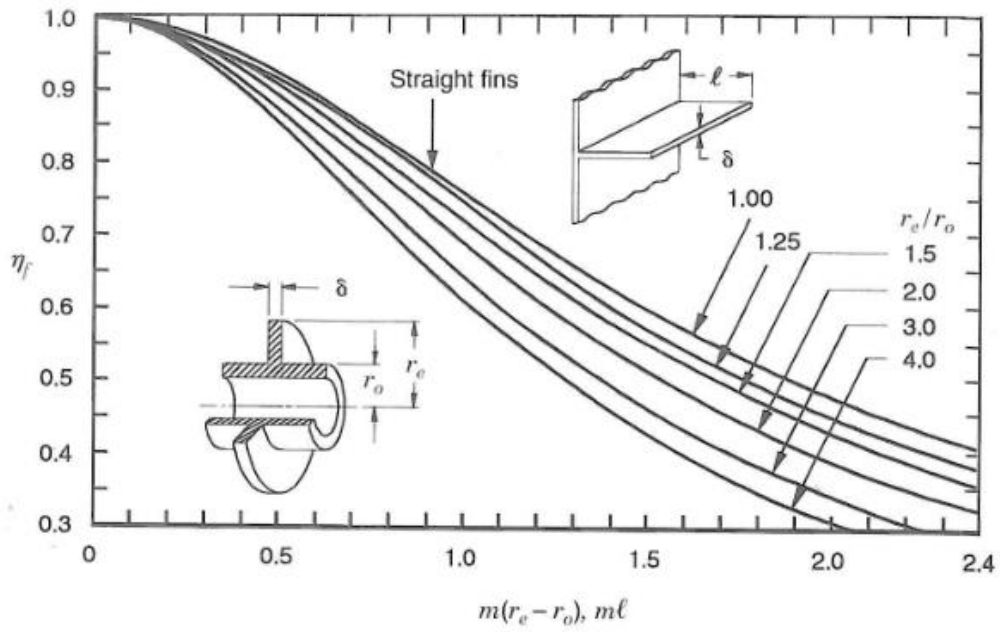


Fig 4-8 Efficiencies of circular and straight fins [118]

- R_2 : Conductive thermal resistance of the evaporator external wall.

$$R_2 = \frac{ln\left(\frac{r_3}{r_2}\right)}{2\pi l_e \lambda_e} \tag{4.31}$$

where, $r_2$is the inner radius of heat pipe evaporator (m), l_e is the evaporator length (m), λ_e is the thermal conductivity of the evaporator external wall (W/mK).

- R_3 : Conductive resistance of the evaporator wick structure.

$$R_3 = \frac{ln\left(\frac{r_2}{r_1}\right)}{2\pi l_e \lambda_{wk}} \tag{4.32}$$

where, $r_1$is the vapour space radius of heat pipe (m), λ_{wk} is the thermal conductivity of the wick structure of the heat pipe (W/mK). In this research, the wick type is wire mesh. The thermal conductivity of the mesh can be calculated from equations based on mesh type, provided by [120]. For wire mesh type, the thermal conductivity of the water-saturated wick of the evaporator (λ_{wk}) can be determined by the equation below,

$$\lambda_{wk} = \frac{\lambda_{\mathrm{wt}}[\lambda_{\mathrm{wt}} + \lambda_{\mathrm{m}} - (1-\epsilon)(\lambda_{\mathrm{m}} - \lambda_{\mathrm{m}})]}{\lambda_{\mathrm{wt}} + \lambda_{\mathrm{m}} - (1+\epsilon)(\lambda_{\mathrm{m}} - \lambda_{\mathrm{m}})} \tag{4.33}$$

and,

$$\epsilon = 1 - \frac{\pi\, N_{wk}\, d_{wk}}{4} \tag{4.34}$$

where, λ_{wt} is the heat pipe working fluid (water) thermal conductivity, λ_{m} is the thermal conductivity of wick material, ϵ is the wick porosity which also calculated based on the wick type and specification, N_{wk} is the number of mesh wires per 1 inch of mesh, $d_{wk}$is the wire diameter of the mesh (in).

- R_7 : Conductive resistance of heat pipe wick structure of the condenser

$$R_7 = \frac{ln\left(\frac{r_2}{r_1}\right)}{2\pi l_c\, \lambda_{wk}} \tag{4.35}$$

- R_8 : Conductive resistance of heat pipe wall of the condenser

$$R_8 = \frac{ln\left(\frac{r_3}{r_2}\right)}{2\pi l_c \lambda_c} \tag{4.36}$$

- R_{11} : Water conductive resistance

$$R_{11} = \frac{ln\left(\frac{r_6}{r_3}\right)}{2\pi l_c \lambda_{\mathrm{wt}}} \tag{4.37}$$

where, l_c is the length of the condenser (m), r_6 is the inner radius of the porous ceramic tube (m), λ_{wt} is the water thermal conductivity ($W/m\,K$).

- R_{12} : Ceramic tube conductive resistance

$$R_{12} = \frac{ln\left(\frac{r_7}{r_6}\right)}{2\pi\, l_{ce}\, \lambda_{w,ce}} \tag{4.38}$$

$$\lambda_{\mathrm{w,ce}} = \frac{\lambda_{\mathrm{wt}}[\lambda_{\mathrm{wt}} + \lambda_{\mathrm{ce}} - (1-\epsilon_{\mathrm{ce}})(\lambda_{\mathrm{wt}} - \lambda_{\mathrm{ce}})]}{\lambda_{\mathrm{wt}} + \lambda_{\mathrm{ce}} - (1+\epsilon_{\mathrm{ce}})(\lambda_{\mathrm{wt}} - \lambda_{\mathrm{ce}})} \tag{4.39}$$

Where, $\lambda_{\mathrm{w,ce}}$ is the thermal conductivity of the water-soaked ceramic tube ($W/m\,K$), r_7 is the outer radius of the ceramic tube (m), λ_{ce} is the thermal conductivity of the ceramic material ($W/m\,K$), ϵ_{ce} is the porosity of the ceramic material.

- R_{13} :Convective resistance in the wet channel between ceramic tube and moist air

$$R_{13} = \frac{1}{h_a\, A_{ce}} \qquad (4.40)$$

where, h_a is the convective heat transfer coefficient in the wet-air channel ($W/m^2\,K$), $A_{ce}$is the surface are of the ceramic tube (m^2).

4.3.3 Heat transfer coefficients

- **Heat-transfer coefficient in the dry-air channel**

The flow in the dry-air side is turbulent and heat transfers by forced convection over the finned heat pipe evaporators. For such configuration, the average Nusselt number of fully developed flow over finned tube can be correlated using the following equation [50].

$$Nu_1 = c_1\, {Re_1}^{c_2}\, Pr_1^{1/3} \qquad (4.41)$$

and

$$Re_1 = \frac{\rho V_d D_H}{\mu} = \frac{V_d D_H}{\nu} = \frac{V_d * 2r_3}{\nu} \qquad (4.42)$$

Where c_1 and c_2 are constant and their values related to the fin geometry, V_d is inlet air velocity, ρ is air density, D_H is hydraulic diameter, μ is the dynamic viscosity, Re and Pr are Reynolds and Prandtl numbers, respectively.

Another correlation can be used, based on the outer diameter of the heat pipe and fin geometry. The equation is restricted for $0.125 < (F_P/F_H) < 0.610$ and $4.5 < \left(F_P/t_{fin}\right) < 8.0$ [121]

$$Nu_d = 0.134\, {Re_1}^{0.681}\ \ Pr_1^{1/3} \left(\frac{F_P}{F_H}\right)^{0.2}\ \ \left(\frac{F_P}{t_{fin}}\right)^{0.113} \qquad (4.43)$$

Thus, the average local heat transfer coefficient can be defined as

$$h_d = \frac{Nu_d}{\frac{2\, r_3}{\lambda_d}} \qquad (4.44)$$

where, $\left(\frac{F_P}{F_H}\right)$ is ratio of the fin pitch to the fin height, $\left(\frac{F_P}{t_{fin}}\right)$ is ratio of the fin pitch to the fin thickness, λ_d is thermal conductivity of air in the dry-air channel.

- **Heat transfer coefficient in the wet-air channel**

The moist air in the wet-air channel flow over the short cylindrical water-saturated tubes. The average local heat transfer coefficient can be determined as follows [122];

$$h_a = \frac{Nu_a}{\frac{2\, r_7}{\lambda_a}} \qquad (4.45)$$

The average local Nusselt number can be defined as function of Reynolds number and cylinder dimensions.

$$Nu_a = 0.123\, {Re_a}^{0.651} + 0.00416 \left(\frac{l_{ce}}{d_7}\right)^{-0.85}\ Re^{0.792} \qquad (4.46)$$

$$7.0 \times 10^3 \leq Re \leq 2.3 \times 10^5 \qquad (4.46\ a)$$

$$1.0 \leq \frac{l_{ce}}{d_7} \leq 7.0 \qquad (4.46\ b)$$

and,

$$Re_a = \frac{\rho V_a D_H}{\mu} = \frac{V_a D_H}{\nu} = \frac{V_a * 2r_7}{\nu} \qquad (4.46\ c)$$

where, Re_a is Reynolds number in the wet-air channel, $\frac{l_{ce}}{d_7}$ is length-to-diameter ratio of the porous tube, V_a is air velocity in the wet-air channel, r_7 is outer radius of the porous tube.

4.4 Computer model

The numerical solution of the governing equations involves derivation of a discrete set of equations and a technique for their solution. Numerical methods provide values of the variables at a discrete number of points in the system domain by employing discretisation process, and, then, determining values of the required variables at each assigned grid points. Accordingly, the physical system is divided into (n) number of differential elements across both the dry- and wet-air channel, as schematically shown in Fig 4-5. Then, the governing differential equations (4.1), (4.11), (4.16), and (4.18) are converted into a set of discrete algebraic equations. The finite difference method with Newton iterative process are used for solution, a computer code using MATLAB programming language was developed for this purpose, as presented in Appendix A. Furthermore, a group of initial and boundary conditions are required for solution, which are given as follows;

- at the inlet of the dry-air channel of the cooler, $x = 0$ and $i = 1$

$$T_d|_{x=0} = T_{in} \text{ and } \omega_d|_{x=0} = \omega_{in}$$

- at the inlet of the wet-air channel which have the same conditions of dry-air channel exit ($x = L$ and $i = n$) of the temperature and moisture content of the supply air,

$$T_d|_{x=L} = T_s \ , \ \omega_d|_{x=L} = \omega_s = \omega_{in}$$

$$T_a|_{x=L} = T_s \ , \ \omega_a|_{x=L} = \omega_d|_{x=L} = \omega_{in}$$

$$\text{and } \dot{m}_a = \dot{m}_d - \dot{m}_s$$

where subscripts "d" refers to inlet air and dry air channel, "a" refers to working air and wet air channel, and "s" refers to supply air.

The overall solution loop for the simulation is illustrated by the computer algorithm presented in Fig 4-9. This algorithm and the iteration process are explained as follows:

1. Given system specifications, air constants, heat pipe specifications, inlet air velocity, and ambient air conditions;

2. Calculate heat pipe heat transfer limitations, thermal resistances, heat transfer and mass transfer coefficients;
3. Initialising values at inlet of the dry-air channel of inlet air temperature T_d , working air temperature T_a, and water temperature T_w, to be equal the prevailing ambient inlet air conditions.
   - Set-up a counter for the differential elements ($i = i + 1$) to the "nth" element,
   - For the first iterative loop J=1, repeat the initial values of (T_d, T_a, T_w) for all control volumes from $i = 1\ to\ n$;
4. Initialising values at exit of the dry-air channel i.e. the inlet of wet-air channel $(i = n)$ of air temperature T_d, and vapour content ω_a to be equal to the aforementioned boundary conditions;
5. Use a counter for the iteration process (J=J+1) to "m" iterations,
6. Calculate parameters (T_d, T_a, T_w, ω_a, $\dot{m}_w$) starting from differential element $i = 1$ till "n-1" element, this for iteration process number (J=J+1),
7. Check for convergence between two consecutive iterations $\left(\left|T_{d(N,J-1)} - T_{d(N,J)}\right| <= 0.01\right)$. If converged, continue. Else go to 5, and assume water temperature of the next iteration process equals water temperature of previous iteration one for the "nth" differential element.
8. Calculate WB and DP effectiveness, cooling capacity, COP, and plot air temperatures profiles along the cooler channels;
9. End programme.

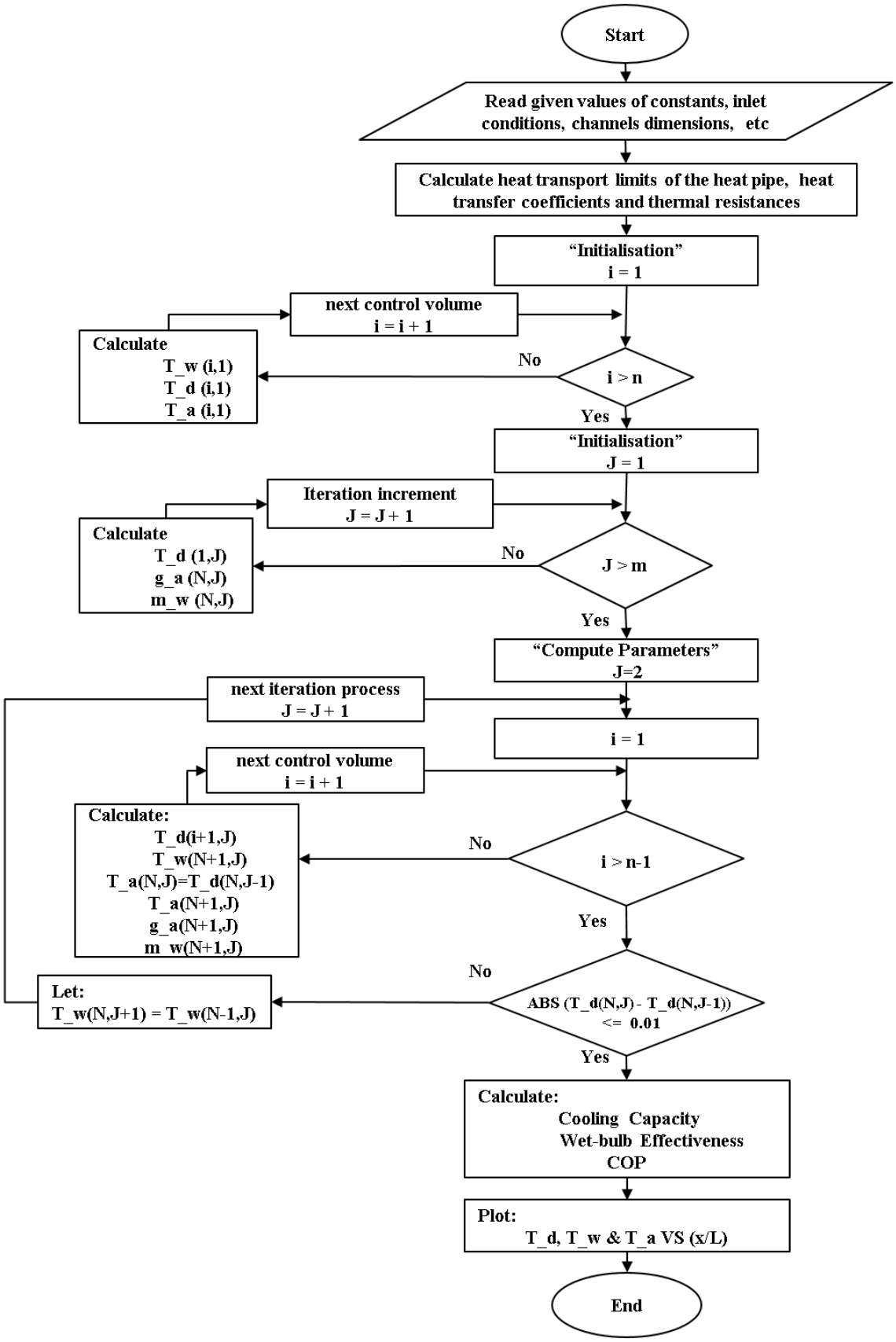


Fig 4-9 Computer model flowchart

4.5 Computer model results

Multiple computer model runs were carried out to investigate the performance of the cooling system and evaluate the effect of geometrical parameters such as channels dimensions, heat pipes numbers, ceramic tube diameter and wall thickness, and wettability factor. Though the computer model was run for selected operating conditions, the parameter under investigation is varied for specific range, while other parameters are set to the pre-set conditions presented in Table 4-1.

Table 4-1 Pre-set conditions of the computer model

Parameter	value	unit
Inlet air temperature	40	℃
Inlet air Relative humidity	35	%
Inlet air wet bulb temperature	26.51	℃
Inlet air velocity	2	m/s
Working-to-inlet air ratio	50	%
Feed water temperature	23	℃
Number of heat pipe rows	14	-
Inner diameter of ceramic tube	0.024	m
Outer diameter of ceramic tube	0.028	m

4.5.1 Effect of channels dimensions

The general configuration of the cooling unit is controlled by and subject to the geometry of the heat pipe, the system casing was built around and according to the dimensions of the heat pipe. The dimensions of the dry-air passage (the bottom channel) is constrained by the dimensions of the finned evaporator i.e. the fin dimensions (width*length). The gap between the external wall and the fins designed to be small to reduce the amount of air escaping without contacting with the fins, and, therefore, eliminate any unfavourable thermal heat conduction issues between the fins and unit outer walls. Similarly, the upper channel (wet-air channel) should be with the same width as the lower channel for the easiness of the fabrication and assembly process of the cooler casing. As a result there is no direct effect of the channel dimensions on the performance of the cooler since the channel dimensions and cross-section area are not related to the heat transfer area of this cooler, as seen from the governing heat and mass transfer equations. The net heat transfer area is represented by the total area of heat transfer of the finned heat pipe includes the area of exposed surface of the heat pipe plus the area of fins. The indirect impact of the channel

dimensions might be limited to the heat transfer coefficient inside the air passages, their values may vary as the channels and the diameter of ceramic tubes change.

4.5.2 Effect of ceramic tube inner and outer diameter

In the numerical model, the tube thickness was kept constant while the inner radius of the ceramic tube was varied from 11 to 16 mm, and other parameters were fixed to their pre-set values presented in Table 4-1. The influence of varying the inner diameter on the supply air temperature and the WB effectiveness is presented in Fig 4-10, it is found that the best results are related to small values of inner radius, such trend can justified by the increase of the thermal resistance (R_{11}), Eq. (4.38), as the inner radius (r_6) increases which results in a decline of the heat transfer rates of the heat pipe. Furthermore, large outer dimensions of the cylinder would effect on the flow pattern as well as convective heat transfer coefficient, this research point can be considered for future study.

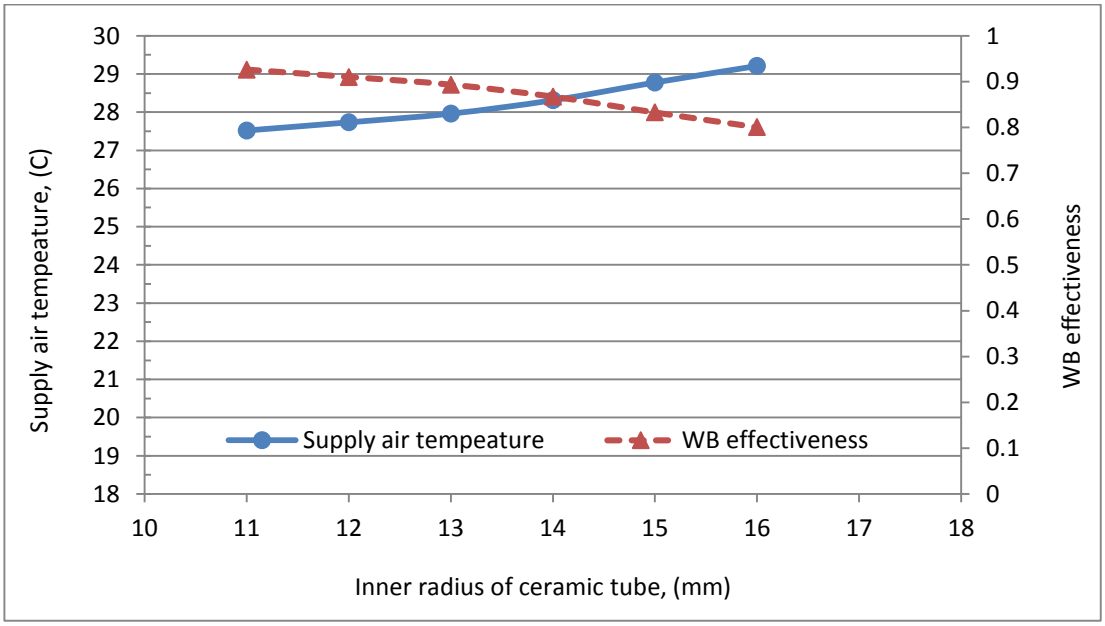


Fig 4-10 Effect of increasing inner radius of ceramic tube on supply temperature and WB effectiveness at inlet conditions of 40 ℃, 35% RH, 2 m/s, and 50% flow rate ratio

These findings comply well with experimental results from [51] who demonstrated that the cooler's effectiveness decrease with increasing the internal and external radius of the ceramic tube. As a result, 12 mm of the inner radius was selected for ceramic tubes. So, a 3

mm gab between the heat pipe condenser and ceramic tube is considered to provide sufficient amount of water to evenly cover the condenser entirely.

4.5.3 Effect of thickness of ceramic tube wall

The direct effect of the wall thickness of the porous cylinders was on the value of the conductive thermal resistance of the wall. As it be seen from Eq. (4.38) and Fig 4-11, both parameters are directly proportional. Consequently high thermal resistance of the tube wall limits the heat transport rate from the condenser side to the air side. Accordingly, the thickness is kept to the minimal value that is consent with materials strength requirements, and maintain sufficient water-retaining characteristic of the ceramic materials.

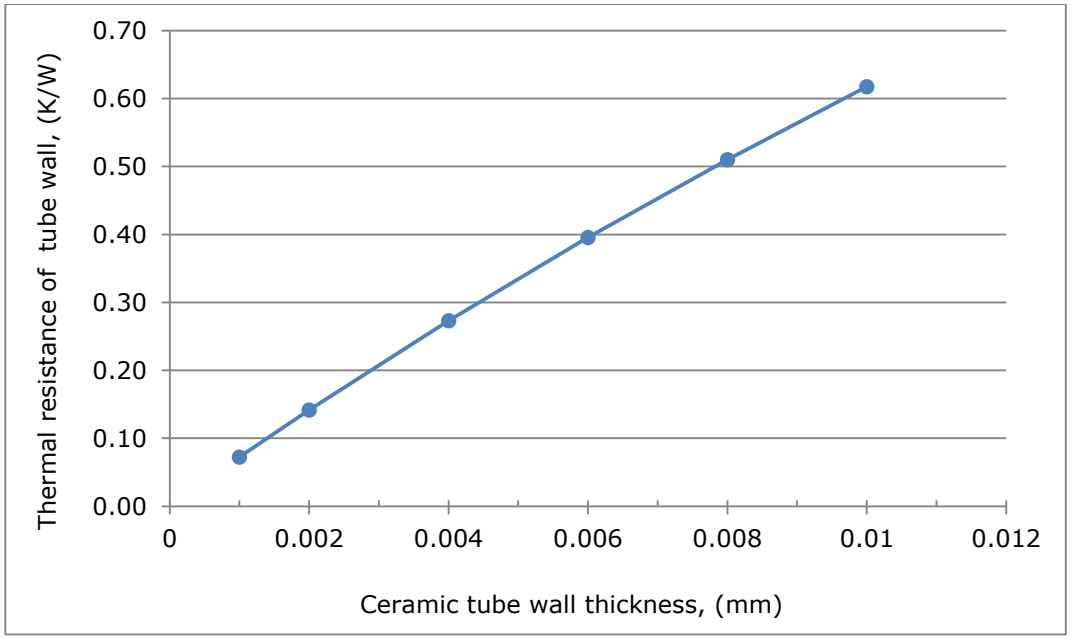


Fig 4-11 Thermal resistance of ceramic tube versus tube wall thickness

4.5.4 Effect of wettability and contact factors

The use of water-filled ceramic tubes as heat dissipation mechanism of this cooler assured sufficient water distribution and complete wettability for the condenser, therefore, a 3mm water jacket is formed evenly around the outer surface of the condenser. So, this design guaranteed 100% wettability i.e. the wettability factor equals to unity. However, the outer surface of the ceramic tube might suffer from insufficient contact between the water film

and working air due to existence of the eddy currents. In other words, the air flow type and pattern might influence the evaporation process by affecting on the total area of water film on the water-saturated ceramic tube. As a result, part of the wetted-ceramic tube area is not in-contact with the working air for evaporation process. To avoid this, a distance of $4d_{ce}$ is considered between cylindrical tubes to minimise the effects of eddy currents and improve heat transfer rate from each porous tube which have been found to be adversely influenced by small distance between cylinders [123]. In addition, the wettability factor of this design is expected to equal 1. In contrast, for plate-type HMX based IEC system, a study showed that the wettability factor should be considered for such configuration, and value of 0.7-0.9 was recommended of the wettability factor [33].

4.5.5 Effect of water film and feed-water rates

Theoretically, water film is anticipated to be thin and evenly covering the porous ceramic tube, based on the physical properties of the ceramic materials and their sufficient water wettability characteristics [102]. Nevertheless, excessive water flow rates might occur which have an effect on heat and mass transfer process due to increase of water film thickness. A proper selection of ceramic porosity tackles this problem, where low porosity ceramic maintains water within the ceramic tube with sufficient water-film formation over the ceramic outer surface. Furthermore, insufficient formation of water film is unlikely to happen because of the good absorption properties and water-retaining abilities of the ceramic material, unless inadequate feed-water rates were supplied which cause dry-out spots on the ceramic tube surface, this would directly effect on the performance of the heat pipe as well as the whole cooling system. Therefore, the water tank was designed to be located on the top of the cooler and to directly feed the ceramic tubes with water.

4.5.6 Effect of number of heat pipes

As the heat pipe being the heat transfer element for the HPHX, it is important to specify how many rows of heat pipes are required for a particular cooling application under certain climate and operational conditions. Using the developed computer simulation, the heat pipe

number of rows was varied from 5-20, while other inlet operation parameter were fixed at their pre-set values shown in Table 4-1. The effect of number heat pipe rows on the WB effectiveness and the supply air temperature of the cooling unit is presented in Fig 4-12. The WB effectiveness steadily increased with the increase of the numbers of heat pips till 14-heat-pipe, after that it slowly rises as the heat pipe number increases above 16-heat-pipe. Similarly, the supply air temperature remarkably drops from 34.72 to 27.08 ℃ as the rows of heat pipes increases from 5 to 15-heat-pipes, whereas the supply air temperature drops by only 1 ℃ as the heat pipe rows rises from 16 to 20. It can be noted that after heat pipe number 15, there was little improvement of the cooler effectiveness comparing to the added numbers of rows, and their associated costs. Therefore, it was decided to keep the number heat pipe rows of the cooling system at 15 units only based on the effectiveness profile, and from economic point of view.

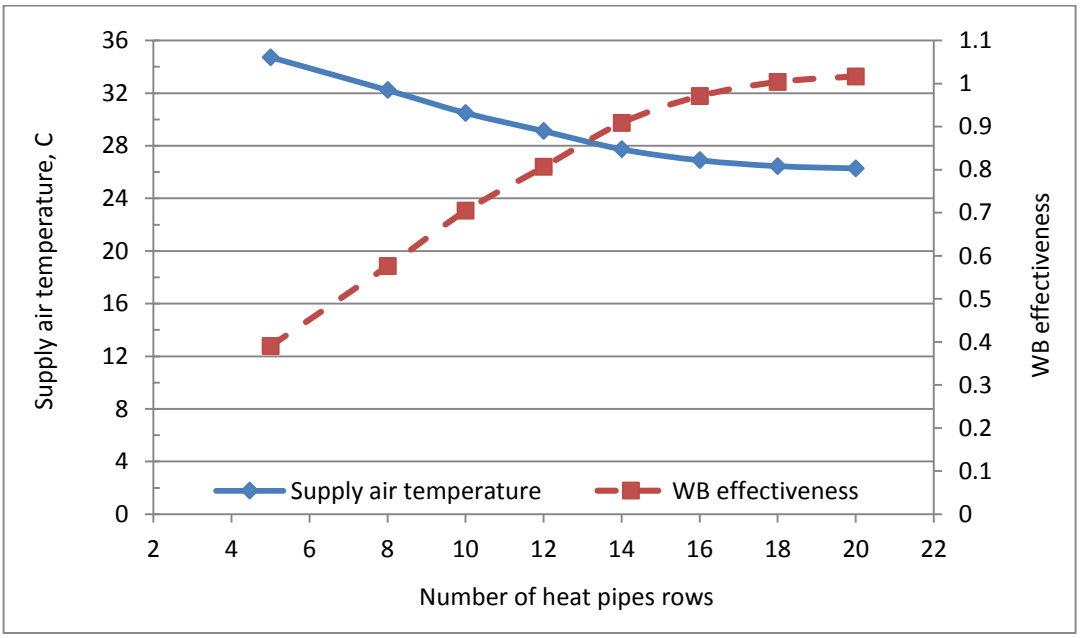


Fig 4-12 Effect of number of heat pipes on the effectiveness and temperature at inlet conditions of 40 ℃, 35% RH, 2 m/s, 23 ℃ water temperature and 50% flow rate ratio

4.5.7 Preliminary computer model results of the cooler performance

The developed simulation was used to predict the performance of the cooling system at for varying inlet ambient conditions of 30, 35, 40, and 45°C with relative humidity of 20, 25, 30, 32% respectively, but at fixed operational conditions of 18 ℃ water temperature, 50%

flow ratio, and 15 heat pipes used. Table 4-2 shows the thermal performance parameters of the proposed sub WBT cooling system at four different inlet flow rates of 60-125 m^3/h.

Table 4-2 Thermal performance parameters of the cooling system

inlet air flow rate (m^3/h)	125	100	75	60
Temperature of inlet air (℃)	30	35	40	45
Wet bulb temperature of inlet air (℃)	15.7	20.23	25.09	29.34
Relative humidity of the inlet air (%)	20%	25%	30%	32%
Supply air flow rate (m^3/s)	0.01716	0.01364	0.00966	0.0079
Supply air temperature (℃)	19.82	23.06	25.59	27.61
Supply air relative humidity (%)	40%	52%	67%	83%
Inlet air temperature reduction (℃)	10.17	11.94	14.4	17.39
Wet-bulb effectiveness	0.712	0.808	0.966	1.11
Cooling capacity (W)	202.56	188.80	161.44	159.35
Coefficient of performance (COP)	6.33	9.14	13.80	17.02
Water consumption rate (l/h)	0.1973	0.2127	0.2260	0.2482

For ambient air conditions of 30-45 ℃ and 20-32% relative humidity, the cooler dropped the inlet air temperature by 10-17.5 ℃. Additionally, of the cooler WB effectiveness was about 0.71 at flow rate of 125 m^3/h, and 1.11 at 60 m^3/h with a respective cooling output of 202 and 160 W. Whereas, the COP ranged from 6 to 17. In regard with water consumption rates, it was in the range of 0.785-1.557 l per 1 kW/h cooling output of the system.

For further evaluation of the performance of this cooling system in terms of meeting the recommended indoor comfort requirements, Typical summer indoor comfort is around 25 ℃ and 50-60% relative humidity, according to ASHRAE 55 [124]. Fig 4-13 presents the supply air temperature and relative humidity profiles versus wide range of inlet air conditions. From the graph, the supply air temperatures ranged from 19.82-27.61 ℃ with humidity of 40-83%, respectively. Also, it is found the cooling system was able to supply air within the recommended levels of comfort as long as the ambient air is below 40 ℃ with relative humidity less than 30%. As the climate condition become hotter i.e. 45 ℃ and 32 % relative humidity, the cooler was considerably able to cool the air by 17.4 ℃, yet the supply air temperature was above the summer comfort standards of 25 ℃ by 2.61 ℃. However, reducing the inlet air flow rate or/and increasing the working-to-inlet air flow ratio can improve the cooling effectiveness of the cooler for extreme hot ambient air conditions.

Therefore, the effect of these operational parameters and others are subject to a parametric study in chapter 6, for further investigation of their impact on the cooler performance.

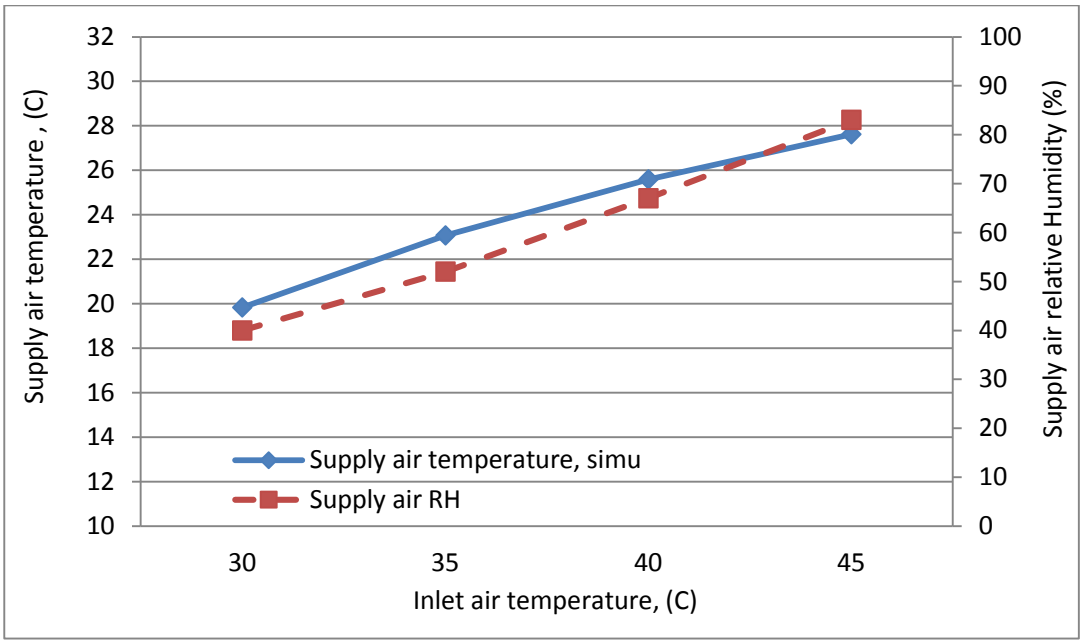


Fig 4-13 Supply air temperature and relative humidity profiles as function of inlet air temperature at inlet conditions of 20-35%RH, 60-125 m^3/h rates, 18 ^oC water temperature, and 50% flow ratio

4.6 Summary

In this chapter, the thermal design and fundamental requirement of the proposed system were discussed. Additionally, a mathematical model was developed to simulate the simultaneous heat and mass transfer process of the cooler. This implies explanation and justification of system components such as the choice of heat pipes type, material, wick structure; and heat pipe numbers; and selection of ceramic tube dimensions. Furthermore, the formulation of computer model is presented which include identification of main energy and mass balance equations, determination of the thermal resistance and heat transfer coefficient, and calculation of heat pipe heat transfer limitations.

Preliminary simulation results of the performance parameters were presented for wide range of working conditions. In addition, the effects of the ceramic tube dimensions, heat pipes numbers, and wettability factor on the cooler performance were discussed. The numerical results show that the cooling system can cool the inlet air up to 17.5^oC, with

cooling capacity ranging 160-203W. Equally, the wet bulb effectiveness of the cooler reached 1.11. Additionally, it was found that thermal performance of the cooler decreases as the inner diameter and the thickness of the porous cylinder increase.

Chapter 5: Construction and experimental investigations

5.1 Prototype construction

The construction of a small-scale prototype sub WBT evaporative cooler was completed to demonstrate the working concept and evaluate the thermal performance. The prototype is made of an outer shell that delimits the air flow channels, cylindrical heat pipes with finned evaporator, ceramic tubes hosting the heat pipe condenser, and a water tank feeding directly the porous ceramic tubes. To make the unit compact, the heat pipes-ceramic tubes modules were arranged in series along three-row. Figure 5-1 shows a 3-D sketch of the prototype where the system is comprised of two adjacent channels; the bottom channel, dry-air passage, in which the ambient air flow through to be cooled along it, and the upper channel, wet-air passage, where the working air, branched from the cooled inlet air stream, passes through for heat removal process from the condenser and wetted ceramic tubes.

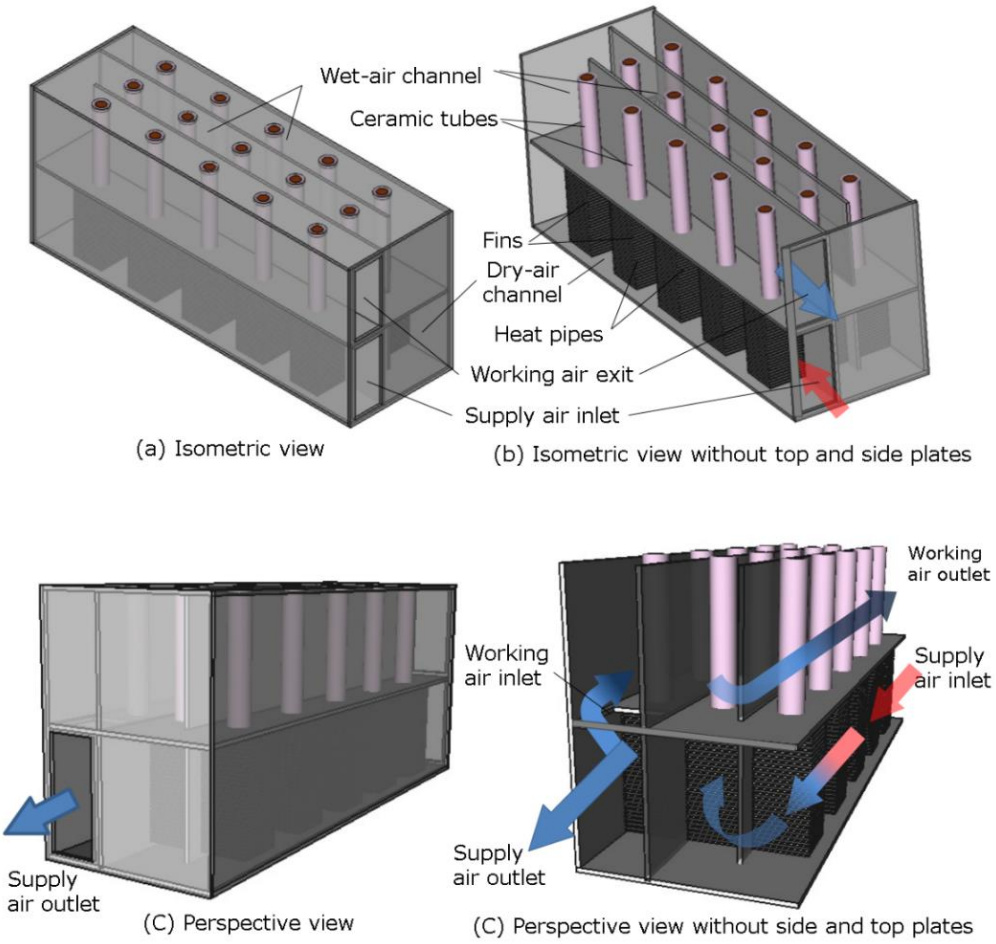


Fig 5-1 Isometric and perspective views of the HPHX and ceramic tube based R-IEC system

For further illustration of the air flow paths of the system, Fig 5-2-a presents counter-flow arrangement of the flow direction inside the cooler channels, while Fig 5-2-b and -c show top views of the flow pattern in the wet-and dry-air passages, respectively.

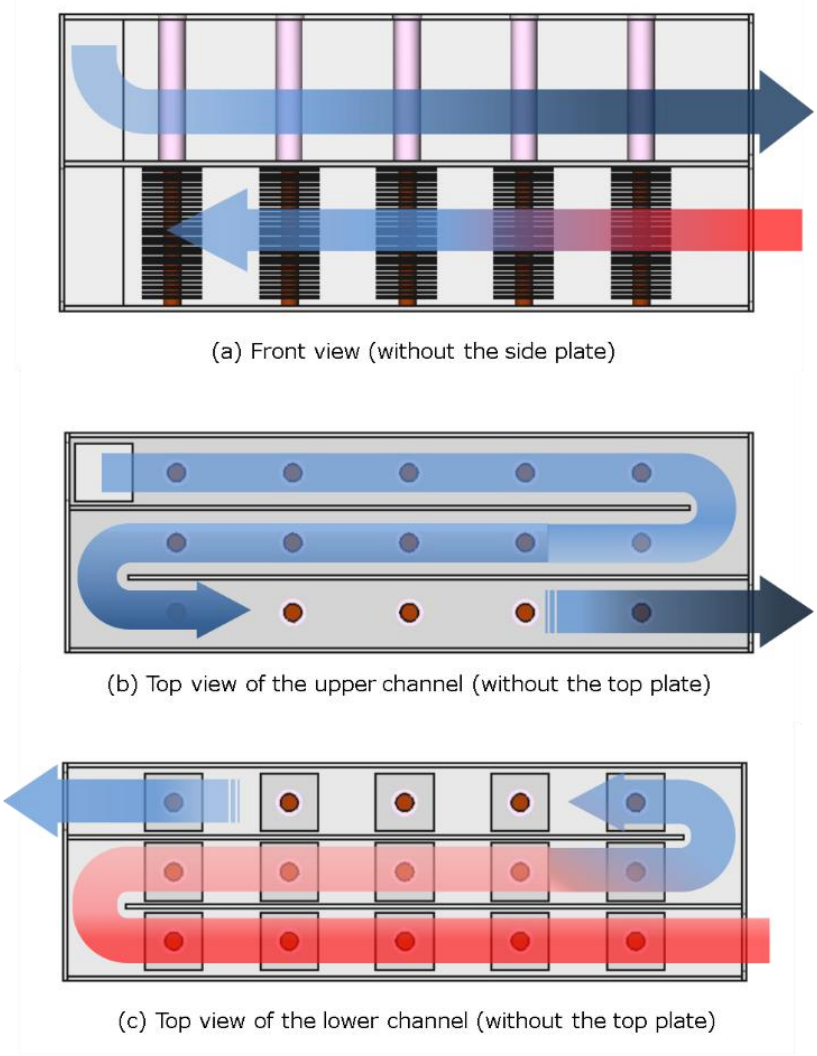


Fig 5-2 flow scheme inside the cooler, (a) dry and wet channels, (b) wet channel, (c) dry channel

The front and side views of the prototype unit with physical dimensions of the different components are presented in Fig 5-3. It can be noted the compact size of the system with overall dimensions of (700mm * 227mm * 300mm). While other dimensions of the cooling unit are illustrated in Table 5-1. Also, supply air centrifugal fan, fan speed controller, and other auxiliary instruments are required for measurements such as thermocouples, data-logger, humidity meters and flow meters. The main specifications and properties of the system components and parts are introduced in the following sections.

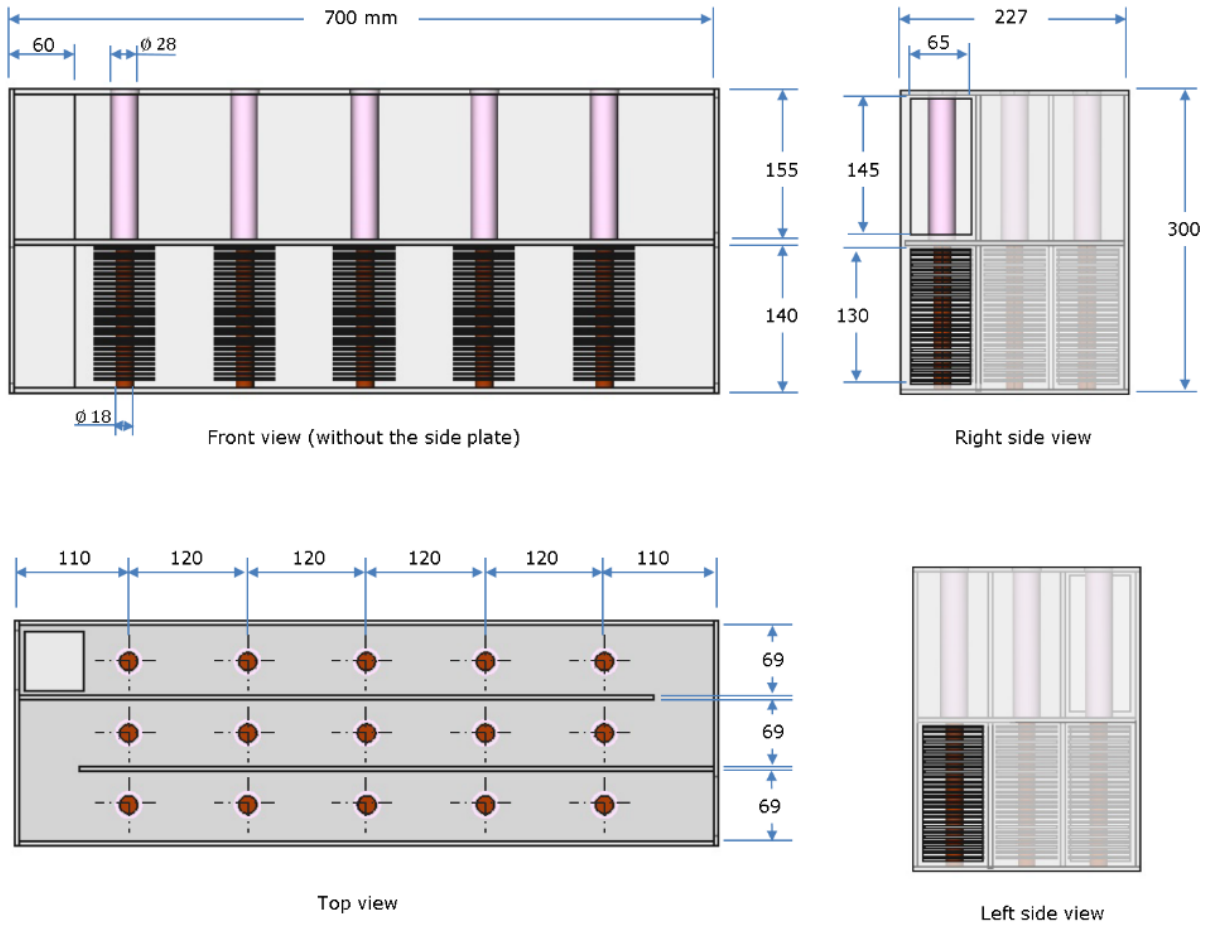


Fig 5-3 Front, sides, and plan views of the cooling unit

5.2 Components assembly

5.2.1 Outer casing

The outer casing of the prototype was made of transparent Perspex sheets for rigidity and facilitating visualisation of airflow in the ducts. The specification of each component of the system is recapitulated in Table 5-1 and Fig 5-3. The outer shell of the unit was formed in the shape of a box where the Perspex sheets were bolted and glued together to form the air channels. Circular holes were drilled in the sheets to accommodate the heat pipes and ceramic tubes. Fig 5-4 shows the assembly of the box with example of heat pipes inserted in place.

Table 5-1 Outer casing specification

Parameter	Value
Wall thickness	5 mm
Length	700 mm
Width	227 mm
Height	300 mm
Diameter of the inlet air opening	13 mm
Diameter of the supply air exit opening	10 mm
Diameter of the working air exit opening	10 mm
The wet surface area of one ceramic cylinder	0.0123 m^2
Total wet-ceramic surface area of the system	0.1845 m^2
Spacing between heat pipes	120 mm



Fig 5-4 The casing of the prototype unit

5.2.2 Heat pipes

The heat pipes were purchased as standard components, they are made from copper with two layers copper wire mesh wick structure and water as working fluid. Table 5-2 shows main specification of heat pipe. In addition, other design parameters and thermodynamic properties of the heat pipe such as vapour space area, capillary radius, porosity for the wick structure, and wick permeability are presented in Appendix B, and Excel spread sheet was created to calculate some of heat pipe design parameters that were not provided by the suppler [113].

Table 5-2 Heat pipe parameters and specifications

parameters	Symbol	Value	Unit
Outer diameter	d_3	0.0180	m
Inner diameter	d_2	0.0158	m
vapour space diameter	d_v	0.01547	m
Length of evaporator	l_e	0.1300	m
Length of condenser	l_c	0.1550	m
Length of adiabatic section	l_a	0.0100	m
Total length of heat pipe	l_t	0.2950	m
Wick structure	-	2 layers screen mesh	
Number of wires per 1in of mesh	N_{wk}	250	$wire/in$
Mesh wire thickness	d_w	0.0016	in

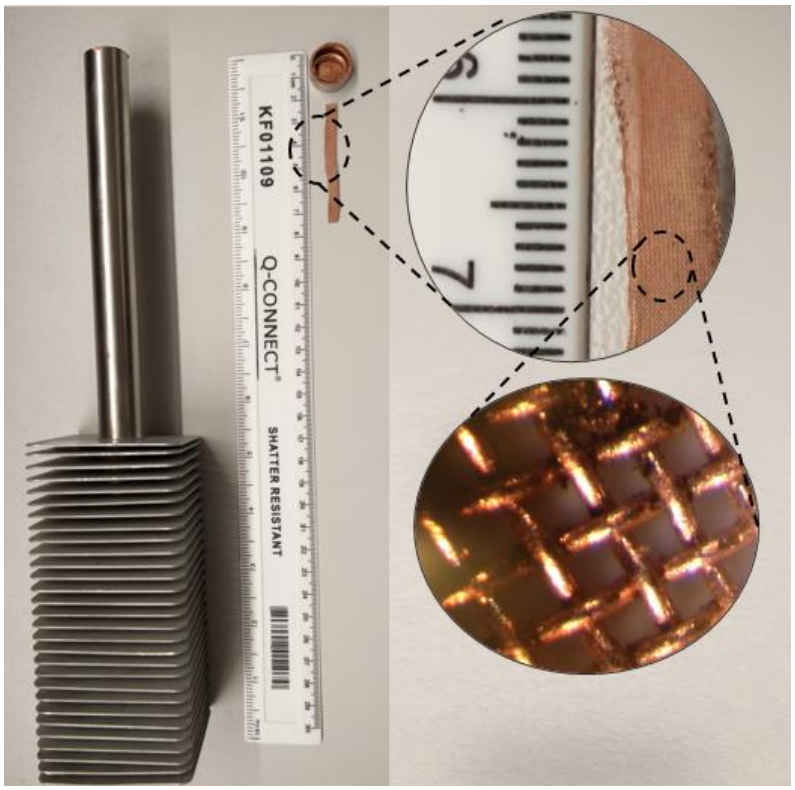


Fig 5-5 Heat pipe element

5.2.3 Porous ceramic pipe

Porous ceramic tubes were specified from specialist ceramic manufacturer who produced the tubes. The main specification parameters of ceramic are given in Table 5-3. Also, Fig 5-6 shows a picture of the produced porous ceramic tube. To control its porosity, the raw ceramic powder is heated in mould in high temperature oven to about 1200 ^{o}C until the different constituents were sintered into a solid structure.

Table 5-3 Porous ceramic tubes specification [125]

Porous Ceramic properties	Specifications
Materials compositions	$25.68\%\ Al_2O_3$, $66.85\%\ Si\ O_2$, 4.03% Albite, 2.07% MAD-10 Feldspar, 0.45% F_e, 0.42% Wollastonite, 0.29% M_gO, 0.11% KCI
Length	150 mm
Inside diameter	24 mm
Outside diameter	28 mm
Porosity	17%
Density	2300 kg/m^3
Thermal conductivity	1.5 W/mK

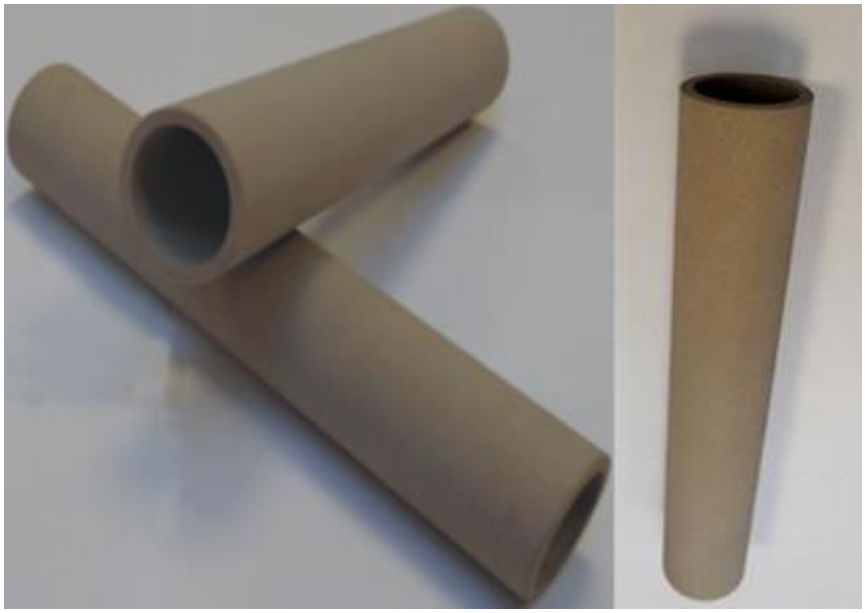


Fig 5-6 Porous ceramic tubes

5.2.4 Air circulating fan and controller

Centrifugal fan is attached to the dry channel inlet and draws air from an environmental chamber using a flexible duct. The fan speed and hence air flow rate is controlled using a speed controller. The specification of the fan and controller are given in Appendix C [126].

5.3 Fully assembled laboratory prototype

The assembly process of all the components is presented by photos in Fig 5-7. Initial assembly of the unit casing to check the accuracy of cut Perspex sheets before the final assembly is shown in Fig 5-7-a. The casing is constructed to form two adjacent channels, starting the assembly from the bottom plate i.e. the base of the cooling unit, and then, heat

pipes, vertical guide walls, and horizontal common plate. After that, the ceramic tubes were inserted to envelop the condensers. The next step was installing the front and the back plates, and the side plates. The fan and its casing were attached to the right side plate i.e. inlet air side, as seen from Fig 5-7-d. Finally, the water tank is constructed and fitted directly on the top plate of the unit, as it is seen in Fig 5-7-f.



Fig 5-7 Construction and assembly process of the cooling system

The complete assembled prototype unit is shown in Fig 5-8. In air flow process of the system, air from the environmental chamber at controlled temperature and humidity is sucked in through the fan and circulated in the dry channel. At the outlet of the dry channel

a portion of the cooled air is supplied for space cooling using a duct damper, and the remaining part is channelled through the wet channel to evaporate the water held in the ceramic tubes and cool the heat pipes condenser, the water tank for wetting the ceramic pipes is located on top of the rig.

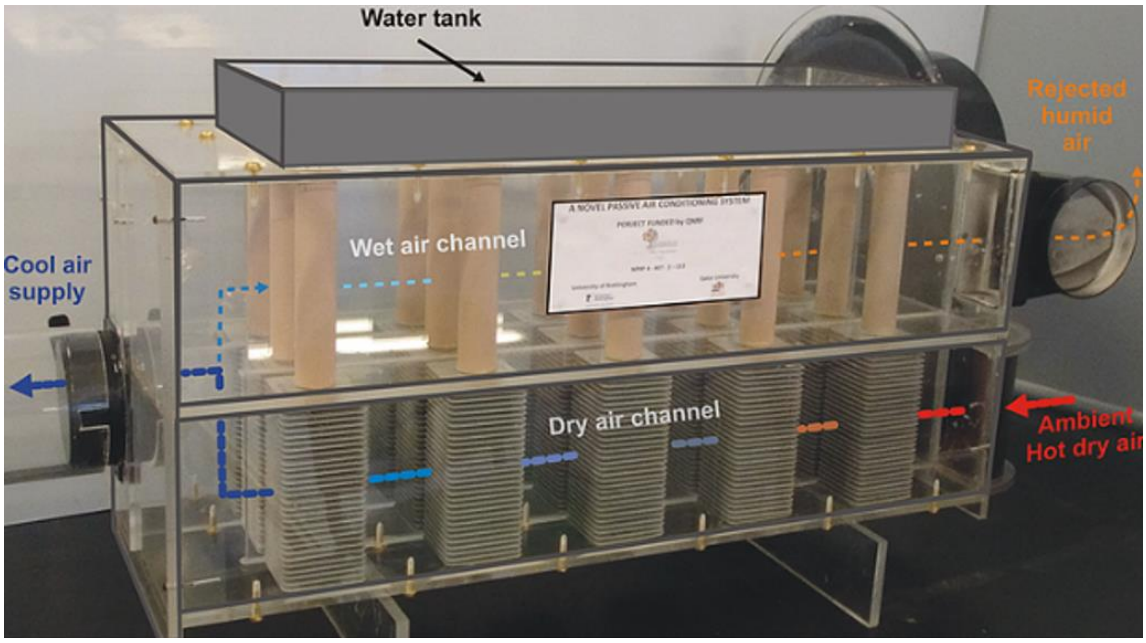


Fig 5-8 Heat pipe and porous ceramic tube based R-IEC system

5.4 Measuring instruments

The system has the following electrical auxiliary devices which help to run the system, measure variables, and save data during testing.

- Thermocouples: K-type thermocouples are located in several points on the middle of air flow passages to measure temperatures simultaneously, as presented in Fig 5-9.
- Data logger: a data-taker, model DT500 series 2, is used. All the thermocouples are connected to this data acquisition device to store readings and save it temporarily. The data taker is connected to a computer which ran a program, DeLogger 4, which read all sent data from the data taker and display it on the monitor. Then, this data is saved on the computer for later analysis.
- Humidity & temperature meters: RS-232 humidity and temperature meter is used to at exist of the wet air channel measuring the humidity and temperature of the

working air, while RS-1365 thermometer is located at inlet of dry air channel measuring the humidity and temperature of the inlet air as shown in Fig 5-9.

- Hotwire anemometer: a portable hotwire anemometer (Testo 405-V1) to measure flow velocity at the inlet and exit of the dry channel and the wet channel exit.

These instruments are located in several points around the test rig in order to measure and record the data required to evaluate the performance of the IEC system. Fig 5-9 shows locations of these measuring devices on the test-rig. Table 5-4 provides a summary of the measured parameters/variables and their corresponding instruments with their measuring ranges and accuracies, and Fig 5-10 shows photos of these instruments.

No.	Instrument
1	Hot wire anemometer
2	Type K thermocouple
3	Humidity meter
4	Type K thermocouple
5	Type K thermocouple
6	Type K thermocouple
7	Hot wire anemometer
8	Type K thermocouple
9	Type K thermocouple
10	Type K thermocouple
11	Humidity meter
12	Hot wire anemometer
13	Type K thermocouple
14	Scale measuring jug

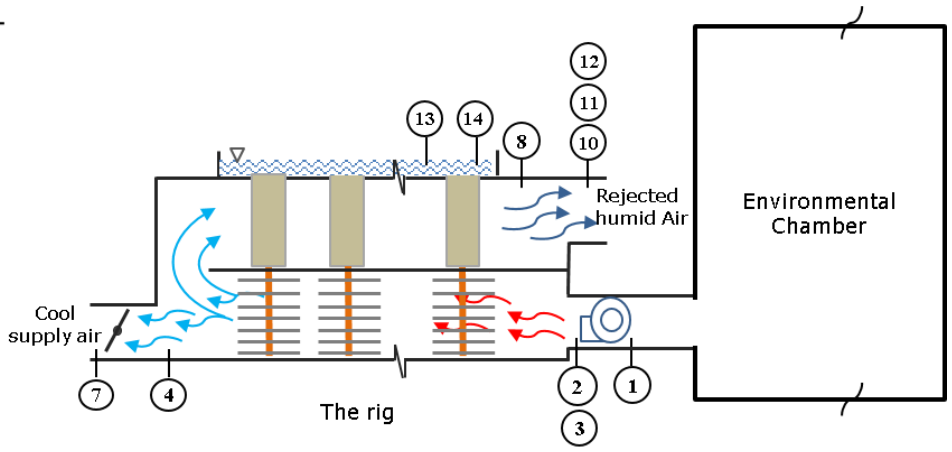


Fig 5-9 Measurement instruments' locations on the rig



Fig 5-10 Photographs of the measurement instruments: (a) Type K thermocouple; (b) hotwire anemometer; (c) RS-232 humidity and temperature meter; (d) RS-1365 thermometer

Table 5-4 Rig instruments and their corresponding measured parameters

No.	Instrument	Variable	range	Accuracy of reading
1	Hotwire anemometer	Inlet air velocity	0 to 10 m/s	±5 %
2	Type K thermocouple	Inlet air temperature	-50 to +250°C	±0.4%
3	Temperature/Humidity meter	Inlet air humidity and temperature	-20 to 60 ℃, 10% - 95% RH	± 1% RH ± 0.5 ℃
4	Type K thermocouple	Supply air temperature after 5 heat pipes	-50 to +250°C	±0.4%
5	Type K thermocouple	Supply air temperature after 10 heat pipes	-50 to +250°C	±0.4%
6	Type K thermocouple	Supply air temperature at dry channel exit	-50 to +250°C	±0.4%
7	Hotwire anemometer	Supply air exit velocity	0 to 10 m/s	± 5%
8	Type K thermocouple	Working air temperature after 5 ceramic tubes	-50 to +250°C	±0.4%
9	Type K thermocouple	Working air temperature after 10 ceramic tubes	-50 to +250°C	±0.4%
10	Type K thermocouple	Working air temperature at the exit of wet channel	-50 to +250°C	±0.4%
11	Temperature/Humidity meter	Working air humidity at the exit of wet channel	-20 to 60 ℃, 10% - 95% RH	± 1% RH ± 0.5 ℃
12	Hotwire anemometer	Working air velocity at the exit of wet channel	0 to 10 m/s	± 5%
13	Type K thermocouple	Feed water temperature	-50 to +250°C	±0.4%
14	Scale measuring jug	Feed water consumption	10 to 500 ml	±2%

5.2 Experiment set-up

The performance parameters of the laboratory prototype were experimentally investigated under controlled temperature and humidity conditions. Fig 5-11 shows the associated rig instruments used in the testing schedule. The cooler is connected to an environmental chamber via a flexible duct, the chamber is used to simulate the required climatic condition by setting and controlling air temperature and humidity via the chamber's control panel. During the testing, hot inlet supply air is drawing from the environmental chamber (point 1) through the duct (point 2) by a variable-speed centrifugal fan (point 3) which draw it throughout the cooling unit (state 4). The inlet air continues to be cooled down as it flows across heat pipes till the exit of the dry-air channel where part of this cool supply air leaves the device and flows toward the conditioned room (point 5), while the other part is diverted and flows through the upper channel (point 6), as working air, for heat removal process form the wetted porous ceramic tubes, and then is reject to the surrounding as hot humid working air (point 7). Meantime, the tap water is supplied to the system via overhead tank,

the water flows down by the gravity effect and fill out the cavity between the outer surface of the heat pipe and ceramic tubes providing even and complete covering of the condenser.

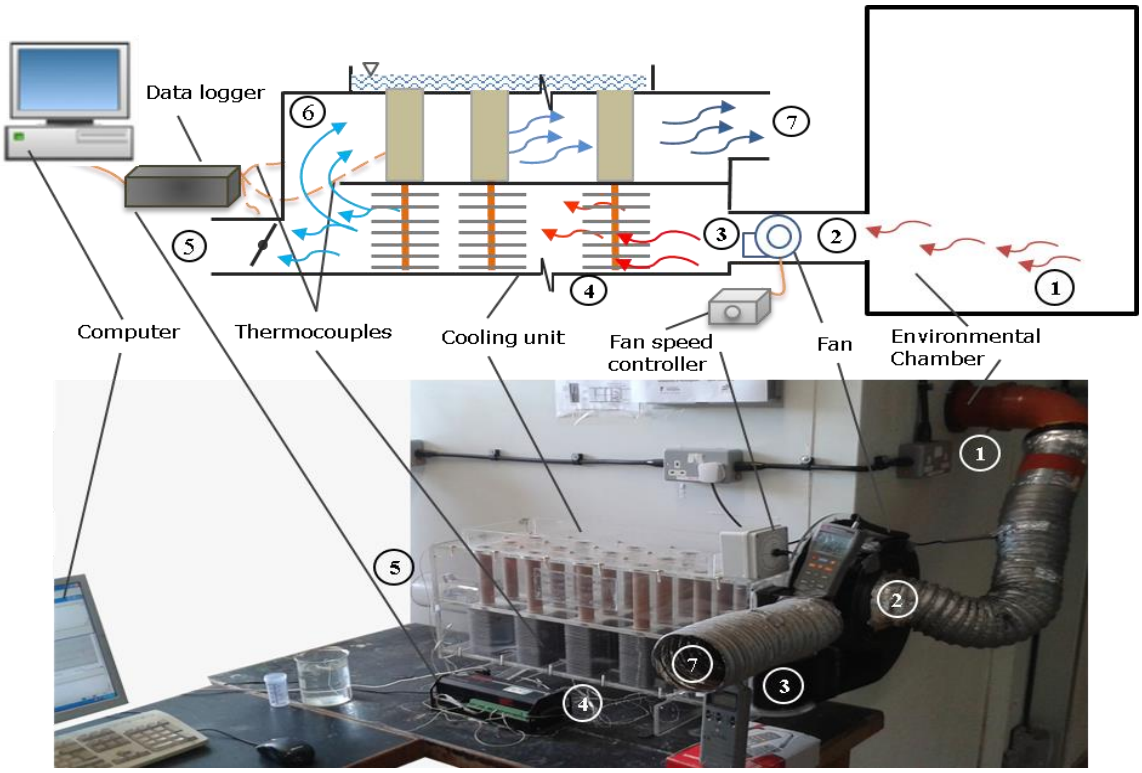


Fig 5-11 Experiment set-up

5.3 Test conditions

Several test conditions were selected in order to investigate of the thermal performance of the laboratory prototype. This was conducted over a range temperature, humidity and air flow rates conditions to represent the climate of hot and dry areas such as the MENA region. Two different test conditions were conducted of experimental tests. The full schedule of experimental work for both cases is summarised in Fig 5-12, and explained as follows:

5.3.1 Constant inlet air temperature and humidity

This experiment was extensive and evaluated the performance of the prototype unit by measuring the effect of one or more of the following variables:

i. Temperature and relative humidity of inlet air,

ii. Inlet supply air velocity,

iii. Working-to-inlet air flow rate ratios,

iv. Water consumption rates.

For this set of tests, three different temperatures (30, 35 and 40 ℃) were selected of the inlet air. Each temperature e.g. 30℃ was tested at three different relative humidity values i.e. 25%, 35%, 45% RH. Then, for each temperature and humidity e.g. 30℃ and 45%, the fan operated at three different speeds (5, 3.5 and 2.5 m/s) with three different flow ratios of the working-to-inlet air of 20, 50, and 70%, as illustrated in Fig 5-12.

5.3.2 Variable inlet air temperature and humidity

The main objective of this test is to evaluate the behaviour of the cooling system under continuous variation of inlet supply air temperature and humidity to replicate real life weather conditions in mid-summer day of the southern Libyan city of Sabha (Latitude: 27 01N, and Longitude: 14 27E). The cooler was operated under variable inlet ambient air conditions but at a constant flow rate and flow ratio, as presented in the Fig 5-12. Initially, it was intended to simulate the operation of the cooler for a day-long operation but due to time limitation in the laboratory, the tests were shorten to 6-hour operation only.

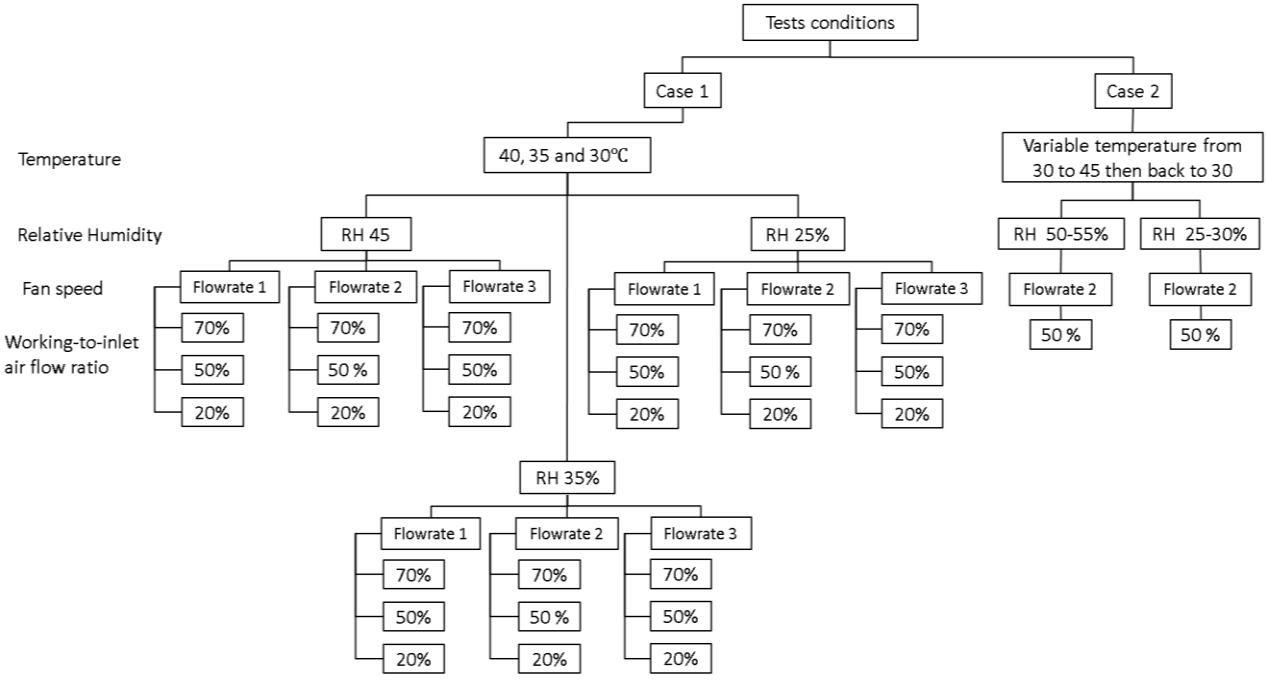


Fig 5-12 Tests plan

5.4 Test procedure

The experiments proceeded as follows:

1. Check the electrical connections of computer, data logger and fan, and also the connections of thermocouples, and duct connections between environmental chamber and cooler.
2. Start the experiment by:
    i. Setting-up the environmental chamber to required temperature and humidity by the control panel, and switch it on. After that, switch the computer and data logger on, and make sure the thermocouples are working properly,
    ii. Switching the fan on as the temperature and humidity inside the chamber reaches the chosen values, and set-up fan speed to the required flow rate of the inlet air by using fan speed controller.
3. Once the system reached steady state condition, open new file on the computer to start recording and monitoring reading of temperatures taken by the thermocouples every 20 second. While, readings of the relative humidity are recorded manually every 2-3 minutes. Meanwhile, tap water is manually added to the overhead tank by using a scale measuring jug.
4. In the first set of tests, the fan speed controller is used to change fan speed to required flow rate, the air flow rates are measured at the inlet and exit of dry-air channel and exit of wet-air channel by using hot wire anemometer for each flow rate ratio setting. Also, velocity and flow rates readings are recorded, while a dumper is used at the exit of the dry-air channel to control the working-to-inlet air flow rate ratio. After running the system for sufficient time i.e. the air temperature curves are stabilised, save the data file on the computer.
5. Once the readings of three fan speeds and three flow rate ratios were recorded and data files saved. Thus, the experiment is finished, but only for one temperature point and one relative humidity value.

6. For other values of relative humidity at the same inlet temperature, change the humidity via the environmental chamber's control panel, and, then, repeat test steps 3 to 5.
7. After recording data for the required periods, save all data files. Therefore, the experiments of only one temperature setting with 3 different humidity values are completed. For other test temperatures, increase the inlet air temperature via the chamber control panel and repeat the previous steps 3-6 of test procedure.

For the second set of experimental tests, a dynamic testing of the cooler operation is carried out under continuously variable inlet air conditions. The experiment procedure, here, is almost similar to that of the first set of experiments apart from that the inlet air temperature and inlet relative humidity are changing with the time while other parameters i.e. inlet flow rate and flow rate ratio are fixed at constant values of 105 m^3/h and 50%, respectively.

All tests recorded data (inlet and supply air temperatures and relative humidity, working air exit temperature and humidity, and water and power consumption) were converted to a spread excel sheet created for the ease of the analysis and interpretation of the experimental results, as presented in

Appendix D.

5.5 Experiment observations and limitations

- **Water droplets formation and porosity issue**

During the first attempts to added water to the overhead water tank, the water smoothly flown from the tank directly to fill out the cavities between the heat pipe and porous tube. So, the porous ceramic material became water-saturated within few minutes which is ideally was anticipated. But as the water tank was is filled up, extra water came out (siphon off) of the ceramic and formed water tears. Hence the water film became thick and developed water droplets over the external surface of the ceramic cylinders, as shown in Fig 5-13. Consequently, water puddles are formed at the base of the ceramic tubes which eventually accumulate and flood the entire channel i.e. the upper passage of the cooler. This possibly because of water static pressure in the tank on the micro pores of ceramic materials and, also, the uncontrolled porosity of the ceramic might be responsible as well. Yet, the manufacturer stated that the porosity of the ceramic is 17%, see Table 5-3.



Fig 5-13 Water droplets formation over ceramic tubes

In order to solve this issue with minimum costs and without affecting the core of the design which is using ceramic tubes to provide a uniform and complete water-cover of the condenser. Initially, fine sand was added to fill out the whole volume of the overhead tank, after that water was poured to the sand-filled tank, therefore, water is anticipated to slowly flow towards the ceramic tubes. This technique helped to reduce the amount of water siphoning off, but still some water escaping and accumulating at the base of the porous ceramic cylinders, as shown in Fig 5-14.

Alternately, the fine sand was added into the ceramic tubes to fill out the cavity between the heat pipe and the ceramic cylinder to reduce the amount of water penetrating from the pores of ceramic material and solve issue of the high porosity, consequently, water siphons properly and form a thin water film over the ceramic surface without causing any water puddles on the upper channel. In addition, the effect of adding fine sand would also improve the heat removal rates from the condenser, owing to the higher thermal conductivity of the water-sand mixture than that of water.

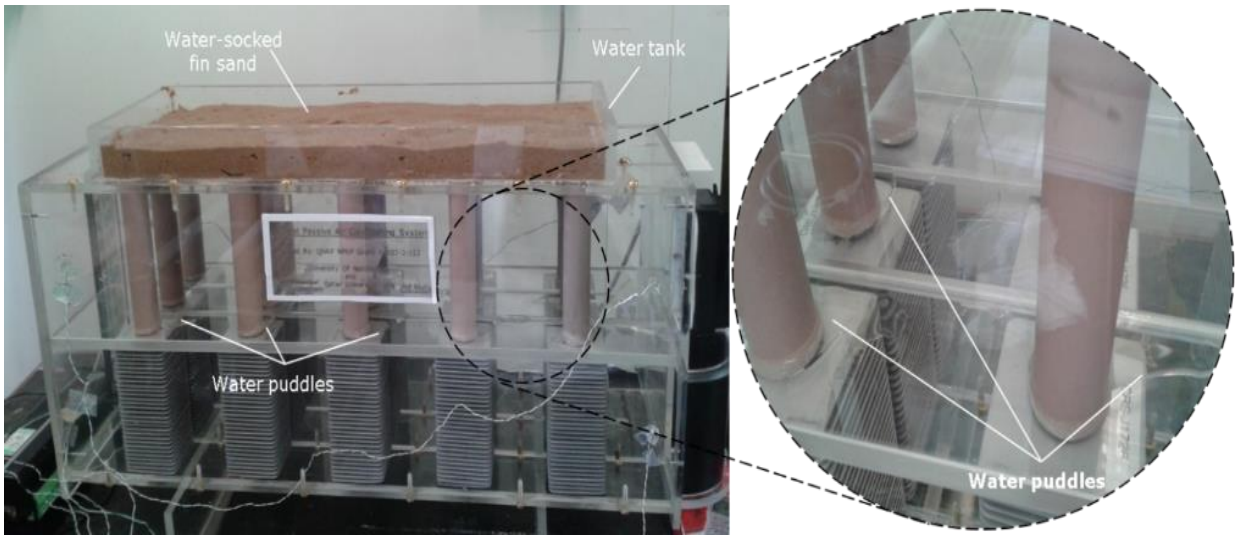


Fig 5-14 Water puddles formation at the base of ceramic tubes

5.6 Preliminary results of experimental work

Table 5-5 provides a quick hint of some of the performance parameters based on the experimental investigation at inlet conditions of 40℃, 45% and 25% RH, 50% working-to-inlet air flow rate ratio and water temperature of 23℃.

Table 5-5 Experimental results of the cooler performance at inlet air conditions of 40 ℃, 25% and 45% RH, and 50% working-to-inlet air flow rate ratio

Parameter	Value			Value		
Temperature of inlet air (℃)		40			40	
Relative humidity of inlet air (%)		25%			45%	
Supply-to-inlet air flowrate ratio		50%			50%	
Wet bulb temperature of inlet air (℃)		23.60			29.1	
Dew-point temperature of inlet air (℃)		16.20			25.8	
Inlet air speed (m/s)	5	3.50	2.50	5	3.50	2.50
Volumetric flowrate of the inlet air (m^3/h)	150.00	105.00	75.00	150.00	105.00	75.00
Supply air temperature (℃)	30.25	28.81	28.30	32.31	31.15	30.64
Supply air relative humidity (%)	43.00	46.00	48.00	68.00	73.00	75.00
Inlet air temperature reduction (℃)	9.75	11.19	11.7	7.7	8.85	9.35
Wet-bulb effectiveness	0.595	0.683	0.713	0.706	0.812	0.858
Dew-point effectiveness	0.410	0.471	0.492	0.542	0.623	0.658
Cooling capacity (W)	233.21	187.86	140.45	186.40	150.37	112.74
Coefficient of performance (COP)	5.45	8.96	13.16	4.29	6.93	9.64
Water consumption rate (l/h)	0.311	0.285	0.280	0.246	0.232	0.233

Under ambient conditions of 40 ℃ of inlet air temperature and 25% relative humidity (RH), the temperature drop of the inlet air was about 11.7 ℃ , achieved at inlet air flow rate of 75 (m^3/h) with WB and DP effectiveness of 0.713 and 0.492, respectively. The cooling capacity was only 140 (W) which considerably can be improved, by 33.5 %, by increasing the inlet air flow rate to 105 ($\mathrm{m^3/h}$), to become 188 (W), with relatively small effect on effectiveness. But, any further increase of the inlet air flow rate would affect the temperature drop of the inlet air as well as the cooler effectiveness. In contrast, at same inlet conditions but higher inlet air humidity of 45%, the WB and DP effectiveness were 0.858 and 0.658, respectively. In regard with the COP of the cooler, it ranged from 5.45 to 13.16, these values of COP corresponds well with COP values of other recently developed R-IEC systems, like [89] and [76], because of low power consumption. Furthermore, the cooler water consumption ranged 0.148-0.318 (l/h) for all conducted tests i.e. 0.841-2.8 (l/kWh).of cooling output.

This considerably represents savings of 30-55% of water consumption comparing with that of the R-IEC system of [88], and the M-IEC system of [89].

5.7 Summary

An experimental investigation was conducted in order to evaluate the performance, and determine the effect of various operation parameters on the prototype. In total 83 laboratory tests were carried out for inlet air temperature varied from 30 to 40℃, relative humidity from 25 to 45%, inlet air flow rate from 75 to 150 $(\mathrm{m}^3/\mathrm{h})$ and working-to-inlet air flow rate ratios from 20% to 70%. The experimental results showed that this indirect evaporative cooler has the potential to provide sufficient cooling effectiveness without increasing the supplied air moisture content. For all performed tests, the WB effectiveness value was close to unity, it varied from 0.425 to 0.91. Equally, the COP ranged 4.62-13.16.

Further result analysis the experimental data, and validation of computer model are presented in the next chapter for broad investigation of the effects ambient and operational parameters on the cooler performance.

Chapter 6: Results analysis and discussion

In this chapter, analysis of the experimental and theoretical results was carried out. In addition, a comparison between the mathematical results and experimental data was presented, this was shown in terms of analysing the effects of various operational parameters on the cooler thermal performance.

6.1. Air flows temperature variation

6.1.1 Constant inlet air temperature and humidity

Fig 6-1 presents temperatures distribution over time of the inlet air, the supply air and the exhaust working air under inlet conditions of 40 ℃, 25% RH, and water temperature of 23℃, the figure illustrates experimental results of three tests at different inlet air flow rates of 150, 105 and 75 (m^3/h) i.e. 5, 3.5, and 2.5 (m/s) respectively. For each inlet flow rate setting, three different ratios of the working-to-inlet air flow rate (20%, 50% and 70%) were tested. During the experiment, the system was operated for couple of minutes without adding water till the inlet air flow rate become steady. After that, the water is gradually supplied to the cooling unit, so, the temperatures curves undergoes transient period before it becomes steadily constant. Meanwhile, it is usually takes from 5-10 minutes approximately for ceramic material to become fully water-saturated.

For temperatures profiles of the inlet air, supply air, and working air in Fig 6-1. Firstly, consider the case of 20% working-to-inlet air flow ratio and 150 ($\mathrm{m^3/h}$) inlet air flow rate, the cooling unit cooled the inlet air from 40 to 34 ℃, while the working air leave the system at lower temperature of 31.6 ℃ , this limited temperature drop of the inlet air because of high flow rate passing through the channels of the cooling unit with limited time for sufficient heat transfer. Additionally, by comparison with other flow rates (105 and 75 m^3/h) at 20% flow ratio, the cooler seems to be unable to effectively remove the heat from the wet-air channel, since low rates of air flowing through it i.e. only 20% of the cooled inlet air flow rate. For instance, at inlet condition of 105 ($\mathrm{m^3/h}$) intake air flow rate and 20% flow

ratio, the working air temperature profile (the green curve) was gradually increasing because of low flow rates of the working air which consequently led to poor heat removal from the ceramic tubes and the wet channel as well, as it can be seen from Fig 6-1. Furthermore, for operating condition of 75 ($\mathrm{m^3/h}$) inlet flow rate and 20% flow ratio, both inlet and working air temperature profiles (the blue and the green curves) rose gradually over the time, this might be due to only 20% of 75 ($\mathrm{m^3/h}$) cooled inlet air flow rate was pumped to the wet-air channel for heat removal process. As a result, the cooling system under such operational conditions was not able to cope with the heat load and high ambient temperature which cause heat accumulation in the wet passage. This eventually effects on the performance of heat pipes. Moreover, at higher inlet air mass flow rates and 20% of working-to-inlet air flow ratio, higher cooling capacities are expected to be achieved due to being 80% of the cooled inlet air flow rate is supplied to the conditioned space. But, low temperature drop of inlet air was achieved at these inlet conditions, therefore, high cooling output with small temperature reduction would not be practically desirable. For example, the cooler only dropped the ambient air temperature, under inlet conditions of 40 ℃, 25% RH and 20% working-to-inlet air flow rate ratio, by 6.10, 7.00 and 7.55 ℃ which corresponds with inlet air flow rates of 150, 105 and 75 (m^3/h), respectively.

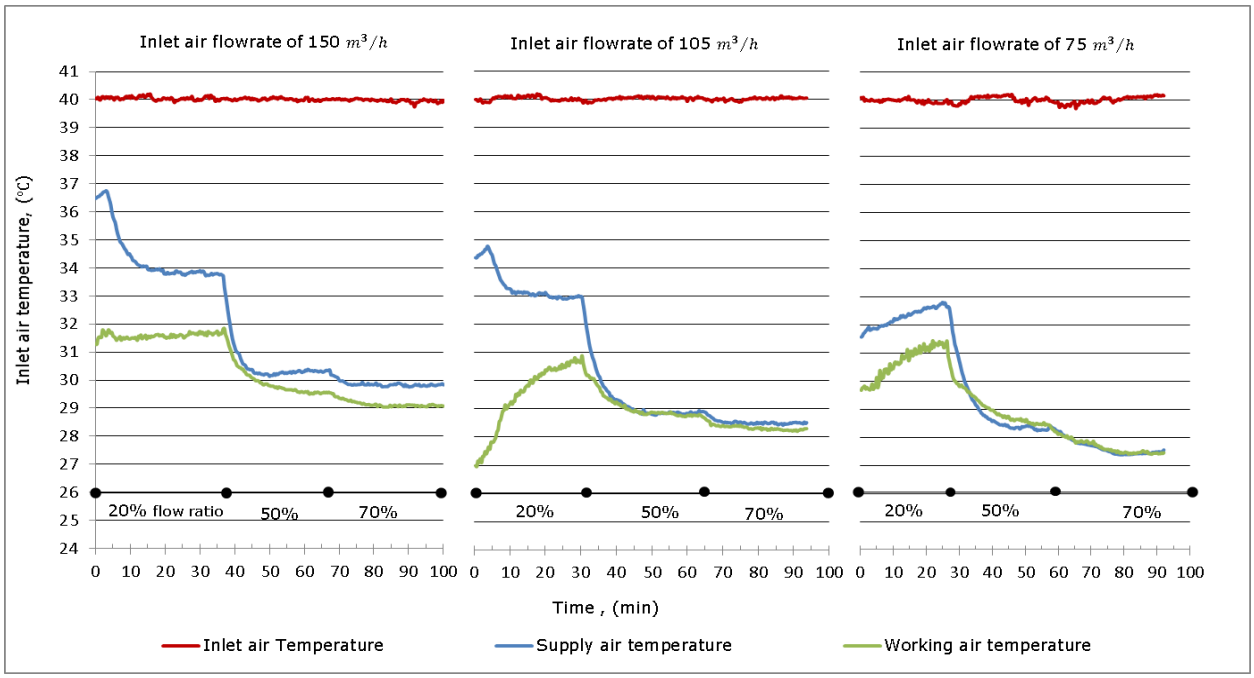


Fig 6-1 Inlet air, supply air and working air temperature profiles over time at inlet conditions of 40 ℃, 25% RH, 150, 105 and 75 $\mathrm{m^3/h}$ inlet flow rates, and of 20, 50 and 70% flow ratios

Secondly, for the case of 50% flow rate ratio, the cooling unit shows improved performance for the three values of the volumetric flow rates used. As it can be seen from Fig 6-1, the inlet air temperature reduction reached about 11.63 ℃ corresponds to the lowest inlet air flow rate of 75 (m^3/h). Also, the cooling outputs would be sufficient since the inlet air volumetric flow rate is equally divided between the condition space and the upper passage. For example, the tendency of supply air and working air temperature curves indicates sufficient heat transfer is undertaken in both channels for all tested inlet air flow rates.

Lastly, under inlet condition of 70% of the working-to-inlet air flow rate ratio, best temperature reductions of the inlet air were harvested at each inlet air flow rates, since large fraction of the cooled inlet air flow is passed to the upper passage, consequently, improving the heat dissipation process from the ceramic cylinders via latent heat of evaporation to the working air. Nevertheless, the cooling output would be considerably small, as only 30% of the cooled inlet air is supplied to the conditioned space. Hence, under such operational conditions, highest inlet air temperature reductions are achieved, but with low cooling outputs of the cooler.

To sum up, the cooler supplies limited inlet air temperature drop but high cooling capacities at condition of 20% of working-to-inlet air ratio, since most of the cooled inlet air is delivered toward the conditioned room. On the contrary, the best values of inlet air temperature drop are achieved at lower inlet air mass flow rates and high working-to-inlet air ratio. In fact, the system is able to achieve temperature reduction of 12.41 ℃ under inlet condition of 40 ℃, 25% RH, inlet flowrates of 75 (m^3/h) and 70% working-to-inlet air flow rate ratio. Nevertheless, at such conditions of low flow rates of the inlet and supply air, the cooling capacity would deteriorate as only 30% of 75 m^3/h of inlet air is supplied to conditioned space, and due to the direct relation between the supply air mass flow rate and the cooling capacity. Thus, as the temperature drop of inlet air and cooling capacity are the main parameters of interest; the 50% working-to-inlet air flow ratio appears to be the most convenient flow ratio which could provide the balance between the desire to achieve high temperature drop of the inlet air and the common need of high cooling capacities.

6.1.2 Variable inlet air temperature and humidity

These tests covered two experiments of dynamic testing of the cooler to investigate the thermal performance under real operating conditions for a-day-long test i.e. 6 hours. For the first test, the cooling unit operated under variable inlet temperature from 30 to 45 ℃ gradually and then falling back 30 ℃, with inlet relative humidity varying from 25 to 30%, at fixed inlet flow rate of 105 m^3/h , 50% flow rate ratio, and 20 ℃ water temperature. Similarly, the second test conducted at the same operating condition, but at higher relative humidity of the inlet air fluctuating between 50% and 55%. The temperature profiles of inlet air, supply air and working air for both cases is presented in Fig 6-2.

In comparison, the performance, the inlet air temperature drop, of the cooler at dryer ambient conditions were better than that of humid operation condition. To illustrate, temperature drop of inlet air was 13.55 ℃ at inlet air temperature of 45℃, while, at the same inlet temperature but relative humidity of 50-55%, the temperature decrease of the inlet air was 9℃. Therefore, the cooler is preferably to operate in hot and dry climates.

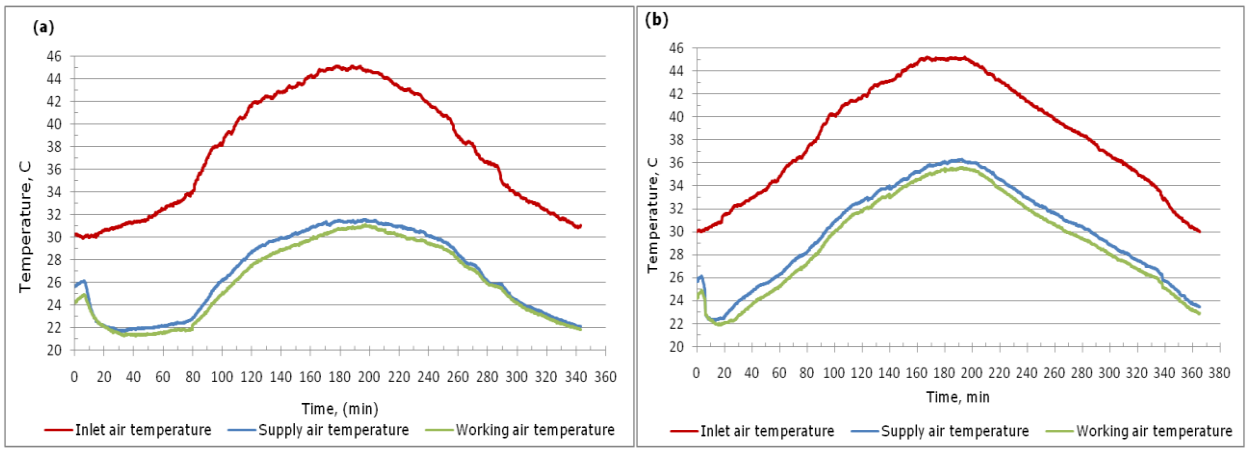


Fig 6-2 Temperature distribution over the time of dynamic testing under conditions of variable inlet air from 30-45-30 ℃ , at fixed inlet flow rate of 105 $\boldsymbol{m^3/h}$ and flow rate ratio of 50%; (a) at inlet relative humidity varying 25-30%, (b) at inlet relative humidity 50-55%,

6.2. Temperatures distribution in the air channels

The validation is carried out by comparing between the experimental and numerical results on the bases of identical operational conditions and the same geometrical properties of the cooler. The selected ambient conditions and the cooler specifications for the model verification process are presented in the Table 6-1

Table 6-1 Pre-set operation conditions and cooler specification

Parameter	value	unit
Inlet air temperature	40	℃
Relative humidity	35	%
Wet bulb temperature of inlet air	26.51	℃
Dew point temperature of inlet air	21.60	℃
Inlet air velocity	2.5	m/s
Supply-to-inlet air ratio	50	%
Feed water temperature	23	℃
Number of heat pipes rows	15	-
Inner diameter of ceramic tube	0.024	m
Outer diameter of ceramic tube	0.028	m

The air flows temperature profiles along the dry and wet channels are shown in the Fig 6-3 for operating conditions shown in Table 6-1. It can be seen that the temperature profiles that the experimental data and modelling results are in good agreement. The maximum deviation between simulation and experimental results of the air temperature and humidity is 3.94% and 4.5%, respectively. Furthermore, the figure shows supply air temperature along the dry-air channel decreasing from 40°C to 28°C. Another important parameter is the moisture content of the working air which, with the working air temperature, reflect heat removal process from the wet-air channel through water evaporation by the increase temperature and vapour content of the working air flow profiles along the passage. The working air enters into the wet-air passage at the same properties of the supply air i.e. 28 °C and 0.0162 kg_{water}/kg_{air} and flows through the water-soaked ceramic cylinders removing heat and, eventually, rejected to the surrounding as hot and humid air at 31.08°C and 0.0216 kg_{water}/kg_{air}.

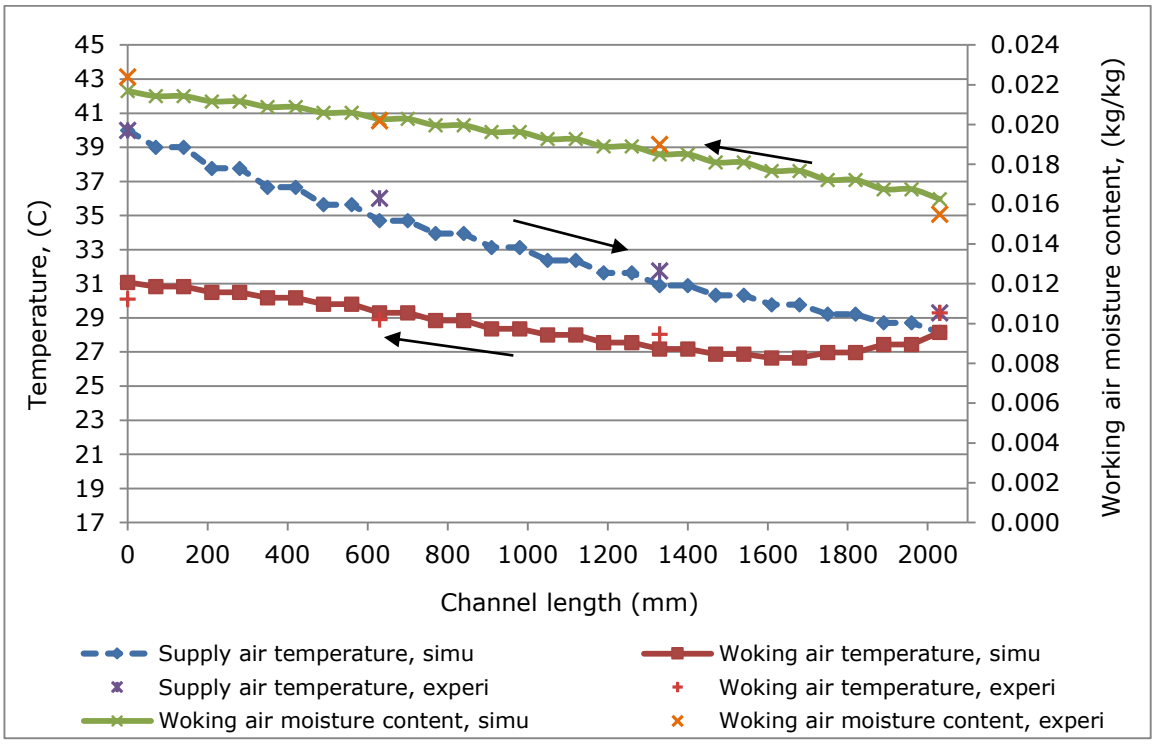


Fig 6-3 comparision between experimental and numerical temperature curves of the inlet supply air and working air, and moisture content of working air along the cooler channels at inlet conditions of 40℃, 35%, 75 m^3/h air flow rate, 50% flowrate ratio

6.3. Psychrometric chart plotting and comfort zone

For further evaluation of the performance of the cooling system in terms of meeting the recommended indoor comfort requirements, several simulation runs performed for wide range of inlet air conditions of 30-45°C, 15-50% RH, 70-150 m^3/h, and 18°C water temperature, while other parameters were fixed at their pre-set values shown in Table 6-1. Fig 6-4 presents the temperature reduction of the supply air of various hot and dry ambient air conditions plotted on the psychrometric chart, the cooler performed adequately in such climatic conditions supplying air within the comfort zone for wide inlet conditions of 30-42 °C and 15-30% RH. But, once the ambient conditions become hotter and moister, higher than 42°C and 35% RH, the cooling effectivity of the system would not fall within the comfort zone as shown in Fig 6-4. However, some operational parameters are to be optimised such as heat pipe numbers, working-to-inlet air flow ratio, and inlet air flow rate to enhance the overall cooling effectiveness for extreme hot weather conditions. The effects of these

parameters and others on the thermal performance of the cooler are discussed in the next section.

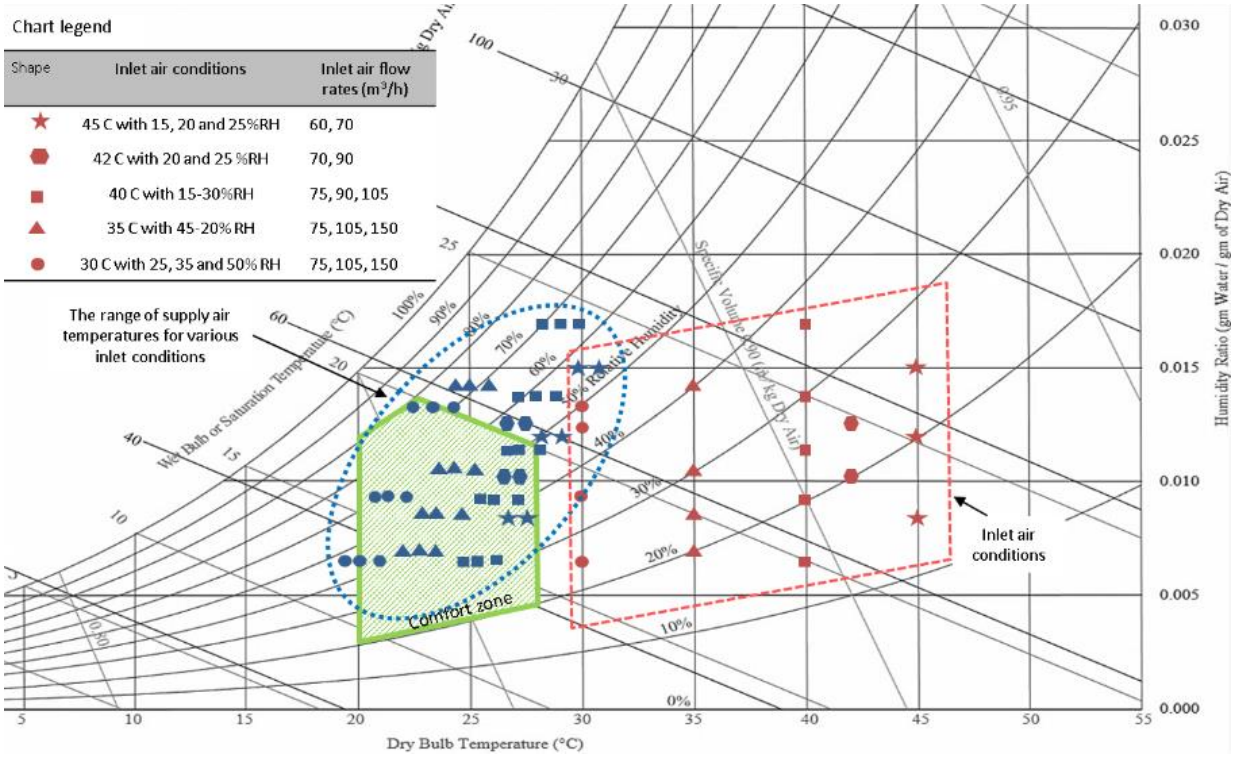


Fig 6-4 Mapping inlet and supply air temperatures on psychrometric chart

6.4. Parametric study

A parametric study was conducted using the developed computer model for further investigation of the effects of ambient and design parameters on the cooling unit performance, and, also, comparison between experimental data and numerical results for validation purposes.

6.4.1 Effect of inlet air temperature

Fig 6-5 presents the WB effectiveness and inlet temperature drop profiles against various inlet air temperatures and under inlet conditions presented in Table 6-1. It was found that the effectiveness of the cooling system increased gradually as the inlet ambient air became hotter, the best WB effectiveness was achieved at a higher inlet air temperature, and the WB effectiveness reached 1.04 at inlet temperature of 45 ℃ and 35% RH.

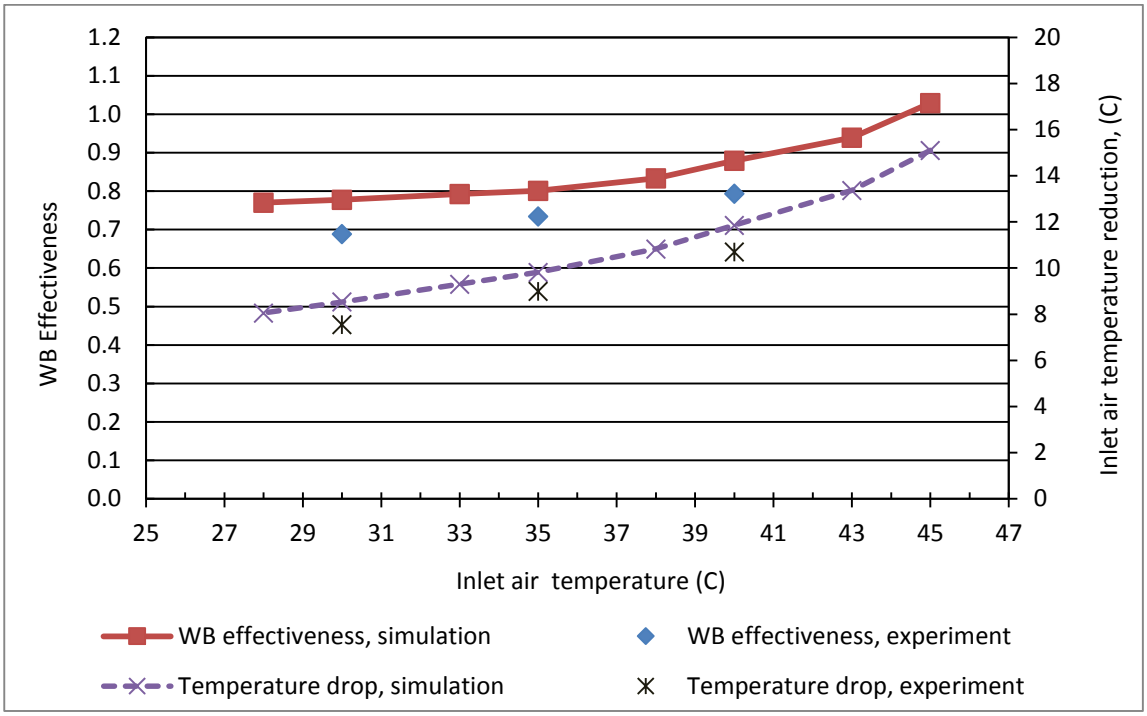


Fig 6-5 WB effectiveness and inlet air temperature drop versus inlet air temperature at operation conditions of 50% flowrate ratio, 75 m^3/h air flow rate, and 35% RH

Furthermore, the inlet air temperature drop is also influenced by the variation ambient air temperature, and its profile undergoes similar trend as for the effectiveness, as it can be seen from Fig 6-5. The highest temperature reduction of the intake air of 15.1 ℃ was at the inlet air condition of 45 ℃, whereas the lowest value of temperature drop of 8 ℃ was at the inlet air condition of 28 ℃. Therefore, the temperature drop of the inlet air through the cooler is improved as the ambient air conditions become hotter. This is obviously one of the advantages of the evaporative coolers over other vapour-compressed cooling systems which their performance decreases as the ambient temperature increases. A good agreement between measured and calculated data of the WB effectiveness and inlet air temperature drop is demonstrated in Fig 6-5 with discrepancy in the range of 8.67-12.9%. Moreover, Fig 6-5 illustrated that the WB effectiveness and inlet air temperature drop are directly proportional to the inlet ambient air temperature.

The effect of the ambient air temperature on the cooling capacity and the COP is presented in Fig 6-6. Under the abovementioned operation conditions, the results clearly reveal that any increase of the inlet air temperature would positively influence on the cooling capacity

and COP of the cooler. For example, the cooling capacity improved about 30%, from 143.17 to 185.66 (W), as the ambient air temperature increased from 40℃ to 45℃. This is possibly because of the direct correlation between the cooling capacity (Q_{cc}) and temperature reduction of the inlet air $(T_{d,1} - T_{d,2})$, see Eq. (3.3). Since the inlet air temperature drop is also directly proportional to the inlet air temperature. The cooling capacity and the COP, therefore, are directly proportional to inlet air temperature.

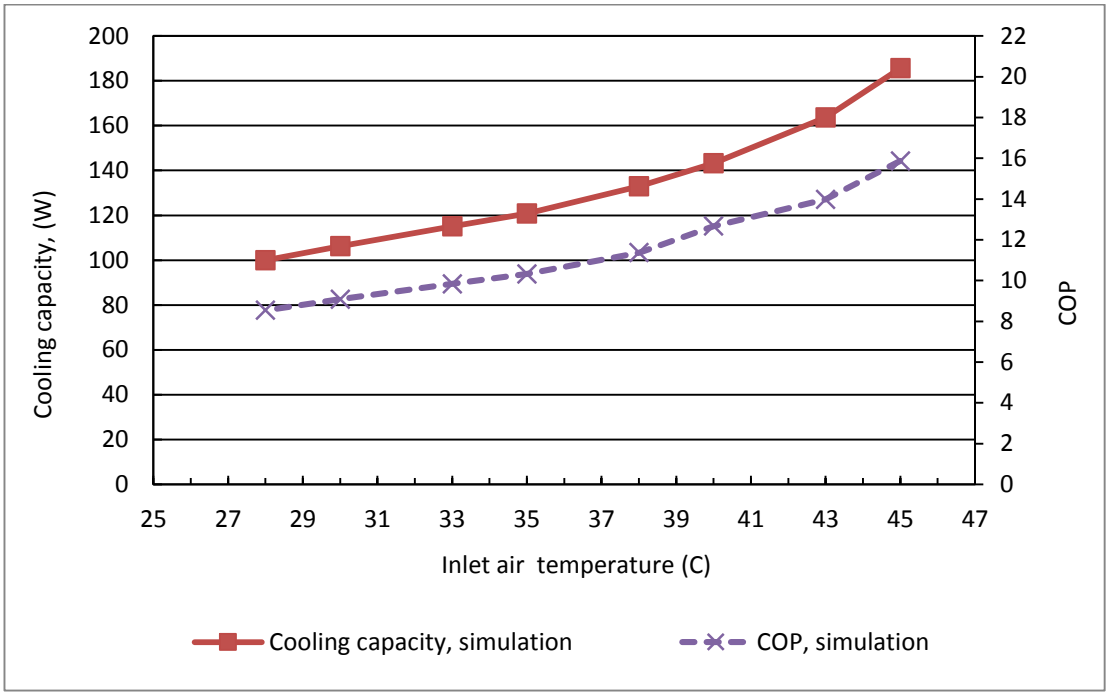


Fig 6-6 Cooling capacity and COP versus inlet air temperature at flow rate ratio of 50%, 75 m^3/h flow rate ratio and 35% inlet relative humidity

6.4.2 Effect of inlet air relative humidity

Another important parameter that influence the thermal performance of IEC system is the inlet air relative humidity i.e. air moisture content. Fig 6-7 shows the effect of the inlet air relative humidity variation (25-60% RH) on the WB effectiveness and the temperature reduction of the inlet air, at inlet conditions of 40 ℃ intake air temperature, 50% flow rate ratio, and 75 m^3/h inlet air flow rate. The results show that increasing the ambient air humidity resulted in the increase in the coolers effectiveness. In contrast, the temperature drop of inlet air decreased as the inlet air humidity increased. This ambiguous contradiction

can be explained by examining the psychrometric chart, at constant DB temperature, the value of the WB temperature depression become smaller at higher values of moisture content and vice versa. Thus, the effectiveness value become smaller at low inlet air humidity ratios because of the numerator of Eq. (3.1) would have a bigger value than that value at higher relative humidity, while the value of the denominator changes but slowly due to limited cooling effect of the cooler. Overall, attention should be given when using the effectiveness as an indicator of system performance. Other performance parameters are recommended to be used along with it for clearer illustration of cooler operation such as inlet air temperature drop, COP and cooling capacity.

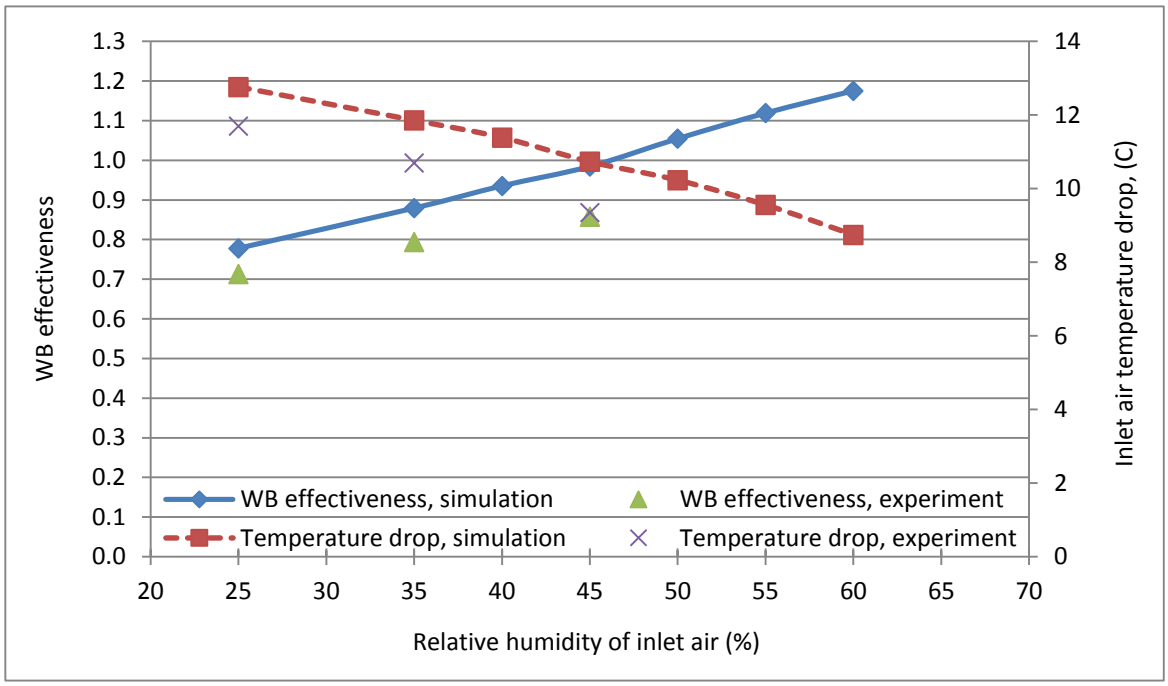


Fig 6-7 WB effectiveness and temperature reduction profiles versus various inlet air relative humidity under inlet air conditions of 40℃ temperature, 50% flow ratio, and 75 m^3/h inlet air flow rate

By considering the profile of inlet air temperature drop in Fig 6-7, the temperature drop of the inlet air decreased as the air humidity rose. For example, at 40℃ and 30% RH ambient air conditions, temperature drop of 11.7℃ was harvested, whereas at the same conditions but 45% RH, the inlet air temperature reduction was only 9.35℃. Additionally, a sufficient consistency found between the predicted results and experimental findings of the WB effectiveness and temperature drop with error ranges 9-14.7% as shown in Fig 6-7.

The effect of ambient air relative humidity on the cooling capacity and COP is presented in Fig 6-8, the values of the cooling capacity and COP gradually decreased as the ambient air moisture content increased. This declining of system performance can be interpreted by linking between the cooling capacity and the temperature drop of the inlet air (Eq. (3.3)) which inversely proportional to the inlet air humidity. Therefore, the cooling output is adversely influenced by the increase of inlet relative humidity, so happen to the COP. As it is seen from the figure below, higher values of the COP and the cooling capacities of the cooler were obtained at lower values of the inlet air relative humidity. For example, both values of COP and cooling capacity declined by about 15.50%, as the inlet air relative humidity rose from 25 to 45℃. It is clear that there an inverse proportionality between the inlet air relative humidity and the COP, cooling capacity, and supply air temperature.

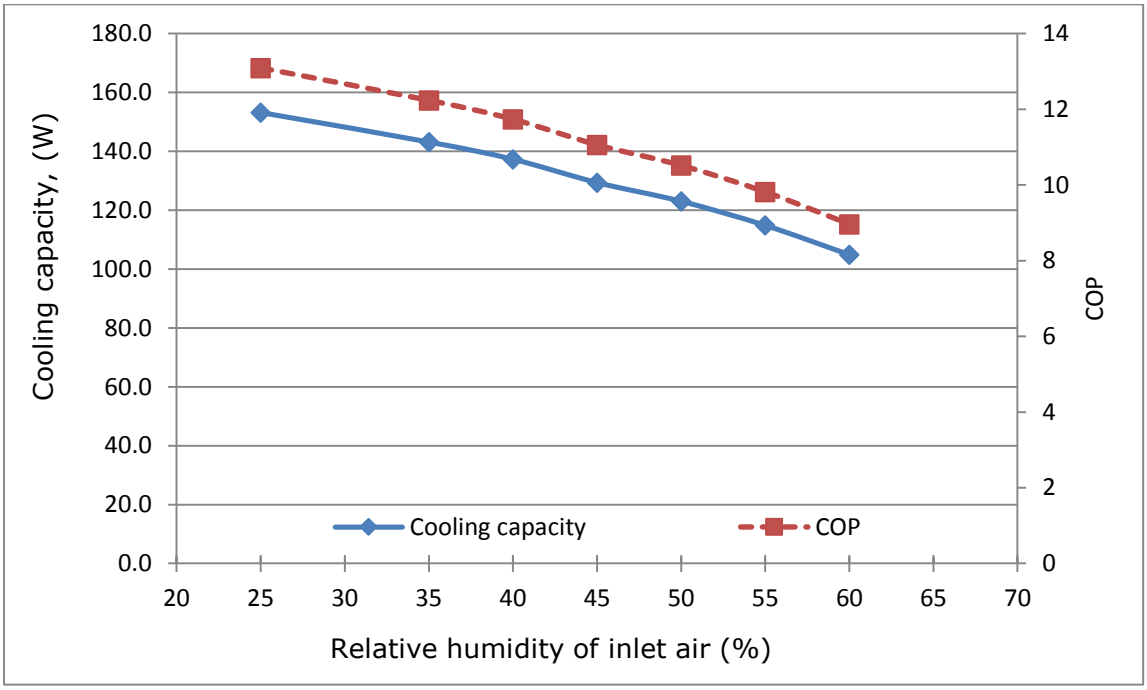


Fig 6-8 Cooling capacity and coefficient of performance profiles over various inlet air relative humidity values at inlet conditions of 40 and 30℃, 75 m^3/h air flow rate and 50% flow rate ratio

6.4.3 Effect of inlet air velocity (inlet air flow rate)

Further evaluation of the cooler performance was conducted at wide range of inlet air flow rates as shown in Fig 6-9, the increase of the inlet air velocity (inlet air flow rate) resulted in a decline of the cooler's effectiveness, while the cooling output considerably improved.

Thus, the inlet air flow rate is directly proportional to the cooling capacity, while it is inversely proportional to the cooler effectiveness.

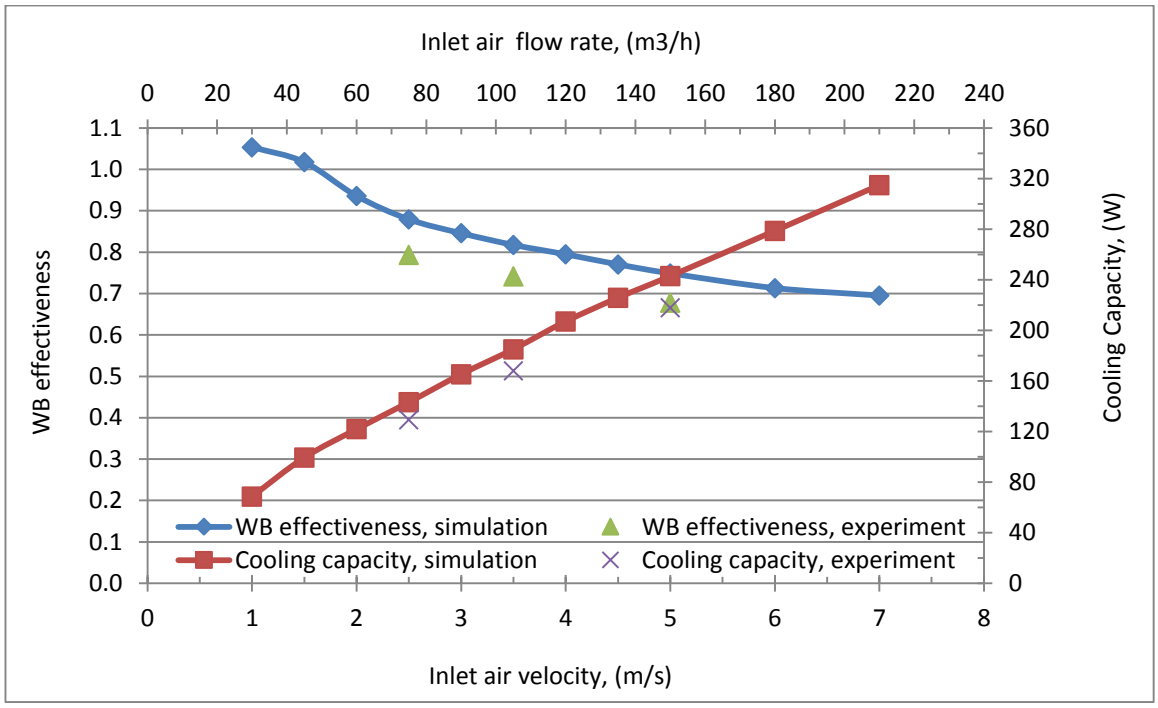


Fig 6-9 WB effectiveness and cooling capacity versus inlet air flow rates at inlet conditions of 40℃, 35% RH and 50% flow rate ratio

From the slope of the effectiveness and the cooling capacity profiles, the impact of the inlet flow rate is relatively small on the effectiveness comparing to that on the cooling capacity. For example, at inlet air velocity of 2 m/s (60 m^3/h), the WB effectiveness was 0.936 and the cooling capacity was 122 (W), as the air velocity is doubled the effectiveness declined by 15.10%, while the cooling capacity increased considerably by almost 70% due to the direct proportional relation between the cooling capacity and inlet air flow rate. Nevertheless, high values of inlet air velocities contribute to the declining of the cooler effectiveness i.e. it minimise the inlet air temperature reduction. Therefore, it is important to notice that not all high values of cooling capacity would necessarily be accompanied with a sufficient temperature drop of the inlet supply air. In some scenarios, high cooling capacity at high inlet flow rates might have limited temperature drop of the inlet air because of the limited contact time of the inlet air and working air with the HPEs and ceramic tubes, respectively. As a result, it is recommended that the inlet air velocity should be controlled between 2-2.5 m/s to compromise between the need of high cooling capacity for cooling

loads and thermal comfort requirements of low temperature of supply air. Also, the Fig 6-9 shows that the theoretical effectiveness and cooling capacity were slightly higher than that of the experimental results, with maximum error of 10.7 and 11.4%, respectively.

6.4.4 Effect of the working-to-inlet air flow rate ratio

Fig 6-10 shows the WB effectiveness and cooling capacity profiles against the change of the working-to-inlet air flow rate ratio from 20% to 80%, at inlet air conditions of 40, 35, and 30 ℃, with constant inlet 35%RH, 3.5 (m/s) inlet air velocity, and 23℃ water temperature. As can be seen in Fig 6-10, the best values of the WB effectiveness were harvested at flow rate ratios higher than 50%. This is a result of having high portion of volumetric flow rate of cooled air is diverted into the wet channel. It can also be seen that for flow rate ratios above 60%, the WB effectiveness remains almost constant and reaches peak of 0.86 at 40℃.

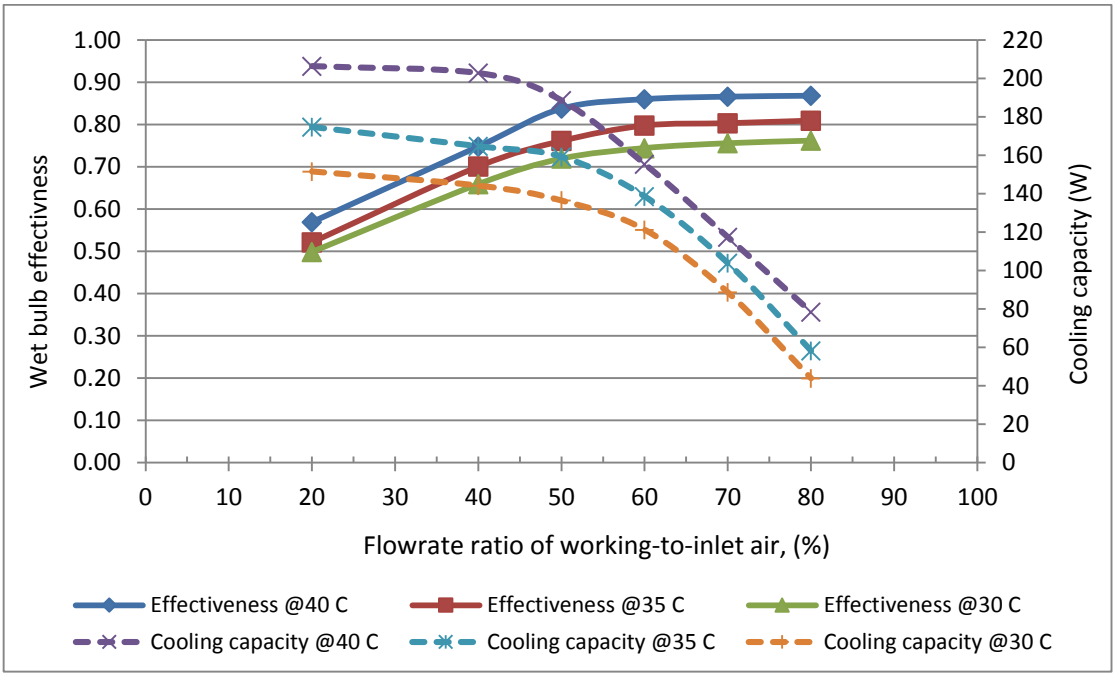


Fig 6-10 WB effectiveness and cooling capacity variation against flow rate ratio of working-to-inlet air at inlet air speed of 3.5m/s, 35% RH and 40, 35, 30℃ inlet air temperatures

In contrast, the cooling capacity profile tends to have opposite tendency of the effectiveness profile. The highest cooling outputs were associated with low flow rate ratios, it reached a peak of 206 (W) at 20% working-to-inlet air flow rate ratio and inlet air temperature of

40℃, then, its value slightly fallen down by 4% as the flow rate ratio increased to 45%. For higher flow rate ratios, >50%, the cooling capacity sharply declined as the flow rate ratio increased. The reason behind low values of cooling capacities at low flow ratios is that a small amount of cooled inlet supply air is pumped to the conditioned space, while most of it is diverted to the wet-air channel as working air, yet the best values of the WB effectiveness were achieved at high flow rate ratio of 80%, as see in Fig 6-10.

As the best values of cooling capacity are related to small flow rate ratios of ≤45%, whereas high values of effectiveness are associated with high flow rate ratios of ≥60%. This yields optimum WB effectiveness and cooling capacity for air flow ratio of 50%. This is consistent with published literature in which IEC systems were designed and recommended to perform at flow rate ratio of the working-to-inlet air of 50%, like [69] and [71].

6.5. Water consumption rate of the cooler

Fig 6-11 presents experimental and theoretical water consumption rates of the cooler as function of the various ambient air temperatures. The simulation results show that the water evaporation rate is directly proportional to the inlet air temperature for a constant inlet air moisture content. Hence, the water consumption at various inlet air temperatures can be estimated roughly from the water evaporation rate of 0.01 $l/h/℃$. The experimental results are in good agreement with simulation results both in trend and in quantity to within a maximum error of 11%, as a result of measurement errors, over saturation of the ceramic materials, and water and air leaking from the system. It is demonstrated in Fig 6-11 that the cooler water consumption rates were in the range of 1.07-2.11 (l/kWh) of cooling output at inlet operating conditions of 25-45$℃, 35\%\ \mathrm{RH}$, 75 m^3/h air flow rate, and 50% flow rate ratio.

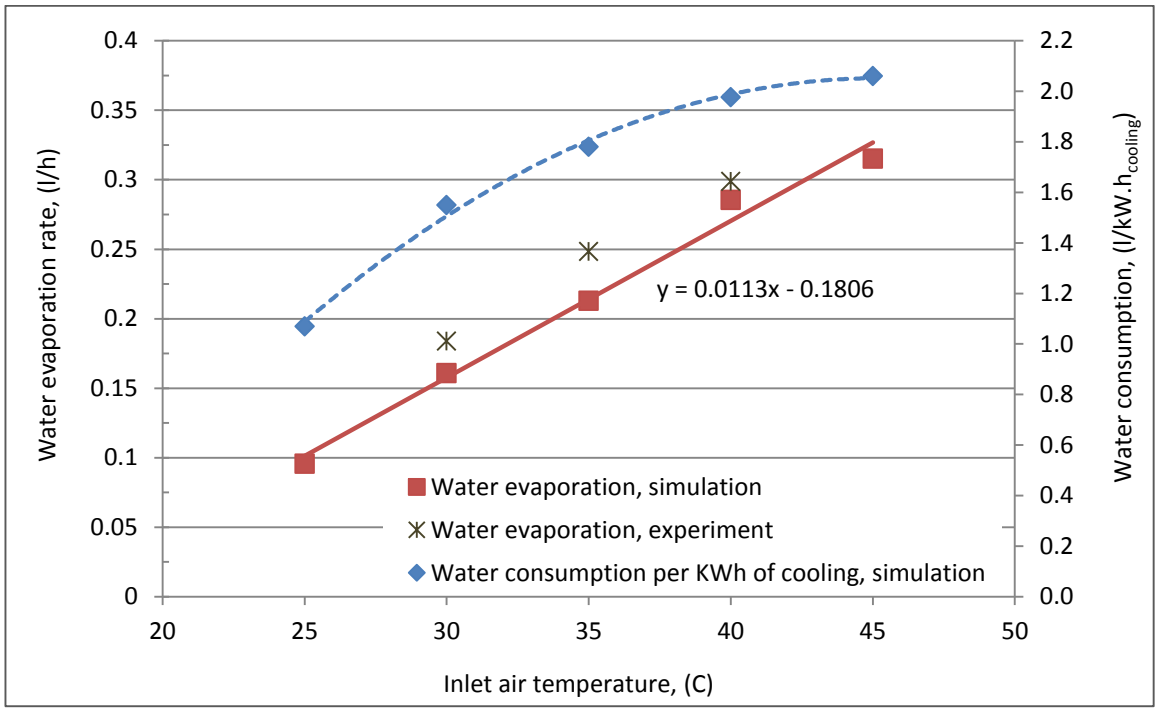


Fig 6-11 Water evaporation rate at working conditions of 75 m^3/h air flow rate, 35% RH, and 50% flow rate ratio

6.6. The discrepancy between computed and measured results

Using the theoretical and experimental methods for evaluation of thermal performance of the cooler revealed differences between measured and calculated findings as shown in the previous sections. Several possible causes for the results' discrepancy are explained as follows:

- Energy loses to the surroundings

In the computer model, it was assumed that heat transfer into or out of the device is neglected due to the insulated outer walls of the cooling unit i.e. adiabatic walls. Nevertheless, the outer walls of the actual unit were not insulated due to the need for transparent walls for monitoring the water distribution and air flows. Yet, the walls are relatively thick and the ambient conditions inside the laboratory with zero air speed that make the convective heat transfer negligible. Nevertheless, a layer of insulation of walls would be preferable to prevent heat transfer with the surroundings, and to comply with the

assumption of adiabatic walls, otherwise a term for "energy losses" should be introduced in the energy balance equations of the system.

- Water distribution system and water leakage

Water distribution mechanism of this cooling system is based on two unique characteristics of porous materials: strong capillary forces and large water holding capacity. This cooling system was designed without water circulation system. The installed porous ceramic tubes, with a proper porosity, works as wick media for the cooler and holds water inside the porous tube with only small amount of water siphon from the ceramic micro-pores, to form thin water film over the outer surface of the ceramic cylinders. In practice, several cases of overdoes of feed water were observed during the tests, some water droplets might be accumulated at the base of the cylinders, it could be mainly related to high porosity of the porous ceramic materials used. For long-term system operation and without controlling feed water flows from the overhead tank, the excessive water would flood the entire wet-air channel with water which ultimately would leak to the lower channel. The leakage can be related to the fabrication process and the accuracy of the machinery work in the laboratory. It is believed that these manufacturing problems would be overcome if the system was assembled at manufacture facility. A few cases were recorded of water droplets spillage from the wet-air passage to the dry-air passage, in such circumstances the results of the experiments were considered void.

- Equivalent diameter of the square fins:

The heat pipe is fitted with square fins to increase heat transfer rates. This type of fin was selected to correspond with the duct geometry and, therefore, ensuring minimal escape of the process air without contacting the fins. Yet, finding the fin efficiency of the square fins is not straightforward, and there is no charts, or equations from which the efficacy could be calculated. An equivalent diameter is used for the square fin to convert it into an equivalent radial fin, as shown in Fig 6-12, using Eq. (4.28). Then, carry on the calculation as if circular fins are employed by using their efficiency graphs. The original square fin is 60*60*0.9 mm

and the equivalent radius of the radial fin would be 33.85 mm. This can be one of the sources of the discrepancy between calculated and measured results.

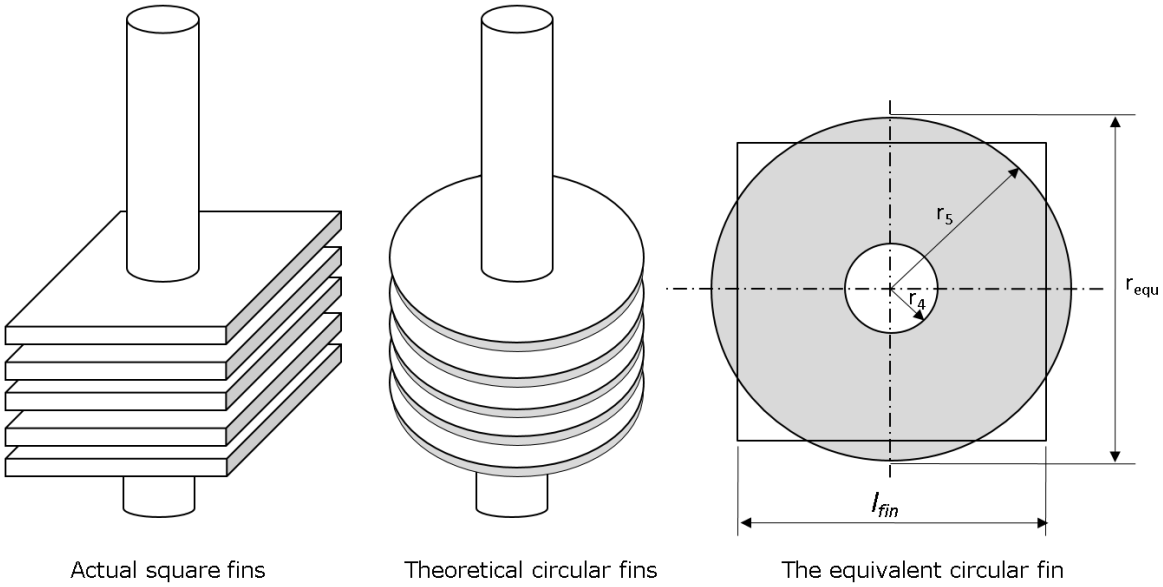


Fig 6-12 Equavalent radial fin

- Contact resistance

From the manufacturing process of the finned heat pipe and machinery method used to fit the fins to the heat pipe evaporator, a contact resistance exist between the fin collar and heat pipe surface that should be included in the thermal resistance equation of the heat pipe, Eq. (4.30). Though some text books, like [118], provide typical values of this resistance of various composite materials, it is hard to precisely predict the contact conductance between both metals in order to determine the thermal resistance [127]. In this study, due to the lack of some of the heat pipe technical information from the suppler, the thermal contact resistance was not considered.

6.7. Effect of increasing numbers of heat pipe and ceramic tube modules

Based on the investigation of the effect of ambient air temperature carried out, it can be inferred that the cooler performance is enhanced as the inlet air temperature increased. But, the cooling effectiveness of the cooler, i.e. the supply air temperature, is still limited

and dependent on the ambient air conditions; temperature and humidity. The supply air temperature rises as the ambient temperature increases, despite the considerable drop of inlet air temperature achieved.

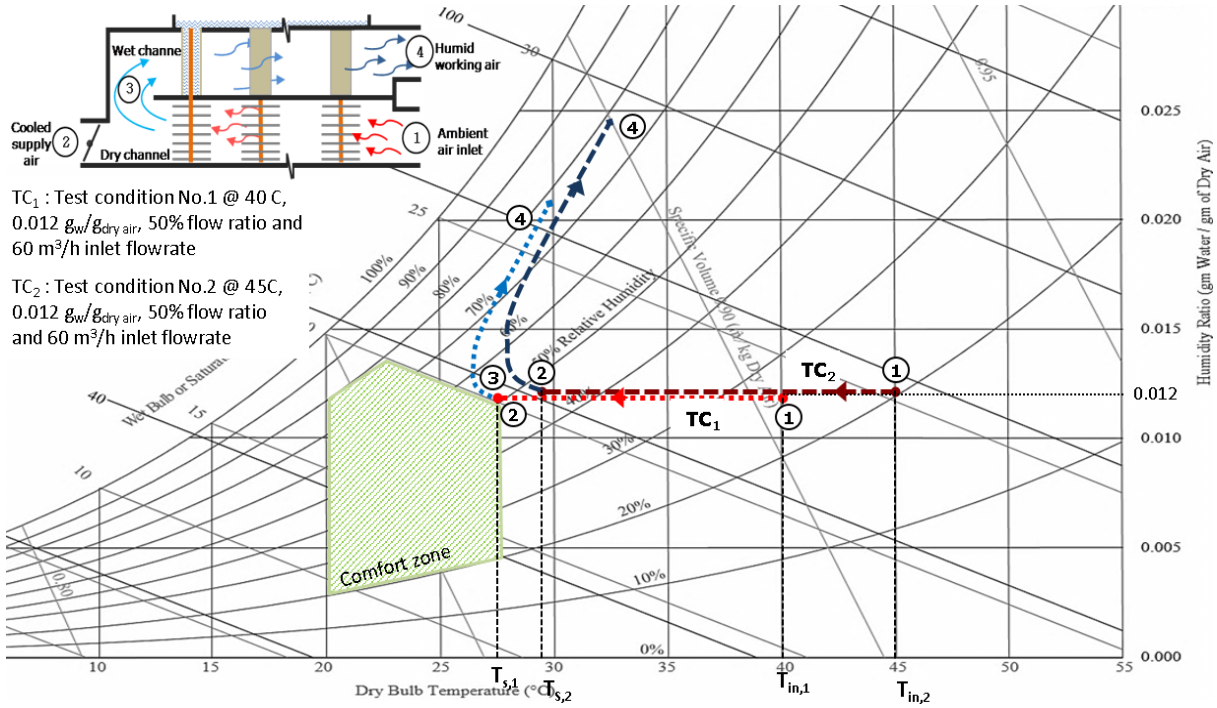


Fig 6-13 Psychrometric plotting of two inlet temperatures under inlet air conditions of 40 and 45℃, constant moisture content of 0.0120 $kg_w/kg_{dry\ air}$, flow rate ratio of 50%, 60 m^3/h flow rate, 23 ℃ water temperature and 15 rows of heat pipe

This is explained further by plotting cooling process through the cooler on the psychrometric chart, as shown in Fig 6-13, for inlet air temperatures of 40℃ and 45℃ with constant moisture content of 0.0120 $kg_w/kg_{dry\ air}$, while other parameters are fixed to their pre-set values presented in Table 6-1. Although inlet air temperature reduction improved as the ambient air temperature increased, the supply air temperature (T_{s1}) increased to $(T_{s,2})$ as the inlet temperature rose from $(T_{in,1})$ to $(T_{in,2})$, as present in Fig 6-13, this possibly due to limited the cooling effectivity of the cooler and incapability to maintain the supply air temperature constant as the inlet condition became hotter. Furthermore, the working air flows through the water-saturated porous tubes exchanging sensible heat and water vapour with the water film, and then is rejected to the environment before reaching 100% saturation condition, as seen on the psychrometric chat of the process (3-4). This means

the working air still have the ability to hold more water vapour. But due to shortage of wet surface area, the working air leaves the cooling system before reaching the full saturation conditions. As a result of this insufficient heat removal from the condenser side of the heat pipes i.e. the wet-air channel, less heat is transported from the evaporator side of the heat pipes i.e. the dry-air channel. This ultimately affected the inlet air temperature reduction and, consequently, the supply air temperatures do not reach the comfort zone for extreme hot climates, particularly for inlet air temperatures above 42 °C, as presented in Fig 6-4.

Principally, two techniques can be implemented to ensure complete saturation of the working air before it is discharged, this would ultimately improve the heat transport from the dry-air channel. First method, using bigger diameters of the ceramic tubes which can relatively increase the wet surface area for heat and mass transfer on the wet-air side. However, the thermal resistance of the water and ceramic tube increase which effect the heat transfer rates from the heat pipe, as presented in Fig 4-10. The other method is adding extra units of heat pipe and ceramic tube modules. Adopting this solution would be beneficial in terms of additional heat is transferred from the dry-air passage to the wet-air passage and, also, increasing the wet surface area for hear and mass transfer without excessively increase the thermal resistance and water usage for each heat pipe. Theoretically, using 20 of heat pipe and ceramic tube units for the cooling system increases the wet surface area by 30.33%. Yet, these extra units would have an effect on the initial cost of the cooling system and higher water consumption as well.

The numerical results are plotted on the psychrometric chart in Fig 6-14, for ambient conditions of 40℃ and 45 ℃ inlet temperature, 0.0120 $kg_w/kg_{dry\ air}$ moisture content, 60 m^3/h flow rate ratio, 23 ℃ feed water temperature, 50% flow rate ratio and 20 heat pipes. As illustrated in Fig 6-14, the thermal characteristic of the air on both air passages of the cooler improved, the working air left the cooling unit at saturation conditions, and the temperature drop of the inlet air increased. Also, it was found that the thermal performance of the cooler enhanced regarding the inlet air temperature drop and the effectiveness, particularly at ambient air temperature of 45 ℃. By comparison between the two cases of

15 and 20 heat pipes, at test condition TC_2 the supply air temperature improved by 3.29 ℃, whereas at TC_1 by about 2.08 ℃ as a result of increasing the number of heat pipes to 20 units. Furthermore, it can be seen from Fig 6-14, the effect of increasing the ambient conditions on the supply air temperature was less than that of the 15-heat-pipe cooler, see Fig 6-13. The supply air temperature increased by almost 0.85 ℃ as the inlet air temperature rose from 40 to 45 ℃. Thus, it is clear that the selection of heat pipe numbers is dependent on the operating temperature ranges i.e. the ambient air temperature. The benefit of adding more heat pipes is obvious at inlet air temperature above 45 ℃, and it is due to the fact that the selection of heat pipe number, i.e. 15-heat-pipe, of this cooler was based on the working conditions of 40℃ intake air temperature.

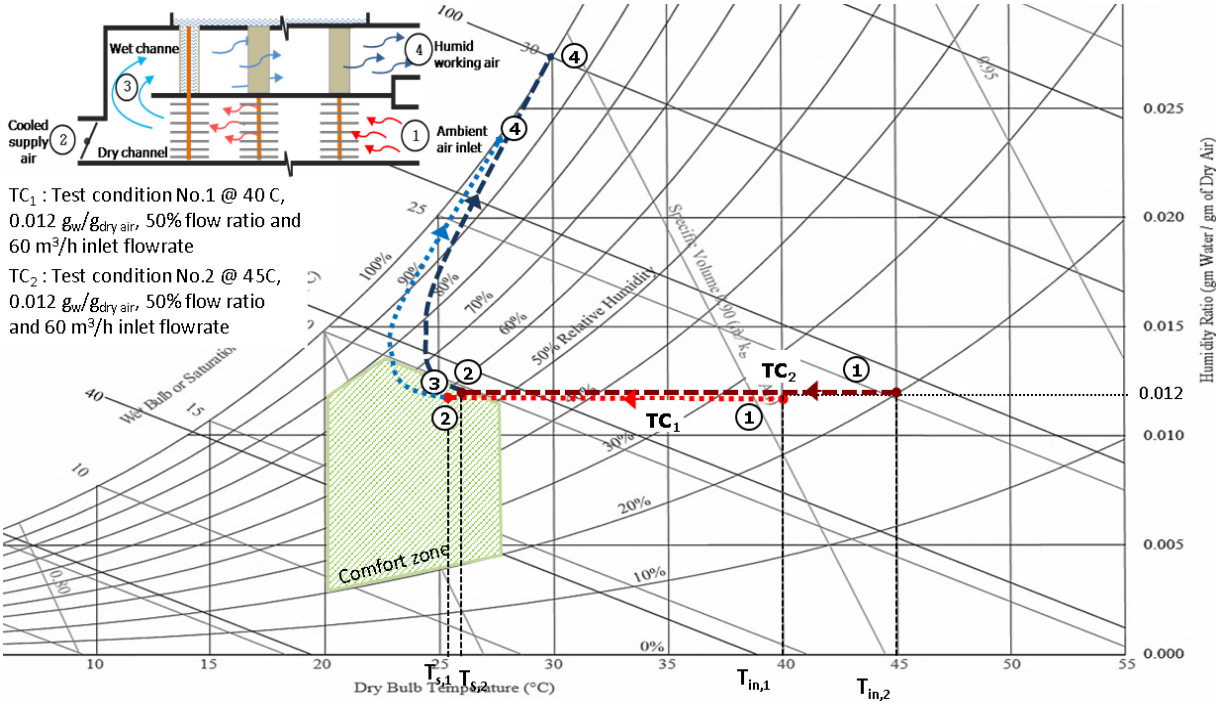


Fig 6-14 Psychrometric plotting of two different inlet temperatures under inlet air conditions of a constant moisture content of 0.0120 $kg_w/kg_{dry\ air}$, flow rate ratio of 50%, 60 m^3/h flow rate, 23 ℃ water temperature and 20 rows of heat pipes

For further numerical evaluation of the impact of the number of heat pipe rows on the cooler performance, Fig 6-15 illustrates the relation between the cooler effectiveness and the number heat pipe rows, for various ambient temperatures and at operational conditions presented in Table 6-1. In modelling, the inlet air temperature was varied from 35 to 45 ℃,

while the number of heat pipe and porous tube modules of the cooler ranged from 6 to 24 units. The numerical results showed that the effectiveness of the cooler improved gradually as the number of heat pipe units increases till certain number of heat pipes, after that any added units have relatively minor effect on the cooler performance. This limit clearly depends on the ambient air conditions. For example, at the inlet air temperature of 35 ℃, 16-heat-pipes would be sufficient to obtain best effectiveness as any extra heat pipes would not contribute in any significant performance improvement. But it may added up in the initial cost and the overall size of the cooler. While, for ambient conditions of 40 and 45 ℃ of inlet air, effectiveness curve tend to remain nearly constant from 18 and 20 heat pipes, respectively.

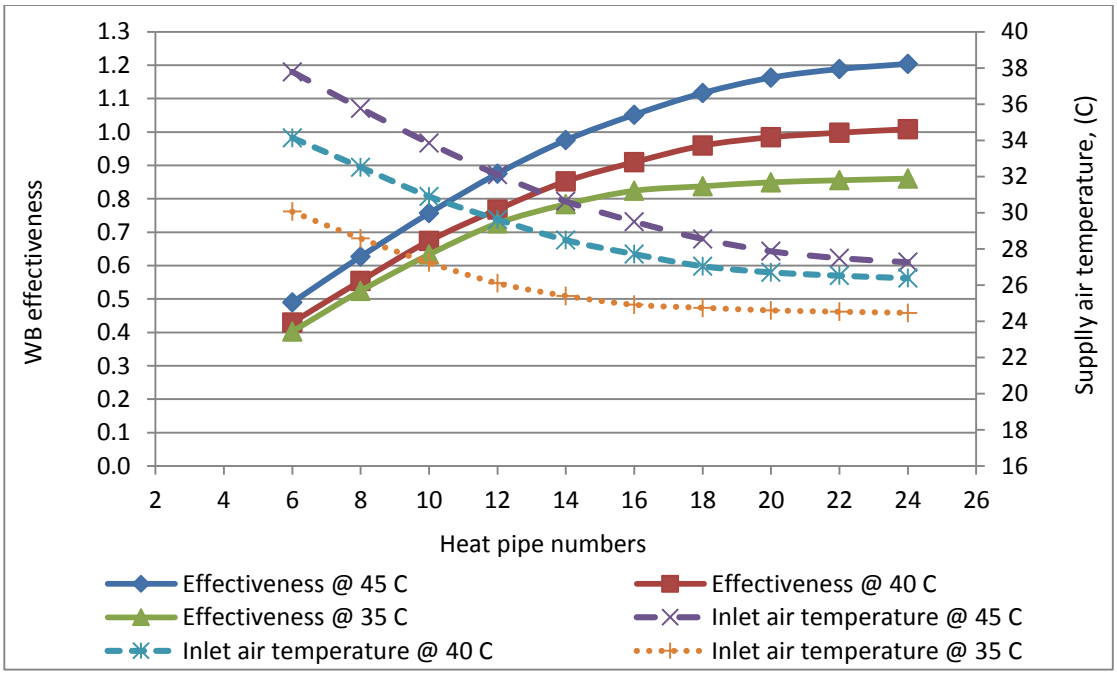


Fig 6-15 Effect of heat pipe numbers on the effectiveness for verious inlet temperatures and under fixed operation condtios of 75 m^3/h air flow rate, 35% RH, and 50% flow rate ratio

To compromise between best number of heat pipe rows number within this wide range of working conditions, 20 heat pipe and porous ceramic units should be installed as the target applications of this cooler intended to operate in arid and semi-arid locations, and hot and dry climate, in which the ambient temperatures soars above 45 ℃ with the relative humidity around 25% [128].

Interestingly, from Fig 6-15, it is noted that the supply air profiles for various inlet temperatures have a turning point at which any increase of heat pipe numbers would not have a noticeable decrease of the supply air temperature. This occurred when supply air temperature reaches 28 and 27℃ for inlet temperatures of 45 and 40℃, respectively. While at operating temperature of 35℃, the curve of the supply temperature is sharply declined till approaching 25℃, after that, the supply air temperature drop barely is improved despite the increase of the number of heat pipe rows. This, possibly, can be related to the performance of each individual heat pipe which is influenced by the decrease of the temperature difference at both ends of the heat pipe i.e. temperature difference between evaporator and the condenser that is the driving force of the heat pipe operation. Further investigation may be required to establish relationship between heat pipe sub-components and heat transfer capacity of the heat pipe, as suggested in the literature that wick type, vapour space diameter, and working fluid type of the heat pipe influence on the performance of the heat pipe [115] and [118].

Chapter 7: Simplified economic and environmental evaluation

7.1 Building cooling loads assessment

In this assessment, a typical domestic building in hot and dry climate region (Benina city, Libya with latitude of 32.086° N and longitude of 20.26° E). A simple square shape form of the house, from [129], with 110 m^2 floor area and facing North, the house floor plan is shown in Fig 7-1. House main details are summarised in Table 7-1, while Table 7-2 presents specification of rooms and main input data of the conditioned spaces i.e. number of people, cloths, lighting, equipment, etc. based on the recommended values from CIBSE Guide A [12]. In addition, the construction of the walls, roof and floor, windows, and doors and their U-values are presented in Table 7-3 and Fig 7-2.

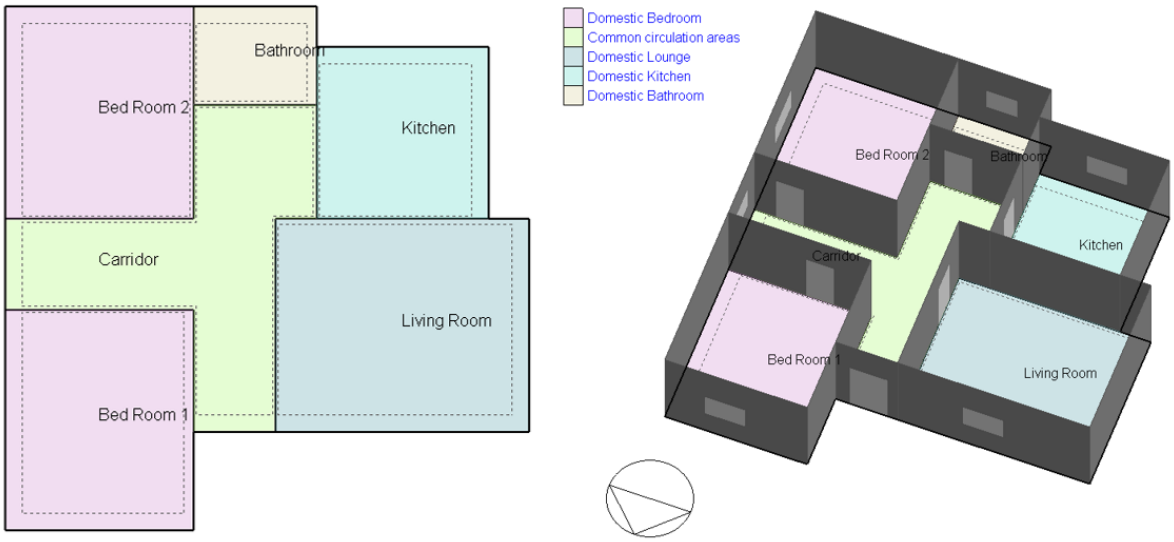


Fig 7-1 House plan view and 3D sketch of the house

Table 7-1 House specifications

Descriptions	QTY	Dimensions/value	unit
Number of floors	1	-	-
Occupied floor area	-	110	m^2
Height of the building	-	3	m
Number of people	6	-	-
Density of people	-	0.054	people/m^2
Windows	6	1.4 x 1.4	m^2
Internal doors	5	0.9 x 2.2	m^2
External door	1	1.2 x 2.2	m^2

Table 7-2 Input data and assumptions of the house rooms

Parameter	Bedroom 1	Bedroom2	Living room	Bathroom	Kitchen	Corridor
Area, m^2	4.9 x 4.0	4.9 x 4.0	5.3 x 5.0	2.85x 1.8	3.7x 3.7	8.0x 1.8 6.0x 1.8
Density (people/m^2)	0.1030	0.2060	0.225	0.183	0.145	0.1194
Activity	0.9	1.0	1.1	0.9	1.0	1.8
Clothing	0.5	0.5	0.65	0.25	0.65	0.65
Min fresh air (l/s-person)	10	10	10	12	12	10
Infiltration (ac/h) always on 24/7	0.05	0.05	0.05	0.05	0.05	0.05
Lighting, lux	100	100	150-300	150	150-300	100
Electrical equipment	Laptop	TV PC	TV	Washing machine	Cooker Oven	-

Table 7-3 Specifications of walls, roof, floor, doors, and windows

Component	Thickness (m)	Specifications	U-value (W/m^2K)
External walls	0.42	5 layers 10mm outermost mortar-cement of plaster, 150mm hollow block, 100mm Polystyrene insulation, 150mm hollow block, and 10mm internal mortar-cement plaster.	0.266
Internal walls	0.141	3 layers of 13mm outermost gypsum plastering, 115mm brickwork, and 13mm innermost gypsum plastering	1.959
Flat roof	0.29	3 layers of 20mm Asphalt, 250mm cast concrete, and 20 mm mortar-cement plaster.	1.171
Floor	1.24	4 layers of 20mm inner ceramic floor tiles, 20mm floor screed, 200mm cast concrete, 1000mm soil.	0.805
External door	0.06	3 layers of 2mm metal surface, 56mm of Glass fibre insulation, and 2mm of metal surface	2.839
Window	0.04	Double clear 6mm/13mm air gap, with internal blinds	2.708

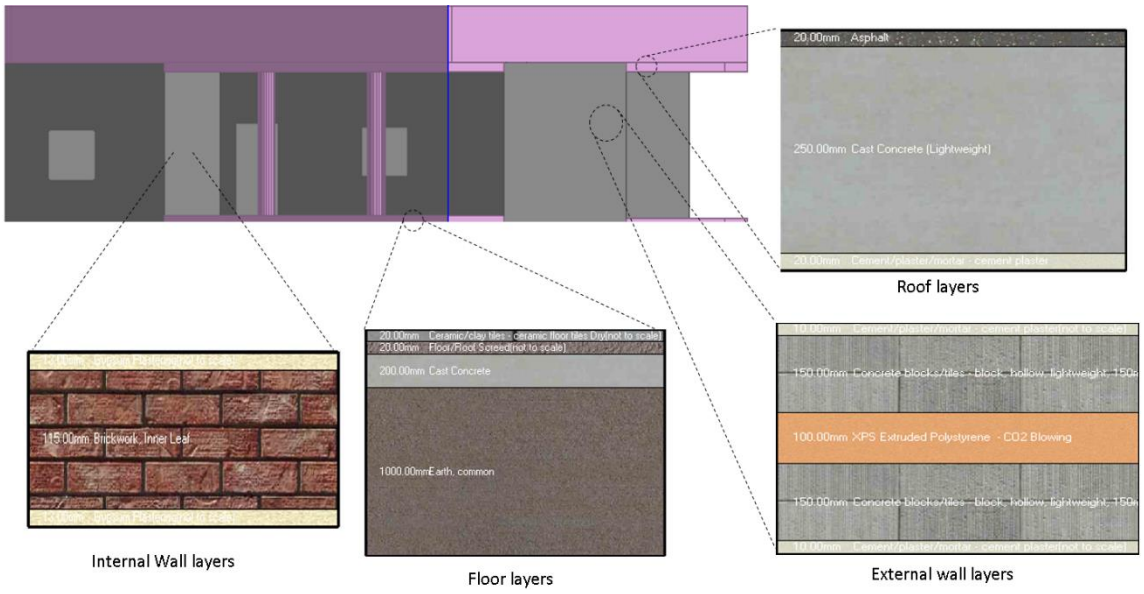


Fig 7-2 Structure of house components

The weather data and building construction and orientation were modified in Design Builder software, powered by EnergyPlus simulation engine, to estimate the cooling load of the entire house in the selected location. The Modelling calculation of the cooling load takes into account the internal loads (people, electrical equipment, appliances, ventilation, lighting, and insulation) and the building envelope components, as given in Table 7-2 and Table 7-3. The daily variation of the cooling load profile of house is presented in Fig 7-3, while Annual cooling load of the house is estimated to be 7400 kWh i.e. 67.27 kWh/m^2.

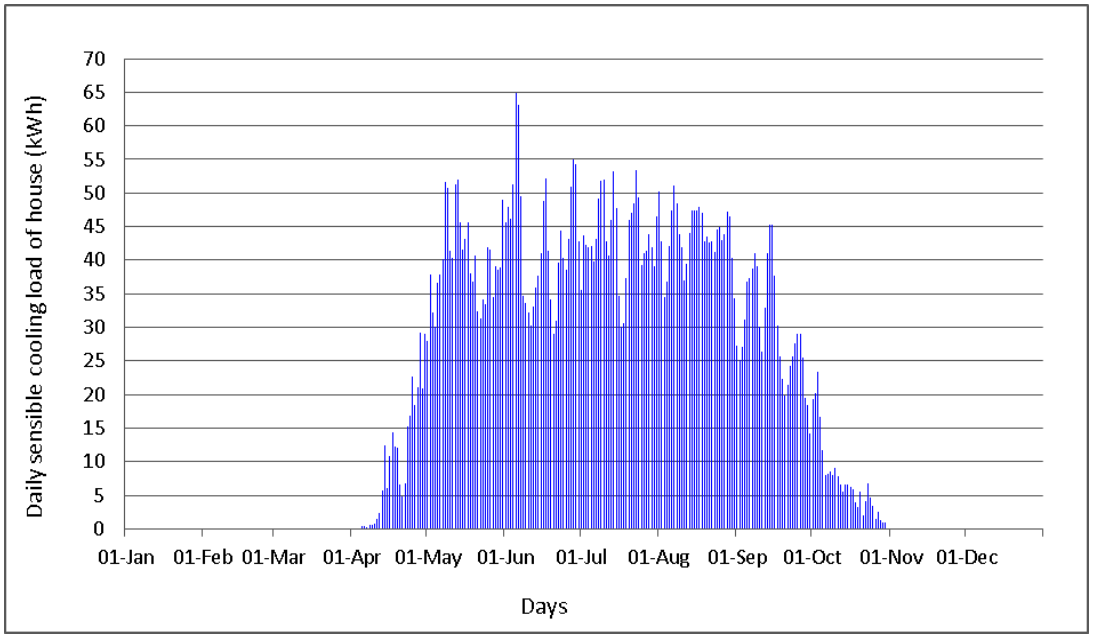


Fig 7-3 Daily sensible cooling load of the house

The outdoor design temperature is 37.5 ℃ with 22% RH based on software database. The indoor temperature of 25 ℃ with 50-60% RH is recommended by ASHRAE [14]. Once the design indoor air temperature of the space is known, the supply air temperature (T_2) of the cooling system can be determined by Eq. (3.1), since the WB effectiveness of the cooler and outdoor design conditions are given as well. Also, the system cooling output (Q_{cc}) can be calculated from Eq. (3.3). Additionally, the COP and the total power consumption of the cooler is determined by using Eq. (3-4) and (3-5), respectively. Water consumption rate (m^3/s) can be calculated from equation (3-6).

7.2 The cooler capacity

The laboratory prototype module can be scaled up to meet the cooling load of considered typical house. Using the developed numerical model, the cooler operational parameters were selected based on number of heat pipes, inlet air velocity, and flow rate ratio. Table 7-4 presents the technical specifications and performance parameters of the cooler under outdoor design temperatures of (37.50℃, 22% RH) of selected location based on 99.6% coverage of the DB temperature.

Table 7-4 Thermal performance of the cooling system

Parameter	unit	value
Heat pipes number of rows	-	20
Wet ceramic area,	m^2	0.2551
Feed water temperature	℃	18
Supply-to-inlet air ratio	%	50
Inlet air dry-bulb temperature	℃	37.50
Inlet air wet-bulb temperature	℃	21.10
Supply air dry-bulb temperature	℃	23.61
Supply air relative humidity	%	49%
Supply air flow rate	m^3/h	37.27
WB effectiveness	-	0.8591
Cooling output	W	167.175
Cooling output per $m^2$of wet surface	W/m^2	655.332
Cooling output per m^3/h of supply air flow rate	$\frac{W}{m^3/h}$	4.486
Water consumption rate	l/h	0.2864
Water consumption rate	$litre/kWh_c$	1.7135
COP	-	14.025

Based on a daily operation of 10 hours, a seasonal operation of 6 month a year (i.e. May to October), as shown in Fig 7-3, corresponding to annual operational hours 1800 hours and a cooler COP of 14.03, the annual consumption of energy and water is summarised in Table 7-5.

Table 7-5 Daily and annual consumption of electricity and water of the IEC system

Parameter	unit	value
Daily cooling capacity of the cooler	$(KWh_c)_{daily}$	1.6717
Daily electricity consumption	$(KWh_e)_{daily}$	0.1192
Daily water consumption	L/day	2.8647
Yearly cooling output of the cooler	$(KWh_c)_{year}$	300.915
Yearly electricity consumption	$(KWh_e)_{year}$	21.4560
Yearly water consumption	$L/year$	515.6389

7.3 Economic assessment

7.3.1 Annual electrical energy consumption

In assessing the feasibility of the current evaporative cooler, a direct comparison with traditional A/C was carried out. The annual electricity consumption of both systems can be determined based on their coefficient of performance. Traditional A/C units operating in hot climates suffer from low COP, with average COP of around 2.0 [20]. Fig 7-4 compares annual power consumption between the proposed evaporative cooler and a vapour compression A/C. It which shows that the performance of the evaporative cooler surpasses by a large margin that of the vapour compression A/C with annual electrical energy savings amounting to 3.172 MWh_e.

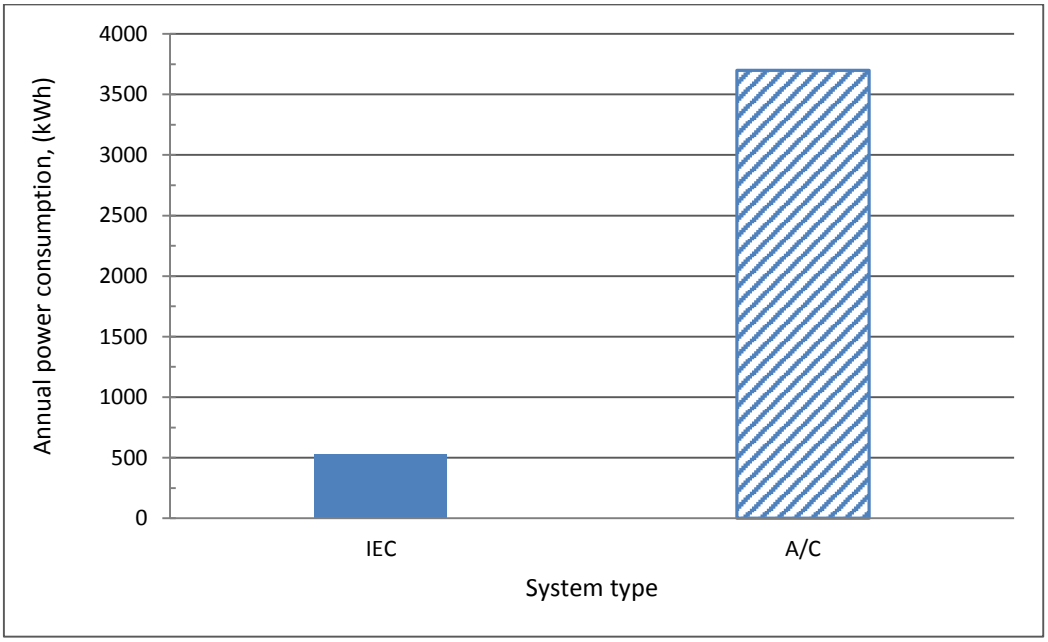


Fig 7-4 Comparison of annual power consumption between the heat pipe-ceramic based IEC and vapour compression A/C.

7.3.2 Annual water consumption

Electricity and desalinated water prices vary widely depending on location, climate, type of power plants and fuel used, and the national demand of each country. Using the current available prices in Libya does not provide realistic results as energy and water are heavily

subsidised by the state. Therefore, an average electricity price of 0.063 €/kWh is considered based on prices from the wider region of Middle East and North Africa (MENA) countries, as presented in Appendix E [130]. Similarly, the prices of desalinated water ranges from 0.4-3 $€/m^3$ depending on desalination method used, size of plant, and type of water [131]. Thus, the water cost would be estimated at a price of 1.50 $€/m^3$. Accordingly, Fig 7-5 presents a comparison between annual operating costs of the EC system and vapour compression A/C, the total running costs of the A/C unit is about 233.09 $€/year$, which is four times higher than that of the EC system.

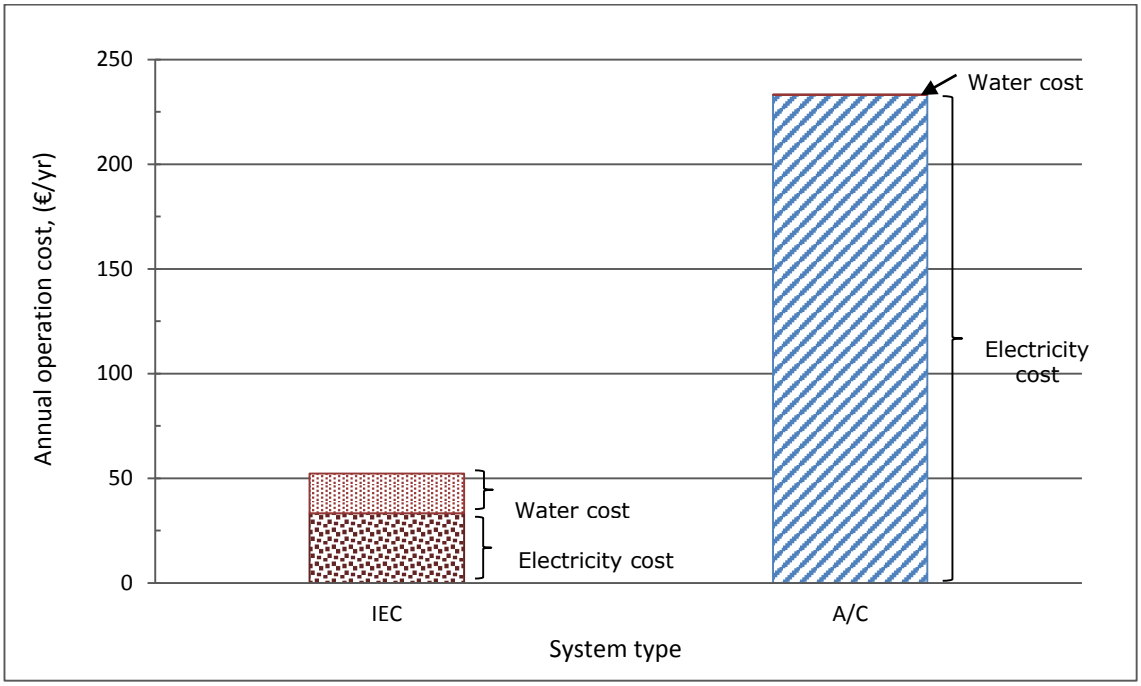


Fig 7-5 Comparison between annual operation cost of vapour compression A/C and the proposed system of 110 m^2 House

It is noted, from the above graph, that the A/C system does not require any water for air cooling process. Nonetheless, it consumes water indirectly via its electricity consumption, which require water at power generation stage. Namely, the A/C unit use large amount of electricity, which would be met by relatively high water demand at power production site, (i.e. so called off-site water consumption). Interestingly, if the water amount required to produce 1 kWh electricity is considered (an average of 3.8 l to generate 1 $\mathrm{kW\,h_e}$ form thermal power plant [132]), thus a comparison between on-site and off-site water

consumption of both cooling systems can be made. By considering the cooling load of 7400 $\mathrm{kWh/yr}$, the A/C system requires an equivalent of 14.059 $\mathrm{m^3/yr}$ off-sit water demand for electricity production to meet this cooling load, while water demand of this IEC system for the same cooling load is 14.684 m^3/yr (i.e. 12.679 m^3/yr on-site water demand and 2.005 m^3/yr off-site water usage). It is obvious that total water-usage of the IEC is almost equal to that of the traditional A/C system. So, this demonstrates strong evidence that IEC systems being environmentally friendly and cost-effective technology. Furthermore, this finding is consistent with results from [13] who performed a comparative study of water-use efficiency between wide ranges of cooling systems including DEC system, IEC system, MVC A/C, MVC A/C with evaporative pre-cooling of condenser inlet air, and combined cooler of IEC and MVC A/C system. It is concluded that the evaporative coolers have considerably reduced annual power demand and their water-use are not higher than that required by the conventional A/C systems.

7.4 Environmental impact

One of the most significant advantages of the IEC is their limited electricity demand, which ultimately leads to low Carbon-related emissions, comparing with conventional A/C systems. Once the emission factor of electricity generation and power consumption saving are known, the annual reduction of $\mathrm{CO_2}$ emissions can be calculated. The total amount of $\mathrm{CO_2}$ emissions saved in this case study is 0.238 tonnes CO_2 per year (i.e. about 85.74% savings of carbon emissions for one household). Besides, another environmental benefit is that this IEC system does not use any dangerous or toxic refrigerants which unfortunately are used by conventional A/C such as CFCs, HCFCs, and HFCs which contribute to the increase of greenhouse gases emissions and the ozone-layer depletion.

Hence, high COP, low power and water consumption, and low environmental impact are the most required characteristics of this IEC system, the heat pipe and porous tube based R-IEC system can play a major role towards green and sustainable air cooling systems and less-carbonised environment for best of people's health and comfort.

7.5 Summary

This chapter outlined a brief economic and environmental assessment of the developed cooler by analysing the performance of the cooling system under real weather data and operational conditions for 110 m^2 house. In this chapter, the annual operational costs and environmental impact were evaluated and compared against conventional air conditioner.

The weather data were based on the Design Builder software database, this programme was used for cooling load estimation of small house in Libya situated in a hot and dry climate, with consideration of building material, people, equipment, ventilation, lighting, and insulation. The Annual cooling load of 110 m^2 house was 7400 kWh.

By comparison with conventional A/C system, the annual electricity consumption of the IEC was less than that of the A/C system by almost 86% that is around 3.172 $\mathrm{MW\,h_e/yr}$ saved from the national power demand, and total money saving in the operational costs of the IEC system was around 180.80 €. While, the reduction of carbon-related emissions was about 0.238 tonnes CO_2 per year which represent 85.7% savings of CO_2 emissions for one household when the IEC system used.

Chapter 8: Conclusion and future work

8.1 Conclusion

In this thesis, the aim was to experimentally and theoretically investigate the thermal performance of new design of regenerative indirect evaporative cooler configured from heat pipe heat exchanger and employing porous ceramic tubes as wet medium of the heat pipe condenser. This heat pipe and porous ceramic tube based IEC system is to be used in the MENA region where the desert climate is prevailing. The cooler is anticipated to overcome some of the disadvantages associated with indirect evaporated coolers such as high water consumption and low performance.

The main key findings to emerge from this research are;

- From experimental work, the manufactured prototype unit was tested under various inlet operating conditions that covers wide range of inlet air temperatures of 30-40 ℃, relative humidity values of 25-45%, inlet air flow rates of 75-150 m^3/h, working-to-inlet air flow rates of 20-70%, and 23℃ water temperature. The cooler performance parameters from all conducted experiments as follows;
  - WB effectiveness ranged from 0.422 to 0.91,
  - Inlet air temperature drop was from 4.50 to 12.41 ℃,
  - Cooling capacity spanned from 72.35 to 233.14 W,
  - COP was 4.62-13.16, and
  - Water consumption rates varied from around 0.841to 2.8 (l/kWh) of cooling capacity.

- Theoretical results were obtained from the developed computer simulation for performance evaluation of the cooler. Several computer simulation runs performed at inlet operation conditions of 30-45 ℃, 25-60% relative humidity, 20-80% working-to-inlet air flow ratio, 30-210 m^3/h, and 23℃ water temperature, the thermal performance indexes are as follows;
  - WB effectiveness widely varied from 0.52 to 1.053,

- Inlet air temperature reduction ranged from 8.05 to 17.1℃,
- Cooling outputs varied from 68.76 to 314.9 W,
- COP spanned from 6.33 to 17.02,
- water consumption rates per 1 kWh of cooling output ranged from 1.08-2.11 (l/kWh), this is about 30-55% saving of water consumption comparing with [99] and [88].

- Regarding with meeting comfort levels recommended by ASHRAE, the cooler is able to supply air at temperatures and humidity within the comfort zone for wide range of ambient air conditions of ≤42 ℃ and ≤30% RH. While for ambient air temperatures above 42 ℃, the range of supply temperatures was above of comfort levels by 0.5-2 ℃. Therefore, it is recommend for such extreme ambient conditions to increase heat pipe numbers to 20 and keep inlet air velocities around 2 (m/s) and working-to-inlet air flow ratio fixed at 50%.

- Computer model verification was conducted by comparing between the experimental data and numerical results. A good agreement were found between the experimental and the predicted results from the numerical model. Though, a small discrepancy between the simulation and the experimental findings results was noted, The computed supply air temperatures were lower than that of the measured data, the maximum error ranged 3.13-4.93%, the theoretical WB was, also, slightly higher than the experimental WB effectiveness, the discrepancy ranged from 8.67 to 12.92%. Moreover, the cooling capacity maximum error was within 11.41%.

Parametric study:

- The effect of the ambient inlet conditions i.e. the temperature and moisture content of the inlet air.
  - It was found that the inlet air temperature is directly proportional to the WB and DP effectiveness, temperature reduction of the inlet air, COP, and cooling capacity. This means the higher the inlet air temperature the grater the inlet air temperature reduction, thus the higher the cooler performance is.

- The effect of inlet air humidity was relatively small comparing with inlet air temperature influence on the cooler effectiveness. But, at a constant inlet air temperature, humidity variation had a notable effect on the cooler efficiency. The relationship was directly proportional between the inlet air humidity and the effectiveness i.e. as the inlet humidity increases as the effectiveness rises. In the contrast, the inlet air temperature reduction, COP, and cooling capacity was inversely proportional to the inlet humidity. For a constant inlet temperature, the best values of the performance parameters were harvested at lower inlet air relative humidity values. In other words, the thermal performance of the cooler is better at hot and dry inlet conditions.

- The impact of operational parameters was considerable on the thermal performance of the system such as the inlet air velocity, the working-to-inlet air flow ratio, ceramic tube radius, ceramic tube wall thickness, and the number heat pipe rows.
  - The thermal performance parameters i.e. the effectiveness, inlet air temperature drop, COP, and cooling capacity are influenced by the inlet air velocity i.e. inlet air flow rate. The best values of the effectiveness and temperature drop of inlet air were achieved at low inlet air velocity i.e. an inverse relationship between inlet air velocity and the effectiveness exist. In contrast, the COP and cooling capacity were adversely affected by reducing inlet air flow rate. Therefore, low inlet air velocities may contribute to larger size of the system at higher initial costs to compensate the low cooling outputs of the cooler as a result of using low inlet air velocities. While, high inlet air velocities improve the COP and the cooling capacities, but this might limit the cooling effectiveness of the unit i.e. temperature drop of inlet air. For optimum design, a compromising between the effectiveness and cooling capacity must be considered. From both experimental and theoretical results, it is recommended to operate the cooler at 2 to 2.5 m/s.
  - The effectiveness and temperature drop of inlet air of the system improved as the working-to-inlet air flow ratio increased, whereas the cooling capacity and the COP sharply declined when this flow ratio go above 50%, due to limited supply air flow rate forward to the conditioned space despite the benefit of improved temperature reduction

of inlet air and high effectiveness achieved at high flow rate ratio. In contrast, low values of the working-to-inlet air flow ratio, the cooling outputs and the COP improved considerably as result of large amount of air flow rate was supplied to conditioned room. Nonetheless, the effectiveness of the cooler is negatively affected by this setting because of limited temperature drop achieved at low flow ratio of the working-to-inlet air. Therefore, it is recommended to use 50% flow ratio to compromise between cooling effectiveness and cooling capacity.

- Also, the effect of ceramic tube wall thickness and increasing the radius of ceramic tube was assessed. It was shown that the increase of ceramic tube diameter and wall thickness are inversely proportional to the cooling system effectiveness.
- As being the only heat transfer mechanism of the cooling system, heat pipes numbers installed in the unit effect on the thermal performance, the increase of the number heat pipe rows led to improvements of the performance but till certain number of heat pipes. So, any added heat pipes would not cause any significant enhancements of the performance, but it may increase costs. It was found that for extreme hot ambient conditions of 45℃, it is recommended to have 20 rows of heat pipes for the cooler. Whereas, for operational conditions below 40℃, 15-heat-pipes are sufficient.

Operating limits:

The proposed cooler provided significant cooling effectiveness and temperature reduction of the intake air with ability to work under various high inlet air temperatures, but the operation of the cooler might be restricted by two elements; the ambient humidity of the inlet air and the heat transfer capacity of heat pipes. It was found that the system performance considerably deteriorated as the relative humidity of inlet air reach above 35% and/or when the ambient inlet temperature drop below 27℃ due to limited temperature difference between both ends of the heat pipe (condenser and evaporator) which is the driving force of heat pipe operation. It is, therefore, recommended to operate the cooler for hot and dry climate, and, also, investigate the effect of using another heat pipe working fluid on the performance of the system.

A small size Libyan house of 110 m^2 was considered as a base line of a case study for economic and environmental investigation of the annual operation performance of the developed cooler. The house required annual sensible cooling load of 7400 kWh/yr, estimated using Design builder software. The annual operational costs of the heat pipe and porous tube based R-IEC was 52.26 $€/yr$ which mainly paid for 572.61 $kW\,h_e/yr$ electricity and 12.67 m^3/yr water consumed by the cooler to meet the cooling loads. By comparing with vapor compression A/C unit used for the same space at the same operational conditions, the annual electricity saving was around 3.172 $\mathrm{MW\,h_e/yr}$, and the annual saving of operational costs was around 77.6% when the IEC system is used. Furthermore, the annual carbon emission of the IEC was in the range 0.04 tonne that is remarkably 85.74% less carbon emissions than that of A/C system.

8.2 Further work

Although this research has shown the remarkable potential of using heat pipe and porous ceramic for indirect evaporative cooling, further research might explore a few opportunities to improve the cooler performance, as follows;

- **Improving heat pipe heat transfer capacities (Heat pipe optimization)**

  Although the heat pipe was selected as standard component of the cooling system, it was found the heat pipe specifications plays vital role in effecting the overall efficiency of the system. Modelling the heat pipe for optimum design is recommended, the internal specifications of het pipe such as working fluid, wick structure, and inner and outer diameters should be analysed as they can considerably contribute toward improving the heat pipe heat transfer capacity.

- **Using extended surfaces on the condenser**

  One of techniques to enhance overall performance of the system is using fins on the condenser. Employing axial fins on the outer surface of the condenser allows smooth

water flow and increases area of heat transfer between the condenser and the surrounding water, as presented in Fig 8-1. Consequently, increasing the effectiveness of the cooler.

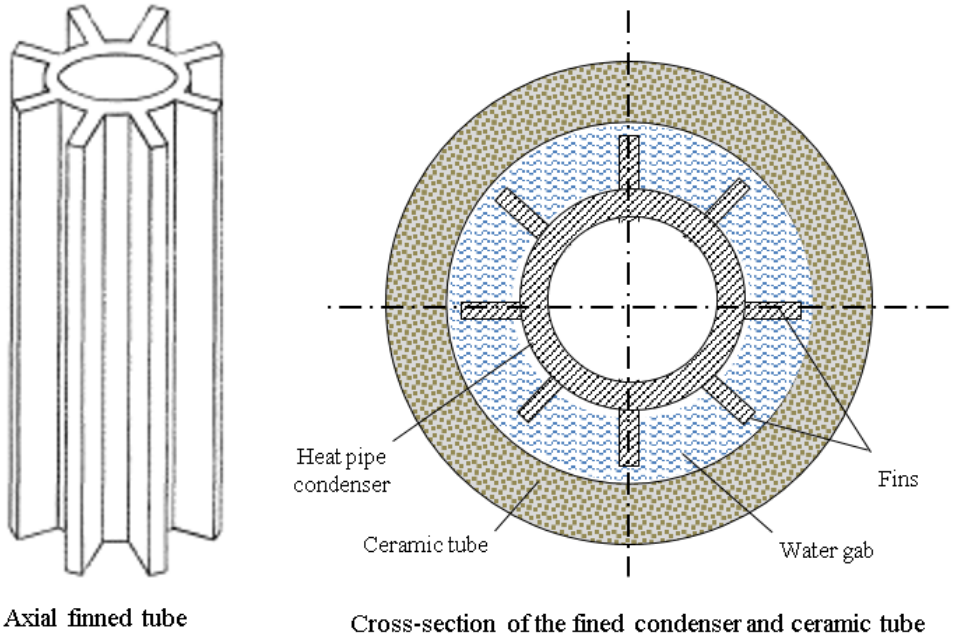


Fig 8-1Schematics of axial fin and cross section of finned condenser and ceramic tube

- **Testing under real weather data for a day-long**

Although the cooling unit was tested under real weather data but it was limited to desert climate with short operating hours of only 6 hrs due to limited opening hours of the laboratory. So, further experimental work might be conducted to determine daily thermal performance of the cooler for typical summer day.

- **Energy recovery of rejected working air**

One of the drawbacks of the sub wet bulb temperature evaporative cooling system is that a portion of the humid and cool air is discharged to the surroundings. Fig 8-2 presents the profiles of temperature and relative humidity of the working air as function of the inlet air temperature, the rejected working air temperature was in the range of 23-34 ℃, with the relative humidity ranged from 73-82%. Thus, there is 7-11 ℃ temperature difference of between the inlet air and the rejected working air, this

considerable amount of cold working air is discharged to the environment which represent a loss of cooling capacity.

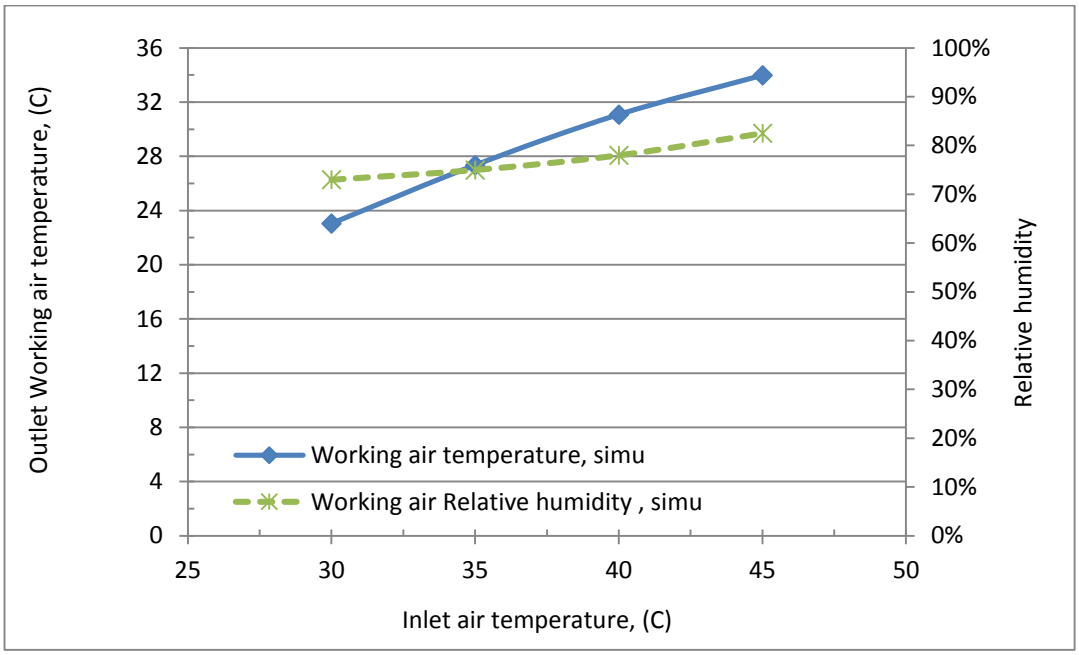


Fig 8-2 Working air temperature and humidity profiles versus inlet air temperature at inlet air conditions 75 m^3/h of flow rate, 35%RH, and 50% flow rate ratio of working-to-inlet air

This energy loss can be recovered in two ways; the first method is to employ a desiccant system to dehumidify the working air to the required levels of humidity and resupply it to the conditioned space. Whereas, the other method is to use a dry-air heat exchanger to pre-cool inlet air using the rejected working air. Each technology has its advantages and limitations in terms of efficiency of the energy recovery and cost of each system.

The use of a desiccant system in conjunction with this R-IEC system is currently the subject of further work research project by another PhD student. Two possible setting of this combined cooling system can be adopted. The first configuration comprises of a desiccant unit followed by the IEC unit. The inlet air, firstly, is dehumidified (process 1-2) and, then, to be cooled by the IEC unit (process 2-3), as presented in Fig 8-3. This configuration has the potential of increasing thermal performance of the current evaporative cooling cooler as well as extend the scope of application to regions of the world with high relative humidity.

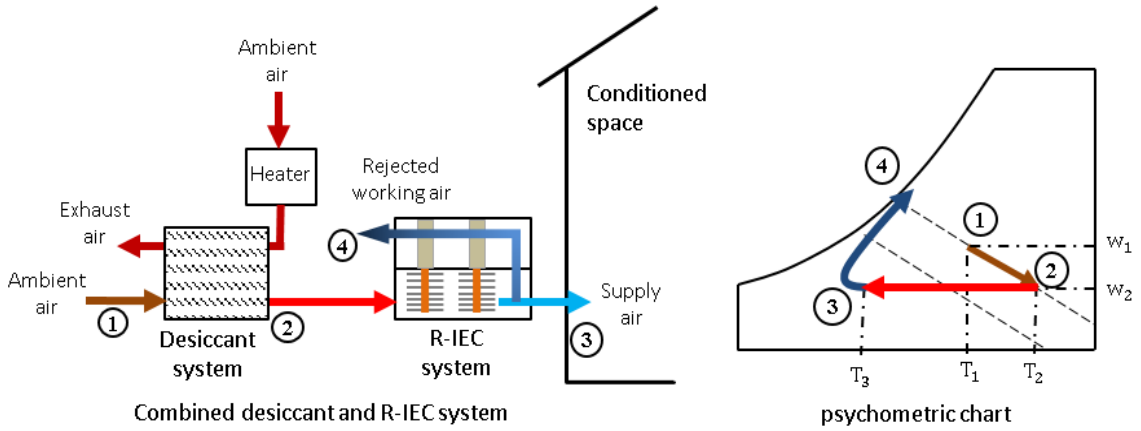


Fig 8-3 First configuration of the combined system

In the second design, a desiccant unit is attached to the exit of the working air stream of the IEC to modify the moisture content of the working air to the thermal comfort levels. In operation, the inlet air is sensibly cooled by the IEC unit (process 1-2) and, then, partly is supplied to the conditioned room, whereas the remaining part is diverted as working air (process 2-3) which eventually leaves the system at worm and humid air (point 3), the rejected working air, then, is drawn through the desiccant unit (process 3-4) to control it moisture content, and leaves the desiccant system drier but at warmer conditions (point 4). After that, the working air is cooled further through the HPHX based IEC system to required levels, as illustrated in Fig 8-4. Using this configuration allows full recovery of cooled inlet air flow rate with zero energy wasted of the cold working air.

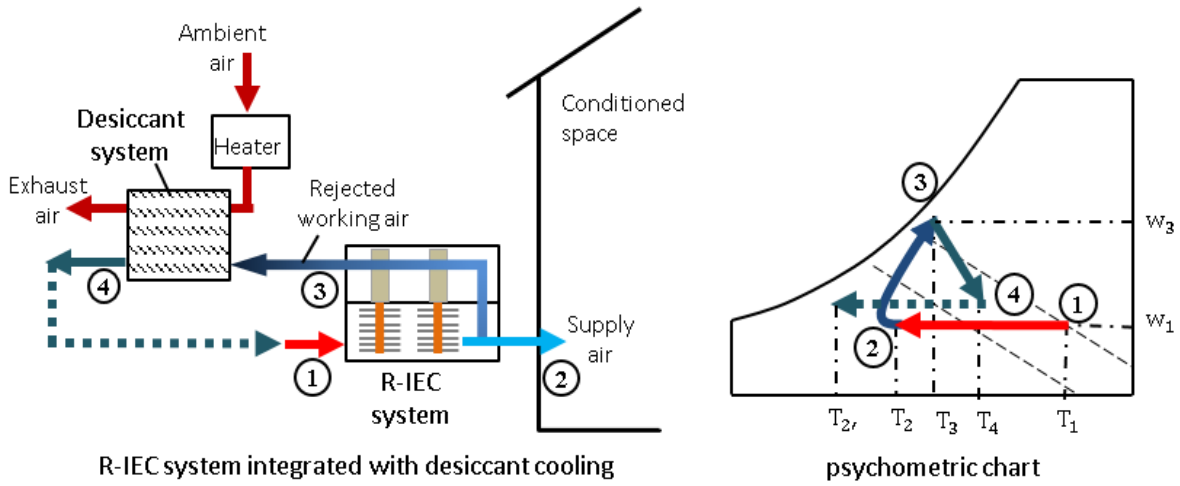


Fig 8-4 Second configuration of the combined system

Employing a dry-air heat exchanger to recover part of the wasted energy via using the cold and humid rejected working air for decreasing the temperature of the inlet air which ultimately improve the overall performance of the cooling system. A dry air-to-air heat exchanger can be used to pre-cool the inlet air of the IEC system using the rejected working air of the IEC system as cold working fluid, and ambient air as hot fluid of the exchanger. Fig 8-5 presents schematic of this configuration. This cooling process involves pre-cooling the ambient air in the dry-air HX (process 1-2) using the rejected working air, and, then, the inlet air is cooled through the IEC system (process 2-3), whereas the working air is fractioned from the supply air stream into the wet-air channel for water evaporation process (process 3-4), and, after that, to be forwarded into the dry-air HX (process 4-5) as cold working fluid. Adopting this configuration offers pre-cooling the inlet air at constant vapour content, and without demanding external heat source.

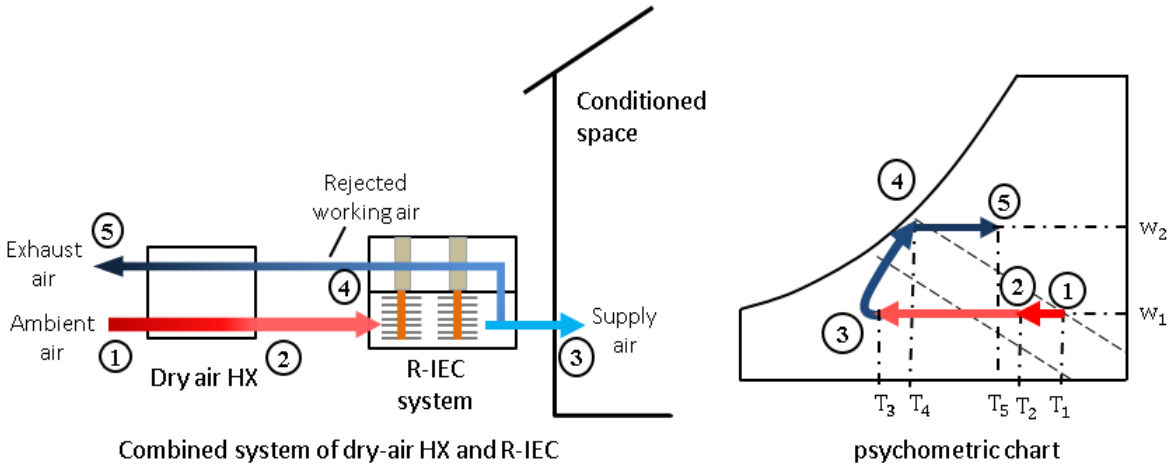


Fig 8-5 Combined configuration of HPHX and ceramic based R-IEC and dry air HX

References

1. Lechner, N., *Heating, cooling, lighting: sustainable design methods for architects*. 2009: John wiley & sons.
2. EIA. *Total Primary Energy Consumption 2014*. U.S. Energy Information Administration 2014 [cited 2015 30.01.2015]; Available from: https://www.eia.gov/beta/international/data/browser/#/?pa=000000001&vs=INTL.44-2-AFRC-QBTU.A&vo=0&v=H&start=1980&end=2014&showdm=y.
3. Sivak, M., *Potential energy demand for cooling in the 50 largest metropolitan areas of the world: Implications for developing countries.* Energy Policy, 2009. **37**(4): p. 1382-1384.
4. Pérez-Lombard, L., J. Ortiz, and C. Pout, *A review on buildings energy consumption information.* Energy and Buildings, 2008. **40**(3): p. 394-398.
5. IEA. *CO_2 emissions from fuel consumption*. International Energy Agency 2016 20.01.2017]; Available from: http://www.iea.org/publications/freepublications/publication/CO2EmissionsfromFuelCombustion_Highlights_2016.pdf.
6. EPA. *Montreal Protocol Frequently Asked Questions and Answers*. Environmental Protection Agency 2010; Available from: http://www.epa.gov/ozone/downloads/MP20_QandA.pdf.
7. Vakiloroaya, V., et al., *A review of different strategies for HVAC energy saving.* Energy Conversion and Management, 2014. **77**(0): p. 738-754.
8. Duan, Z., et al., *Indirect evaporative cooling: Past, present and future potentials.* Renewable and Sustainable Energy Reviews, 2012. **16**(9): p. 6823-6850.
9. Jones, W., *Air conditioning engineering*. 2012: Routledge.
10. ASHRAE, *ASHRAE Handbook HVAC Systems and Equipment (SI)*. 2008, American Society of Heating, Refrigerating Air-Conditioning Engineers, Inc. Atlanta, GA, USA.
11. Xuan, Y.M., et al., *Research and application of evaporative cooling in China: A review (I) – Research.* Renewable and Sustainable Energy Reviews, 2012. **16**(5): p. 3535-3546.
12. CIBSE, G.A., *Environmental design.* The Chartered Institution of Building Services Engineers, London, 2006.
13. Pistochini, T. and M. Modera, *Water-use efficiency for alternative cooling technologies in arid climates.* Energy and Buildings, 2011. **43**(2–3): p. 631-638.
14. ASHRAE Standard, *ASHRAE Standard 55-2004.* Thermal environmental conditions for human occupancy, 2004.
15. Haines, R.W. and C.L. Wilson, *HVAC systems design handbook*. 2003: McGraw-Hill.
16. Wu, J.M., X. Huang, and H. Zhang, *Numerical investigation on the heat and mass transfer in a direct evaporative cooler.* Applied Thermal Engineering, 2009. **29**(1): p. 195-201.
17. Eicker, U., *Low energy cooling for sustainable buildings*. 2009: Wiley. com.
18. Marshall, P. *Evaporative cooler schematic*. HVAC Education Australia 2014 [cited 2014 28.01.2014]; Available from: http://www.hvaceducationaustralia.com/Resources/Images/evap_cooler_schematic.png.
19. APOGEE. *Evaporative Cooling*. Online Solutions for the Energy Industry 2014 [cited 2014 28.01.2014]; Available from: http://smud.apogee.net/comsuite/content/ces/?utilid=smudid=962&id=1069.
20. Duan, Z., *Investigation of a novel dew point indirect evaporative air conditioning system for buildings*. 2011, University of Nottingham.
21. inspections, k.c.h. *Evaporative coolers*. Professional Inspection Services 2012 [cited 2014 20.03.2014]; Available from: http://www.kansas-city-home-inspections.com/Swamp-Cooler.html.

22. Kolokotsa, D., et al., *3.19 - Passive Solar Architecture*, in *Comprehensive Renewable Energy*, A. Sayigh, Editor. 2012, Elsevier: Oxford. p. 637-665.
23. Fardeheb, F. *Examination and Review of Passive Solar Cooling Strategies in Middle Eastern and North African Vernacular Architecture*. in *Proceedings of ISES World Congress 2007 (Vol. I–Vol. V)*. 2009. Springer.
24. Hughes, B.R., H.N. Chaudhry, and S.A. Ghani, *A review of sustainable cooling technologies in buildings.* Renewable and Sustainable Energy Reviews, 2011. **15**(6): p. 3112-3120.
25. Wikipedia. *Wind catcher*. Wikipedia 2014 [cited 2014 10.03.2014]; Available from: http://en.wikipedia.org/wiki/Windcatcher.
26. Riangvilaikul, B. and S. Kumar, *An experimental study of a novel dew point evaporative cooling system.* Energy and Buildings, 2010. **42**(5): p. 637-644.
27. Riangvilaikul, B. and S. Kumar, *Numerical study of a novel dew point evaporative cooling system.* Energy and Buildings, 2010. **42**(11): p. 2241-2250.
28. Rey Martínez, F.J., et al., *Comparative study of two different evaporative systems: an indirect evaporative cooler and a semi-indirect ceramic evaporative cooler.* Energy and Buildings, 2004. **36**(7): p. 696-708.
29. Pescod, D., *A heat exchanger for energy saving in an air-conditioning plant.* ASHRAE Transactions, 1979. **85**(2): p. 238-251.
30. Maclaine-Cross, I. and P. Banks, *A general theory of wet surface heat exchangers and its application to regenerative evaporative cooling.* Journal of heat transfer, 1981. **103**(3): p. 579-585.
31. Stoitchkov, N.J. and G.I. Dimitrov, *Effectiveness of crossflow plate heat exchanger for indirect evaporative cooling: Efficacité des échangeurs thermiques à plaques, à courants croises pour refroidissement indirect évaporatif.* International Journal of Refrigeration, 1998. **21**(6): p. 463-471.
32. José Alonso, J.F.S., et al., *Simulation model of an indirect evaporative cooler.* Energy and Buildings, 1998. **29**(1): p. 23-27.
33. Guo, X.C. and T.S. Zhao, *A parametric study of an indirect evaporative air cooler.* International Communications in Heat and Mass Transfer, 1998. **25**(2): p. 217-226.
34. Kettleborough, C. and C. Hsieh, *The thermal performance of the wet surface plastic plate heat exchanger used as an indirect evaporative cooler.* Journal of heat transfer, 1983. **105**(2): p. 366-373.
35. Sekulic, D. and R. Shah, *Fundamentals of heat exchanger design*. 2002, Wiley, New York.
36. Velasco Gómez, E., et al., *Description and experimental results of a semi-indirect ceramic evaporative cooler.* International Journal of Refrigeration, 2005. **28**(5): p. 654-662.
37. An, C.S. and D.H. Choi, *Analysis of heat-transfer performance of cross-flow fin-tube heat exchangers under dry and wet conditions.* International Journal of Heat and Mass Transfer, 2012. **55**(5–6): p. 1496-1504.
38. Martín, R.H., *Numerical simulation of a semi-indirect evaporative cooler.* Energy and Buildings, 2009. **41**(11): p. 1205-1214.
39. Wan, J.W., J.L. Zhang, and W.M. Zhang, *The effect of heat-pipe air-handling coil on energy consumption in central air-conditioning system.* Energy and Buildings, 2007. **39**(9): p. 1035-1040.
40. Abd El-Baky, M.A. and M.M. Mohamed, *Heat pipe heat exchanger for heat recovery in air conditioning.* Applied Thermal Engineering, 2007. **27**(4): p. 795-801.
41. Calautit, J.K., et al., *Comparison between evaporative cooling and a heat pipe assisted thermal loop for a commercial wind tower in hot and dry climatic conditions.* Applied Energy, 2013. **101**(0): p. 740-755.
42. Xu, J., et al., *Modulated porous wick evaporator for loop heat pipes: Experiment.* International Journal of Heat and Mass Transfer, 2014. **72**(0): p. 163-176.
43. Mathur, G. *Enhancing performance of an air conditioning system with a two-phase heat recovery loop retrofit*. in *Energy Conversion Engineering Conference, 1996. IECEC 96., Proceedings of the 31st Intersociety*. 1996. IEEE.

44. Noie-Baghban, S.H. and G.R. Majideian, *Waste heat recovery using heat pipe heat exchanger (HPHE) for surgery rooms in hospitals.* Applied Thermal Engineering, 2000. **20**(14): p. 1271-1282.
45. Herrero Martín, R., F.J. Rey Martínez, and E. Velasco Gómez, *Thermal comfort analysis of a low temperature waste energy recovery system: SIECHP.* Energy and Buildings, 2008. **40**(4): p. 561-572.
46. Riffat, S.B. and G. Gan, *Determination of effectiveness of heat-pipe heat recovery for naturally-ventilated buildings.* Applied Thermal Engineering, 1998. **18**(3): p. 121-130.
47. Martínez, F.J.R., et al., *Design and experimental study of a mixed energy recovery system, heat pipes and indirect evaporative equipment for air conditioning.* Energy and Buildings, 2003. **35**(10): p. 1021-1030.
48. Beckwith, W.B., *Novel application of heat pipes for economical dehumidification in air conditioning systems.* American heat pipes , Inc.
49. Shirey, D. *Demonstration of efficient humidity control techniques at an art museum*. in *the 1993 Winter Meeting of ASHRAE Transactions. Part 1, Chicago, IL, USA, 01/23-27/93*. 1993.
50. Riffat, S.B. and J. Zhu, *Mathematical model of indirect evaporative cooler using porous ceramic and heat pipe.* Applied Thermal Engineering, 2004. **24**(4): p. 457-470.
51. Riffat, S. and J. Zhu, *Experimental investigation of an indirect evaporative cooler consisting of a heat pipe embedded in porous ceramic.* J Res, 2003. **1**: p. 46-52.
52. Huang, X., et al., *Theory and applications of evaporative cooling air conditioning.* China Architecture & Building Press, Beijing, 2010.
53. X.J. Wang, X.H., J.M. Wu, *Analysis of a novel indirect evaporative cooler with heat pipe heat exchanger.* Fluid Machinery, 2004. **32**(2): p. 72-74.
54. X.J. Wang, *Theoretical and experimental analysis of a novel heat pipe indirect evaporative cooler.* China: Xi'an Polytechnic University, 2006.
55. J.J. Zheng, X.H., X.J. Wang, Y.H. Di, *Experimental study on two stage heat pipe type evaporative cooling air conditioning system.* Journal of Xi'an University of Engineering Science and Technology, 2007. **21**(1): p. 122-125.
56. Maisotsenko, V., et al., *Method and plate apparatus for dew point evaporative cooler*. 2003, Google Patents.
57. Elberling, L., *Laboratory Evaluation of the Coolerado Cooler Indirect Evaporative Cooling Unit.* Pacific Gas and Electric Company, 2006.
58. Heidarinejad, G., et al., *Experimental investigation of two-stage indirect/direct evaporative cooling system in various climatic conditions.* Building and Environment, 2009. **44**(10): p. 2073-2079.
59. El-Dessouky, H., H. Ettouney, and A. Al-Zeefari, *Performance analysis of two-stage evaporative coolers.* Chemical Engineering Journal, 2004. **102**(3): p. 255-266.
60. Bourne, R.C., *Developement of an improved two-stage enaporative cooling system.* California Energy Commission 2004.
61. Higgins C and R. H, *Desert CoolAire^{TM} Package UnitTechnical Assessment Field Performance of a Prototype Hybrid Indirect Evaporative Air-conditioner.* New Buildings Institute, 2007.
62. Goldsworthy, M. and S. White, *Optimisation of a desiccant cooling system design with indirect evaporative cooler.* International Journal of Refrigeration, 2011. **34**(1): p. 148-158.
63. Heidarinejad, G. and H. Pasdarshahri, *Potential of a desiccant-evaporative cooling system performance in a multi-climate country.* International Journal of Refrigeration, 2011. **34**(5): p. 1251-1261.
64. La, D., et al., *Development of a novel rotary desiccant cooling cycle with isothermal dehumidification and regenerative evaporative cooling using thermodynamic analysis method.* Energy, 2012. **44**(1): p. 778-791.
65. Kim, M.-H., et al., *Energy conservation potential of an indirect and direct evaporative cooling assisted 100% outdoor air system.* Building Services Engineering Research and Technology, 2011. **32**(4): p. 345-360.

66. Kim, M.-H. and J.-W. Jeong, *Cooling performance of a 100% outdoor air system integrated with indirect and direct evaporative coolers.* Energy, 2013. **52**(0): p. 245-257.
67. Farmahini-Farahani, M. and G. Heidarinejad, *Increasing effectiveness of evaporative cooling by pre-cooling using nocturnally stored water.* Applied Thermal Engineering, 2012. **38**(0): p. 117-123.
68. Maisotsenko, V., et al. *Method of indirect-evaporative air cooling in household electrical appliances*. in *Proc. of World Electrotechnical Congress*. 1977.
69. Zhao, X., J.M. Li, and S.B. Riffat, *Numerical study of a novel counter-flow heat and mass exchanger for dew point evaporative cooling.* Applied Thermal Engineering, 2008. **28**(14–15): p. 1942-1951.
70. Lee, J. and D.-Y. Lee, *Experimental study of a counter flow regenerative evaporative cooler with finned channels.* International Journal of Heat and Mass Transfer, 2013. **65**(0): p. 173-179.
71. Zhan, C., et al., *Comparative study of the performance of the M-cycle counter-flow and cross-flow heat exchangers for indirect evaporative cooling – Paving the path toward sustainable cooling of buildings.* Energy, 2011. **36**(12): p. 6790-6805.
72. Zhao, X., et al., *Feasibility study of a novel dew point air conditioning system for China building application.* Building and Environment, 2009. **44**(9): p. 1990-1999.
73. Zhao, X., et al., *Dynamic performance of a novel dew point air conditioning for the UK buildings.* International Journal of Low-Carbon Technologies, 2009. **4**(1): p. 27-35.
74. Hasan, A., *Indirect evaporative cooling of air to a sub-wet bulb temperature.* Applied Thermal Engineering, 2010. **30**(16): p. 2460-2468.
75. Hasan, A., *Going below the wet-bulb temperature by indirect evaporative cooling: Analysis using a modified ε-NTU method.* Applied Energy, 2012. **89**(1): p. 237-245.
76. Bruno, F., *On-site experimental testing of a novel dew point evaporative cooler.* Energy and Buildings, 2011. **43**(12): p. 3475-3483.
77. Zhan, C., et al., *Numerical study of a M-cycle cross-flow heat exchanger for indirect evaporative cooling.* Building and Environment, 2011. **46**(3): p. 657-668.
78. Boukhanouf, R., et al., *Investigation of a sub-wet bulb temperature evaporative cooler for buildings*, in *Sustainable Building Conference 2013*. 2013: Coventry University.
79. Cui, X., et al., *Studying the performance of an improved dew-point evaporative design for cooling application.* Applied Thermal Engineering, 2014. **63**(2): p. 624-633.
80. Hsu, S.T., Z. Lavan, and W.M. Worek, *Optimization of wet-surface heat exchangers.* Energy, 1989. **14**(11): p. 757-770.
81. Cui, X., K.J. Chua, and W.M. Yang, *Numerical simulation of a novel energy-efficient dew-point evaporative air cooler.* Applied Energy, 2014. **136**: p. 979-988.
82. Rogdakis, E.D., I.P. Koronaki, and D.N. Tertipis, *Experimental and computational evaluation of a Maisotsenko evaporative cooler at Greek climate.* Energy and Buildings, 2014. **70**: p. 497-506.
83. Lin, J., et al., *Study on dew point evaporative cooling system with counter-flow configuration.* Energy Conversion and Management, 2016. **109**: p. 153-165.
84. Fakhrabadi, F. and F. Kowsary, *Optimal design of a regenerative heat and mass exchanger for indirect evaporative cooling.* Applied Thermal Engineering, 2016. **102**: p. 1384-1394.
85. Moshari, S. and G. Heidarinejad, *Numerical study of regenerative evaporative coolers for sub-wet bulb cooling with cross- and counter-flow configuration.* Applied Thermal Engineering, 2015. **89**: p. 669-683.
86. Bozorgmehr, M., *Mathematical modeling of one dimensional heat and mass transfer in evaporative cooling and performance evaluation of indirect/direct cooling systems*. 2009, PhD thesis 2009, Tarbiat Modares University, Tehran, Iran.
87. Pandelidis, D., et al., *Comparison of desiccant air conditioning systems with different indirect evaporative air coolers.* Energy Conversion and Management, 2016. **117**: p. 375-392.
88. Duan, Z., et al., *Experimental study of a counter-flow regenerative evaporative cooler.* Building and Environment, 2016. **104**: p. 47-58.

89. Jradi, M. and S. Riffat, *Experimental and numerical investigation of a dew-point cooling system for thermal comfort in buildings.* Applied Energy, 2014. **132**(0): p. 524-535.
90. Porumb, B., et al., *A Review of Indirect Evaporative Cooling Technology.* Energy Procedia, 2016. **85**: p. 461-471.
91. Porumb, B., et al., *A Review of Indirect Evaporative Cooling Operating Conditions and Performances.* Energy Procedia, 2016. **85**: p. 452-460.
92. Zhao, X., S. Liu, and S.B. Riffat, *Comparative study of heat and mass exchanging materials for indirect evaporative cooling systems.* Building and Environment, 2008. **43**(11): p. 1902-1911.
93. Lee, D.-Y., J. Jin, and B. Kang, *Momentum boundary layer and its influence on the convective heat transfer in porous media.* International journal of Heat and Mass transfer, 2002. **45**(1): p. 229-233.
94. Ibrahim, E., L. Shao, and S.B. Riffat, *Performance of porous ceramic evaporators for building cooling application.* Energy and Buildings, 2003. **35**(9): p. 941-949.
95. Chen, W., *Thermal analysis on the cooling performance of a wet porous evaporative plate for building.* Energy Conversion and Management, 2011. **52**(5): p. 2217-2226.
96. Naticchia, B., et al., *Energy performance evaluation of a novel evaporative cooling technique.* Energy and Buildings, 2010. **42**(10): p. 1926-1938.
97. Musa, M.a., *Novel evaporative cooling systems for building applications*. 2009, University of Nottingham.
98. He, J. and A. Hoyano, *Experimental study of cooling effects of a passive evaporative cooling wall constructed of porous ceramics with high water soaking-up ability.* Building and environment, 2010. **45**(2): p. 461-472.
99. Alharbi, A., *Investigation of sub-wet bulb temperature evaporative cooling system for cooling in buildings*. 2014, University of Nottingham.
100. Ahmad, A., S. Rehman, and L.M. Al-Hadhrami, *Performance evaluation of an indirect evaporative cooler under controlled environmental conditions.* Energy and Buildings, 2013. **62**: p. 278-285.
101. Bellemo, L., et al. *Modeling of a regenerative indirect evaporative cooler for a desiccant cooling system*. in *4th IIR Conference on Thermophysical Properties and Transfer Processes of Refrigerants*. 2013.
102. Boukhanouf, R., et al., *Computer modelling and experimental investigation of building integrated sub-wet bulb temperature evaporative cooling system.* Applied Thermal Engineering, 2017. **115**: p. 201-211.
103. Anisimov, S. and D. Pandelidis, *Theoretical study of the basic cycles for indirect evaporative air cooling.* International Journal of Heat and Mass Transfer, 2015. **84**: p. 974-989.
104. Pandelidis, D. and S. Anisimov, *Numerical analysis of the heat and mass transfer processes in selected M-Cycle heat exchangers for the dew point evaporative cooling.* Energy Conversion and Management, 2015. **90**: p. 62-83.
105. Bolotin, S., B. Vager, and V. Vasilijev, *Comparative analysis of the cross-flow indirect evaporative air coolers.* International Journal of Heat and Mass Transfer, 2015. **88**: p. 224-235.
106. Chengqin, R. and Y. Hongxing, *An analytical model for the heat and mass transfer processes in indirect evaporative cooling with parallel/counter flow configurations.* International Journal of Heat and Mass Transfer, 2006. **49**(3–4): p. 617-627.
107. Tulsidasani, T., et al., *Recent research on an indirect evaporative cooler (IEC) part 1: optimization of the COP.* International journal of energy research, 1997. **21**(12): p. 1099-1108.
108. Kim, M.-H., et al., *Annual operating energy savings of liquid desiccant and evaporative-cooling-assisted 100% outdoor air system.* Energy and Buildings, (0).
109. Maheshwari, G.P., F. Al-Ragom, and R.K. Suri, *Energy-saving potential of an indirect evaporative cooler.* Applied Energy, 2001. **69**(1): p. 69-76.
110. Boukhanouf, R., et al., *Experimental and numerical study of a heat pipe based indirect porous ceramic evaporative cooler*, in *International Journal of Environmental Science and Development* 2015. p. 104.

111. Chaudhry, H.N., B.R. Hughes, and S.A. Ghani, *A review of heat pipe systems for heat recovery and renewable energy applications.* Renewable and Sustainable Energy Reviews, 2012. **16**(4): p. 2249-2259.
112. Faghri, A., *Review and advances in heat pipe science and technology.* Journal of Heat Transfer, 2012. **134**(12): p. 123001.
113. CRS-Engineering-ltd. *CRS Engineering Heat pipes and systems*. 2015 [cited 2015 26/05/215]; Available from: http://www.heat-pipes.com/.
114. Shabgard, H., et al., *Heat pipe heat exchangers and heat sinks: Opportunities, challenges, applications, analysis, and state of the art.* International Journal of Heat and Mass Transfer, 2015. **89**: p. 138-158.
115. Reay, D., R. McGlen, and P. Kew, *Heat pipes: theory, design and applications*. 2013: Butterworth-Heinemann.
116. Hubbeling, L., *Cooling of high-density and power electronics by means of heat pipes*. 1980, CERN.
117. Halasz, B., *A general mathematical model of evaporative cooling devices.* Revue Générale de Thermique, 1998. **37**(4): p. 245-255.
118. Lee, H.S., *Thermal design: heat sinks, thermoelectrics, heat pipes, compact heat exchangers, and solar cells*. 2010: John Wiley & Sons.
119. Cui, X., et al., *Fundamental formulation of a modified LMTD method to study indirect evaporative heat exchangers.* Energy Conversion and Management, 2014. **88**: p. 372-381.
120. Chi, S., *Heat Pipe Theory and Practice: A sourcebook*. 1976, Washington: Hemisphere Pub. Corp.
121. Butterworth, D., *Introduction to heat transfer*. Vol. 18. 1977: Oxford University Press for the Design Council, the British Standards Institution and the Council of Engineering Institutions.
122. Sun, S.-H. and T.R. Marrero, *Experimental study of simultaneous heat and moisture transfer around single short porous cylinders during convection drying by a psychrometry method.* International Journal of Heat and Mass Transfer, 1996. **39**(17): p. 3559-3565.
123. Sahim, K. and D. Puspitasari, *Convective heat transfer of one row arrangement of elliptical cylinder.* Frontiers in Heat and Mass Transfer (FHMT), 2017. **8**.
124. ASHRAE, *ASHRAE Handbook-2005 ASHRAE Fundamentals.* American Society of Heating, Refrigeration and Air-conditioning Engineers Inc, 2005.
125. Multi-Lab. *Multi-Lab Quartz and Ceramic Technology*. 2014 [cited 2015 28/01/2015]; Available from: http://www.multi-lab.co.uk/.
126. Ebm-papst. *EC/AC centrifugal fans – RadiCal*. Ebm-papst 2015 [cited 2015 03/03/2015]; Available from: http://www.ebmpapst.co.uk/media/content/infocentre_media/downloads/content_dl/catalogues/EC_AC_Centrifugal_Fans_-_RadiCal_05-2013.pdf.
127. Wang, C.-C., R.L. Webb, and K.-Y. Chi, *Data reduction for air-side performance of fin-and-tube heat exchangers.* Experimental Thermal and Fluid Science, 2000. **21**(4): p. 218-226.
128. Met-office. *Climate zones*. 2017 [cited 2017 09/03/2017]; Available from: http://www.metoffice.gov.uk/climate-guide/climate/zones.
129. Almabrok, A.A., *The analysis of the possibilities of using heat energy for water heating, space heating and air conditioning in the domestic sector*, in *Faculty of electrical engineering and communication, Department of electrical power engineering*. 2014, Brno University of Technology: Brno, Czech republic.
130. Talavera, D.L., et al., *A worldwide assessment of levelised cost of electricity of HCPV systems.* Energy Conversion and Management, 2016. **127**: p. 679-692.
131. Karagiannis, I.C. and P.G. Soldatos, *Water desalination cost literature: review and assessment.* Desalination, 2008. **223**(1): p. 448-456.
132. Webber, M.E., *Chapter 2.2.6 - Water for Electricity Generation in the United States A2 - Ziolkowska, Jadwiga R*, in *Competition for Water Resources*, J.M. Peterson, Editor. 2017, Elsevier. p. 212-232.

Appendices

Appendix A

Computer code

For inlet operational conditions of 40℃ , 20%RH, $2.5\ m/s$, and 50% flow rate ratio

```
            %** Heatpipe porous ceramic cooler modelling **%
 %Subscripts are used to refer as follows:
clear                           % "d" refers to dry channel
clc                             % "a" refers to wet channel
                                % "w" refers to water
                                % "f" refers to fin
% Channels dimentions
   L=0.700;    %Channel length, (m)
   W=0.069;   %Channel width, (m)
   Y=0.13;    %Channel height, (m)
% Heat pipe & ceramic tube dimentions
   r1=0.007; %Vapour space radius of heat pipe (m)
   r2=0.008; %Inner radius of heat pipe container (m)
   r3=0.009; %Outer radius of heat pipe container (m)
   r6=0.012;  %Inner radius of ceramic container (m)
   r7=0.014;  %Outer radius of ceramic container (m)
   l1=0.130;  %Evaporator length of heat pipe (m)
   l2=0.155;  %condenser length of heat pipe (m)
   l3=0.010;  %adiabatic length of heat pipe (m)
   l4=0.160;  %length of ceramic tube (m)
   t_f=0.0009; %Thickness of the fin (m)
   l_f=0.060; %length of the fin (m)
   w_f=0.060; %wedith of the fin (m)
   N_f=29;    %Number of fins
   d_3=0.018; %Outer diameter of heat pipe container (m)
   r_eq=0.0344;  %equivalent fin diameter

%Coefficients,
   k1=0.0271;    %Air thermal conductivity in drt-air passage  @ 40c (W/m K)
   Lambda_e=401; %Conductivity of heat pipe evaporator (W/m K)
   Lambda_c=401; %Conductivity of heat pipe condenser (W/m K)
   Lambda_ws=0.9; %Water-sand mix conductivity (W/m K)
```

```
   Lambda_ce=1.50;  %Ceramic tube conductivity (W/m K), given by manufacturer
   Lambda_wk=1.70;  %Conductivity of evaporator wick strecture(W/m K)


%Inlet conditions
   T1=40;       % Inlet temperature of dry air channel,(C) & 20%RH
   RH_1=0.20;   % Inlet air relative hmodity in the dry air channel
   T1_wb=22.05;  %Inlet wet bulb temperature of dry air channel,(C) & 25%RH
   T1_dp=12.85;  % dew point temperature of dry air channel,(C) & 25%RH
   Patm=101325;  %Atmospheric pressure,(Pa)
   P1_s=610.7*10^((7.5*T1)/(237.3+T1));  %Saturated Vapour Pressure,(Pa)
   P1_p=RH_1*P1_s;    %Partial vapour pressure of inlet air,(Pa)
   g1=0.622*(P1_p/(Patm-P1_p)); % moisture content of Inlet air in dry air
passage ,(kg_vapour/kg_dryair)
   Tw=23; %Water temperature,(C)


%Thermal resistances
   V1=2.50; %Air velocity of dry air passage  (m/s)
   visc1= 0.00001697; %Air kinematic viscosity of dry-air channel  @ 40c
(m2/s)
   D_h=2*r3; %Hydrolic diameter (m)
   A_b=(2*pi()*r3*l1)-N_f*(t_f*d_3); %The exposed base surface area of the
evaporator (m)
   A_f_rectan=2*(l_f*w_f-(pi()*r3^2))+(2*(l_f+w_f)*t_f); %The area of square
fin(m2), 2 faces of the fin
   A_f=2*pi()*(r_eq^2-r3^2)+2*pi()*r3*t_f;  %The area of circular fin(m2
At=A_b+(N_f*A_f); %The net surface area of the evaporator with fins (m)
   Re1=(V1*D_h)/visc1;  %Reynolds number in the dry-airpassage
   Nud=0.94*(Re1^0.538); %Nusselt number of dry-air passage
   h1=Nud/(2*r3/k1); %heat transfer coefficient of dry-air passage(W/m2 K)
   etha_f=0.82; % fin effectivness
   etha_o=1-((N_f*A_f/At)*(1- etha_f)); % the fin efficiency
%R1: Heat pipe evaporator external surface resistance
R1=1/(h1*At);  %Heat pipe evaporator external surface resistance
%R2: Evaporator wall radial conductance resistance, R2
R2=(log(r3/r2))/(2*pi()*l1*Lambda_e);
%R3:Evaporator wick resistance, R3
R3=log(r2/r1)/(2*pi()*l1*Lambda_wk);
%R7:Condenser wick resistance, R7
R7=log((r2/r1))/(2*pi()*l2*Lambda_wk);
%R8: Condenser wall resistance, R8
R8=log(r3/r2)/(2*pi()*l2*Lambda_c);
```

```
%R10: Water-sand mix thermal conductive resistance, R10
R11=log(r6/r3)/(2*pi()*l2*Lambda_ws);
%R11: Ceramic tube conductive resistance, R11
R12=log(r7/r6)/(2*pi()*l4*Lambda_ce);
Rt1=R1+R2+R3+R7+R8; %The sum of thermal resistances between T1 and Tc (C/W)
   Rho_d=1.12;  %Air density in the dry channel (kg/m3) @ 40C&25%
   VFR1=0.0208;  % flow rate of air in passage1 (m3/s)@ 2.5m/s inlet speed
   m_d=VFR1*Rho_d; %Air massflow rate in in dry channel (kg/s)
   Cp_1=1007.00; %Air specific heat,(J/kg.K)
   VFR_s=0.011;  % flow rate of supply air(m3/s)@ 2.5 m/s inlet speed
   Rho_2=1.14 ;  %Air density (kg/m3) @ 33C&37%
   m_s=VFR_s*Rho_2; %flow rate of supply air (kg/s)@ inlet speed of 5 m/s
   m_a=m_d-m_s;     %Air massflow rate in in moist air channel (kg/s)
   Cp_w=4180;     %Water specific heat, (J/kg.K)
   hfg_Tce=2260000; % Water lathent heat of vaporzation ,(J/kg)
   visc_a=0.000016;   %Air kinematic viscosity of moist air channel @ 30c
(m2/s)
   V_a=3.86;          %Air velocity of passage 2 (m/s)/ FOR THE CASE OF 50%
OF FLOWRATE RATIO//
   k_a=0.0250;        %Air thermal conductivity of passage 2 (W/m K)
   Re_a=V_a*2*r7/visc_a; %Reynolds number  in the the wet channel (passage 2)
   Pr=0.72; %Prendtal number @30C
   Nu_a=0.193*(Re_a^0.618)*(Pr^(-1/3));
 %R12: Convection resistance btwn the air and ceramic tube in the wet
channel, R12
  ha=Nu_a/(2*r7/k_a);   % Convective heat transfer cofficient (W/m2.C)
   R13=1/(ha*2*pi()*r7*l4);
   Ace=2*pi()*r7*l4; %Ceramic tube surface area (m2)
  N=30;   %number of sections
  m=100;  %number of iteration;
  K=1;


%First loop
  for I=1:1:N;         % from diffren. element 1 to N
      T_w(I,1)=Tw;    % water temperature
      T_d(I,1)=T1;    % temperature of dry air
      T_w(I,1)=T_d(I,1)-(Q(I)*Rt1); % water temperature
      T_a(I,1)=T1;    % temperature of mist working air
      q(I,1)=Q(I);    % Capillary limit of heat transport,W
  end
```

```
    for J=1:1:m;        % from iteration loop 1 to m loops
        T_d(1,J)=T1;    % water temperature
        q(N,J)=Q(30);   % Capillary limit of heat transport,W
        g_a(N,J)=g1;    % moisture content of moist working air
        Cp_da(N,J)=(1.005+(1.35*10^(-8))*(T_a(N,1)+30)^2)*1000;  % Specific
heat of dry air as function of T
      Cp_v(N,J)=(1.8684+0.009*(T_a(N,1)/100)+0.00373*(T_a(N,1)/100)^2)*1000;
% Specific heat of vapour as function of T
        Cp_a(N,J)=Cp_da(N,J)+g_a(N,J)*Cp_v(N,J);  % Moist air specific heat
        hm(N,J)=ha/(Cp_a(N,J));      % mass heat transfer coffient(kg/m2.s)
        m_w(N,J)=hm(N,J)*Ace*(g_swn-g_a(N,J)); % vapour mass flowrate(kg/s)
    end

 % Second stage of loops
 for J=2:1:m;     % from iteration loop 2 to m loops
         K=K+11;    % a counter
     for I=1:2:N-1; %I=1,3,5,7,...29
           q(I+1,J)=Q(I+1);
           T_d(I+1,J)=T_d(I,J)-(q(I+1,J)/(m_d*Cp_1)); % air temperature at
dry-air passage as function of Q1
           T_w(N+1-I,J)=T_d(N+1-I,J-1)-(q(N+1-I,J-1)*Rt1);
           T_a(N,J)=T_d(N,J-1);
           Cp_da(N+1-I,J)=(1.005+(1.35*10^(-8))*(T_a(N+1-I,J)+30)^2)*1000;  %
Specific heat of dry air as function of T
           Cp_v(N+1-I,J)=(1.8684+0.009*(T_a(N+1-I,J)/100)+0.00373*(T_a(N+1-
I,J)/100)^2)*1000; % Specific heat of vapour as function of T
           Cp_a(N+1-I,J)=Cp_da(N+1-I,J)+g_a(N+1-I,J)*Cp_v(N+1-I,J);  % Moist
air specific heat
           hm(N+1-I,J)=ha/(Cp_a(N+1-I,J)); % Mass transfer cofficent(kg/m2.s)
           m_w(N+1-I,J)=hm(N+1-I,J)*Ace*(g_swn-g_a(N+1-I,J)); % mass flowrate
for each ceramic tube(kg/s)
           T_a(N+1-I-1,J)=T_a(N+1-I,J)+((ha*Ace/(m_a*Cp_a(N+1-
I,J)))*(T_w(N+1-I,J)-T_a(N+1-I,J)));
           g_a(N+1-I-1,J)=g_a(N+1-I,J)+(m_w(N+1-I,J)/m_a);
           T_w(N+1-I-1,J)=T_w(N+1-I,J);
          if I<29
             T_d(I+2,J)=T_d(I+1,J);
             T_a(N-I-1,J)=T_a(N-I,J);
             g_a(N-I-1,J)=g_a(N-I,J);
          end
    end
```

```
        if abs((T_d(N,J)-T_a(N,J)))<=0.01; % Checking the convergence
            fprintf('Converged, K=%d, ABSLUTE(T_d-T_a)=%d\n',K,
abs((T_d(N,J)-T_a(N,J))))
            Q_cc=m_s*Cp_1*(T_d(1,J)-T_d(N,J))  %Cooling Capacity
            Eff_wb=(T_d(1,J)-T_d(N,J))/(T_d(1,J)-T1_wb) %WB effectiveness
            Eff_dp=(T_d(1,J)-T_d(N,J))/(T_d(1,J)-T1_dp) %DP effectiveness
            mw=m_w(:,J);
            mm=sum (mw)  % total water consumption (kg/s)

            break
        end

    end

    %Plotting

    hold on;
    j=J;
    xo=1:30;
    Td=T_d(:,j);
    Ta=T_a(:,j);
    Tw=T_w(:,j);
    %ga=g_a(:,j);
    %Twp=polyfit(xo,Tw,2);
    plot(xo,Td,'g-',xo,Ta,'r-',xo,Tw,'+b','LineWidth',2) %
    legend('T_d','T_a','T_w')
    xlabel('N/L')
    ylabel('Temperature,(C)')

    title('Temperature change alonge the ICE','Fontsize',12)
    grid
```

Appendix B

Heat transfer limitations of heat pipe

Heat pipe specifications and properties

parameters	Symbol	Value	Reference [118]
Outer diameter of heat pipe, m	d_o	0.0180	Supplied by manufacturer
Inner diameter of heat pipe, m	d_i	0.0158	Supplied by manufacturer
vapour space diameter, m	d_v	0.01547	measurement
Length of heat pipe evaporator, m	l_e	0.1300	measurement
Length of heat pipe condenser, m	l_c	0.1550	measurement
Adiabatic length of heat pipe, m	l_a	0.0100	measurement
Total length of heat pipe, m	l_t	0.2950	Supplied by manufacturer
Effective length of heat pipe, m	l_{eff}	0.1525	$l_{eff} = l_a + l_c/2 + l_e/2$
Heat pipe inclination angle, °	φ	-90	Condenser above evaporator
2 layers of #250 $wire/in$	N_{wk}	250	measurement
Mesh wire thickness, $in\ or\ mm$	d_w	0.0016 or 0.041	measurement
Capillary radius, m	r_c	5.080E-05	$r_c = 2.54 */(1000 * 2\ N_{wk})$
Wick thickness for two layers, m	t_{wk}	1.626E-04	$t_{wk} = 2 * 2 *\ d_w$
Vapour space area, m^2	A_v	0.00019	$A_v = \pi(d_v/2)^2$
Cross-sectional flow area of wick structure, m^2	A_{wk}	7.986E-06	$A_{wk} = \pi\left(d_i^2 - d_v^2\right)/4$
Wetted perimeter, m	P_{wk}	0.0983	$P_{wk} = \pi(d_i + d_v)$
Hydraulic radius of wick at vapour-wick interface, m	$r_{h,s}$	1.626E-04	$r_{h,s} = 2\ A_{wk}/P_{wk}$
Porosity for the wick structure, -	ε	0.6858	$\varepsilon = 1 - ((\pi\ N_{wk}\ d_w)/4)$
Wick permeability, m^2	K	4.43E-11	$K = \left({d_w}^2\ \varepsilon^2\right)/(122(1-\varepsilon)^2)$
Water-saturated wick effective thermal conductivity, $W/m\ K$	$\lambda_{wk,eff}$	1.30	See equation (4.40)
Water thermal conductivity, $W/m\ K$	λ_{wt}	0.68	
Copper thermal conductivity, $W/m\ K$	λ_{copp}	401.0	
Nucleation radius, m	r_n	2.54E-6	Constant

Thermdynamic properties of the heat pipe working fluid " water"

Properties	temperature, ℃						
	10	20	30	40	50	80	100
Latent heat,	2476000	2454000	2431000	2407000	2384000	2310000	2254000
Liquid density, kg/m^3	1002.2	998.6	994.8	990.4	985.8	969.7	961
Vapour density, kg/m^3	0.009426	0.017364	0.03046	0.05134	0.083217	0.29303	0.58
Liquid thermal conductivity, W/m°C	0.5815	0.5997	0.6157	0.6298	0.642	0.6685	0.6795
Liquid viscosity, N.s/m^2	0.001313	0.001013	0.000806	0.000657	0.000548	0.00040	0.00028
Vapour viscosity, N.s/m^2	9.46E-06	9.75E-06	1.01E-05	1.04E-05	1.07E-05	1.1E-05	1.3E-05
Vapour pressure, ,bar	0.0122	0.02	0.0423	0.07	0.1231	0.470	1.022
Liquid surface tension ,N/m	0.07423	0.07275	0.07121	0.06961	0.06796	0.06269	0.0584

Excel spread sheet was created to calculate heat transfer limitation of the heat pipe;

Capillary limit of the heat pipe heat transport (Q_c) is determined by

$$Q_c = \frac{\rho_l \, i_v \, K \, A_{wk}}{\mu_l \, l_{eff}} \left(\frac{2\sigma_l}{r_c} - \rho_l g l_t \sin\varphi - \rho_l g \, l_t \cos\varphi \right), \qquad W$$

The maximum heat transport due to entrainment limit is given by

$$Q_e = \pi r_1^2 i_v \sqrt{\frac{\rho_v \, \sigma_1}{2 \, r_{h,s}}}, \qquad W$$

The maximum heat transfer rate due to boiling limitations can be determined by equation

$$Q_b = \frac{4\pi \, l_{eff} \, \lambda_{eff} \, T_v \, \sigma_l}{i_{fg} \, \rho_v \, \ln\frac{r_i}{r_v}} \left(\frac{1}{r_n} - \frac{1}{r_c} \right), \qquad W$$

The sonic heat transport limit is expressed by the following equation

$$Q_s = A_v \, \rho_v \, i_{fg} \sqrt{\frac{\gamma_v \, R_v \, T_v}{2(1+\gamma_v)}} =, \qquad W$$

The overall heat transport due to the viscous limit is expressed as follow [120]

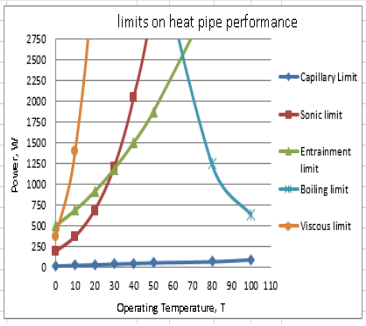
$$Q_v = \frac{A_v \, r_v^2 \, \rho_v \, i_{fg} \, P_v}{16 \, \mu_v \, l_{eff}}, \qquad W$$

Hear pipe working fluid properties (WATER)										
Working fluid temperature	units	0.1	10	20	30	40	50	80	100	
Latent heat,	J/kg	2498000	2476000	2454000	2431000	2407000	2384000	2310000	2254000	
Liquid density,	kg/m3	1005.5	1002.2	998.6	994.8	990.4	985.8	969.7	961	
Vapor density	kg/m3	0.00485	0.009426	0.017364	0.03046	0.05134	0.083217	0.29303	0.58	
Liquid thermal conductivity	W/m•C	0.5611	0.5815	0.5997	0.6157	0.6298	0.642	0.6685		
Liquid viscosity,	Ns/m2	0.001761	0.001313	0.001013	0.000806	0.000657	0.000548	0.00040	0.00028	
Vapor viscosity	Ns/m2	9.172E-06	9.46E-06	9.75E-06	1.01E-05	1.04E-05	1.07E-05	1.1E-05	1.3E-05	
Vapor pressure,	bar	0.0061	0.0122	0.02	0.0423	0.07	0.1231	0.470	1.022	
Liquid surface tension	N/m	0.07566	0.07423	0.07275	0.07121	0.06961	0.06796	0.06269	0.0584	
Gamma of water vapour		1.33	1.33	1.33	1.33	1.33	1.33	1.33	1.33	
R water vapor	J/kg.K	462	462	462	462	462	462	462	462	

Heat pipe properties			
Outer dia of heat pipe surf	d_o	0.0180	m
Inner dia of heat pipe surf	d_i	0.0158	m
vapour space dia	d_v	0.01547	m
max vapor space area	A_v	0.00019	m^2
Length of HP evaporator	L_e	0.1300	m
Length of HP condenser	L_c	0.1550	m
Adibatic length of HP	L_a	0.0100	m
Total length of HP	L_t	0.2950	m
Effective length of HP	L_eff	0.1525	m
water thermal conductivity	k_wt	0.68	W/m.C
Copper thermal conductivit	k_p	401.0	W/m.C
Vapour core hydraulic radi	r_hv	0.0077	m
Heat pipe inclination angle		-90	

Assumptions:					
2 layers of #250/in copper mesh	N	250	units	9.84E+03	wire/m
wire thickness, d_w =		0.0016	inch	0.04064	mm
Capillary radius =w+d/2= 1/(2*N)	r_c,e	0.0508	mm	5.08E-05	m
wick thickness for two layers	t_w	0.1626	mm	1.63E-04	m
vapour space dia	d_v	15.475	mm		
internal diameter of the heat pip	d_i	15.800	mm		
cross-sectional flow area of the w	A_w	7.986	mm^2	7.99E-06	m^2
The wetted perimeter	P	98.253	mm	9.83E-02	m
hydraulic radius of wick , r_h,w	r_h,s	0.1626	mm	1.63E-04	m
porosity for the screen wick	e	0.6858			
wick permeability	K	4.43E-11	m^2		
Wick screen effective thermal con	k_eff	1.300	W/m.C		
The nucleation site radius may be	r_n	2.54E-06	m		

Operating Temperature	C	0.1	10	20	30	40	50	80	100	
Capillary Limit	W	19.462774	25.50034	32.25589	39.50917	47.14191	54.940757	68.1038	90.4262	
max. Mach number (= 0.2)	M_v =	0.2								
Sonic limit	Q_s,max	186.68795	366.0901	680.1104	1201.862	2038.569	3324.611	11858.6	23542.8	
		432.40762	847.9398	1575.275	2783.759	4721.744	7700.4814	27466.9	54529.9	W
Entrainment limit	q_e,max	499.13622	683.1631	909.7846	1180.977	1500.937	1870.086	3265.8	4327.1	
Boiling limit	Q_b,max	65149.67	34383.56	19108.85	11130.89	6735.07	4226.65	1248.84	636.50	W
Viscous limit	Q_v,max	371.83	1389.41	4033.24	14382.54	38539.25	105643.45	1299135	4816949	



Appendix C

Fan specification

ErP2015

EC centrifugal fans – RadiCal

backward curved, Ø 220



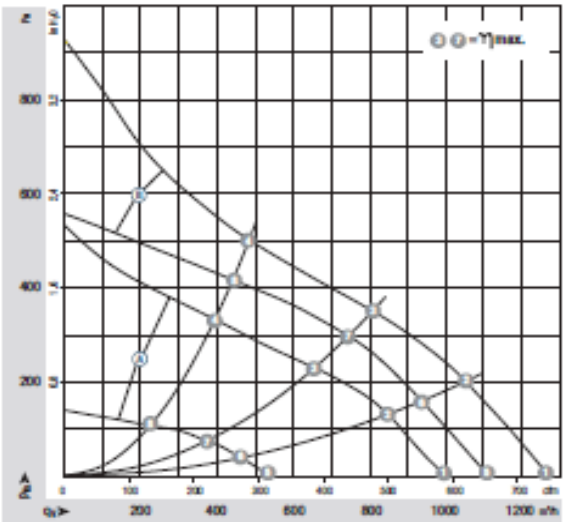
- **Material:** Housing: PA plastic 6, fibreglass-reinforced
  Impeller: PA plastic 6, fibreglass-reinforced
  Rotor: Thick layer passivated
  Electronics enclosure: Die-cast aluminium
- **Number of blades:** 7
- **Direction of rotation:** Clockwise, seen on rotor
- **Type of protection:** IP 54
- **Insulation class:** "B"
- **Mounting position:** Any
- **Condensate discharges:** None, open rotor
- **Mode of operation:** Continuous operation (S1)
- **Bearings:** Maintenance-free ball bearings

Nominal data		Curve	Nominal voltage range	Frequency	Speed/typ.n1	Max. input power1	Max. current drawn1	Perm. amb. temp.	Technical features and electrical connection
Type	Motor		VAC	Hz	rpm	W	A	°C	
*3G 220	M3G055-BI	Ⓐ	1~ 200-240	50/60	2580	85	0,70	-25..+60	p. 164 / H3)
*3G 220	M3G055-CF	Ⓑ	1~ 200-240	50/60	3230	168	1,40	-25..+50	p. 164 / H3)
*3G 220	M3G055-BI	Ⓒ	1~ 200-240	50/60	2580	85	0,70	-25..+60	p. 165 / H4)
*3G 220	M3G055-CF	Ⓓ	1~ 200-240	50/60	2790	115	1,10	-25..+50	p. 163 / H5)
*3G 220	M3G055-CF	Ⓔ	1~ 200-240	50/60	3230	168	1,40	-25..+50	p. 165 / H4)

subject to alterations

(1) Nominal data in operating point with maximum load and 230 VAC

Curves:
2 Speed stages



		n rpm	P_{ed} W	I A	L_{WA} dB(A)
Ⓐ	❶	2765	79	0,67	71
Ⓐ	❷	2700	85	0,69	67
Ⓐ	❸	2580	85	0,70	65
Ⓐ	❹	2630	85	0,70	66
Ⓐ	❺	1505	16	0,18	57
Ⓐ	❻	1485	16	0,20	54
Ⓐ	❼	1470	17	0,21	51
Ⓐ	❽	1485	17	0,19	52
Ⓑ	❶	3540	168	1,40	77
Ⓑ	❷	3370	168	1,40	73
Ⓑ	❸	3230	168	1,40	70
Ⓑ	❹	3310	168	1,40	72
Ⓑ	❺	3000	100	0,85	74
Ⓑ	❻	2955	110	0,95	70
Ⓑ	❼	2900	120	1,00	68
Ⓑ	❽	2930	115	0,97	70

Air performance measured as per ISO 5801, installation category A, with ebm-papst inlet nozzle without protection against accidental contact. Suction-side noise levels: L_{WA} as per ISO 13347, L_{pA} measured at 1 m distance to fan axis. The acoustic values given are only valid under the measurment conditions listed and may vary depending on the installation situation. With any deviation to the standard set-up, the specific values have to be checked and reviewed once installed or fitted! For detailed information see page 172 ff.

- **Technical features:** See electrical connections p. 163 ff.
- **EMC:** Interference emission acc. to EN 61000-6-3
  Interference immunity acc. to EN 61000-6-2
  Harmonics acc. to EN 61000-3-2/3
- **Touch current:** < 3,5 mA acc. to IEC 60990 (test circuit, illustration 4)
- **Cable exit:** Variable
- **Protection class:** I (if customer has provided connection for protective earth)
- **Product conforming to standards:** EN 60335-1, CE
- **Approvals:** VDE, UL, CSA, CCC, GOST are applied for



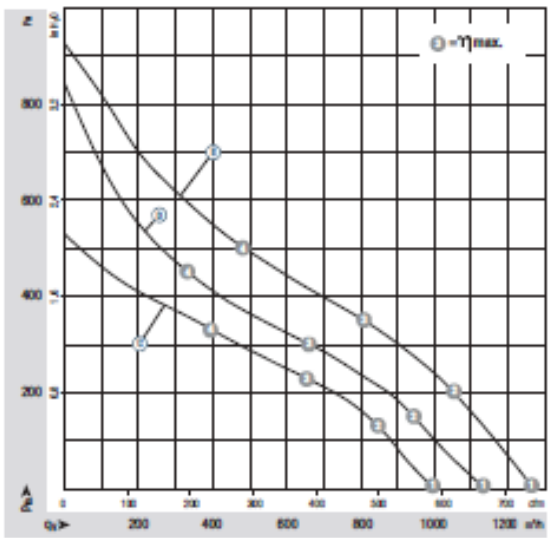
Mass of centrifugal fan



Mass of centrifugal module with support basket

Centrifugal fan	kg	Centrifugal module w. support basket	kg
R3G 220-RC05 -01	1,13	K3G 220-RC05 -01	2,03
R3G 220-RD53 -01	1,53	K3G 220-RD53 -01	2,43
R3G 220-RC05 -03	1,20	K3G 220-RC05 -03	2,10
R3G 220-RG19 -01	1,40	K3G 220-RG19 -01	2,00
R3G 220-RD53 -03	1,53	K3G 220-RD53 -03	2,43

Curves:
Speed-controlled



		n rpm	P_{ed} W	I A	L_{WA} dB(A)
C	1	2765	79	0,67	71
C	2	2700	85	0,69	67
C	3	2580	85	0,70	65
C	4	2635	85	0,70	66
B	1	3085	115	1,10	74
B	2	2935	115	1,10	69
B	3	2790	115	1,10	66
B	4	2940	115	1,10	70
B	1	3540	168	1,40	77
B	2	3370	168	1,40	73
B	3	3230	168	1,40	70
B	4	3310	168	1,40	72

Air performance measured as per ISO 5801, installation category A, with elbow-piped inlet nozzle without protection against accidental contact. Suction-side noise levels: L_{WA} as per ISO 13347, L_{pA} measured at 1 m distance to fan axis. The acoustic values given are only valid under the measurment conditions listed and may vary depending on the installation situation. With any deviation to the standard setup, the specific values have to be checked and reviewed once installed or fitted! For detailed information see page 172 ff.

Appendix D

Experimental results spread sheet

Experimental results of inlet conditions 40℃ and relative humidity of 45,35, and 25%

5	Temperature	40	40	40	40	40	40	40	40	40	40	40	40	40	40	40	40	40	40	40	40	40	40	40	40	40	40	40	40
6	Humidity of inlet air	45%				45%	0.0211								35%,	0.0163								25%	0.0115				
7	Fanspeed (m/s)	5			3.5			2.5			5			3.5			2.5			5			3.5			2.5		
8	Working to inlet air Ratio (Q_supp/Q_in)	20%	50%	70%	20%	50%	70%	20%	50%	70%	20%	50%	70%	20%	50%	70%	20%	50%	70%	20%	50%	70%	20%	50%	70%	20%	50%	70%
9	T_wb (C)=	29.1			29.1			29.1			26.6			26.6			26.52			23.6	23.6	23.6	23.6	23.6	23.6	23.6	23.6	23.6
10	T_dp (C)=	25.8			25.8			25.8			21.6			21.6			21.6			16.2	16.2	16.2	16.2	16.2	16.2	16.2	16.2	16.2
11	Air density (kg/m^3)	1.113			1.113			1.113			1.116			1.116			1.116			1.119			1.119			1.119		
12	Cp (kJ/kg K)	1.045			1.045			1.045			1.036			1.036			1.036			1.027			1.027			1.027		
13	Q_in (m^3/s)	0.0417	0.0417	0.0417	0.0292	0.0292	0.0292	0.0208	0.0208	0.0208	0.0417	0.0417	0.0417	0.0292	0.0292	0.0292	0.0208	0.0208	0.0208	0.0417	0.0417	0.0417	0.0292	0.0292	0.0292	0.0208	0.0208	0.0208
14	Supp Air exit speed (m/s)	4.22	2.65	1.61	2.98	1.86	1.15	2.12	1.32	0.80	4.22	2.65	1.61	2.98	1.85	1.15	2.1200	1.3300	0.8000	4.2200	2.6500	1.6100	2.9800	1.8600	1.1200	2.1200	1.3300	0.8000
15	Q_supp (m^3/s)	0.03	0.02	0.01	0.02	0.01	0.01	0.02	0.01	0.01	0.03	0.02	0.01	0.02	0.01	0.01	0.0167	0.0104	0.0063	0.0331	0.0208	0.0126	0.0234	0.0146	0.0088	0.0167	0.0104	0.0063
16	Reject Air exit speed	1.05	2.66	3.70	0.75	1.86	2.55	0.54	1.34	1.85	1.05	2.66	3.70	0.75	1.87	2.56	0.5400	1.3300	1.8500	1.0500	2.6600	3.7000	0.7500	1.8600	2.5900	0.5400	1.3300	1.8500
17	Q_ext (m^3/s)	0.0082	0.0209	0.0291	0.0059	0.0146	0.0200	0.0042	0.0105	0.0145	0.0082	0.0209	0.0291	0.0059	0.0147	0.0201	0.0042	0.0104	0.0145	0.0082	0.0209	0.0291	0.0059	0.0146	0.0203	0.0042	0.0104	0.0145
18	Q_supp/Q_in= %	79.56	49.96	30.35	80.26	50.09	30.97	79.932	49.769	30.163	79.555	49.958	30.352	80.255	49.823	30.971	79.932	50.146	30.163	79.555	49.958	30.352	80.255	50.092	30.163	79.932	50.146	30.163
19	Q_ext/Q_in= %	20	50	70	20	50	69	20	51	70	20	50	70	20	50	69	20	50	70	20	50	70	20	50	70	20	50	70
20	sum	99.35	100.10	100.10	100.45	100.18	99.65	100.29	100.29	99.92	99.35	100.10	100.10	100.45	100.18	99.92	100.29	100.29	99.92	99.35	100.10	100.10	100.45	100.18	99.92	100.29	100.29	99.92
21	T_in 0	40.00	40.00	40.00	40.00	40.00	40.00	40.00	40.00	40.00	40.00	40.00	40.00	40.00	40.00	40.00	40.00	40.00	40.00	40.00	40.00	40.00	40.00	40.00	40.00	40.00	40.00	40.00
22	T_5HP 5	37.17	35.83	35.63	36.97	35.35	35.03	36.5	34.9	34.4	37	35.23	34.96	36.92	34.71	34.56	36.51	34.41	33.79	37.76	35.41	35.05	37.25	35.05	34.14	36.76	34.04	33.27
23	T_10HP 10	35.65	33.67	33.52	35.34	33.04	32.63	34.8	32.45	32	35.4	32.86	32.65	35.2	32.08	31.88	34.63	31.75	31.02	35.71	32.45	32.17	35	31.71	30.49	34.17	30.25	29.33
24	T_supp out 15	34.80	32.30	32.00	34.04	31.15	30.80	33.80	30.65	30.10	34.04	31.20	31.05	33.55	30.00	29.70	32.85	29.30	28.85	33.88	30.25	29.83	33.10	28.81	28.53	31.54	28.30	27.59
25	T_5ce 10	34.39	31.78	31.55	33.30	30.84	30.25	32.9	30.5	29.44	33.16	30.73	30.46	33.28	29.30	28.87	32.03	28.44	28.22	33.05	29.75	28.53	32.57	27.91	26.92	32.05	26.93	25.85
26	T_10ce 5	35.04	32.45	32.30	33.95	31.55	31.03	33.65	30.86	30.15	33.68	31.47	31.13	33.59	30.17	29.83	32.68	29.26	28.98	32.67	29.06	28.35	32.03	28.06	27.45	31.82	27.62	26.65
27	T_15ce 0	35.98	33.56	33.86	34.98	33.16	32.84	34.63	32.48	31.95	34.65	32.68	32.71	34.8	31.88	31.64	33.87	30.46	31.2	31.9	29.78	29.1	30.9	28.7	28.4	31.34	29.25	28.61
28	Inlet air tepe rature reduc	5.20	7.70	8.00	5.96	8.85	9.20	6.20	9.35	9.90	5.96	8.80	8.95	6.45	10.00	10.30	7.15	10.70	11.15	6.12	9.75	10.17	6.90	11.19	11.47	8.46	11.70	12.41
29	E_wb	0.477	0.706	0.734	0.547	0.812	0.844	0.569	0.858	0.908	0.445	0.657	0.668	0.481	0.746	0.769	0.530	0.794	0.827	0.373	0.595	0.620	0.421	0.682	0.699	0.516	0.713	0.757
30	E_dp	0.366	0.542	0.563	0.420	0.623	0.648	0.437	0.658	0.697	0.324	0.478	0.486	0.351	0.543	0.56	0.389	0.582	0.606	0.257	0.410	0.427	0.290	0.470	0.482	0.355	0.492	0.521
31	Cooling capacity (W)	200.46	186.40	117.66	162.24	150.37	96.65	120.07	112.74	72.35	228.39	211.76	130.85	174.5	168	107.6	137.64	129.23	81.0	233.1	233.21	147.79	185.6	187.9	116	161.88	140.45	89.61
32	Cooling capacity (W/m^2)	1047.73	974.25	614.96	848.00	785.94	505.15	627.57	589.28	378.15	1193.7	1106.8	683.90	912.3	878.05	562.19	719.43	675.43	423.4	1218	1218.92	772.45	970.0	981.9	606.04	846.12	734.1	468.37
33	**COP**	**4.62**	**4.29**	**2.71**	**7.48**	**6.93**	**4.45**	**10.26**	**9.64**	**6.18**	**5.26**	**4.88**	**3.01**	**8.04**	**7.74**	**4.96**	**11.76**	**11.04**	**6.92**	**5.45**	**5.45**	**3.45**	**8.85**	**8.96**	**5.53**	**15.17**	**13.16**	**8.40**
34	Humidity of exhusted wor	100.00	86.50	85.50	100.00	93.50	92.80	100.00	99.50	99.00	94.00	75.50	73.70	98.50	81.00	80.00	100.00	92.50	90.50	94.00	64.00	61.00	100.00	73.50	72.00	100.00	79.00	77.50
35	Water added (ml)	75.00	82.00	109.00	85.00	120.00	94.00	100.00	140.00	136.00	130.00	145.00	142.00	180.00	190.00	100.00	154.00	172.00	90.00	150.00	166.00	168.00	133.00	152.00	145.00	105.00	140.00	142.00
36	test duration (min)	21.00	20.00	25.00	27.00	31.00	25.00	27.00	36.00	30.00	32.00	32.00	30.00	43.00	40.00	20.00	32.00	37.00	25.00	35.00	32.00	33.00	29.00	32.00	30.00	23.00	30.00	34.00
37	total water consumpt (l/h	0.214	0.246	0.262	0.189	0.232	0.226	0.222	0.233	0.272	0.244	0.272	0.284	0.251	0.285	0.300	0.289	0.279	0.216	0.257	0.311	0.305	0.275	0.285	0.290	0.274	0.280	0.251

Experimental results of inlet conditions 35℃ and relative humidity of 45,35, and 25%

45	Temperature					T_in(C)=	35	Tin=35C							T_in(C)=	35								T_in(C)=	35				
46	Humidity of inlet air	45%				45%	0.0159				35%				35%	0.0123						25%				25%	0.0088			
47	Fanspeed (m/s)	5			3.5			2.5			5			3.5			2.5			5			3.5			2.5			
48	Working to inlet air	20%	50%	70%	20%	50%	70%	20%	50%	70%	20%	50%	70%	20%	50%	70%	20%	50%	70%	20%	50%	70%	20%	50%	70%	20%	50%	70%
49	T_wb (C)=	25.07			25.07			25.07			22.75			22.75			22.75			20.23			20.23			20.23		
50	T_dp (C)=	21.3			21.3			21.3			17.2			17.2			17.2			12			12			12		
51	Air density (kg/m^3)	1.135			1.135			1.135			1.137			1.137			1.137			1.14			1.14			1.14		
52	Cp (kJ/kg K)	1.035			1.035			1.035			1.028			1.028			1.028			1.021			1.021			1.021		
53	Q_in (m^3/s)	0.042	0.042	0.042	0.029	0.029	0.029	0.021	0.021	0.021	0.042	0.042	0.042	0.029	0.029	0.029	0.021	0.021	0.021	0.042	0.042	0.042	0.029	0.029	0.029	0.021	0.021	0.021
54	Supp Air exit speed (m/s)	4.220	2.640	1.610	2.980	1.860	1.150	2.120	1.340	0.800	4.220	2.640	1.610	2.980	1.860	1.150	2.120	**1.340**	0.800	4.220	2.640	1.610	2.980	1.860	1.120	2.120	1.340	0.800
55	Q_supp (m^3/s)	0.033	0.021	0.013	0.023	0.015	0.009	0.017	0.011	0.006	0.033	0.021	0.013	0.023	0.015	0.009	0.017	0.011	0.006	0.033	0.021	0.013	0.023	0.015	0.009	0.017	0.011	0.006
56	Reject Air exit speed	1.100	2.660	3.700	0.750	1.860	2.550	0.540	1.320	1.850	1.100	2.660	3.700	0.750	1.860	2.550	0.540	**1.320**	1.850	1.100	2.660	3.700	0.750	1.860	2.590	0.540	1.320	1.850
57	Q_ext (m^3/s)	0.009	0.021	0.029	0.006	0.015	0.020	0.004	0.010	0.015	0.009	0.021	0.029	0.006	0.015	0.020	0.004	0.010	0.015	0.009	0.021	0.029	0.006	0.015	0.020	0.004	0.010	0.015
58	Q_supp/Q_in=	0.80	0.50	0.30	0.80	0.50	0.31	0.799	0.505	0.302	0.796	0.498	0.304	0.803	0.501	0.310	0.799	0.505	0.302	0.796	0.498	0.304	0.803	0.501	0.302	0.799	0.505	0.302
59	Q_ext/Q_in=	**0.21**	**50%**	**70%**	**20%**	**50%**	**69%**	**20%**	**50%**	**70%**	**21%**	**50%**	**70%**	**20%**	**50%**	**69%**	**20%**	**50%**	**70%**	**21%**	**50%**	**70%**	**20%**	**50%**	**70%**	**20%**	**50%**	**70%**
60	sum	1.003	0.999	1.001	1.005	1.002	0.996	1.003	1.003	0.999	1.003	0.999	1.001	1.005	1.002	0.996	1.003	1.003	0.999	1.003	0.999	1.001	1.005	1.002	0.999	1.003	1.003	0.999
61	T_in 0	35.00	35.00	35.00	35.00	35.00	35.00	35.00	35.00	35.00	35.00	35.00	35.00	35.00	35.00	35.00	35.00	35.00	35.00	35.00	35.00	35.00	35.00	35.00	35.00	35.00	35.00	35.00
62	T_5HP 5	32.71	31.51	31.12	32.57	31.04	30.85	32.27	30.70	30.35	32.77	31.15	30.83	32.30	30.50	30.31	32.06	30.10	29.74	32.43	30.93	30.60	32.18	30.39	29.86	31.97	29.68	29.08
63	T_10HP 10	31.46	29.64	29.13	31.24	29.07	28.79	30.87	28.74	28.45	31.30	28.95	28.56	30.98	28.33	28.04	30.52	27.80	27.74	30.97	28.61	27.95	30.50	27.84	27.25	30.10	26.87	26.04
64	T_supp out	30.61	28.40	28.00	30.20	27.60	27.35	29.78	27.10	26.84	30.3	27.52	27.15	29.65	26.48	26.2	29.2	**26**	25.45	29.68	26.99	26.48	28.9	25.7	25.15	28.38	24.55	23.6
65	T_5ce 10	30.03	28.03	27.83	29.64	26.60	26.34	28.97	26.88	26.06	29.70	27.04	26.72	29.05	26.23	25.74	28.65	**25.21**	25.15	29.48	26.88	25.85	28.68	24.92	24.52	27.70	24.17	23.17
66	T_10ce 5	30.57	28.73	28.74	30.10	28.00	27.72	29.64	27.60	26.94	30.14	28.11	27.75	29.45	26.95	26.54	29.40	26.25	26.37	29.88	27.73	26.45	29.03	26.27	25.71	28.23	25.12	24.18
67	T_15ce 0	31.88	30.18	30.38	31.38	29.40	29.35	30.58	29.00	28.77	31.11	29.41	29.28	30.19	28.00	27.75	30.35	**27.95**	27.29	30.47	29.20	28.10	30.16	27.56	27.50	29.00	26.68	26.14
68	Inlet air tepe rature reduc	4.39	6.60	7.00	4.80	7.40	7.65	5.22	7.90	8.16	4.7	7.48	7.85	5.35	8.52	8.80	5.80	**9.00**	9.55	5.32	8.01	8.52	6.10	9.30	9.85	6.62	10.45	11.40
69	E_wb	0.44	0.66	0.70	0.48	0.75	0.77	0.53	0.80	0.82	0.38	0.61	0.64	0.44	0.70	0.72	0.47	0.73	0.78	0.36	0.54	0.58	0.41	0.63	0.67	0.45	0.71	0.77
70	E_dp	0.32	0.48	0.51	0.35	0.54	0.56	0.38	0.58	0.60	0.26	0.42	0.44	0.30	0.48	0.49	0.33	0.51	0.54	0.23	0.35	0.37	0.27	0.40	0.43	0.29	0.45	0.50
71	Cooling capacity (W)	170.92	160.76	103.98	131.97	126.99	81.17	102.10	97.67	60.23	182.08	181.28	116.02	146.36	145.48	92.90	112.88	110.71	70.14	205.23	193.31	125.40	166.18	158.13	100.85	128.30	128.01	83.37
72	Cooling capacity (W/m^2)	893.38	840.25	543.48	689.79	663.75	424.25	533.66	510.49	314.80	951.67	947.51	606.42	764.97	760.38	485.58	589.98	578.66	366.58	1072.70	1010.39	655.42	868.56	826.51	527.12	670.57	669.07	435.76
73	COP	3.94	3.70	2.40	6.08	5.85	3.74	8.73	8.35	5.15	4.20	4.18	2.67	6.74	6.70	4.28	9.65	9.46	5.99	4.79	4.52	2.93	7.92	7.54	4.81	12.02	12.00	7.81
74	Humidity of exhusted wor	96.00	80.50	79.00	100.00	86.00	86.30	100.00	91.50	91.00	87.30	71.00	68.50	95.00	80.00	81.00	99.50	82.00	83.50	87.50	64.00	61.00	97.00	69.00	67.00	100.00	75.00	74.00
75	Water added (ml)	90	**77**	88	90	110	90	80	96	98	134	120	91	140	145	125	140	174	160	115	151	148	100	150	153	128	190	138
76	test duration (min)	32	27	27	27	35	25	28	32	37	39	31	23	44	40	33	42	42	41	31	38	36	28	35	35	30	48	35
77	total water consumpt (l/h)	0.169	0.171	0.196	0.200	0.189	0.216	0.171	0.180	0.159	0.206	0.232	0.237	0.191	0.218	0.227	0.200	0.249	0.234	0.223	0.238	0.247	0.214	0.257	0.262	0.256	0.238	0.237

Experimental results of inlet conditions 30℃ and relative humidity of 45,35, and 30%

Temperature				T_in(C)=	30	Tin=30 C							T_in(C)=	30					0.007			T_in(C)=	30		0.008	0.0087	
Humidity of inlet air				45%		0.012							35%		0.009				30%	30%	30%	30%	30%	30%	30%	30%	30%
Fanspeed (m/s)		5			3.5			2.5			5			3.5			2.5			5			3.5			2.5	
Working to inlet air Ratio	20%	50%	70%	20%	50%	70%	20%	50%	70%	20%	50%	70%	20%	50%	70%	20%	50%	70%	20%	50%	70%	20%	50%	70%	20%	50%	70%
T_wb (C)=		21.06			21.06			21.06			19.03			19.03			19.03		18	18	18	18	18	18	18	18	18
T_dp (C)=		16.8			16.8			16.8			12.9			12.9			12.9		10.6	10.6	10.6	10.6	10.6	10.6	10.6	10.6	10.6
Air density (kg/m^3)		1.156			1.156			1.156			1.158			1.158			1.158			1.16			1.16			1.16	
Cp (kJ/kg K)		1.028			1.028			1.028			1.022			1.022			1.022			1.017			1.017			1.017	
Q_in (m^3/s)	0.042	0.042	0.042	0.029	0.029	0.029	0.021	0.021	0.021	0.042	0.042	0.042	0.029	0.029	0.029	0.021	0.021	0.021	0.042	0.042	0.042	0.029	0.029	0.029	0.021	0.021	0.021
Supp Air exit speed (m/s)	4.220	2.640	1.610	2.980	1.860	1.150	2.120	1.340	0.800	4.220	2.640	1.610	2.980	1.860	1.150	2.120	1.340	0.800	4.220	2.640	1.610	2.980	1.860	1.120	2.120	1.340	0.800
Q_supp (m^3/s)	0.033	0.021	0.013	0.023	0.015	0.009	0.017	0.011	0.006	0.033	0.021	0.013	0.023	0.015	0.009	0.017	0.011	0.006	0.033	0.021	0.013	0.023	0.015	0.009	0.017	0.011	0.006
Reject Air exit speed	1.100	2.660	3.700	0.750	1.860	2.550	0.540	1.320	1.850	1.100	2.660	3.700	0.750	1.860	2.550	0.540	1.320	1.850	1.100	2.660	3.700	0.750	1.860	2.590	0.540	1.320	1.850
Q_ext (m^3/s)	0.009	0.021	0.029	0.006	0.015	0.020	0.004	0.010	0.015	0.009	0.021	0.029	0.006	0.015	0.020	0.004	0.010	0.015	0.009	0.021	0.029	0.006	0.015	0.020	0.004	0.010	0.015
Q_supp/Q_in=	0.80	0.50	0.30	0.80	0.50	0.31	0.799	0.505	0.302	0.796	0.498	0.304	0.803	0.501	0.310	0.799	0.505	0.302	0.796	0.498	0.304	0.803	0.501	0.302	0.799	0.505	0.302
Q_ext/Q_in=	21%	50%	70%	20%	50%	69%	20%	50%	70%	21%	50%	70%	20%	50%	69%	20%	50%	70%	21%	50%	70%	20%	50%	70%	20%	50%	70%
sum	1.00	1.00	1.00	1.00	1.00	1.00	1.00	1.00	1.00	1.003	0.999	1.001	1.005	1.002	0.996	1.003	1.003	0.999	1.003	0.999	1.001	1.005	1.002	0.999	1.003	1.003	0.999
T_in 0	30.00	30.00	30.00	30.00	30.00	30.00	30.00	30	30.00	30	30	30	30	30	30	30	30	30	30	30	30	30	30	30	30	30	30
T_5HP 5	28.10	27.00	26.50	27.90	26.65	26.20	27.70	26.3	25.90	27.9	26.6	26.5	27.9	26.3	25.75	27.6	26.2	25.5	28.6	27.05	26.65	27.75	26.18	25.53	27.47	26.13	25.31
T_10HP 10	27.20	25.50	25.10	26.90	25.60	24.50	26.50	24.6	24.10	26.9	25.1	24.9	26.7	24.5	23.9	26.4	24.3	23.55	27.55	25.1	24.7	26.55	24.37	23.77	26.32	24.02	23.2
T_supp out	26.40	24.25	23.90	26.00	23.60	23.24	25.35	23.50	22.75	25.90	23.70	23.60	25.50	22.85	22.43	25.10	22.45	21.75	25.80	23.61	23.42	25.40	22.70	22.28	25.00	22.11	21.60
T_5ce 10	26.10	24.00	23.50	25.72	23.16	22.75	25.12	23	22.27	25.53	23.15	23.05	24.84	22.18	21.83	24.81	22.07	21.28	25.08	23.1	22.8	25.25	22.05	21.82	24.65	21.57	20.66
T_10ce 5	27.00	24.90	24.56	26.04	24.04	24.00	25.50	24.02	23.38	26.2	24.14	23.71	25.78	22.86	22.75	25.5	22.71	22	25.88	23.63	23.55	25.81	23.05	22.55	25.54	21.87	21.15
T_15ce 0	28.05	26.16	25.90	26.82	25.84	25.80	26.20	25.55	25.00	27	25.73	25.42	26.97	23.77	24.22	26.42	23.57	23.35	26.9	24.31	24.52	27.15	24.16	23.45	26.53	23.8	22.3
Inlet air teperature reduct	3.60	5.75	6.10	4.00	6.40	6.76	4.65	6.50	7.25	4.10	6.30	6.40	4.50	7.15	7.57	4.90	7.55	8.25	4.20	6.39	6.58	4.60	7.30	7.72	5.00	7.89	8.40
E_wb	0.403	0.643	0.682	0.447	0.716	0.756	0.520	0.727	0.811	0.374	0.574	0.583	0.410	0.652	0.690	0.447	0.688	0.752	0.350	0.533	0.548	0.383	0.608	0.643	0.417	0.658	0.700
E_dp	0.273	0.436	0.462	0.303	0.485	0.512	0.352	0.492	0.549	0.240	0.368	0.374	0.263	0.418	0.443	0.287	0.442	0.482	0.216	0.329	0.339	0.237	0.376	0.398	0.258	0.407	0.433
Cooling capacity (W)	141.79	141.68	91.66	111.25	111.11	72.56	92.01	81.29	54.13	160.8	154.59	95.78	124.65	123.61	80.92	96.56	94.04	61.35	164.22	156.31	98.16	127.01	125.81	80.11	98.21	97.96	62.26
Cooling capacity (W/m^2)	741.12	740.53	479.10	581.50	580.72	379.24	480.91	424.90	282.94	840.6	808.0	500.6	651.49	646.10	422.94	504.68	491.51	320.65	858.35	816.97	513.04	663.86	657.56	418.73	513.34	512.02	325.44
COP	3.27	3.26	2.11	5.13	5.12	3.34	7.86	6.95	4.63	3.71	3.56	2.21	5.74	5.70	3.73	8.25	8.04	5.24	3.84	3.65	2.29	6.06	6.00	3.82	9.20	9.18	5.84
Humidity of exhusted work	88.00	77.00	77.30	98.00	83.00	85.00	100.00	86.50	86.00	85.00	70.00	68.00	91.00	75.00	73.50	95.00	78.00	78.00	78.50	59.50	58.00	83.00	69.00	68.00	90.00	72.00	66.00
Water added (ml)	80.00	90.00	90.00	82.00	77.00	85.00	66.00	120.00	88.00	88.00	92.00	88.00	95.00	90.00	75.00	84.00	92.00	74.00	88.00	100.00	110.00	88.00	145.00	155.00	70.00	94.00	80.00
test duration (min)	37.00	34.00	32.00	31.00	36.00	31.00	24.00	37.00	30.00	27.00	31.00	29.00	32.00	30.00	21.00	29.00	30.00	20.00	30.00	35.00	35.00	27.00	33.00	40.00	19.00	25.00	20.00
total water consumpt (ml/	129.73	158.82	168.75	158.71	128.33	164.52	165.00	194.59	176.00	195.6	178.1	182.1	178.13	180.00	214.29	173.79	184.00	222.00	176.00	171.43	188.57	195.56	263.64	232.50	221.05	225.60	240.00

Appendix E

Electricity price of some of MENA region countries for domestic use 2014

Country	Electricity price (€/kW h)
Egypt	0.022
Iran	0.053
Iraq	0.016
Israel	0.133
Jordan	0.115
Kuwait	0.021
Lebanon	0.058
Libya	0.016
Saudi Arabia	0.042
Tunisia	0.087
Average	0.063